UNCLASSIFIED

AD NUMBER

AD874361

NEW LIMITATION CHANGE

TO

Approved for public release, distribution unlimited

FROM

Distribution authorized to U.S. Gov't. agencies and their contractors; Critical Technology; AUG 1970. Other requests shall be referred to Air Force Flight Dynamics Lab., Attn: FDFM, Wright-Patterson AFB, OH 45433.

AUTHORITY

Air Force Wright Aeronautical Labs ltr dtd 30 Jul 1980

THIS PAGE IS UNCLASSIFIED

AFFDL-TR-70-99

ANALYSIS AND DESIGN OF GAS-LUBRICATED TILTING-PAD JOURNAL BEARINGS
FOR MINIATURE CRYOGENIC TURBOMACHINERY

W. Shapiro
R. Colsher

Technical Report AFFDL-TR-70-99

August 1970

D D C

RECEIVED
SEP 16 1970

C

173

AFFDL-TR-70-99

ANALYSIS AND DESIGN OF GAS-LUBRICATED TILTING-PAD JOURNAL BEARINGS
FOR MINIATURE CRYOGENIC TURBOMACHINERY

W. Shapiro
R. Colsher

August 1970

This document is subjected to special export controls and
each transmittal to foreign government or foreign nationals
may be made only with prior approval of the Air Force Flight
Dynamics Laboratory, FDFM, Wright-Patterson Air Force Base,
Ohio.

The distribution of this report or its abstract is limited
because it covers an area of technology that is embargoed
under the Department of State International Traffic in Arms
Regulations and U. S. Export Control Act of 1949.

D D C

SEP 16 1970

C
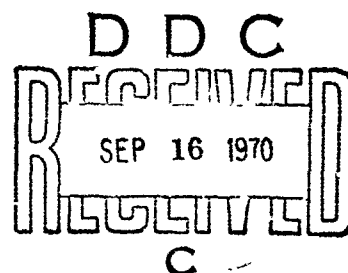
FOREWORD

The final technical report was prepared by The Franklin Institute Research Laboratories (FIRL), Philadelphia, Pennsylvania, under USAF Contract No. F33615-69-C-1718. The contract was initiated under Project No. 1470, "Cryogenic Cooling Technology", Task No. 147002, "Cryogenic Bearings and Seals". The contract was administered by the Air Force Flight Dynamics Laboratory, Air Force Systems Command, Wright-Patterson Air Force Base, Ohio, Mr. Phillip R. Eklund (FDFM), Project Engineer. The technical and program assistance of Mr. Forrest R. Stidham of the Cryogenics Group, (FDFE) is also acknowledged.
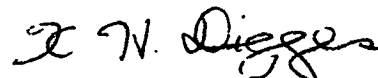
Mr. Wilbur Shapiro, Manager, Friction and Lubrication Laboratory, Mechanical and Nuclear Engineering Department of The Franklin Institute Laboratories, project engineer, was responsible for the program. He was assisted by Messrs. S. Heller, E. Jones, R. Colsher and C. Bognar. Mr. Otto Decker also participated in a managerial capacity prior to his departure from FIRL.

This report covers work performed during the period May 1969 to May 1970. It was submitted by the authors in June 1970.

Information in this report is embargoed under the Department of State International Traffic in Arms Regulations. This report may be released to foreign governments by departments or agencies of the U. S. Government subject to approval of the Air Force Flight Dynamics Laboratory, or higher authority within the Department of the Air Force. Private individuals or firms require a Department of State export license.

Publication of this report does not constitute Air Force approval of the report's findings or conclusions. It is published only for the exchange and stimulation of ideas.

This report has been reviewed and is approved.

KENNERLY H. DIGGES
Chief, Mechanical Branch
Vehicle Equipment Division
AF Flight Dynamics Laboratory

ii

ABSTRACT

Extensive steady-state and dynamic design information has been generated for tilting pad journal bearings with emphasis on miniature cryogenic turbomachinery applications. Coverage includes bearing length to diameter ratios of from 0.5 to 2.0 and values of the compressibility parameter from 1.5 to 20. Information was put into a format for use by design engineers and a separate section discusses design procedures plus practical considerations. An experimental program was completed, using room temperature air as the lubricant, which substantiated the analytical information.

Variable grid computerized analysis was required to avoid numerical problems at high values of the compressibility parameter Λ. These methods proved very successful and represent a significant improvement over constant grid techniques.

TABLE OF CONTENTS

TABLE OF CONTENTS (Cont.)

LIST OF FIGURES

LIST OF TABLES

1. INTRODUCTION

1.1 Primary Objective

The whirl-free characteristics of tilting-pad journal bearings es-
tablished them as the favored candidates for use in miniature cryogenic
turbomachinery. (See Reference 1.) A limited amount of design informa-
tion for this bearing was developed in a previous program described in
Reference 1. The objective of the present effort was to produce extended
verified design information for the tilting-pad journal bearing over a
sufficient range to cover operating conditions anticipated for future
hardware.

1.2 Basic Configuration

The tilting-pad journal bearing is schematically shown on Figure 1.
It is a three-pad bearing, and the pad pivots are equally spaced around
the pivot circle. The tri-pad arrangement ensures that pivot positions
remain on a single circle. One pad is generally spring-loaded to main-
tain a specified pre-load and allow for centrifugal and thermal expansions
of the shaft. The information developed treats both the fixed pivoted
bearing and the spring-loaded configuration. The position of the pivot was
fixed at 65% from the leading edge of the pad, since this position is optimum
with respect to load capacity over a wide operating range. Also, the over-
all pad angle was 100 degrees for all investigations.

1.3 Range of Data Generated

The original study (Reference 1) covered values of the compressibility
parameter (Λ) up to 3.5. Because of possible variations in the clearance/
radius ratio, speed, ambient pressure and lubricant viscosity, and also to
design away from unstable regimes, it was decided to extend the range of
Λ to 20. Performance for additional length to diameter ratios from that of

1
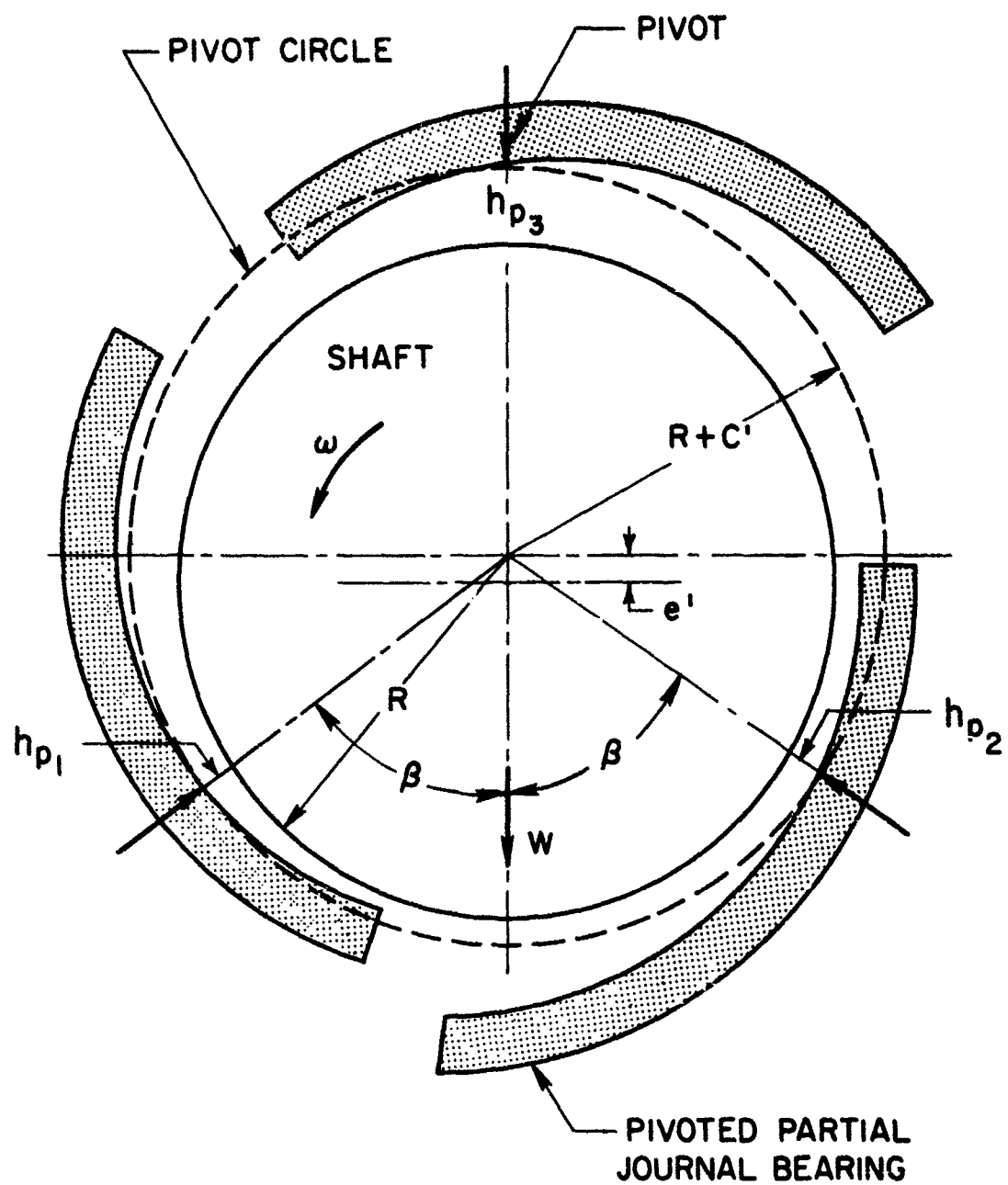
Figure 1. Schematic Representation of Pivoted-Pad Journal Bearing

Reference 1 was also accomplished. Figure 2 is a summary chart that shows the range of variable covered for the steady-state analysis and Figure 3 depicts the parameters covered by the dynamic analyses. It was not originally anticipated to do dynamic analyses for $\Lambda = 5$, but examination of the data between $\Lambda = 3.5$ and $\Lambda = 10$ indicated that an interim value would be beneficial.

1.4 Experimental Program

The primary purpose of the experimental program was to verify analytical predictions, both steady-state and dynamic. This was accomplished on a comparatively large size rig to facilitate installation of instrumentation and measurement, using air as the gaseous medium.

1.5 Design Methods

A secondary objective of the program was to present the data in a format that could readily be used by design engineers. A separate section (Section 4) is devoted entirely to design procedures and practical considerations, for the benefit of design engineers charged with the responsibility of establishing gas-lubricated journal bearing configurations for cryogenic applications.

3

		$\Lambda = 1.5$	3.5	5	10	20
R/L = 0.25	S.P.	✓	✓	X	X	X
OR L/D = 2.0	F.B.	✓	✓	X	X	X
R/L = 0.5	S.P.	✓	✓	X	X	X
OR L/D = 1.0	F.B.	✓	✓	X	X	X
R/L = 1.0	S.P.	✓	✓	X	X	X
OR L/D = 0.5	F.B.	✓	✓	X	X	X

KEY: R = Shaft radius

L = Bearing length

D = Shaft diameter

SP = Single pad

FB = Full bearing (3 pads)

✓ = Accomplished under original contract

X = Accomplished under present contract

Full bearing data generated for displacements directly between pads and directly at pads for both fixed pivot configuration and for single spring loaded shoe.

Figure 2.   Steady-State Summary Chart

	H_p	$\Lambda = 1.5$	3.5	5	10	20
R/L = 0.5	0.25	✓	X	X	X	X
or L/D = 1.0	0.5	✓	✓	X	X	X
	0.75	✓	X	X	X	X
R/L = 1.0	0.25	X	X	X	X	X
or L/D = 0.5	0.5	X	X	X	X	X
	0.75	X	X	X	X	X

KEY: R = Radius of shaft.

L = Bearing length.

D = Shaft diameter.

H_p = Dimensionless pivot film thickness.
   = h_p/C where h_p = pivot film thickness and C = radial clearance.

✓ = Accomplished under initial contract.

X = Accomplished under present contract.

Figure 3. Dynamic Summary Chart

($\alpha = 100°$; $\phi/\alpha = 0.65$)

5

2. ANALYSIS

2.1 Steady-State Analysis

The analytical procedure for obtaining steady-state performance is comprehensively described in Reference 1. For completeness, portions are repeated and elaborated upon in Appendix I. Since a major objective of this program was the generation of design data, it was decided to automate the analytical procedures so that a large amount of performance information could be economically produced. The sequential steps were as follows:

2.1.1 Production of Single-Pad Steady-State Data

The foundation of the steady-state analysis is determining the relationship between the pivot film thickness and performance parameters such as load coefficient, viscous friction coefficient and minimum film thickness for a single pad. This data is then transposed into full three pad bearing performance. Appendix I describes the computerized analyses used to generate the single-pad data for a known bearing size and pivot position.

2.1.2 Completion of Curve Fitting Routines for Single-Pad Steady-State Data

After single pad data is generated as a function of the pivot film thickness, it is necessary to put results in a convenient form for further use. By utilizing curve-fitting routines, it was possible to establish polynomial expressions over varying ranges of the pivot film thickness that accurately described the data from the computer program used to establish single-pad performance.

6

2.1.3 Generation of Computer Program to Determine Full-Bearing Performance

After single-pad data was described by analytical expressions as a function of pivot-film thickness, as described in paragraph 2.1.2 above, it was not difficult to assemble another program whose function was to produce full bearing data. A total of four conditions were considered, as follows:

1. Three-pad bearing, fixed pivots, displacement between shoes.

2. Three-pad bearing, fixed pivots, displacement directly at pivot of one pad.

3. Three-pad bearing, one pad spring loaded, displacement directly between two fixed pads.

4. Three-pad bearing, one pad spring loaded, displacement directly at pivot of spring loaded pad.

Performance was established as a function of eccentricity ratio and pivot circle pre-load. Appendix I contains the analytical procedure for converting from single pad to full bearing performance and also contains the complete set of steady-state performance curves. The use of these curves is described in Section 4, Design Procedures.

2.1.4 Automatic Plotting of Full Bearing Performance

An automatic plotting routine, which generated performance curves for the full bearing proved successful and was extensively applied. The computer plots, accomplished by a Calcomp X-Y plotter allowed great savings in manpower and time in production of the design curves.

2.2 Samples of Steady-State Results

Figure 4 shows single pad load coefficient *vs.* pivot film thickness for values of the compressibility ratio Λ, of 1.5 and 3.5 It is essentially this data that is converted to polynomial format and coefficients determined by insuring a very accurate curve fit. Then, by utilizing

7
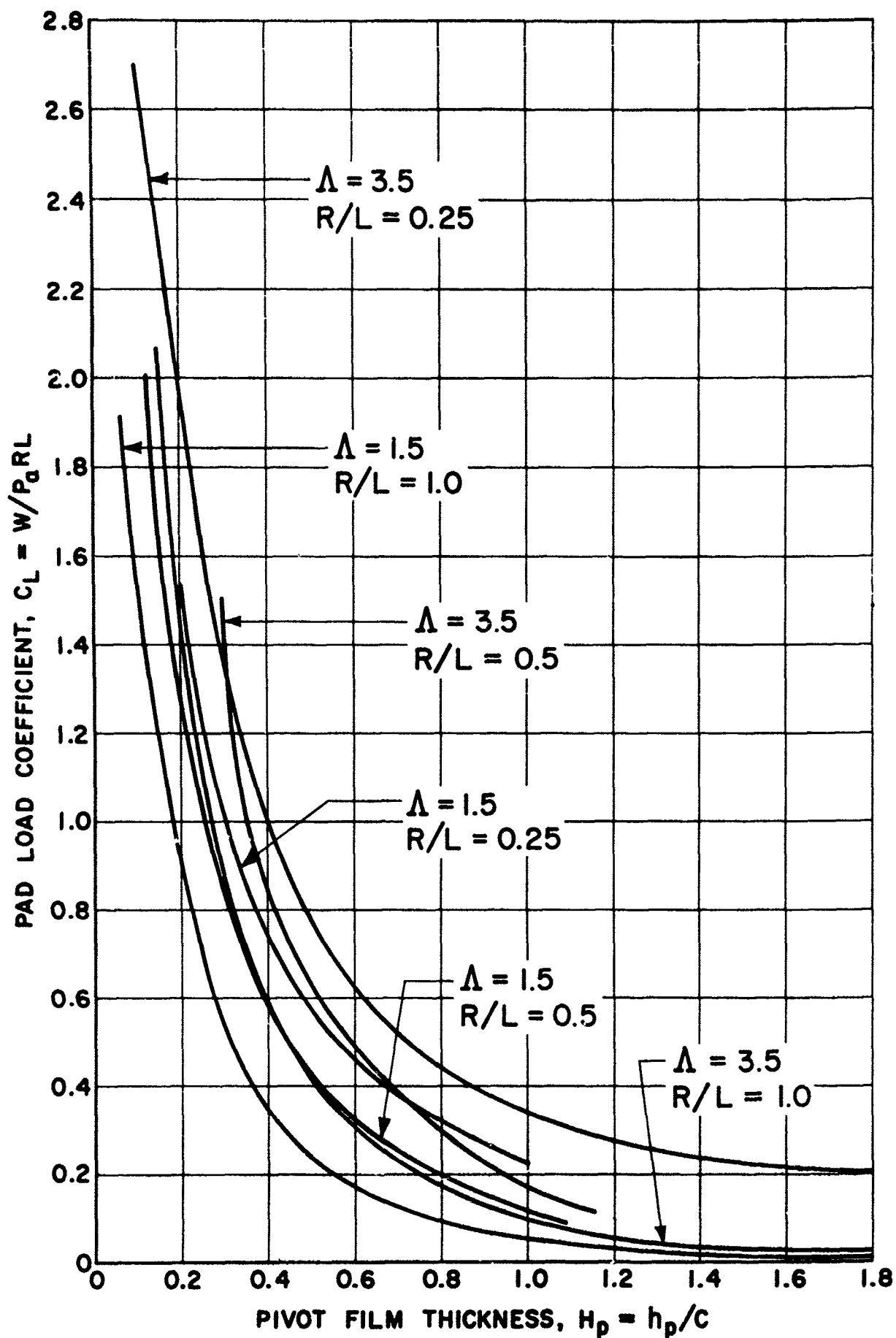
Figure 4. Individual Pad Load vs. Pivot Film Thickness

procedures described in Appendix I full bearing data is determined as a function of eccentricity ratio ϵ' and the pad pre-load parameter C'/C. From this data curves are automatically generated (from additional curve fitting routines) to produce performance plots as shown on Figure 5. Here the full bearing load coefficient is plotted as a function of bearing eccentricity ratio for various pre-loads. Thus, for a given design load, proper pre-load to satisfy a specific eccentricity (which can be related to pivot and minimum film thickness) can be established. The curves also give pivot film thickness on all three shoes. The series of curves shown on Figure 5 also permit determining off-design performance. Figures 6 and 7 show the other two parameters of primary interest namely, pad friction coefficient and minimum film thickness. This information was developed for individual pads and not the whole bearing. For friction, it is necessary to accumulate the effect of each separate pad.

There are quite a voluminous number of curves similar to Figures 4 through 7 covering the range and conditions described in Section 1. Their use for determining steady state performance will be shown by example in Section 4, Design Procedures.

2.3 High Lambda (Λ) Analysis

Numerical difficulties were encountered because of the rapid pressure changes in the bearing trailing edge film at high Λ's. These changes were so severe that dividing the bearing circumference with a uniform grid spacing resulted in the computer solution becoming unstable or converging to the wrong solution. By designing a system with variable grid spacing, this convergence problem was eliminated. The technique merely increases grid spacing where the pressure changes slowly (i.e., leading edge) and decreases grid spacing where the pressure changes rapidly (i.e., trailing edge).

The steady-state portion of the computer program was modified to incorporate this variable grid technique. Figure 8 is a plot of the non-dimensional pressure distribution in the circumferential direction,

9
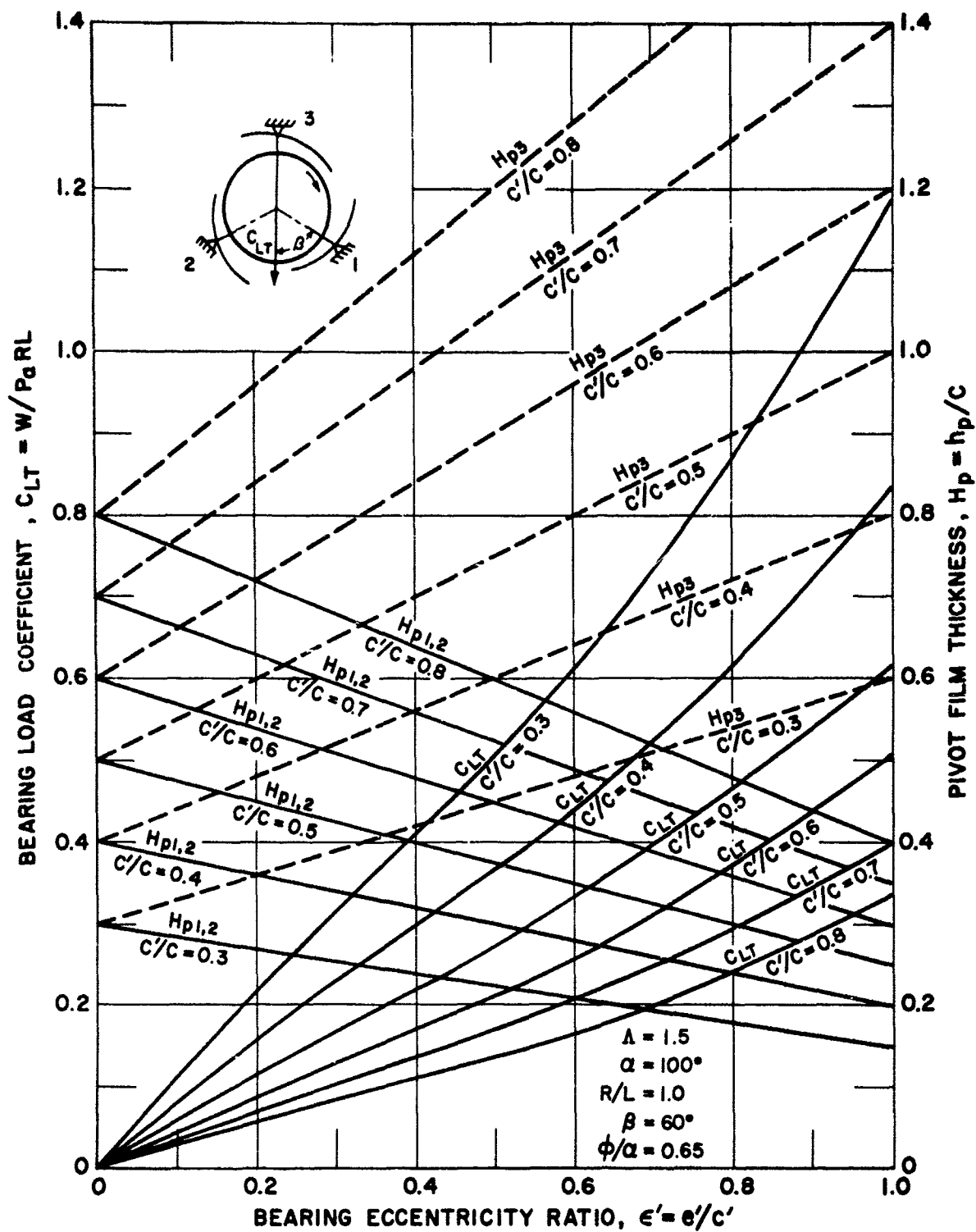
Figure 5.   Bearing Load Coefficient vs. Eccentricity Ratio, Load
"Between" Pads Λ = 1.5, R/L = 1.0

10
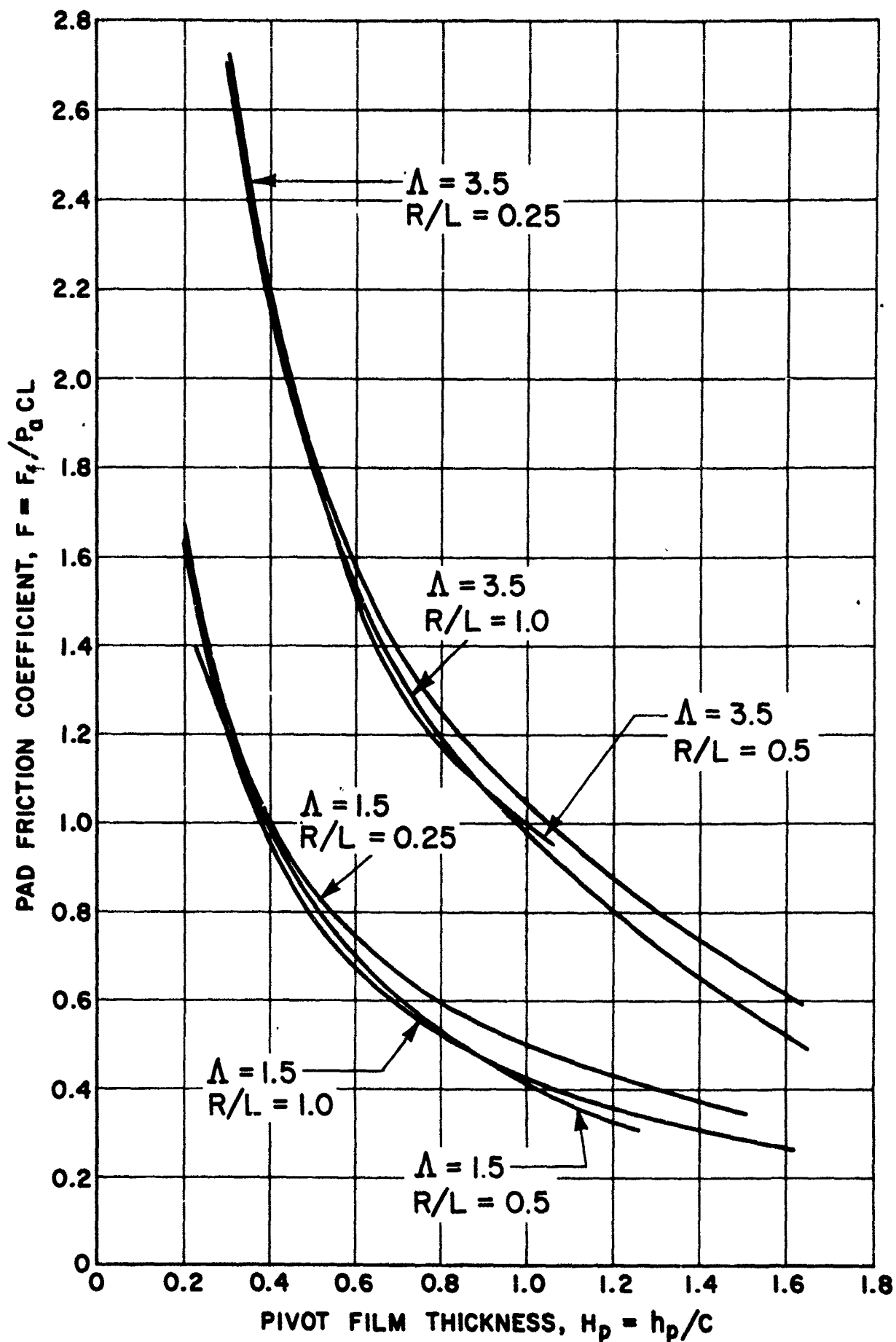
Figure 6. Individual Pad Friction $vs.$ Pivot Film Thickness

11
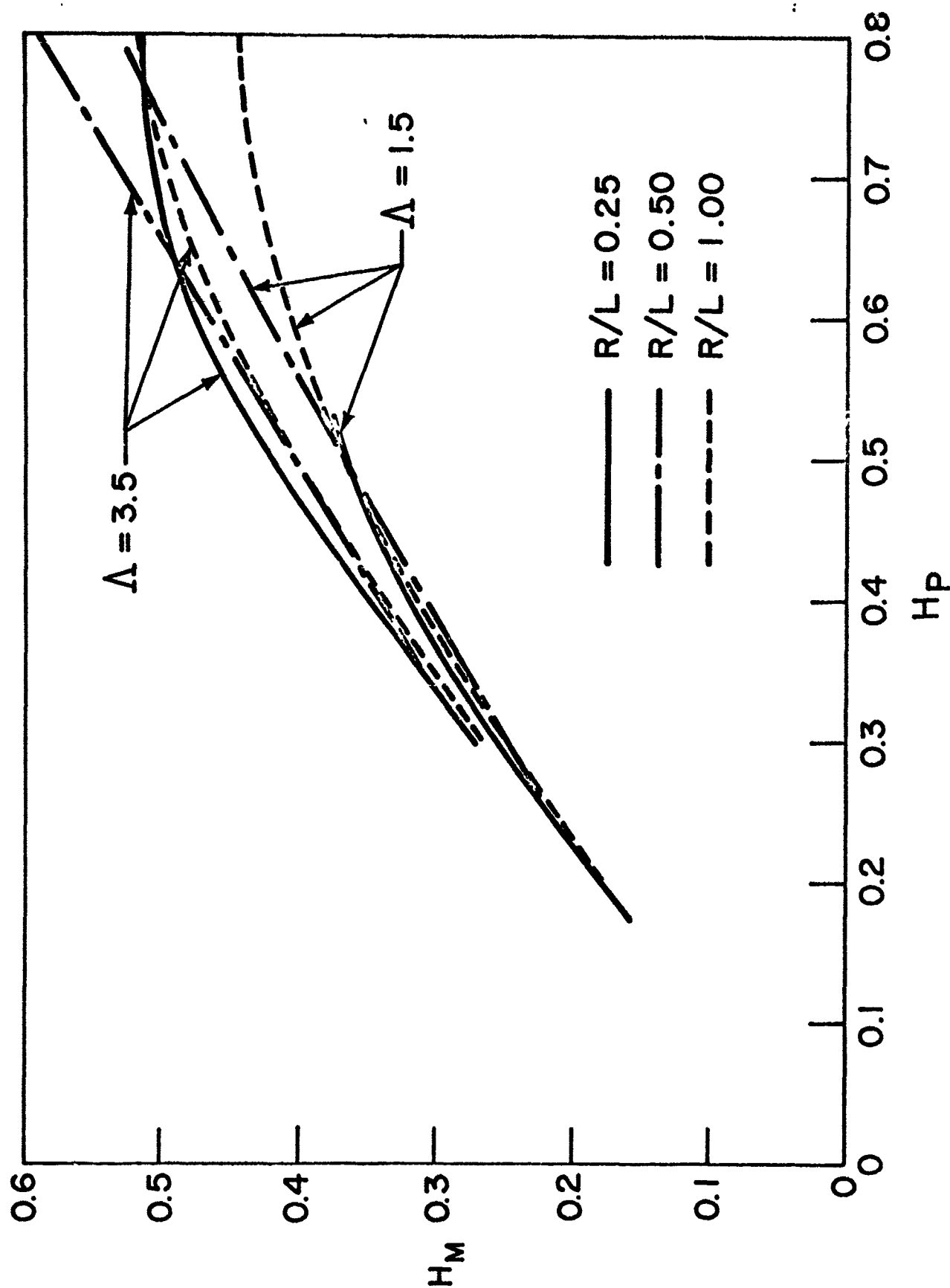
Figure 7. Individual Pad Minimum Film *vs.* Pivot Film Thickness
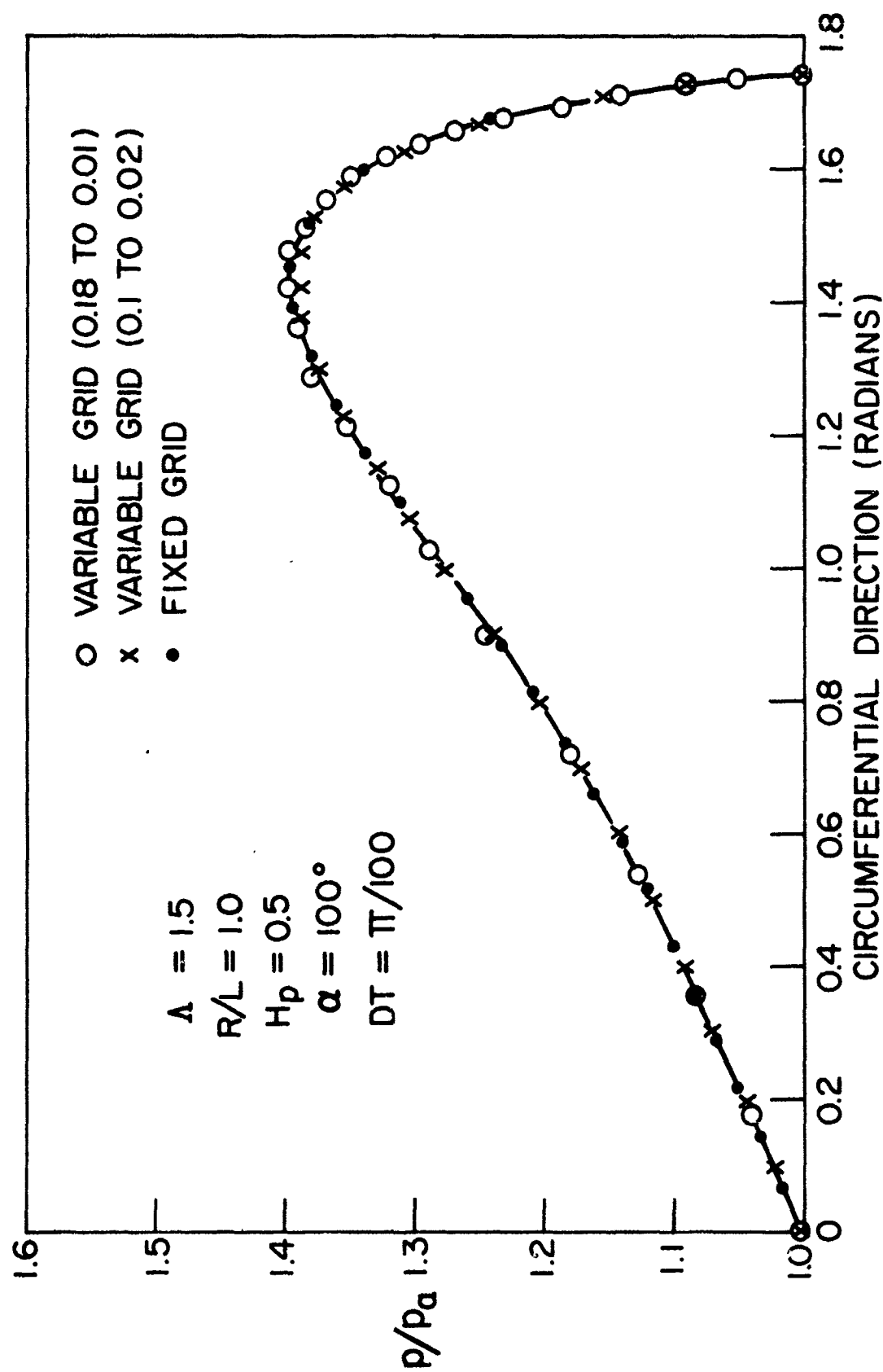
Figure 8. Circumferential Pressure Distribution, Variable vs. Fixed Grid at $\Lambda = 1.5$

13

(i.e., in the direction of rotation) taken at the center of the pad. A small lambda value (Λ = 1.5) was used to check the validity of the variable grid approach. The solid line is the pressure distribution using a fixed grid (circumferential increment = 0.0727 radians). The values of pressure signified by X and 0 are values using two different variable grid spacings.

0   range from 0.18 radians at leading edge to
    0.01 radians at trailing edge.

X   range from 0.10 radians at leading edge to
    0.02 radians at trailing edge.

A high Λ test case was run to check out the modified variable grid technique. Figure 9 is the pressure distribution at Λ = 20 using fixed and variable grid spacings. The dotted line uses a fixed grid and the solid line uses a variable grid. The variable grid generates the correct pressure distribution while the fixed grid generates a pressure profile obviously suffering from numerical instability. Figure 10 presents the corresponding film thickness distribution. Appendix II describes the theory for implementation of the variable grid concept.

2.4 Dynamic Analysis

The big advantage of tilting-pad gas bearing as compared to other types is their relative freedom from self-excited fractional frequency whirl. However, for the unusually severe conditions encountered with miniature cryogenic turbomachinery, shoe flutter could cause problems. Reference 2 describes an analytical technique that determines whether flutter will be excited and cause bearing failure. The technique is called the "Step-Jump" method. The bearing is assumed to be in its normal equilibrium position as if it were to be stable. The journal and pads are then given sequential slight disturbances in their various degrees of freedom. Since the fluid film is compressible the response to the disturbances is not immediate, but occurs over some discrete time interval. The responses are obtained by numerical solution of the time-dependent compressible Reynolds' equation; thus, they are obtained very accurately. They are then transposed to a polynomial form so they can be continuously re-used in the equations governing the dynamics of the

14
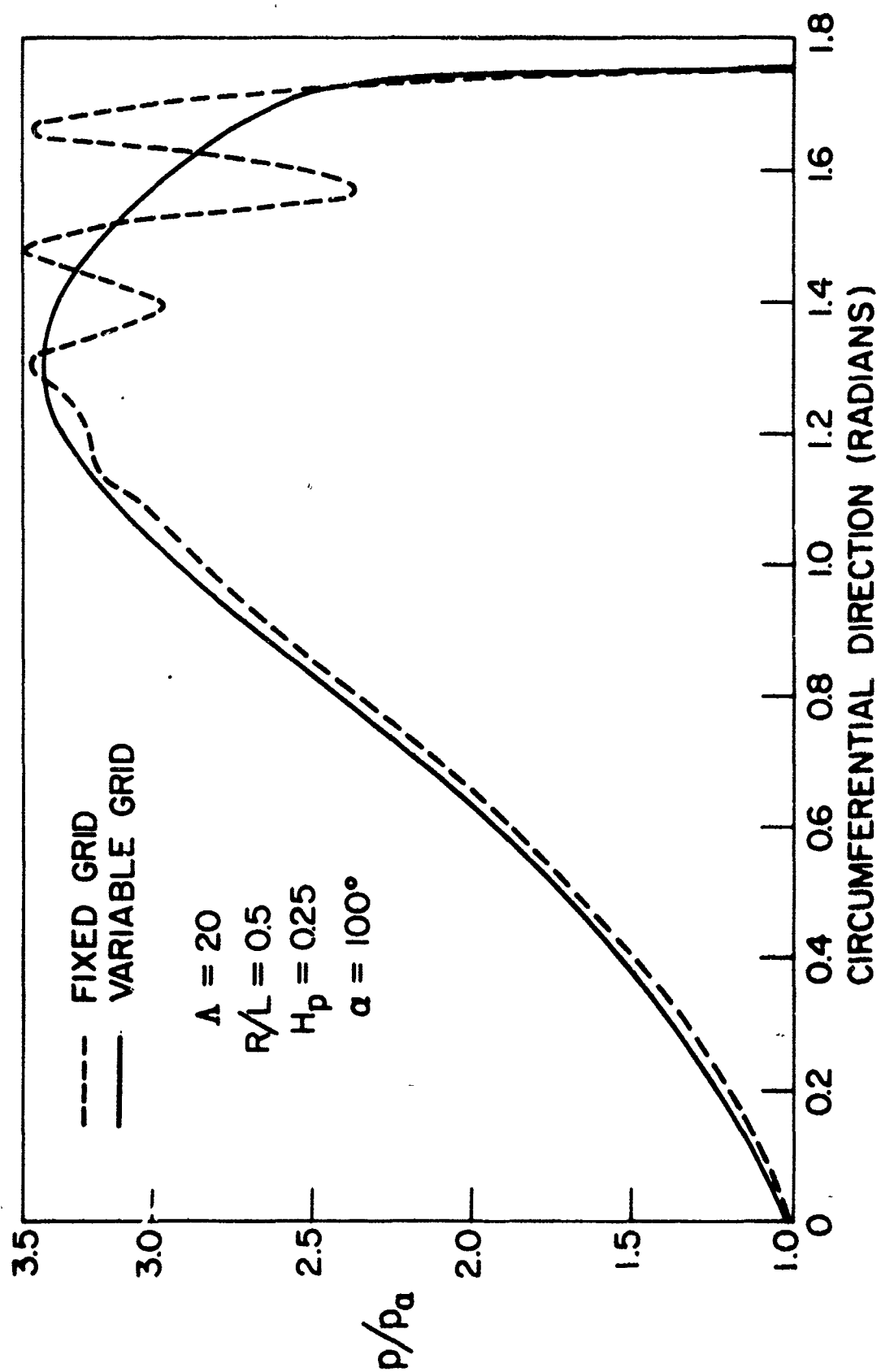
Figure 9. Circumferential Pressure Distribution, Variable vs. Fixed Grid at Λ=20.
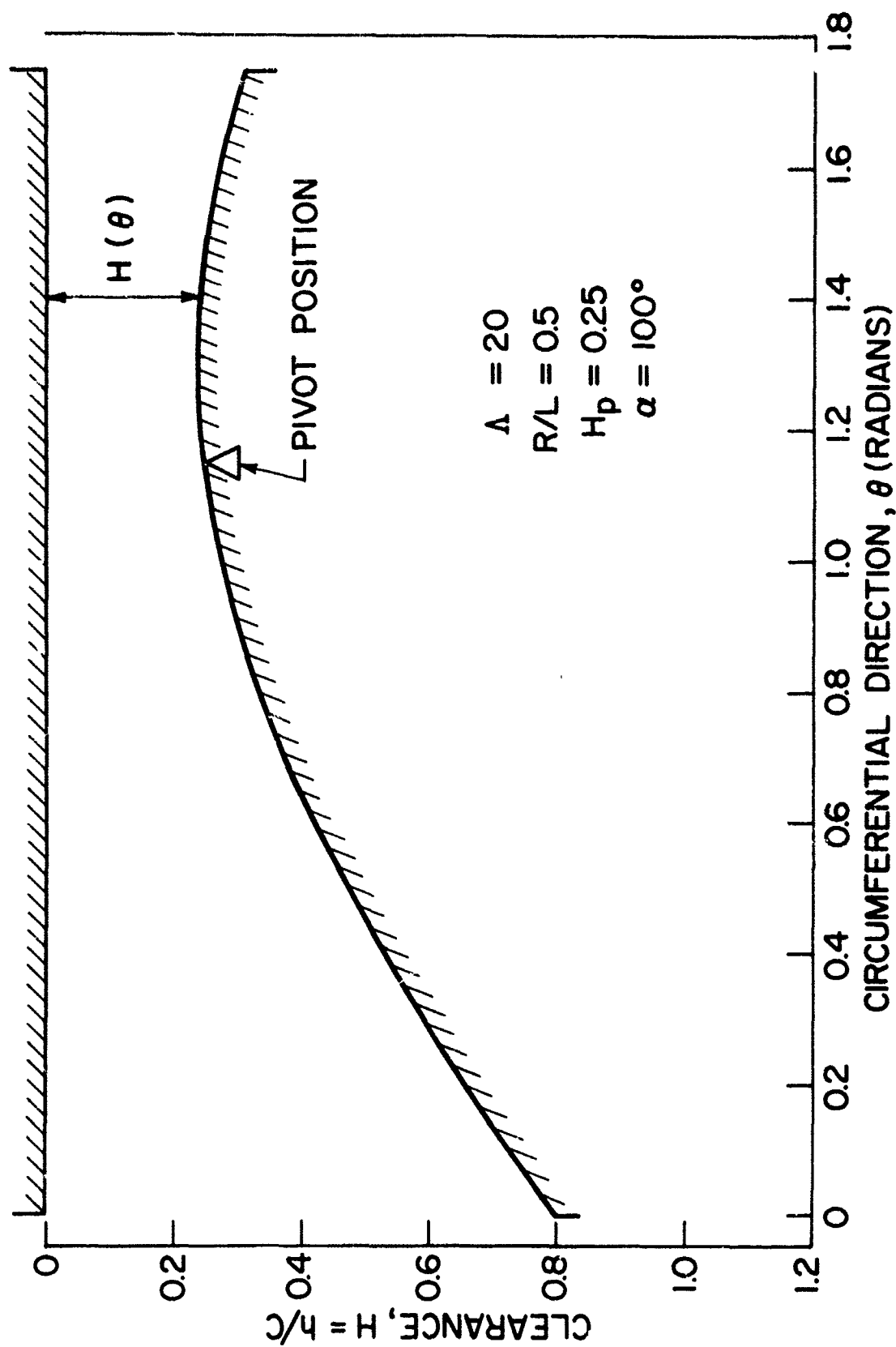
Figure 10. Circumferential Film Thickness Distribution Used for Grid Comparative Studies at Λ=20.

16

system. Then, inertias, masses and spring properties of the dynamic
system can be changed and the equations solved without resolving Reynolds'
equation for the fluid film forces. It is the solution of Reynolds'
equation that consumes computer time. Solution of the dynamics equation
determines whether the response to a disturbance in a particular degree
of freedom will grow or decay. If it grows the system is unstable; if it
decays the system is stable. The main advantage of the "Step-Jump" method
is expeditious determination of stability thresholds. Using this method
(2) a three shoe bearing was analyzed in a system that permitted a total
of 5 degrees of freedom. These included the x and y translations of the
shaft and the pitch of each shoe. These are the predominant motions for
any tilting-pad journal bearing system.

Examples of the results of the analyses are shown on Figure 11. The
bearing system is stable if the shoe inertia and shaft mass are such that
the operating point is below the stability threshold shown on Figure 11.
This plot is for a specific compressibility parameter Λ, length to diameter,
L/D ratio, and various valves of pivot film thickness Hp. The analysis is
confined to one three-pad bearing with fixed pivots operating in the con-
centric position. This is considered a representative model for the high
speed, low-load conditions encountered by miniature cryogenic turbomachinery.
The curve indicates that as the shaft mass increases, so does the stable
range. This is contrary to a whirl type instability in which an increased
mass aggravates the whirl problem. Thus the indications are that the in-
stability is due to pad flutter.

For high Λ, variable grid geometry was again utilized to avoid numerical
instability. All other aspects of the analysis were identical to the con-
stant grid situation.

Appendix III presents all dynamic performance curves such as that
shown on Figure 11 for the range of variables described in Section 1.
Section 4 describes procedures for determining stability of a particular
bearing configuration.

17
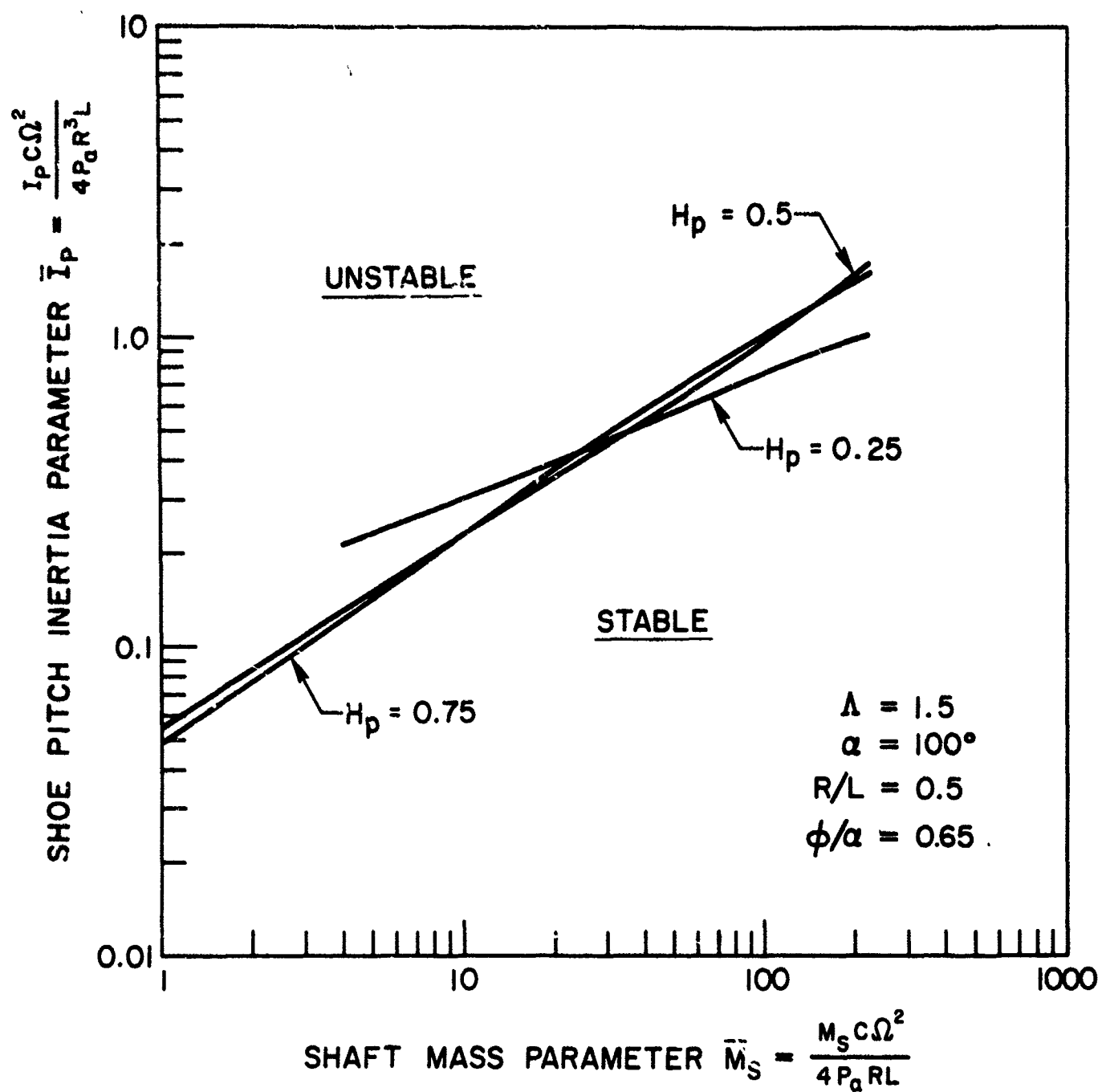
Figure 11. Stability Map, Λ=1.5, L/D = 1.0

2.5 Limitations of the Analysis

There are a number of restrictions of the analysis of which potential users should be aware. Removal of these limitations would increase complexity and make the production of design information impractical. Most of the restrictions are concerned with secondary effects and do not materially reduce the usefulness of the design information.

a. Pivot friction is assumed to be zero. Naturally pivot designs should be as frictionless as possible.

b. The pivot point is assumed to be located at the surface of the pad. Thus, no account is taken of the surface viscous drag moment about the pivot which is usually negligible. It is good practice to locate the pivot as close to the pad surface as practical. (See Section 4.)

c. The dynamic stability thresholds were developed for a model consisting of a three-pad bearing in the concentric position with pad motion restricted to pitch mode only. This is the primary mode. As discussed in Section 4, the thresholds can also be applied to loaded bearings (non-concentric) by considering individual pads rather than a complete bearing.

d. Unbalance and other external excitations are not considered in the dynamic analysis. The methods treat self-excited instabilities due to fluid film forces only. Normal balance limitations, however, have proven more than adequate for gas-bearing miniature cryogenic turbomachinery, although operation should not be in the vicinity of critical speeds computed on the basis of steady-state bearing stiffness.

19

3. EXPERIMENTAL PROGRAM

A decision was made in the early stages of the project to utilize a large tilting-pad journal bearing test rig (4-inch diameter shaft) that was available at FIRL from previous programs. The reasons for using this rig rather than going directly to the small (1/2-inch diameter) cryogenic test rig used on the previous studies (Reference 1) were as follows:

a. The rig has a prior history of providing excellent capabilities for conducting experimental tests on tilting pad journal bearings.

b. The larger size permits much more accurate and easily obtainable measurements.

c. The rig incorporates a test chamber that will allow variations in the environment to get up to the high lambda values necessary for steady state testing.

d. It could be made available for testing with no major modifications or major preliminary check-out work.

The usual operating conditions for this rig are shaft speeds up to 18,000 rpm.

3.1 Description of Test Rig

Figure 12 shows the test rig mounted on its wooden base for atmospheric testing. Behind the rig is the environmental chamber that was employed for high Λ tests. The rig was inserted in the chamber, which was subsequently sealed and evacuated for high Λ testing.

The rig contains two bearing pedestals that support the tilt-pads. The pedestals contain provisions for mounting of capacitance probes for monitoring the shaft and selected pads. A mylar foil supported by pulley mechanisms is used to apply loads to the shaft. The loading mechanism

20
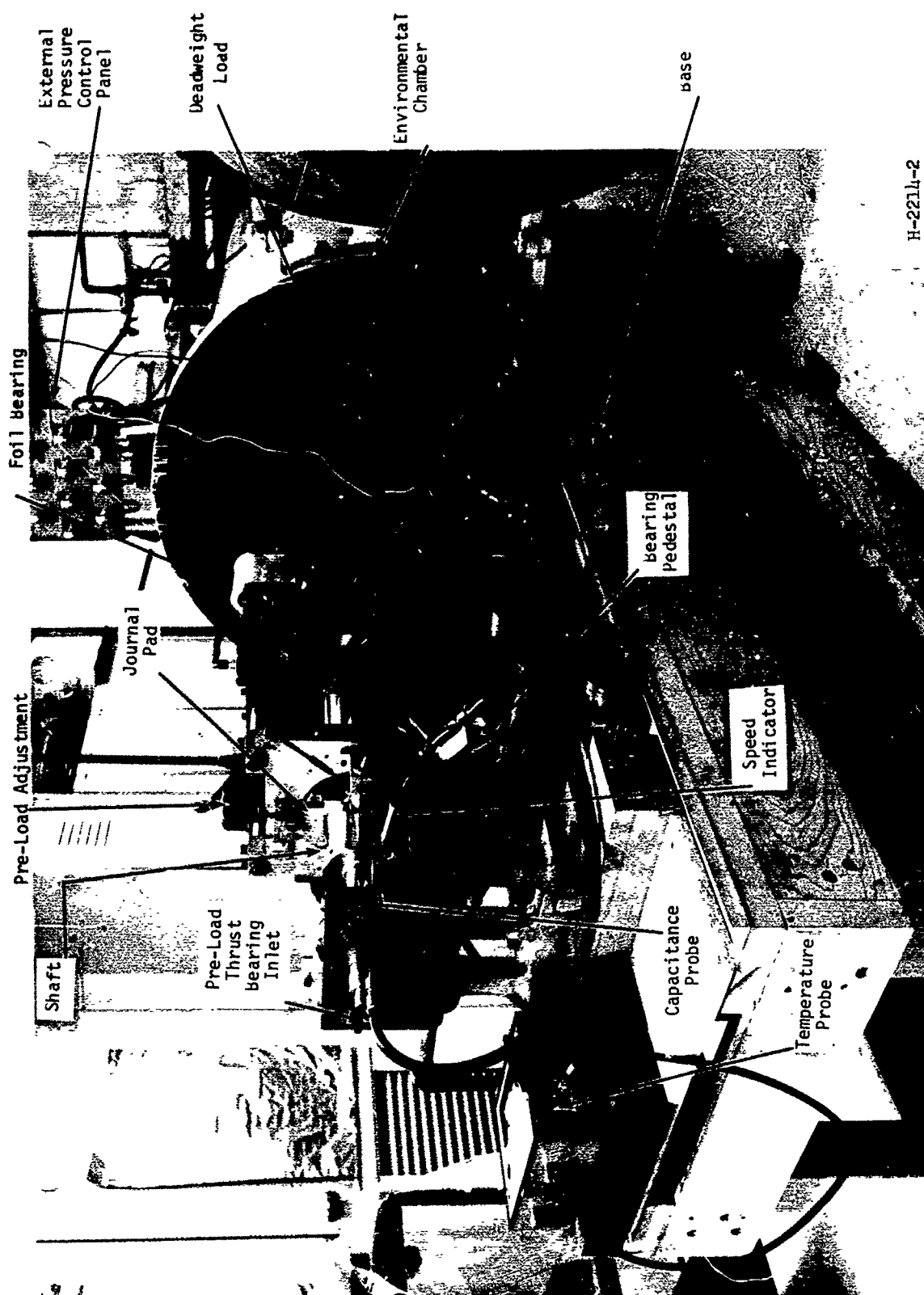
Figure 12. Front-View of Test Rig Ready for Atmospheric Testing

H-2214-2

21

for atmospheric testing employed calibrated dead weights. Note that
the loading mechanism lifts upward on the shaft and is designed to
remove the dead weight shaft load from the bearing. The total shaft
weight is 92 lbs., so the load range on each bearing can vary between
0 and 46 lbs. Figure 13 shows the test rig from the opposite side
and gives a better view of the turbine drive and thrust bearing. Also
indicated is the external pressure lines that feed the bearing pads
through the pivots for start-up and shut-down.

Figure 14 shows the test rig modified for high Λ testing. Since
this testing is accomplished inside the environmental chamber, it is
cumbersome to use dead weight loading. A bellows load cell was con-
structed and loading applied through air-pressure. Calibrated strain
gages were used to establish applied loads. Figure 15 shows the tank
sealed up with the rig inside, ready for vacuum environmental (high Λ)
testing.

3.2 Instrumentation

Instrumentation was utilized to determine the following measurements:

a. X and Y translatory motions or alternatively
    orbit traces of the shaft at each journal
    bearing location.

b. Relative pad pitch to shaft motions of one
    fixed pivot pad.

c. Absolute pitch motions of one fixed pivot pad.

d. Gross shaft displacement.

e. Shaft speed.

f. Shaft loads.

g. External pressure to pad pivots (start-up,
    shut-down and operation below 10,500 rpm).

On Figure 15 is shown the strain gage read-out bridge used for de-
termining load applied by the pressurized bellows. The pressure gage is
fed through a six-way valve and is used for establishing pivot pressure
in each of the six pads. Mounted above the tank are four Wayne-Kerr

22
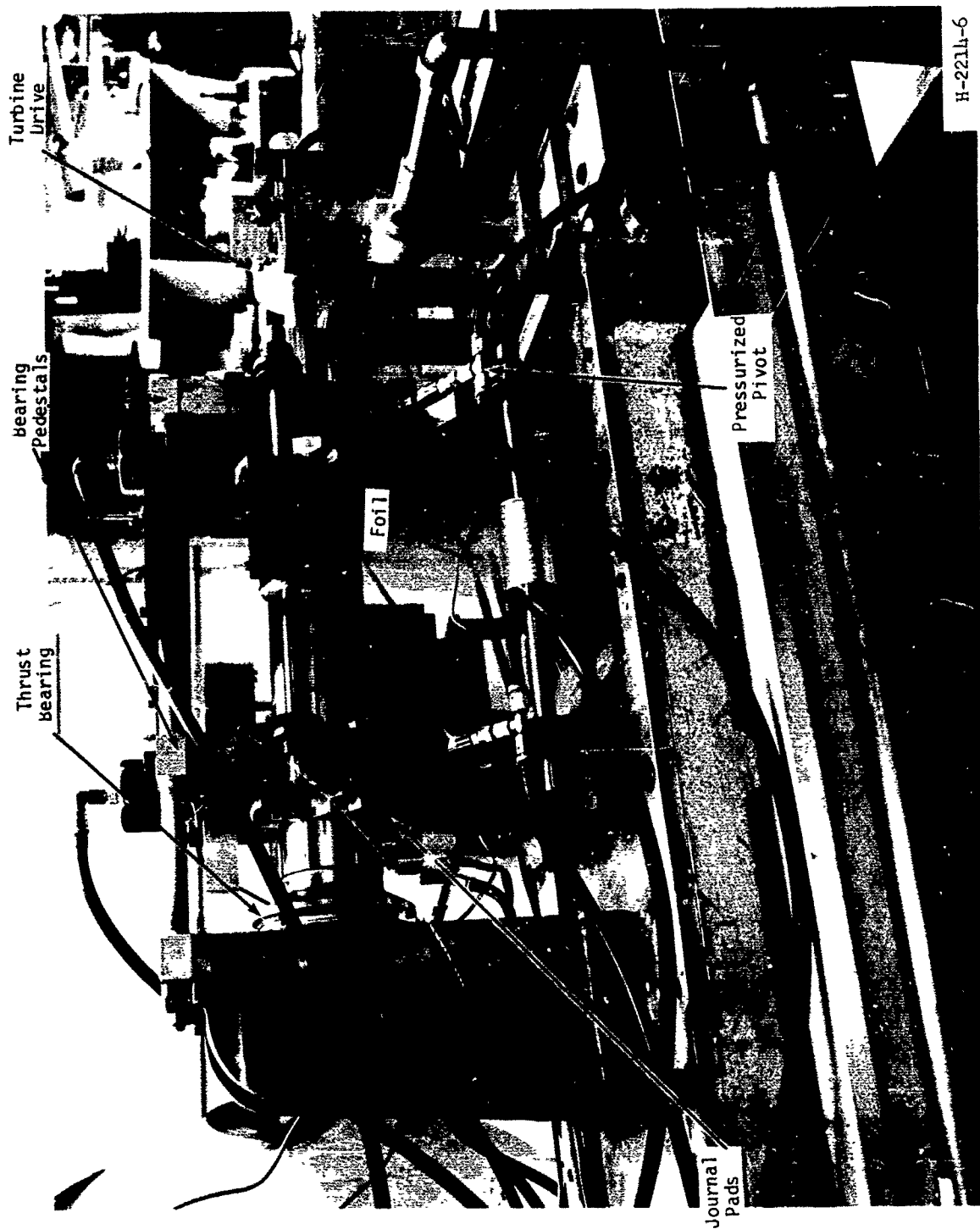
Figure 13. Side-View of Test Rig Geared for Atmospheric Testing
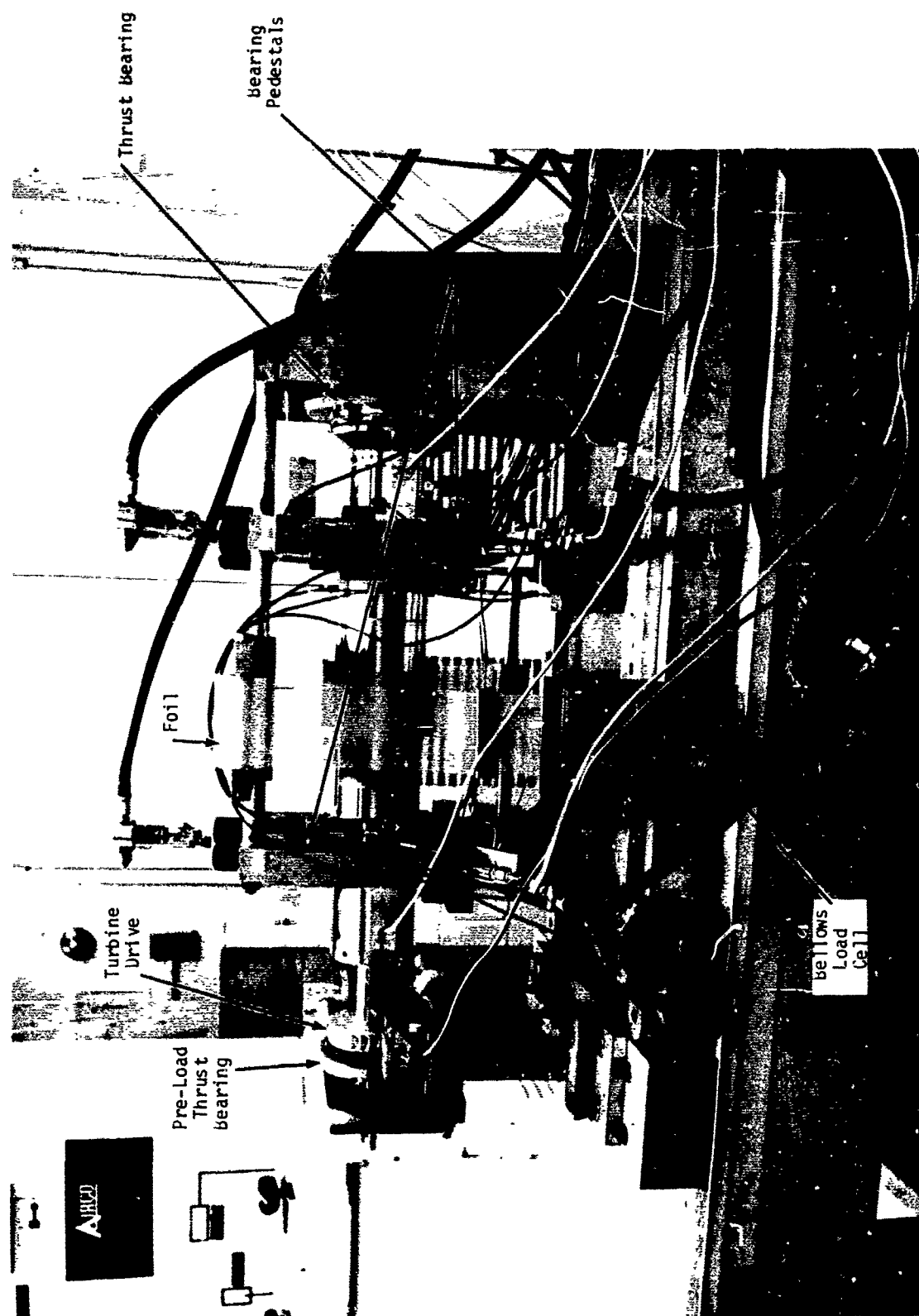
Figure 14. Test Rig with Pressurized Bellows Loading Device

24
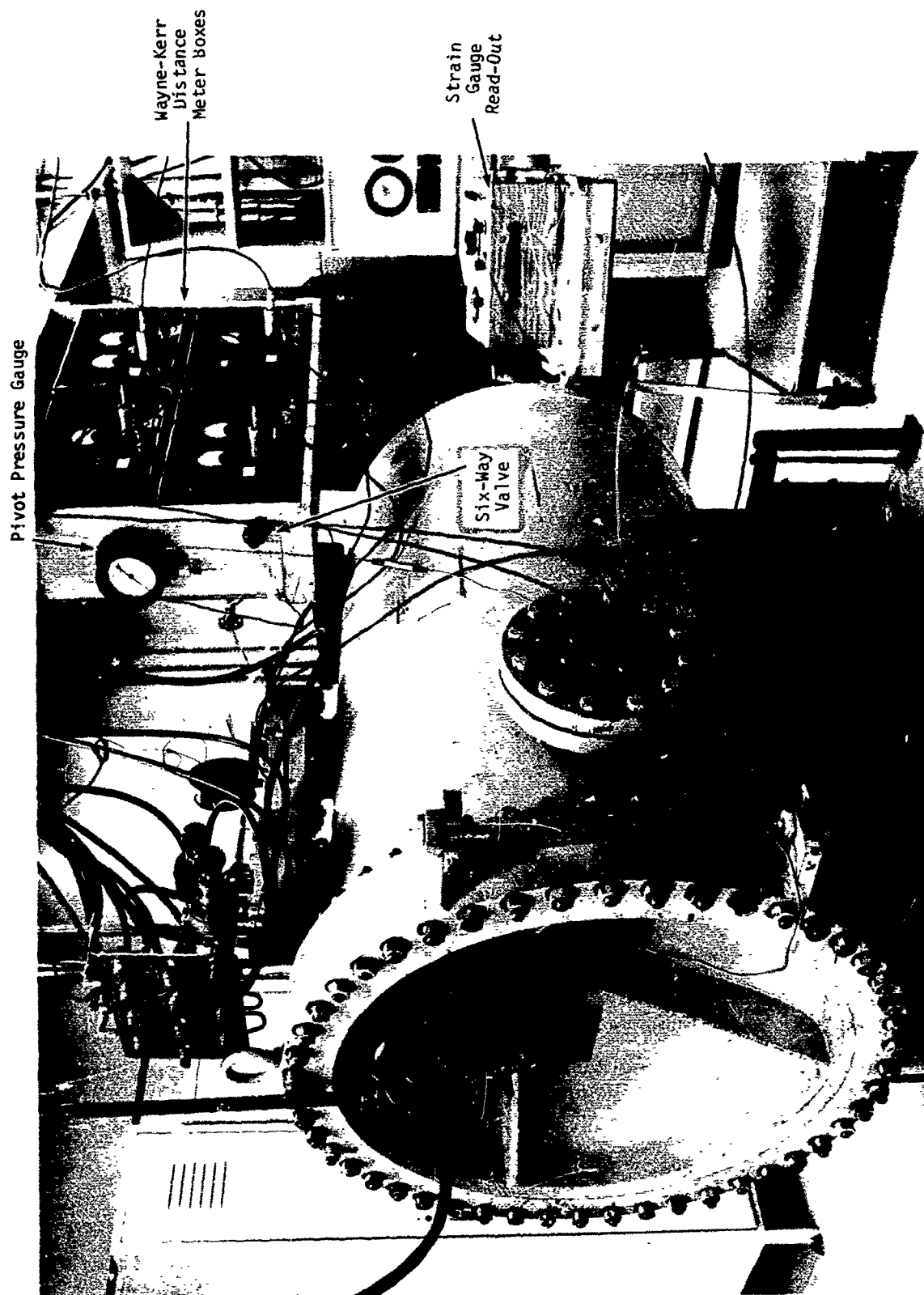
Figure 15. Test Rig Inside Tank for High Λ Testing

25

distance meter boxes that amplify capacitance probe signals and convert into voltage output for driving dual beam oscilloscopes. The oscilloscopes measure individual vibrations monitored by the probes or the probe outputs can be combined to provide orbit traces. Also probe outlets are fed into a Wayne-Kerr electronic micrometer, which measures gross displacements of the shaft. The electronic micrometer and oscilloscopes are shown on Figure 16.

3.3 Pad Configurations

Figure 17 depicts a cross-sectional drawing of the two fixed pivoted pads. A photograph of the two pads are shown on the bottom of Figure 17. The inlet orifice and surrounding recess are clearly shown. The variance in pad configuration was necessary to permit installation of all three pads around the circumference of the bearing. Probes for measuring absolute pitch motion are also indicated. Note that the angular distance between pads are not equal for the test rig. This differs from the recommended configuration of the bearings considered for miniature cryogenic machines and for which design information has been generated. However, the objective of the testing was to validate the analytical tools, and for this purpose a special analysis of the test bearing was completed.

To accomplish high Λ stability testing it was necessary to produce sets of light pads since it was anticipated that the existing heavy pads would go unstable prior to reaching the high Λ condition. The two different pads are shown on Figure 18. The buttons on the pads are used as monitor surfaces for the capacitance probes for measuring absolute pitch, roll or yaw. When the light shoes were installed, relative pitch motions between the pad and shaft were measured by physically attaching the probes to the pad.

3.4 Difficulties Encountered During Testing

Two major problem areas occurred during testing. The first was concerned with the tilting-pad thrust bearing originally installed. This was a self-equalizing Kingsbury type thrust bearing with cylindrical pivots used on the leveling plates. The pad orientation, when operating in the

26
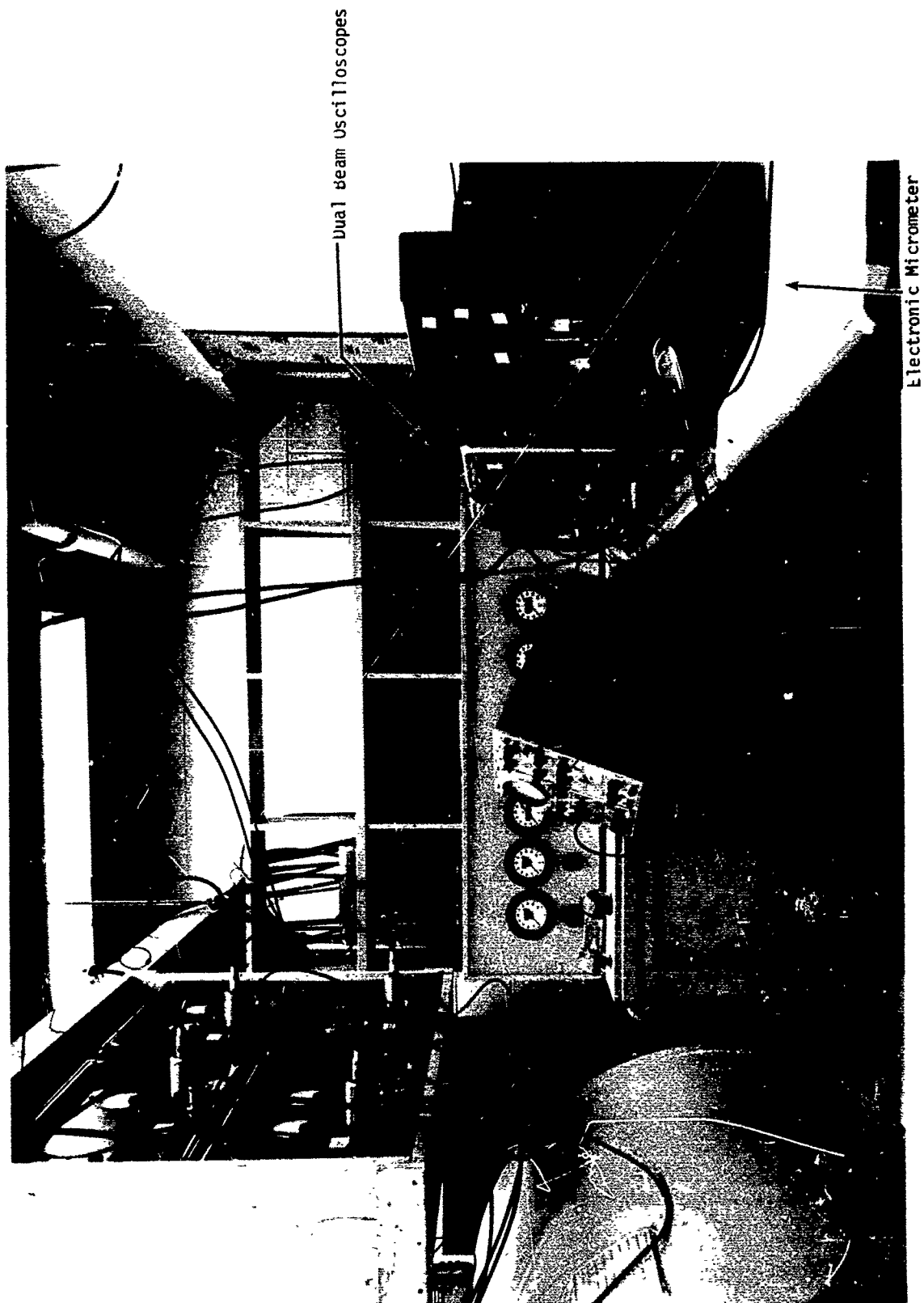
Figure 16. Instrumentation of Test Rig
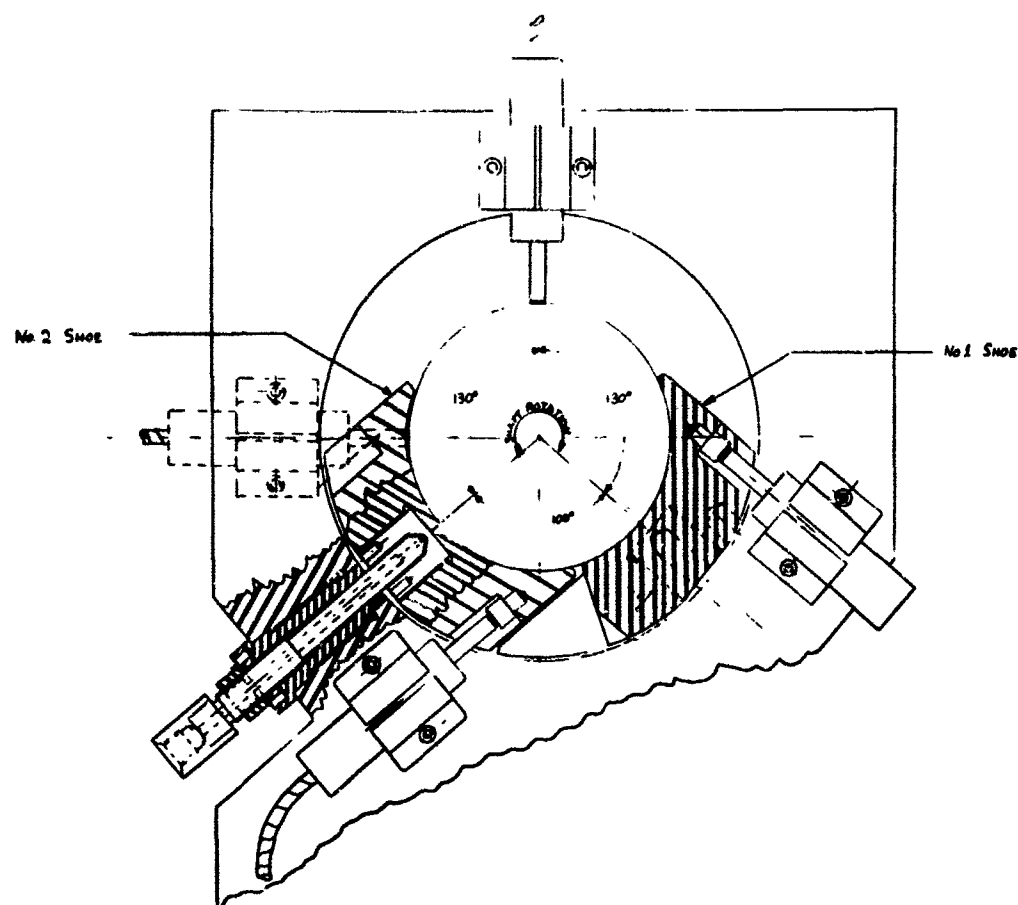
SHOE CONFIGURATION NO. 1   SHOE CONFIGURATION NO. 2

Figure 17. Test Bearing Configuration
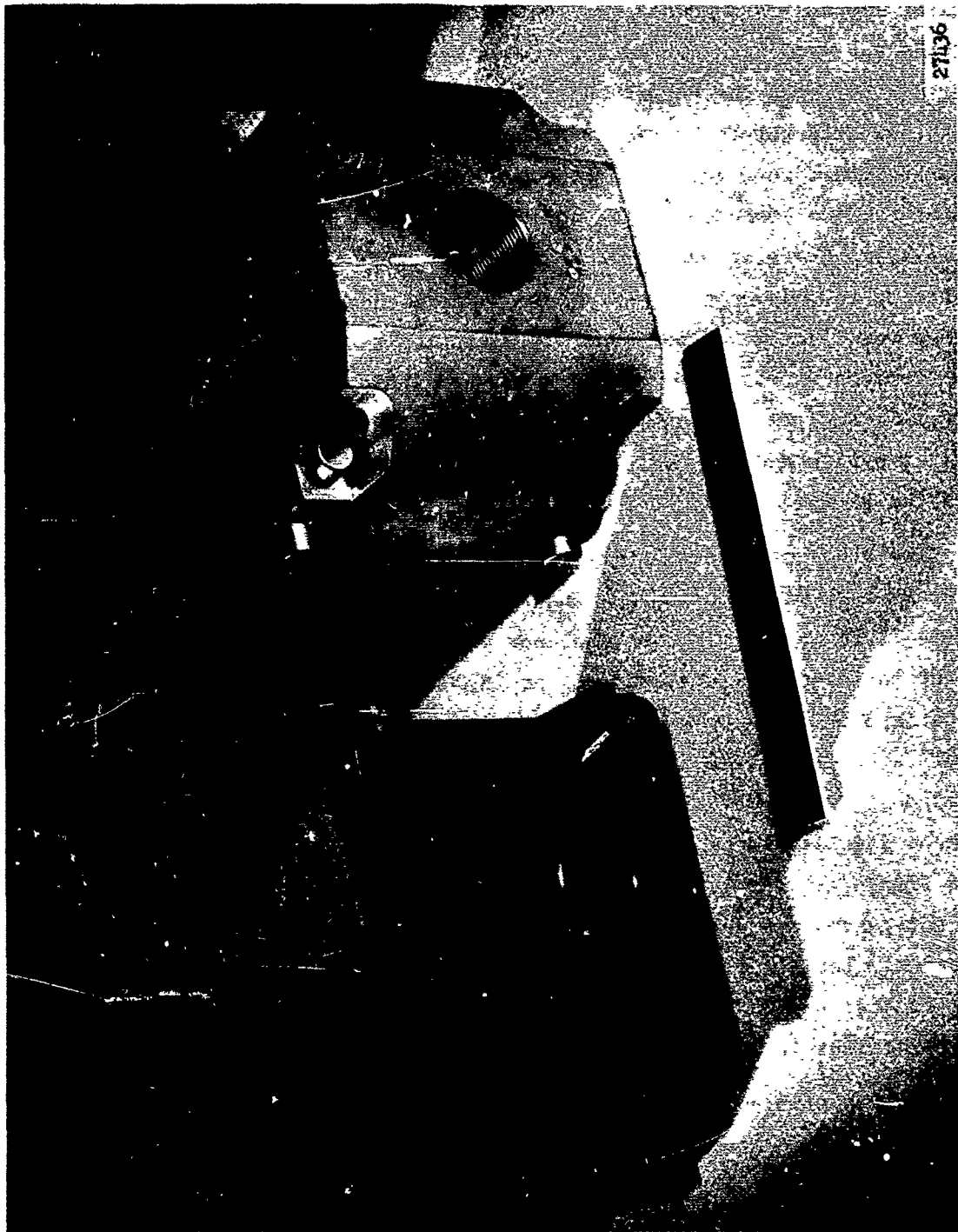
Figure 18. Light and Heavy Pads

horizontal altitude was such that diverging films occurred on the pad
leading edges. This caused rubbing contact to occur between the shoes
and the runner, which caused friction-induced whirl and increased journal
bearing orbits at the thrust end. To alleviate this situation a new com-
pliant surface thrust bearing was constructed. The bearing consists of
separate pads, each pad supported on a rubber mount. Deformations of the
rubber produce some equalizing action and tilting of each pad to form the
necessary converging wedge for hydrodynamic load capacity. The absence
of having to support the pads on pivots eliminated any tendency for pad hang-
up and very smooth and satisfactory operation resulted. Figure 19 shows
orbit traces at both journals with the original thrust bearing installed.
Figure 20 depicts traces with the compliant surfaces installed. The
smaller orbits and absence of sub-synchronous concepts are clearly evident
with the revised thrust bearing.

The other major difficulty occurred during testing to determine the
effects of varying unbalance. Unbalance response results are shown in
Figure 21 for a 0.0884 gram unbalance weight located at the turbine end
of the shaft on a 2-inch radius. At 18,000 rpm ($\Lambda = 3.5$) the unbalance
force is 5.59 lbs. Comparison of scope traces with those for the balanced
rotor for similar operating conditions, shows no apparent effects of the
unbalance. The unbalance weight was then increased to 0.4508 grams (5X)
with no significant effects apparent. (See Figure 22.) Also shown on
this figure are results for a gross unbalance of 1.56 grams. The speed
was not taken past 13,500 rpm, as dangerously high responses were in
evidence. The rotor was decelerated for shut-down. At 6,500 rpm excess
shoe flutter caused bearing contact. The unit did not seize but damage
was sufficient to warrant re-surfacing of the shaft and bearings.

A minor problem occurred during check-out of the rig with the light
shoes installed. Attempts to balance the shaft directly in the rig were
not successful. It was necessary to use a conventional machine to balance
the shaft. Balancing could be accomplished with the heavier shoes in-
stalled (which also had greater pivot friction). The significance is that
the lighter shoes appeared to respond much more sensitively to unbalance
than the heavier shoes.

30

WEST JOURNAL BEARING
TURBINE END

EAST JOURNAL BEARING
THRUST BEARING END
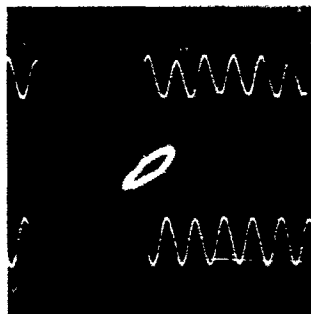
14,000 rpm
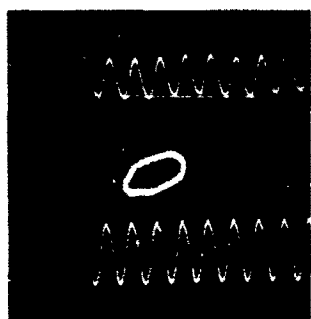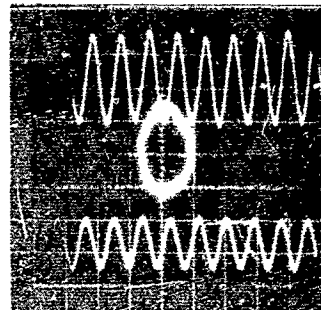
15,000 rpm
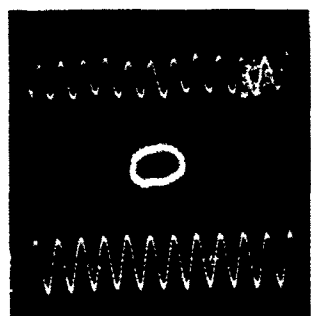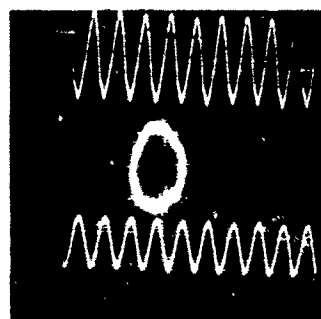
16,000 rpm
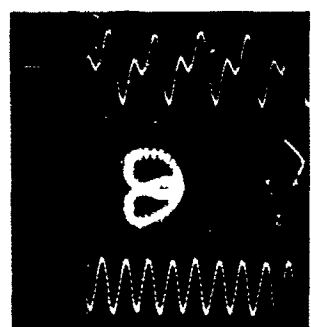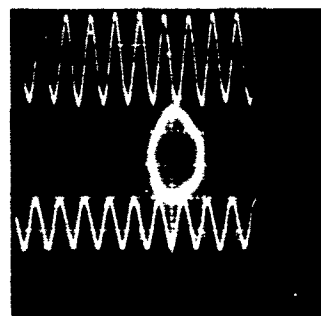
16,750 rpm
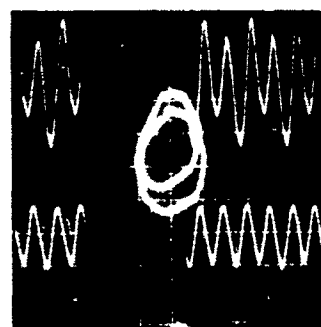
Figure 19. Checkout Runs with Pivoted Thrust Bearing.
Sensitivies are 100μ-in/cm and 5 m.sec/cm-
Full Load.

31

EAST JOURNAL BEARING
THRUST BEARING END
X-5 and Y-4

WEST JOURNAL BEARING
TURBINE END
X-1 and Y-2
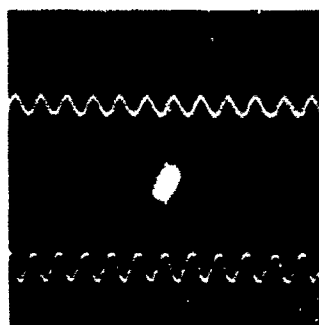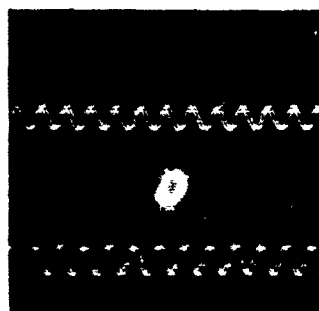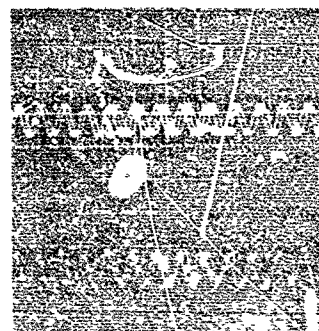
15,000 rpm

16,000 rpm

17,000 rpm

18,000 rpm
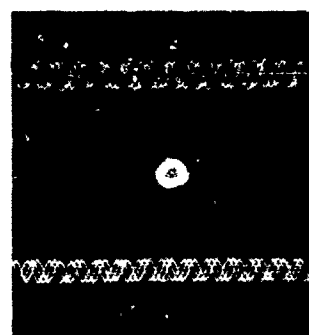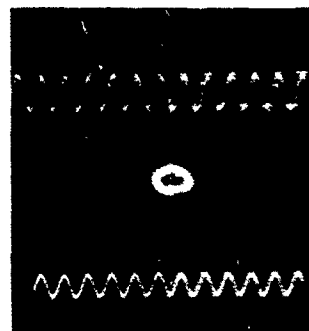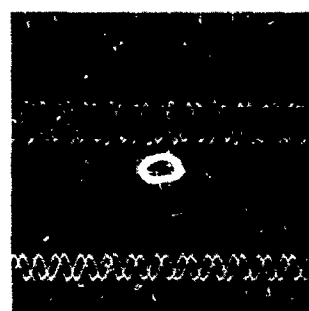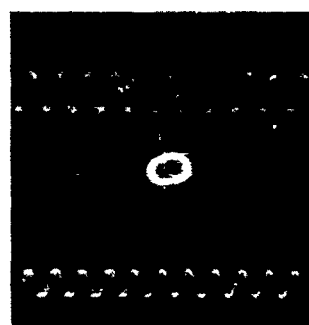
Figure 20. Checkout Runs with Compliant-Surface Thrust Bearing.
Sensitivies are 100μ-in/cm and 5 m.sec/cm-Full Load.

32

Shoe Pitch Motion
X1-D & Y2-A Probe
200 μ-in./cm
lm-sec/cm

Shaft Orbit
X5 & Y5 Probes
200 μ-in./cm
lm-sec/cm
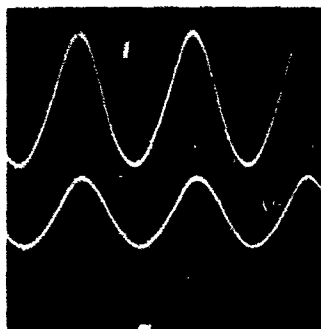
Shaft Weight = 85 lb.
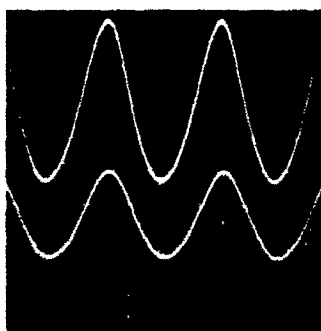
Shaft Weight = 56.7 lb.
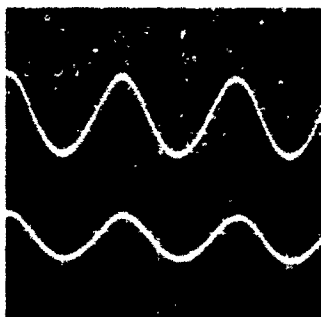
Shaft Weight = 28.4 lb.

Shaft Weight = 0 lb.
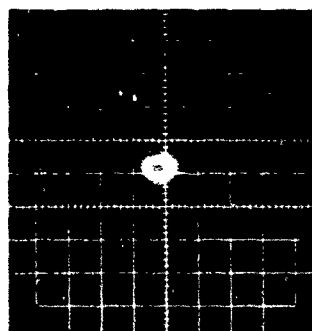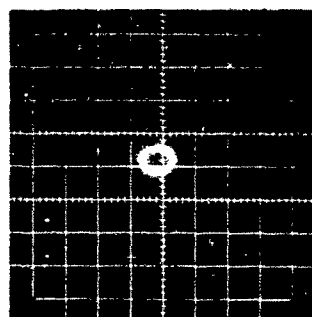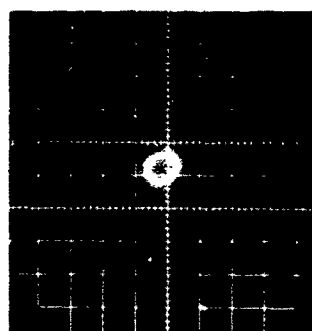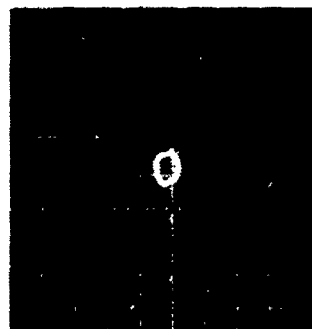
Figure 21.   Unbalance Response of Bearing No. 1 (West or Turbine End.)
Unbalance of 0.0884 Grams at Turbine End of Shaft.   Speed
is 18,000 rpm

33

Shoe Pitch Motion
X5-B & Y4-C
100 μ-in./cm
1m-sec/cm
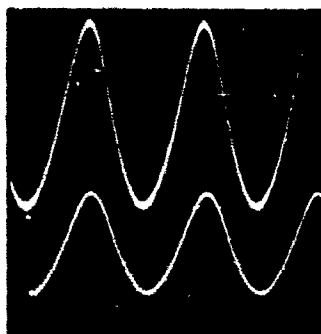
Shaft Orbit
X5 & Y4
100 μ-in./cm
1m-sec/cm

Speed = 18,000 RPM, Unbalance Weight = 0.4508 gm.

Speed = 13,000 RPM
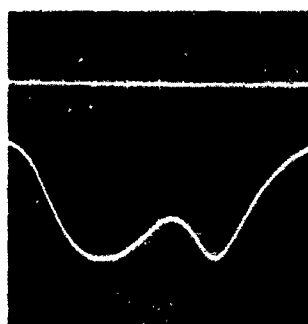
Speed = 6,500 RPM

Unbalance Weight = 1.5608

Figure 22.   Unbalance Response of Bearing No. 1 (West or Turbine
End.) Unbalance Weights of 0.4508 and 1.5608 Grams.

34

3.5 Steady-State Test Results

Steady-state verification testing was accomplished at atmospheric conditions ($\Lambda = 3.5$) with the heavier set of pads installed. Attempts at high Λ steady-state testing inside the evacuated environmental chamber with the heavy pads proved difficult and dangerous because of the inherent tendency to produce instabilities as loads on the bearings were reduced.

3.5.1 Comparison Between Theory and Experiment

Figure 23 shows the comparison between theory and test for a single pad steady-state load *vs*. pad film thickness. Test results on the full journal were converted to single pad results for convenience of comparing with theory, and it eliminates another variable, namely the spring pre-load. As indicated on Figure 23 comparative results agree very well with theoretical predictions and demonstrate the validity of the governing equations and methods of solution.

3.6 Dynamic Test Results

The most significant dynamic testing was accomplished with the light shoes at high Λ conditions, since this provides the best environment for pad instability. Dynamic testing with the heavy shoes at low Λ (3.5) was inconclusive.

Table 1 is a summary of the pertinent dynamic runs conducted with the light shoes. Variables included the bearing pre-load, ambient pressure and external load. Combined pre-load and external load was converted to that on a single fixed pad to facilitate comparisons between theory and experiment.

Figure 24 shows oscilloscope orbit traces of the two bearings at 18,000 rpm at atmospheric pressure ($\Lambda = 3.5$). The orbit size for the thrust end journal is approximately twice that of the turbine end journal. The conical orbit, which was characteristic for the light pad installation, could be due to slight residual unbalance or possibly influence of the thrust bearing.

35
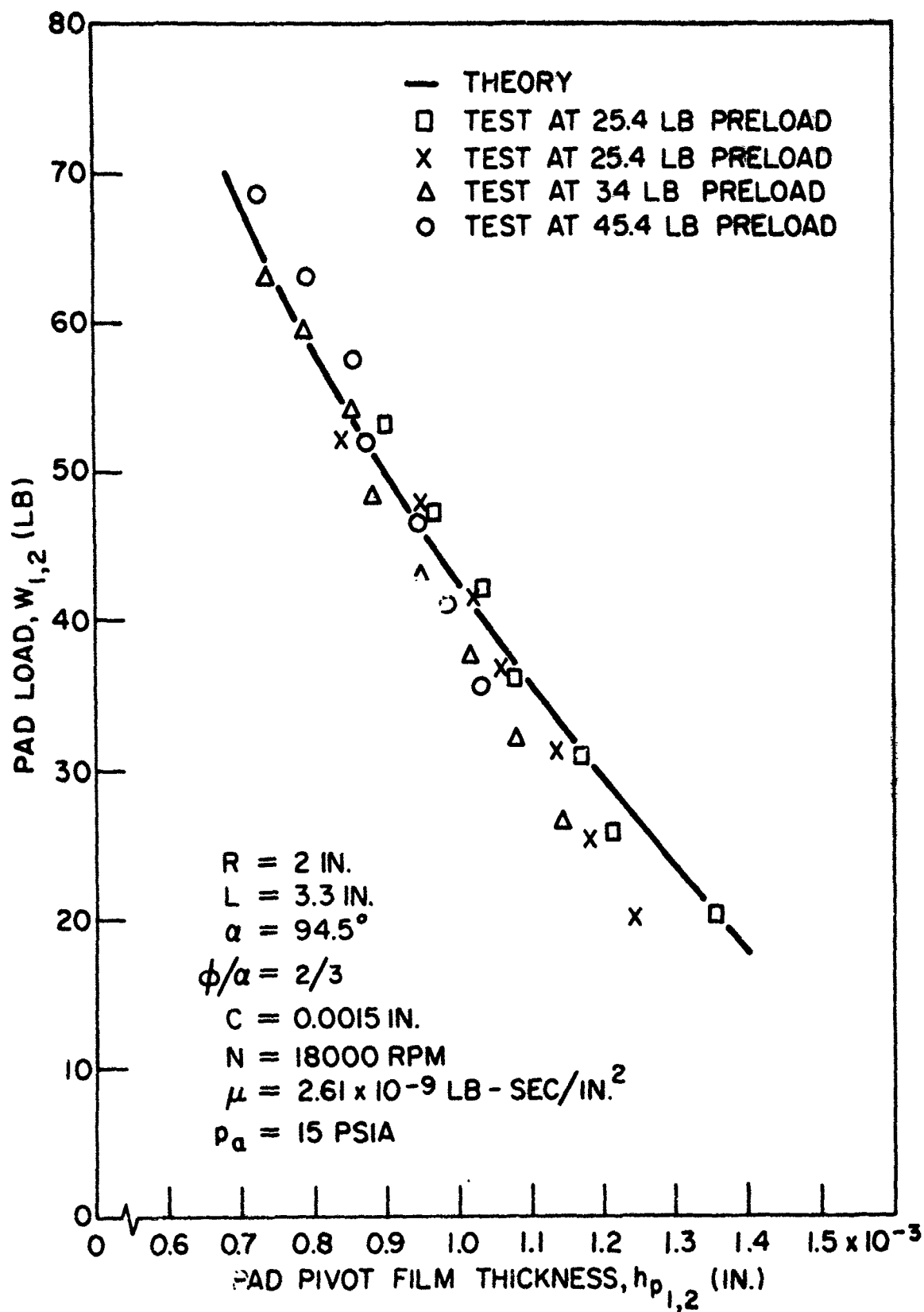
Figure 23. Comparison of Theory and Test for Steady-State Pad Load vs. Pivot Film Thickness.

TABLE 1

Summary of Results of Dynamic Testing of Light Pad Bearings

Shaft speed = 18,000 rpm

$\mu = 2.61 \times 10^{-9}$ lb.-sec./in.^{2}

Shaft diameter = 4 inches

C = 0.0015 inch

Pad size = 94.5 degrees, 3.3 inches long

Pad weight = 2.2 lbs.

Shaft weight = 92.5 lbs.

Pad Inertia = 0.0135 lb.-sec.^{2}-in.

Test No.	Pre-Load	Ambient Pressure psia	Foil Load lbs.	Pad Load lbs.	Λ	Remarks
1	22.2	15.0	0	53.2	3.5	
2			20	42.2		
3			30	36.7		
4			40	31.2		
5			45	28.5		Threshold between 45 - 50 lbs. foil load. Pad load ≃ 27 lbs.
6		12.0	0	53.2	4.37	
7			10	47.7		
8			20	42.2		
9			30	36.7		
10			40	31.2		Threshold between 40 - 45 lbs. foil load. Pad load ≃ 30 lbs.
11		8.75	0	53.2	6.0	
12			≃10	47.7		Threshold
13		7.5	0	53.2	7.0	
14		6.25	0	53.2	8.4	Threshold at $P_a \simeq 6$ psia @ 53.2 pad load, rub occured.

TABLE 1
(Cont'd.)

Test No.	Pre-Load	Ambient Pressure psia	Foil Load lbs.	Pad Load lbs.	Δ	Remarks
15	36.5	15.0	0	64.4	3.5	
16			10	58.9		
17			25	50.6		
18			40	42.4		
19		11.75	0	64.4	4.47	
20		8.75			6.0	
21		7.5			7.0	Threshold
22	7.9	15.0	0	42.1	3.5	
23			10	36.6		
24			15	33.9		
25			20	31.1		
26		12.5	0	42.1	4.2	
27		10.0			5.25	Threshold @ ambient ≈ 9.5 psia.
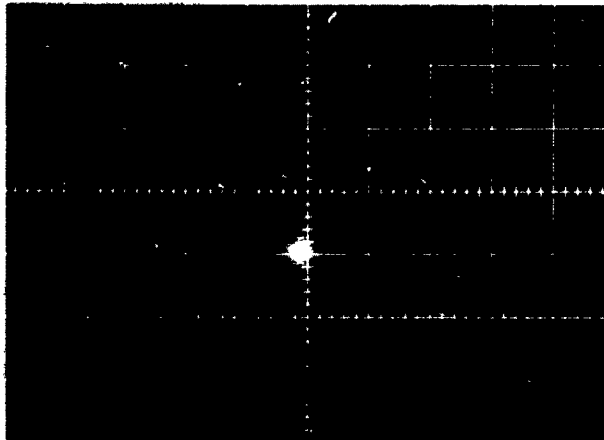
West Shaft Orbit
Turbine End
Sensitivity is 300 μ in./cm.
Orbit Size is ≃ 100 μ in.
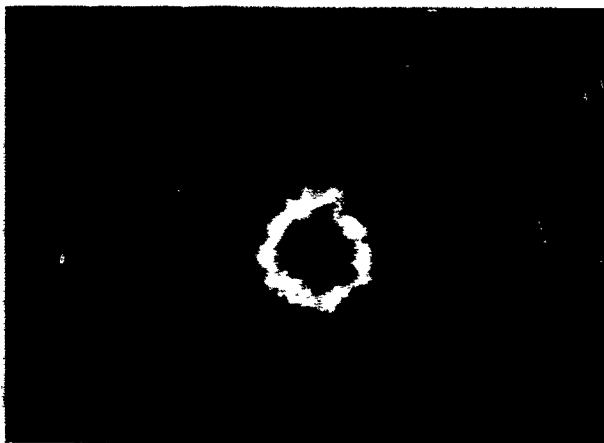
East Shaft Orbit
Thrust Bearing End
Sensitivity is 100 μ in./cm.
Orbit Size is ≃ 200 μ in.

Shaft Orbits at 18,000 RPM;

Ambient Pressure is 15 psia;

Bearing Pre-Load is 22.2 lbs., (c´/c = .92);

Pad Inertia is .0135 lb.-in.-sec.^{2}

Figure 24. Bearing Shaft Orbit, 18,000 rpm, 15 psia, 22.2 lbs
Preload

Figure 25 shows the effect of varying bearing load and pre-load on the thrust end bearing (higher orbit end). Vertical columns have constant pre-load in descending order left to right. Bearing load increases upward. In the first column a relatively heavy pre-load is applied (36.5 lbs.). The bearing showed no signs of distress until the bearing load was reduced to some 9 lbs. (not shown) when evidence of instability was detected. When the pre-load was reduced to 22.2 lbs., instability set in at a bearing load of approximately 13 lbs. A further reduction in pre-load to 7.9 lbs., resulted in an instability setting in at approximately 30 lbs. load.

Figure 26 shows the effects of variations in ambient pressure and pre-load. Bearing load was maintained at a constant value. Lowering the ambient pressure reduces the stable regime. It was not possible to obtain photographs of the instabilities for each situation because it occurs very suddenly. Increasing pre-load to a limit is beneficial, but if pre-load is excessive (overloaded bearing) instability again sets in.

Thus, summarizing it can be said that:

1. Instabilities set in very rapidly.

2. Increasing pre-load is usually beneficial.

3. Decreasing ambient pressure (increasing Λ) reduces stability.

3.6.1 Comparison Between Theory and Experiment

Figure 27 depicts stability threshold as a function of pad load coefficient and compressibility parameter Λ. Experimental points fall reasonably close to predicted values except at the high Λ condition, where the theoretical curve is conservative.

Reasons for variations between experiment and theory are as follows:

a. The analysis does not account for unbalance response. It only examines self-excited instabilities.

40
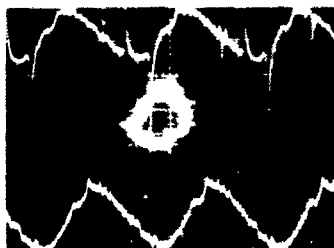
Bearing Load = 39.2 lbs.   Bearing Load = 32 lbs.   Bearing Load = 39.2 lbs.
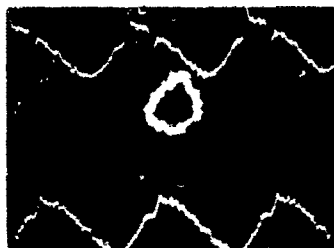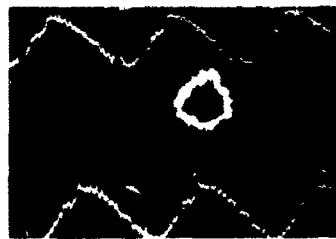
Bearing Load = 28.6 lbs.   Bearing Load = 25 lbs.   Bearing Load = 35.6 lbs.
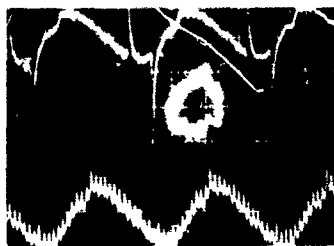
Bearing Load = 18.0 lbs.   Bearing Load = 18 lbs.   Bearing Load = 32.1 lbs.
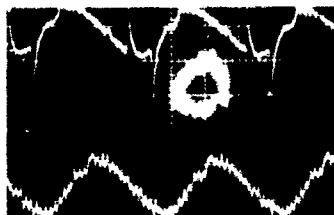
Bearing Load = 10.9 lbs.   Bearing Load = 14 lbs.
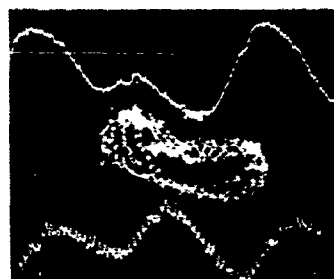
Bearing Pre-Load = 36.5 lbs. (c´/c = .75)   Bearing Pre-Load of 22.2 lbs., (c´/c = .92)

Bearing Pre-Load = 7.9 lbs. (c´/c = 1.2)

Figure 25.   Effects of Varying Load and Pre-Load, East Shaft Motion
(Thrust Bearing End), Shaft Speed is 18,000 rpm; Sensitivities
are 100μ in/cm and 1 m.sec/cm; Pad Inertia is 0.0135
lb-in-sec^2.

41

Ambient Pressure = 15 psia
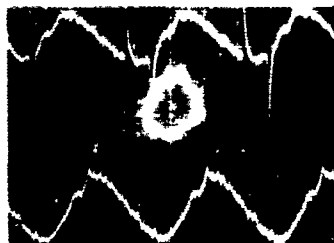
P_a = 15 psia
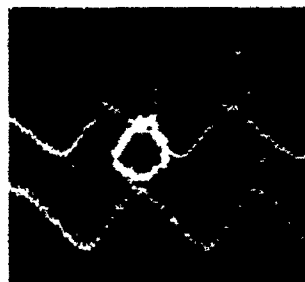
Ambient Pressure = 15 psia
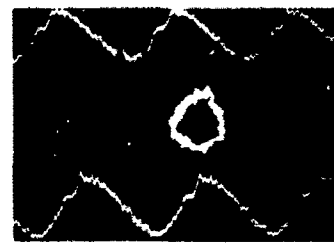
Ambient Pressure = 11.8 psia
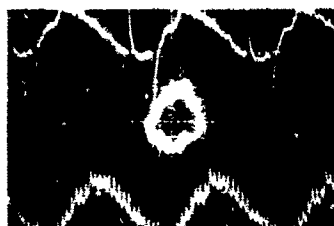
P_a = 12 psia

Ambient Pressure = 12.5 psia
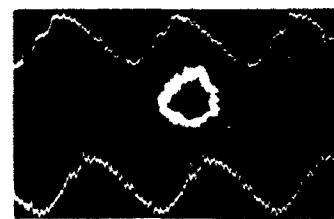
Ambient Pressure = 8.8 psia
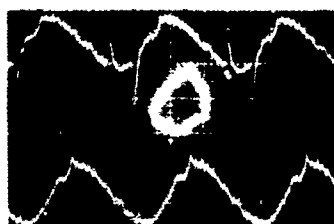
Ambient Pressure = 10 psia

P_a = 7.5 psia
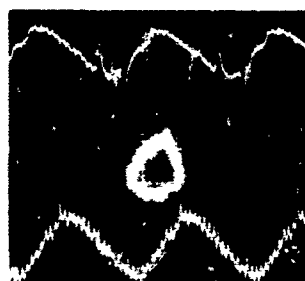
Ambient Pressure is 7.5 psia (Λ = 7)

Ambient Pressure is 9.5 psia, (Λ = 5.5)
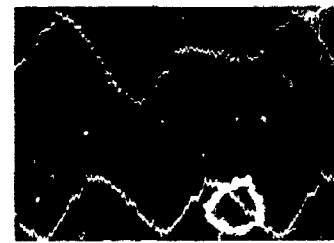
Bearing Pre-Load of 22.2 lbs.

Bearing Pre-Load = 36.5 lbs.

Bearing Pre-Load = 7.9 lbs.

Figure 26. Effects on Varying Ambient Pressure and Pre-Load, East Shaft Motion (Thrust Bearing End). Sensitivities are 100μ in/cm and 1 m.sec/cm; Shaft Speed is 18,000 rpm, Bearing Load is 46.25 lbs., Pad Inertia is 0.0135 lb-sec²-in.

42
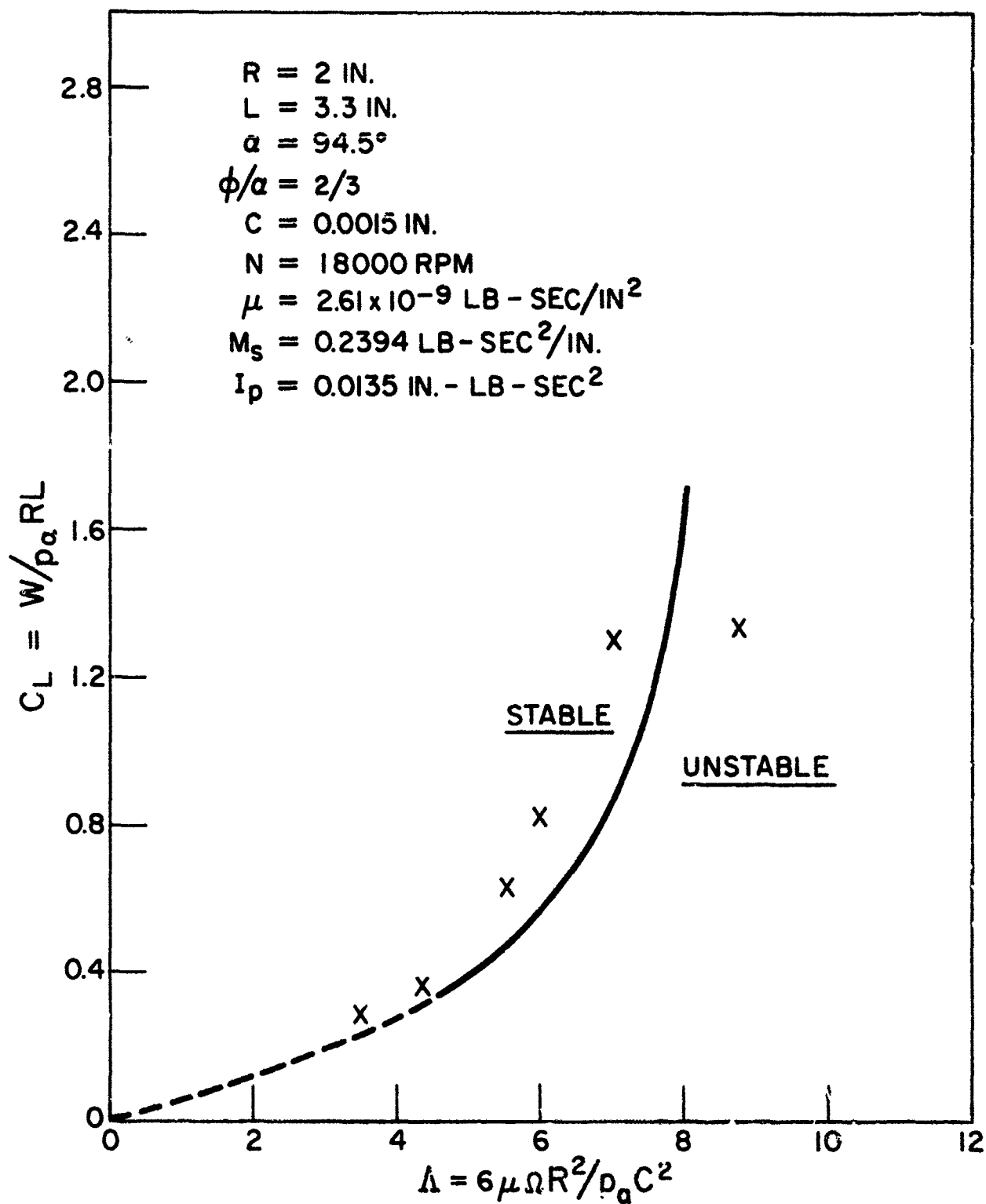
Figure 27. Verification of Theoretical Stability Threshold

b. The dynamic analysis is a small perturbation
   theory and cannot predict bounded orbits.

c. The effects of pivot friction are not accounted
   for.

d. In the test rig, pivot film thicknesses are not equal on all
   pads at zero applied load, as is assumed in the analysis.
   This is significant at high Λ where the analysis
   predicts that stability is sensitive to pivot
   film thickness. (See Appendix III).

44

4. DESIGN PROCEDURES

The intent of this section is to present general computational
methods for establishing geometrical and performance parameters using
the design information included in the appendices. A complete and
all-inclusive design guide was beyond the scope of the program, but
this report contains adequate design information and sufficient pro-
cedural discussion to enable designers, reasonably well versed in gas
bearing technology, to produce a successful design. In addition, a
practical design configuration which has had good success at FIRL is
suggested. The computations are divided into two major areas:
(a) establishing steady-state performance and (b) determining whether
the selected system is stable. Much of the material presented below
has been extracted from Reference 1 with some minor modifications and
extensions for off-design operation.

4.1 General Procedure for Establishing Steady-State Performance

1. Given: For any problem the following information is generally
   given.

   a. ambient pressure, p_a, psia
   b. shaft speed, N, rpm
   c. shaft diameter, D, in.
   d. maximum bearing load, W, lbs.
   e. lubricant viscosity, μ, lb.-sec./in.^{2}

2. Primary considerations for determining the
   length of the bearing are maximum load, startup
   and roll stability. At startup the bearing
   is only subjected to gravity load.

   $$\frac{W}{2RL} \leq 3 \text{ psi} \quad \text{for startup where W = start-up load on bearing}$$

45

$\dfrac{W}{2RL} \le 10$ psi for max loading when operating

A general rule of thumb is to limit L/D < 1.5
to prevent roll dynamic problems.

3. Initially investigate performance at a compress-
    ibility parameter $\Lambda = 1.5$, in order to optimize
    the design for minimum power loss (3). Establish
    machined in clearance C from:

$$C = \sqrt{\frac{6\mu\Omega}{p_a \Lambda}} \times R$$

4. Compute load coefficient C_{LT} for three shoe bearing.

$$C_{LT} = \frac{W}{p_a RL}$$

5. Enter the appropriate full bearing design chart in
    Appendix I at the computed value of C_{LT}. For vary-
    ing values of the pre-load factor C´/C tabulate the
    following:

    a. Bearing eccentricity ratio, $\varepsilon´$.

    b. Pivot film thicknesses H_{P1}, H_{P2} and H_{P3}. H_{P1}
        will always equal H_{P2} for the geometries con-
        sidered. When shaft displacement is between
        pads, H_{P1} and H_{P2} will be less than H_{P3}. When
        displacement is directly into pad 3, H_{P3} will
        be less than H_{P1} and H_{P2}.

    c. Proper interpretation of the curve requires
        the following procedure:

        1. The intersection of the value of C_{LT} with
            a selected C´/C curve establishes $\varepsilon´$.

        2. At the established $\varepsilon´$ go to the $H_{P1,2}$ and
            H_{P3} curves at the corresponding values of
            C´/C and read off the pivot film thicknesses
            from the right hand ordinate. Compute di-
            mensional pivot film thicknesses from:

            $h_{pi} = H_{pi} \times C$ i = 1, 2, 3.

46

6. Determine the non-dimensional minimum film thickness for each pad from the appropriate minimun film *vs.* pivot film thickness curve. Then dimensionalize by:

$$h_m = H_m \text{ X C.}$$

7. Determine the pad friction coefficient F for each pad from the appropriate F *vs.* H_p curve. The friction force for each pad F_{fi} is determined from:

$$F_{fi} = FP_a \text{ CL} \qquad i = 1, 2, 3$$

and the friction power loss in watts is determined from:

$$P_f = \frac{\Sigma F_{fi} \text{ X R}}{63,000} \text{ N X 746.}$$

8. From appropriate individual pad load coefficients *vs.* pivot film thickness curve establish pre-load on spring-loaded shoe:

$$W = C_L P_a \text{RL.} \quad (W = \text{load or preloaded pad})$$

9. From the above procedure major operating performance at the design condition is established. With regards to selection of the pre-load setting C′/C, there are a number of constraints that are applicable.

   a. C′/C is the ratio of the pivot circle clearance to the machined clearance of a pad. A small value implies tight film thickness with a consequently large power loss. A large value may unload the shoe excessively with possibilities of shoe vibration. Also, large values of C′/C can also cause a phenomenon known as leading edge lockup, where the leading edge of the shoe is forced into the rotating shaft. As a general rule:

      $$0.3 \leq C′/C \leq 0.8.$$

      In no instance should C′/C exceed unity.

   b. If the bearing design is to incorporate a spring-loaded shoe, then the pre-load factor C′/C is directly related to the spring pre-load. For a spring-loaded shoe C′/C equals the pivot film thickness H_{p3}. From this the load on the spring

47

loaded shoe can be determined. The spring design should be such that normal shoe displacements will cause negligible change in the spring pre-load, or C'/C, and the bearing will behave as predicted.

10. Other constraints are power loss and minimum film thickness. Maximum power loss is dependent upon the application, and allowable minimum film thickness depends upon the size, production accuracy, and dimensional changes caused by structural and thermal deformations. For shaft sizes 1/2 inch and less a suggested absolute minimum is 0.00025 in. and for shafts up to 1 inch a suggested minimum is 0.0005 in.

11. Once a design is selected, it is often desirable to determine off-design operation. The procedure varies depending upon whether the pad is spring loaded or whether the pivot circle is considered fixed (three fixed pads).

   a. Spring-loaded shoe - Over the shaft displacement range the spring pre-load variation is insignificant, and thus the load on the spring-loaded shoe is constant. A constant load implies a constant pivot film thickness H_{p3}, and off-design performance is obtained by following lines of constant H_{p3} on the appropriate full bearing load *vs.* eccentricity plots. The curves in Appendix I are segregated into fixed pivots on all three pads and one spring-loaded pad with two fixed pivoted pads. For most cryogenic applications a spring-loaded pad is recommended because of strong thermal and centrifugal growth.

   b. Fixed pads - If all pads are fixed, and thermal or centrifugal shaft growth will not change the original pivot circle relationship, then the pre-load varies and performance is obtained by following lines of constant C'/C on the proper fixed pivot performance curves.

4.2 Sample Problem - Steady-State Performance

As a sample problem the design of a typical bearing for a miniature cryogenic turbomachine will be described. The following information is given:

48

1. Shaft Diameter, $D = 0.5$ inches

2. Ambient pressure, $p_a = 15$ psia

3. Shaft speed, $N = 200,000$ RPM

4. Fluid temperature, $T = 100°K$

5. Bearing radial load, $W = 2.5$ lbs. (maximum, primarily due to unbalance loading)

6. Lubricant is gaseous nitrogen with viscosity, $\mu = 1.01 \times 10^{-9}$ lb.-sec./in.^{2}

   a. bearing length

   $$\frac{W}{2RL} \leq 10$$

   $$L_{min} = \frac{W}{20R} = \frac{2.5}{20\ (\frac{1}{4})} = 0.5 \text{ inches.}$$

   This length was used as the first approximation, and was found to be satisfactory in all respects.

   b. machined in clearance

   $$C = \sqrt{\frac{6\mu\Omega}{P_a \Lambda}} \times R$$

   $$C = 7.27 \times 10^{-4}\ \Lambda^{-1/2}$$

   To optimize the bearing for viscous power loss, $\Lambda = 1.5$. Dimensional inaccuracies, thermal growth of the shaft, etc. would result in reduction of the tip pad clearances, C; therefore, a $\Lambda = 3.5$ was also considered to provide performance estimates over the possible clearance range.

Λ	C
1.5	5.937×10^{-4} in.
3.5	3.887×10^{-4} in.

   c. load coefficient

   $$C_{LT} = \frac{W}{P_a RL} = \frac{2.5}{15 \times 0.25 \times 0.5} = 1.333$$

   d. following the procedures of steps 5, 6, 7 of paragraph 4.1. Table 2 can be produced. The numbered columns are generated as described below:

49

TABLE 2

Tilting Pad Journal Bearing Performance

L = 0.5 in; D = 0.5 in.; N = 200,000 RPM; p_a = 15 psia; 1.01 x 10^{-9} lb-sec/in.²; α = 100°; β = 60°; φ/α 65; n = 3 shoes; W_t = 2.5 lb

C'/C	ε' (1)	$H_{p1,2}$ (2)	H_{p3} (3)	$F_{1,2}$ (4)	F_3 (5)	ΣF (6)	F_f x10³ (7)	M_f x10³ in.-lb (8)	P_f watts (9)	$h_{p1,2}$ x10⁴ in. (10)	h_{p3} x10⁴ in. (11)	h_{m3} x10⁴ in. (12)
Λ = 1.5; Load Directed Into Pivot; C - 5.937 x 10^{-4} in.												
.3	.575	.392	.12	1.1	1.7	3.9	4.34	4.34	10.2	2.33	0.71	0.59
.4	.625	.53	.15	.79	1.62	3.2	3.56	3.56	8.4	3.15	0.89	0.77
.5	.680	.667	.16	.64	1.595	2.87	3.20	3.20	7.5	3.96	0.95	0.80
.7	.76	.962	.17	.432	1.57	2.45	2.73	2.73	6.4	5.71	1.01	0.83
.8	.795	1.12	.172	---	---	---	---	---	---	---	---	---
Λ = 3.5 Load Directed Into Pivot; C = 3.887 x 10^{-4} in.												
.5	.567	.65	.115	1.45	4.95	7.85	5.72	5.72	13.4	2.53	.45	.35
.6	.615	.78	.130	1.25	4.70	7.20	5.25	5.25	12.3	3.03	.51	.43
.7	.650	.93	.150	1.05	4.40	6.50	4.73	4.73	11.1	3.62	.58	.51
.8	.682	1.08	.160	0.95	4.25	6.15	4.48	4.48	10.5	4.20	.62	.56
Λ = 1.5 Load Between Pivots; C = 5.937 x 10^{-4} in.												
.2	.820	.12	.36	1.72	1.07	4.51	5.02	5.02	11.8	.71	2.14	.64
.3	.963	.155	.59	1.62	0.72	3.96	4.41	4.41	10.4	.92	3.50	.83
.5	1.27	.185	1.135	1.52	0.37	3.41	3.80	3.80	8.9	1.10	6.74	.95
Λ = 3.5 Load Between Pivots; C = 3.887 x 10^{-11} in.												
.2	.56	.145	.31	4.50	2.65	11.65	8.49	8.49	20.0	.564	1.205	.466
.3	.68	.20	.505	3.75	1.85	9.35	6.81	6.81	16.0	.777	1.963	.680
.5	1.04	.235	1.02	3.30	1.0	7.6	5.54	5.54	13.0	.91	3.96	.780

50

(1) From appropriate Figure of C_{LT} $vs.$ $\epsilon^{\prime}$ at intersection of C_{LT} and $C^{\prime}/C$ curve.

(2),(3) Maintain $\epsilon^{\prime}$ and read H_p from intersection of $\epsilon^{\prime}$ with $C^{\prime}/C$

(4),(5) From figure of friction power loss

(6) $\Sigma F = F_1 + F_2 + F_3 = 2F_1 + F_3$

(7) $F_f = \Sigma F \times P_a \, C \, L$

(8) $M_f = F_f \times R$

(9) $P_f = \dfrac{M_f \times N}{63,000} \times 746$

(10),(11) $h_p = H_p \times C$

(12) $h_m = H_m \times C$ where H_m from appropriate curve of H_m $vs.$ H_p

The minimum film thickness and power loss $vs.$ pre-load parameter are plotted on Figures 28 and 29. Note that the minimum film thickness approaches a limiting value for most cases considered, and an optimum value of $C^{\prime}/C$ is about 0.5, since it provides nearly maximum film thickness and reasonable power loss.

4.3 Sample Problem - Dynamics

Given, information of the type presented in Appendix III, the designer is now in a position to design both tilting pad bearings and rotors which will be stable over the desired operating range. All the important parameters such as speed, ambient pressure, viscosity, and shoe and shaft mass and inertia properties, as well as bearing dimensions such as bearing diameter, length, clearance, pivot location and pad arc, can be specified by the designer to assure a stable system. As an example, given a desired operating speed, ambient pressure and gas, the designer can calculate the required bearing dimensions and mass, and rotor properties that will result in a stable bearing-rotor system. On the other hand, if the designer has the bearing and rotor properties, he can establish the threshold of instability and, consequently, specify the upper speed limit above which the bearing-rotor system is unsatisfactory.
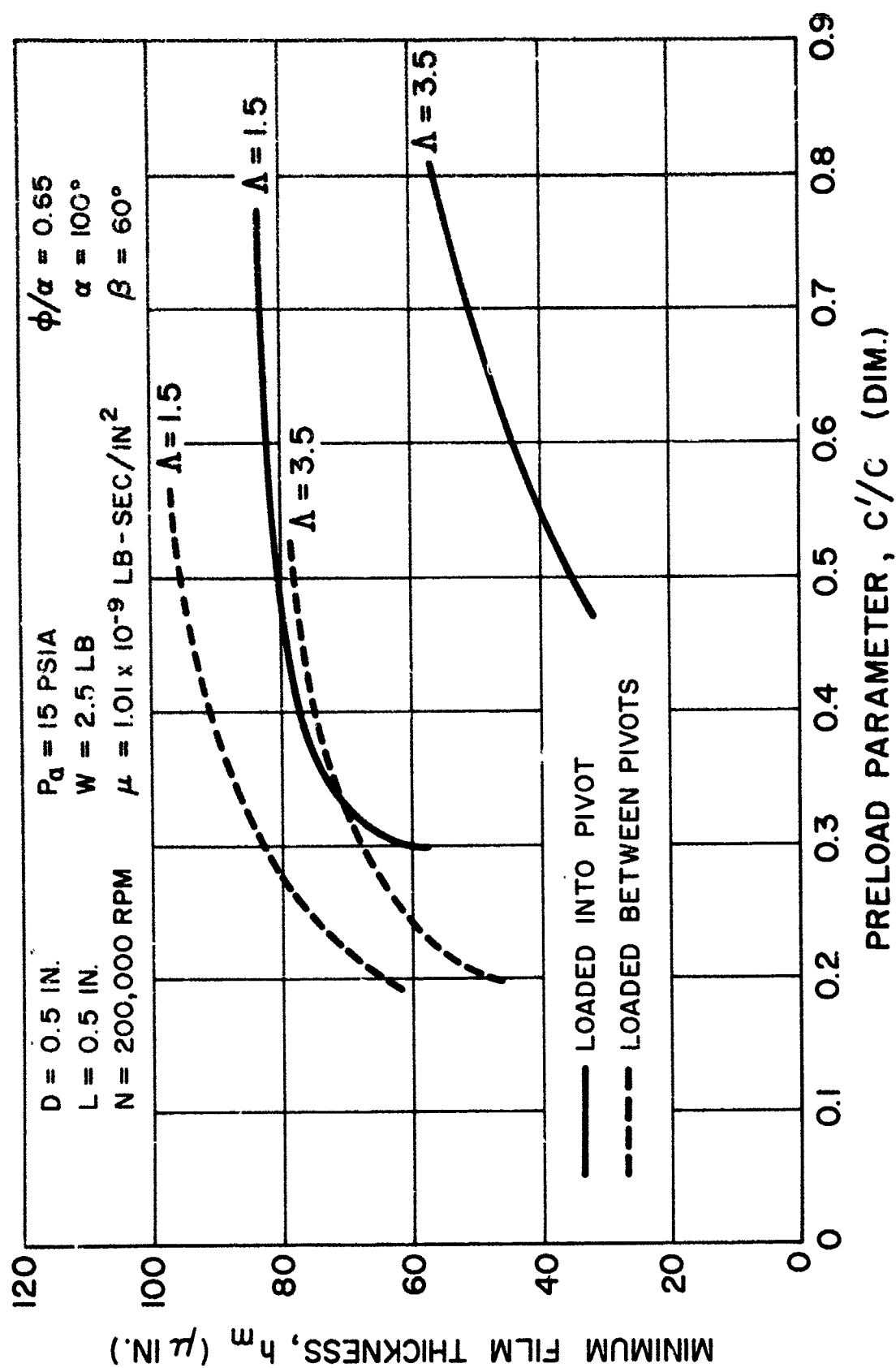
Figure 28. Minimum Film Thickness vs. Pre-Load Parameter at Design Conditions, Sample Problem
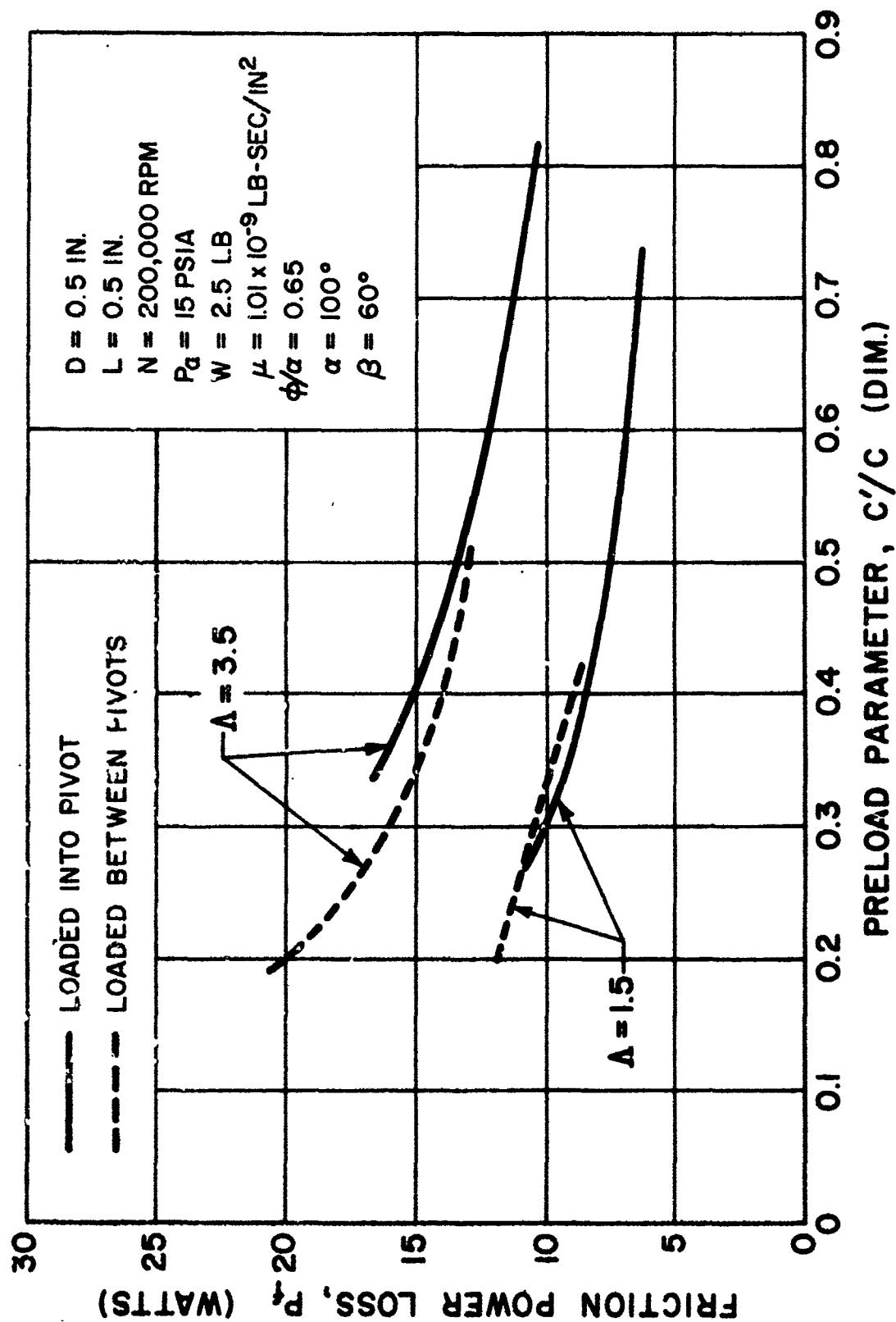
Figure 29. Friction Power Loss vs. Pre-Load Parameter at Design Conditions, Sample Problem

As an example, consider the typical cryogenic tilting-pad bearing-shaft combination design for which the steady-state analysis has been described. The pitch moment of inertia for a particular pad configuration was given as:

$$I_p = .0205 \times 10^{-4} \, \gamma \text{ lb.-sec.}^2\text{-in.}$$

where

$$\gamma = 0.283 \text{ lb./in.}^3 \text{ for steel}$$
$$= 0.162 \text{ lb./in.}^3 \text{ for titanium.}$$

The shaft mass is:

$$M_s = 1.2081 \times 10^{-3} \, \gamma \text{ lb.-sec.}^2/\text{in.}^4$$

Operating conditions for which it is required to determine stability are specified as:

N = 200,000 rpm

P_a = 15 psia

C = 0.0003887 in.

R = 0.25 in.

L = 0.50 in.

To enter the stability curves of Figures 30 and 31, it is necessary to compute the dimensionless mass parameter for the shaft, $\overline{M}_s$, and the dimensionless shoe inertia parameter, $\overline{I}_p$. These computations follow:

$$\overline{M}_s = \frac{M_s C \Omega^2}{4 p_a RL} = \frac{(1.2081 \times 10^{-3} \gamma)(.0003887)(\frac{2\pi}{60} 200,000)^2}{(4)(15)(0.25)(0.5)} = 0.2746 \times 10^2 \gamma$$

Inserting values for γ one obtains:

$\overline{M}_s$ = 7.77 for a steel shaft

$\overline{M}_s$ = 4.45 for a titanium shaft

and

$$\overline{I}_p = \frac{I_p C^2}{4 p_a R^3 L} = \frac{(.0205 \times 10^{-4} \gamma)(.0003887)(\frac{2\pi}{60} 2000,000)^2}{(4)(15)(.25)^3(.5)} = .738 \, \gamma$$

54

For steel shoes, $\gamma = .283$ lb./in.^{3} and

$$\overline{I}_p = .209$$

For titanium shoes, $\overline{I}_p = .120$

Figures 30 and 31 show the various combinations of shoe and shaft materials for operation at $\Lambda = 1.5$ and 3.5 respectively. The combination of the titanium pads and steel shaft provide stable performance at both values of Λ and should be the selected combination.

This sample problem describes one possible use of the dynamic stability design charts. Instead of material combinations, it would have been also possible to vary the inertia properties of the pads or the mass of the shaft.

The limitation of concentric operation may be circumvented by examining what occurs on a single pad rather than the entire bearing. For example, for a heavily loaded situation, the lightly loaded pad would have a high pivot-film thickness H_p, and its dynamic stability can be established by the corresponding H_p threshold curve. Similarly for the loaded pads. On Figure 30 the titanium pads steel shaft combination is stable for both high and low values of pivot film thickness, H_p, so that acceptable operation over a wide load range could be anticipated.

4.4 Practical Design Considerations

A useful design concept, which is a ramification and improvement of a design which has been successfully employed at FIRL is shown on Figure 32. It consists of a split housing to permit locking of the adjustable fixed pivot pins. The pivot pins themselves are accessible through ports in the outer housing sleeve. The spring mounted pivot is loaded through a beam type spring which can be pre-loaded a desired amount by adjusting screws and pre-load mount. The pivots are the ball and socket type with the socket diameter slightly larger than the pivot diameter. The pivots are located close to the face of the pad to: (1) keep pitch inertia low; (2) keep lock-up friction moment low; and (3) minimize camming during initial alignment.
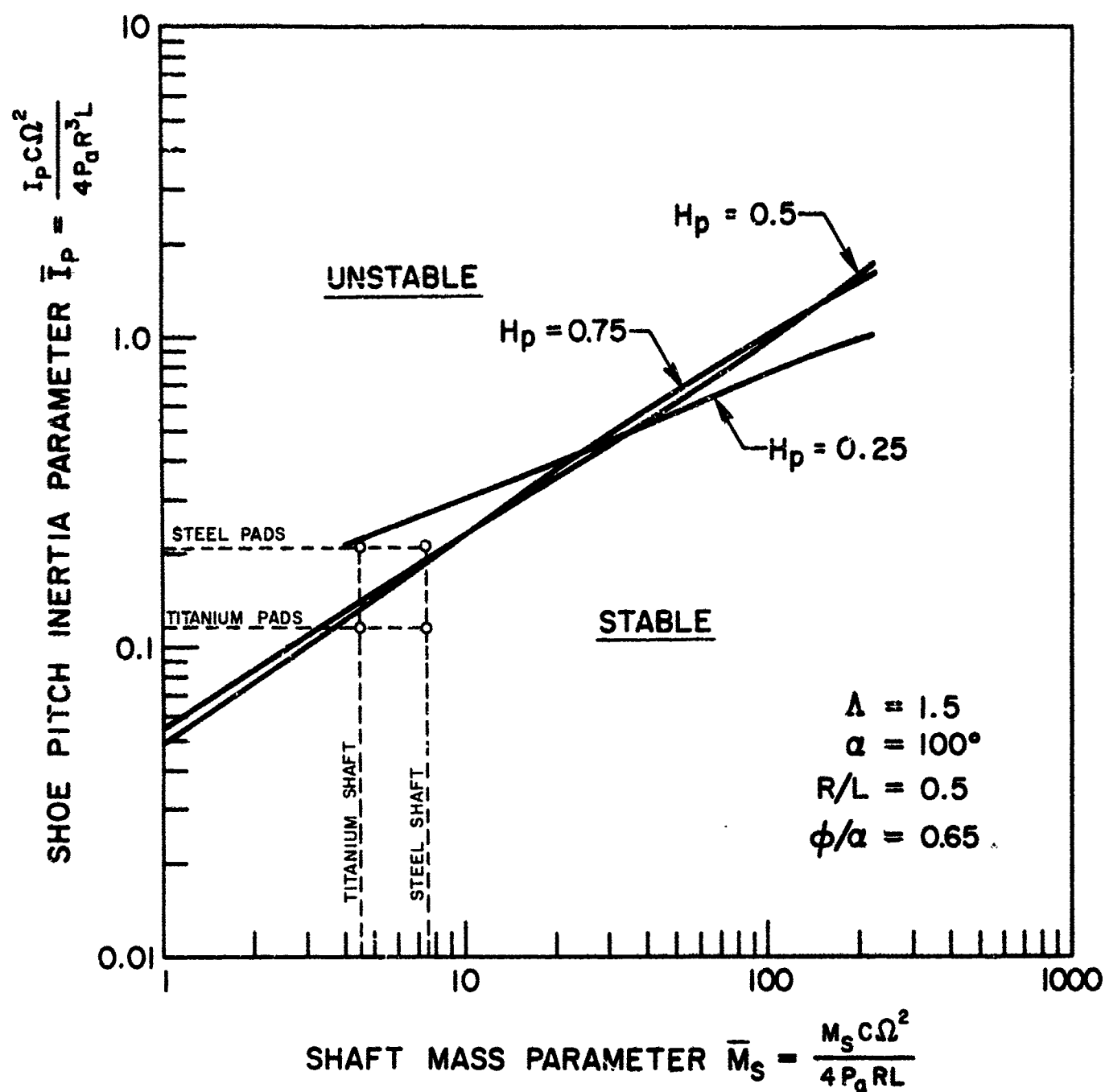
55

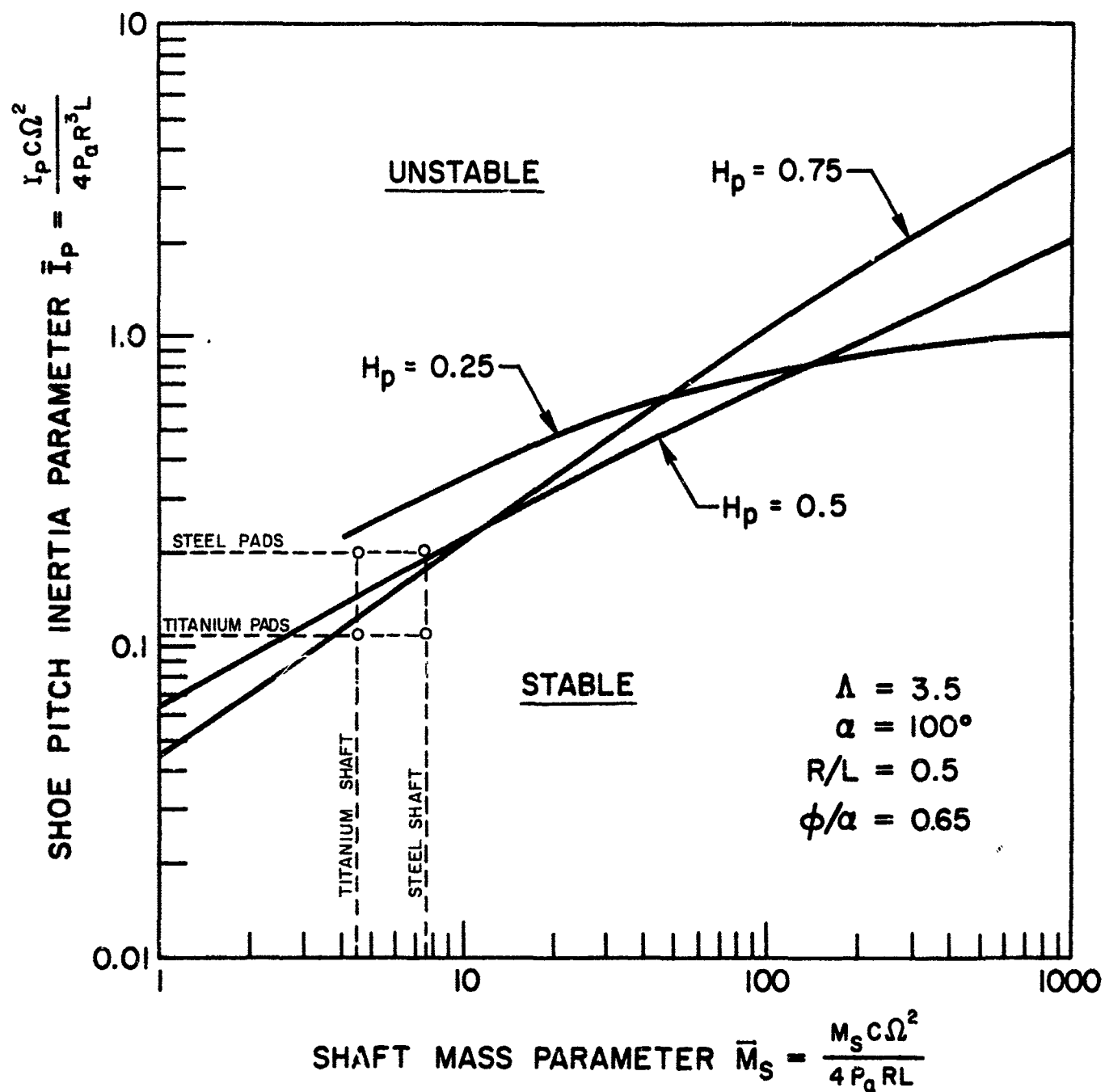Figure 30. Dynamic Stability Curve for Λ=1.5, Sample Problem

Figure 31. Dynamic Stability Curve for Λ=3.5, Sample Problem
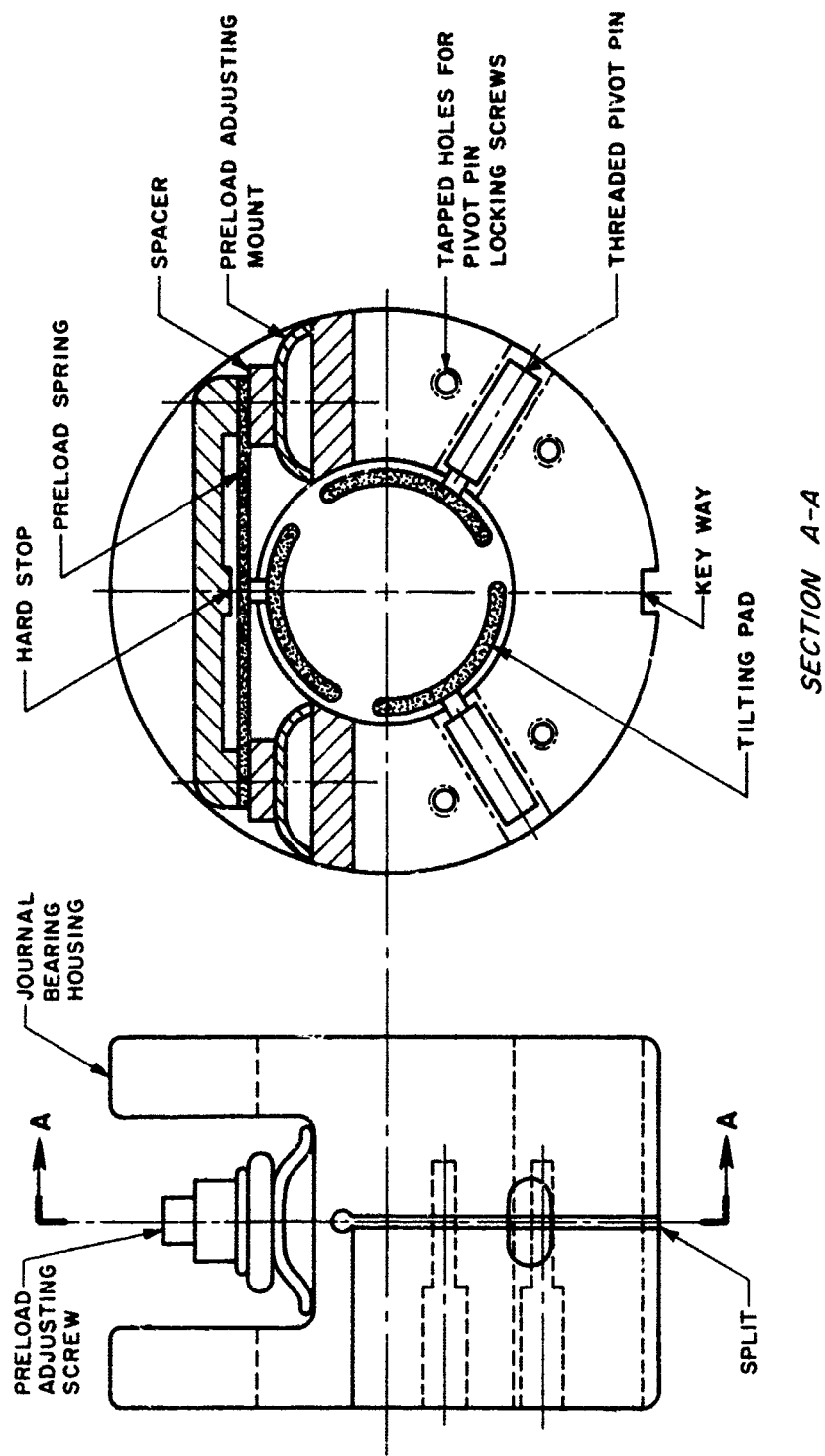
SECTION A-A

Figure 32. Journal Bearing Assembly

58

In general it is desirable to include the following capabilities in design:

a. Have a cartridge type assembly for ease of replacement.

b. Make pivots adjustable for flexibility in pivot clearance setting and to facilitate alignment of the thrust bearing.

c. Insure that pre-load of spring-mounted pivot is externally adjustable.

d. Keep pre-load spring soft so that pre-load
   · remains essentially constant and centrifugal and thermal growths can be readily accomodated.

Successful materials include tungsten carbide coated surfaces applied to 410 stainless steel base material against stainless or titanium shafts. It is also possible to coat the pads with aluminum oxide and mate with a journal coated with nickel chromium bonded chromium-carbide. A flame plated tungsten carbide journal against P692 carbon graphite pads is another possibility.

5. REFERENCES

1. "Selection and Performance of Gas-Lubricated Bearings for Miniature
   Cryogenic Turbomachinery", W. Shapiro, S. Heller, O. Decker, Technical
   Report AFFDL-TR-69-22, dated March 1969, for Air Force Flight Dynamics
   Laboratory, U. S. Air Force Systems Command, Wright-Patterson Air
   Force Base, Ohio.

2. "Stability Considerations for a Gas-Lubricated Tilting-Pad Journal
   Bearing, Part 1: Analytical Methods", T. Y. Chu, J. T. McCabe,
   H. G. Elrod, *Trans. ASME*, Journal of Lubrication Technology, Vol. 90,
   Series F, No. 1, January 1968, pp. 162 ·· 172.

3. "Research and Development of High-Performance Axial-Flow Turbomachinery,
   Volume 3: Des · of Back-up Gas Bearings", W. Shapiro, T. Y. Chu,
   J. T. McCabe, NASA Contractor Report NASA CR-802.

4. "Transient Dynamics of Tilting-Pad Gas Bearing System", V. Castelli,
   J. T. McCabe, *Trans. ASME*, Journal of Lubrication Technology, Vol.
   89, Series F, No. 4, October 1967, pp. 499 - 509.

5. "Analysis and Performance of the Gas-Lubricated Tilting-Pad Thrust
   Bearing", W. Shapiro, R. Colsher, *Trans. ASLE*, Vol. 12, No. 3,
   July 1969, pp. 206 - 215.

6. NOMENCLATURE

C   = machined clearance, in.

C'   = pivot circle clearance, in.

C'/C = preloaded factor

C_L = pad load coefficient $= W/P_a RL$

C_{LT} = bearing load coefficient $= W_t/P_a RL$

D   = diameter (shaft), in.

DT   = dimensionless time step

e'   = Shaft displacement, in.

F   = dimensionless friction $= F_f/p_a CL$

F_f = viscous friction force, els.

F_t = viscous friction force on shaft, lbs.

H   = dimensionless film thickness $= \dfrac{h}{c}$

H_M = dimensionless minimum film thickness $= h_m/C$

H_p = dimensionless pivot thickness $= h_p/C$

h   = film thickness, in.

h_m = minimum film thickness, in.

h_p = pivot film thickness, in.

I_p = pitch moment of inertia of shoe, lb-sec^2-in.

$\overline{I_p}$ = dimensionless pitch moment of inertia of shoe $= \dfrac{I_p C \Omega^2}{4p_a R^3 L}$

L   = bearing length, in.

M_f = dimensional viscous friction moment, in-lbs

M_S = shaft mass, lb-sec^2/in.

$\overline{M_S}$ = dimensionless shaft mass $= \dfrac{M_S C \Omega^2}{4p_a RL}$

N   = shaft speed, rpm

$\overline{n}$ = normal unit vector

p   = pressure, psia

p_a = ambient pressure, psia

P_f = total bearing power loss, watts

61

R = shaft radius, in.

s = length

T = temperature, °K

t = distance in length direction

t = time, seconds

$\bar{\bar{V}}$ = velocity vector

v = volume, in.^{3}

W ≈ bearing or pad load, lbs

α = pad angle, rad

β = angle from load vector to pivot, rad

γ = specific weight, lb/in.^{3}

ε' = bearing eccentricity ration = e'/C

ζ = mass density $\frac{\text{lb-sec}^2}{\text{in}^4}$

θ = circumferential distance, radians

Λ = compressibility parameter = $\frac{6\mu\Omega R^2}{P_a C^2}$

μ = lubricant viscosity, lb-sec/in.^{2}

φ = angle from leading edge of shoe to pivot

Ω = shaft angular speed rad/sec

APPENDIX I
STEADY-STATE ANALYSIS AND DESIGN CURVES FOR TILTING PAD JOURNAL BEARING

1. INTRODUCTION

The design charts for pivoted pad bearings (three pads) are included in this appendix. The charts have been developed for the following parameters:

Compressibility Number Λ	R/L
1.5	
3.5	0.25
5.0	0.50
10.0	1.0
20.0	

The pivot location $\phi/\alpha = 0.65$, and the angular extent of the pad $\alpha = 100°$, and the angular distance between pivots $2\beta = 120°$ are constant for all information shown.

For each combination the following design charts are included:

a) Bearing Load Coefficient, C_{LT} and Pivot Film Thickness, Hp vs. Bearing Eccentricity Ratio ϵ' with or without a spring loaded pad for load between pads

b) Same as a) for load into pad

c) Friction Coefficient, F vs. Pivot Film Thickness, H_p, for a single pad

d) Lift Coefficient, C_L, vs. Pivot Film Thickness, H_p, for a single pad

63

e) Minimum Film Thickness, H_M vs. Pivot Film Thickness, H_p for a single pad

2. PROCEDURE FOR GENERATING STEADY-STATE BEARING PERFORMANCE CURVES

The usual procedure for determining steady-state performance of a gas-lubricated tilting-pad journal bearing is to develop field maps for individual pads with the aid of a steady-state computer program. The pivot position is output, since it is the center of pressure and cannot be known until the pressure distribution is formulated. From these field maps, three pad bearing performance can be obtained.

For every combination of Λ and R/L, the generation of field plots require many data points and a considerable amount of computer time. In addition, since the optimum pivot location ϕ/α is 0.65, many of the field plot data points are extraneous, and unnecessary. Thus a new scheme was devised that was much more efficient in the production of pertinent steady-state data. Reference (4) describes an analysis for obtaining dynamic performance of a Tilting-Pad Bearing System. The method discretizes time into small finite elements. The process starts from a fixed shaft position and pivot position and an arbitrary pitch angle. Also it starts with an assumed pressure distribution on the pad. The sequence for obtaining steady-state data using the dynamics program is as follows:

1. Compute film thickness distribution of the pad which is strictly a function of the pivot clearance and pitch angle.

2. Integrate pressure to obtain pitch torque on the pad about the pivot position.

3. Integrate the pad dynamics equations through one time interval to obtain the pitch of the pad.

4. Solve Reynolds equation for new pressure distribution.

5. Repeat steps 1 through 4 until the pad has steadied and pitch angles and pressures do not vary through successive time intervals.

64

6. Print load capacity, pivot film thickness, minimum film thickness, pitch angle, friction coefficient.

By selecting proper values of pad inertia this process can converge very rapidly. Since the pivot position is known beforehand, this method obviates the necessity of producing field maps and obtains steady-state data very expeditiously. Using this technique, single pad performance information can be determined as a function of pivot clearance for a particular set of conditions, $(\Lambda, R/L, \phi, \alpha, \delta)$.

From the single pad information full bearing performance (three pads) can be readily computed. Figure 33 shows the bearing geometry. For the load direction between pads,

$$h_{p1} = h_{p2}$$

$$h_{p1} = C' - e' \cos\beta$$

$$H_{p1} = \frac{h_{p1}}{C} = \frac{C'}{C} [1 - \varepsilon' \cos\beta] \tag{1}$$

$$H_{p3} = \frac{C'}{C} [1 + \varepsilon'] \quad \text{for no spring} \tag{2a}$$

$$H_{p3} = \frac{C'}{C} \quad \text{for a soft spring (stiffness of} \tag{2b}$$
$$\text{spring} <<$$
$$\text{stiffness of bearing film}$$

Using the single pad load coefficient vs pivot clearance curve and eq. [1] and [2] the bearing load coefficient can be determined.

$$C_{L1} = C_{L2}$$

$$C_{LT} = 2 C_{L1} \cos\beta - C_{L3} \tag{3}$$

Note for the spring load pad C_{L3} is also obtained from the single pad information but it must also equal the spring force. Therefore, the spring is designed using C_{L3} as its load.

65
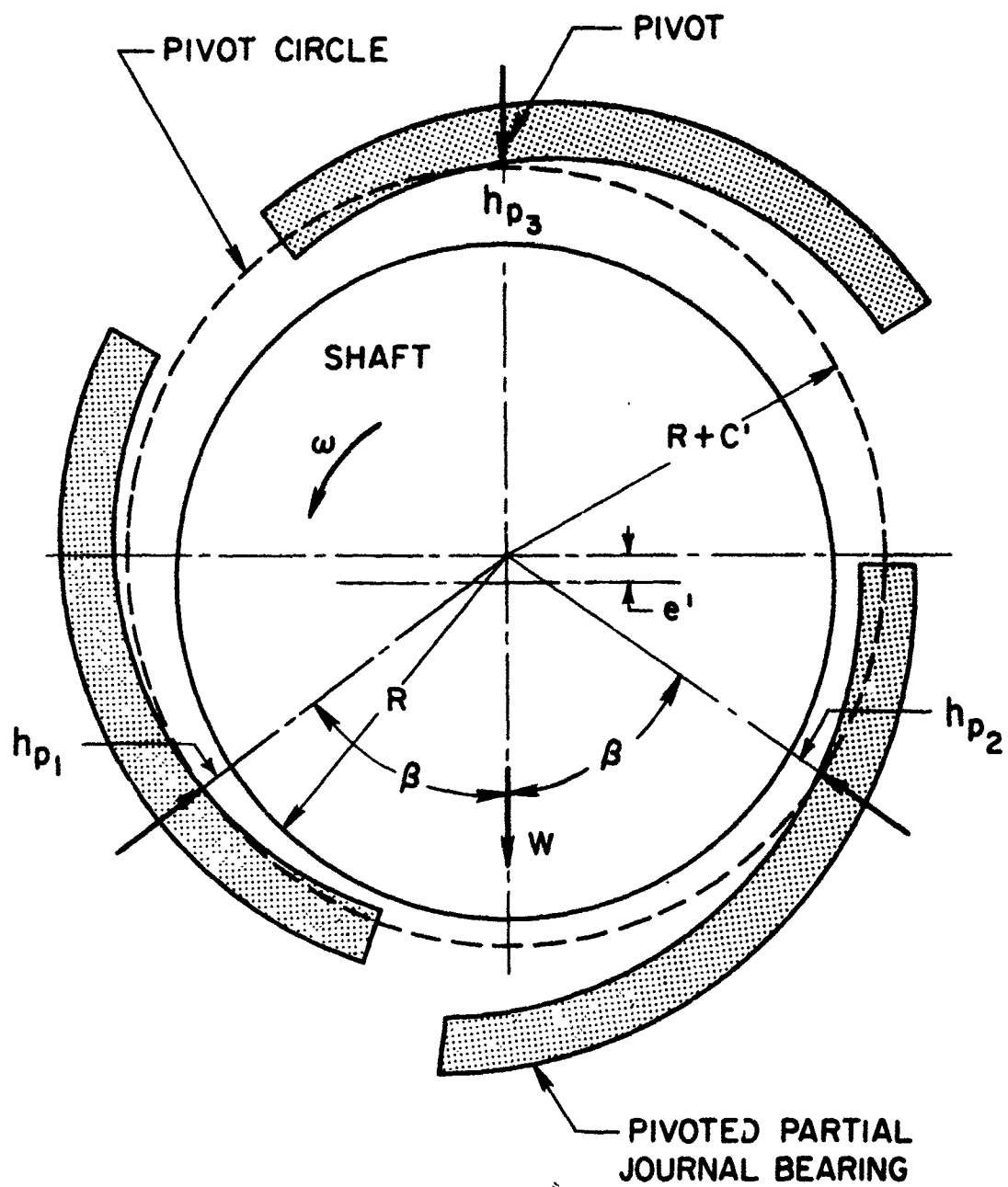
Figure 33. Schematic Representation of Pivoted-Pad Journal Bearing

For the load direction into pad number 3

$$h_{p1} = h_{p2}$$

$$h_{p1} = C' + e' \cos\beta$$

$$H_{p1} = \frac{h_{p1}}{C} = \frac{C'}{C} [1 + \varepsilon' \cos\beta] \qquad [4]$$

$$H_{p3} = \frac{C'}{C} \quad \text{for spring} \qquad [5a]$$

$$H_{p3} = \frac{C'}{C} [1 - \varepsilon'] \quad \text{for no spring} \qquad [5b]$$

Therefore

$$C_{LT} = C_{L3} - 2 C_{L1} \cos\beta \qquad [6]$$

Total friction coefficient (F_T) is

$$F_T = F_1 + F_2 + F_3 \qquad [7]$$

The minimum clearance for the bearing is

$$H_M = H_{M1} = H_{M2} \quad \text{for load between pads}$$

$$H_M = H_{M3} \qquad \text{for load direction at pad 3}$$

Therefore bearing performance can be obtained from the single pad information.

3. SINGLE PAD PERFORMANCE vs. PIVOT CLEARANCE
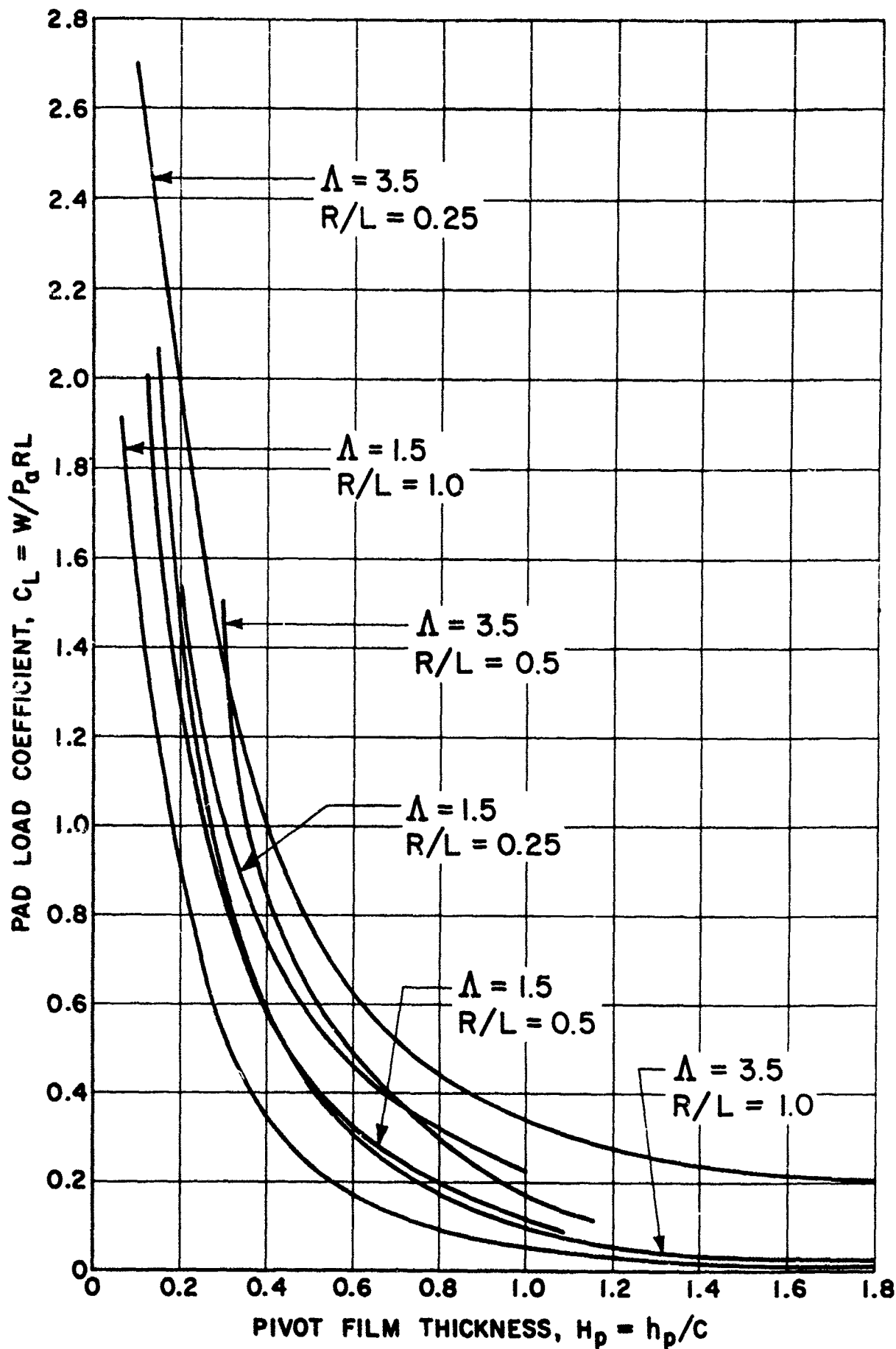
Figure 34. Single Pad Load Coefficient as a Function of Pivot Clearance, $\Lambda = 1.5$, 3.5
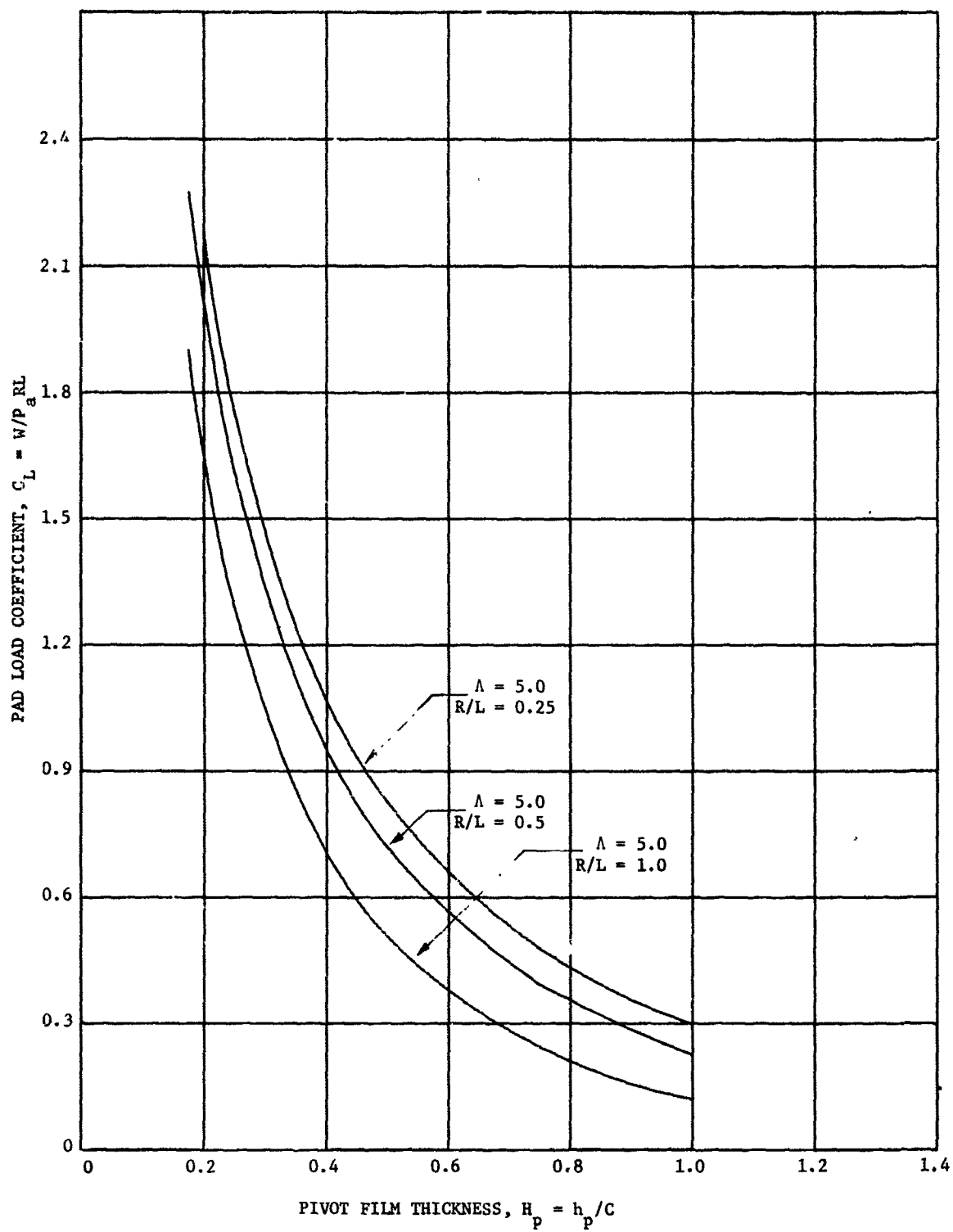
Figure 35. Single Pad Load Coefficient as a Function of Pivot Clearance,
            $\Lambda = 5$

70
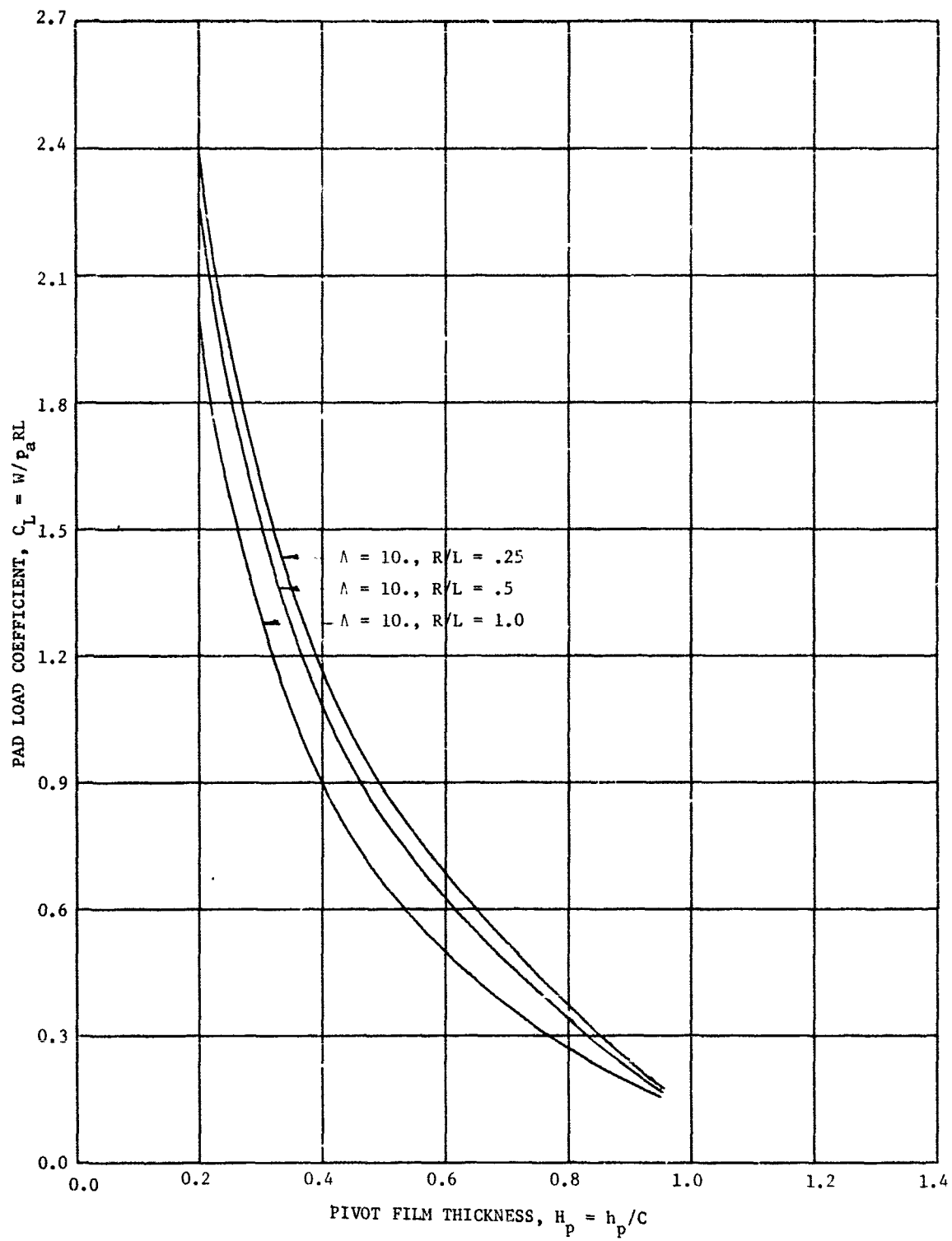
Figure 36. Single Pad Load Coefficient as a Function of Pivot Clearance, $\Lambda = 10$

71
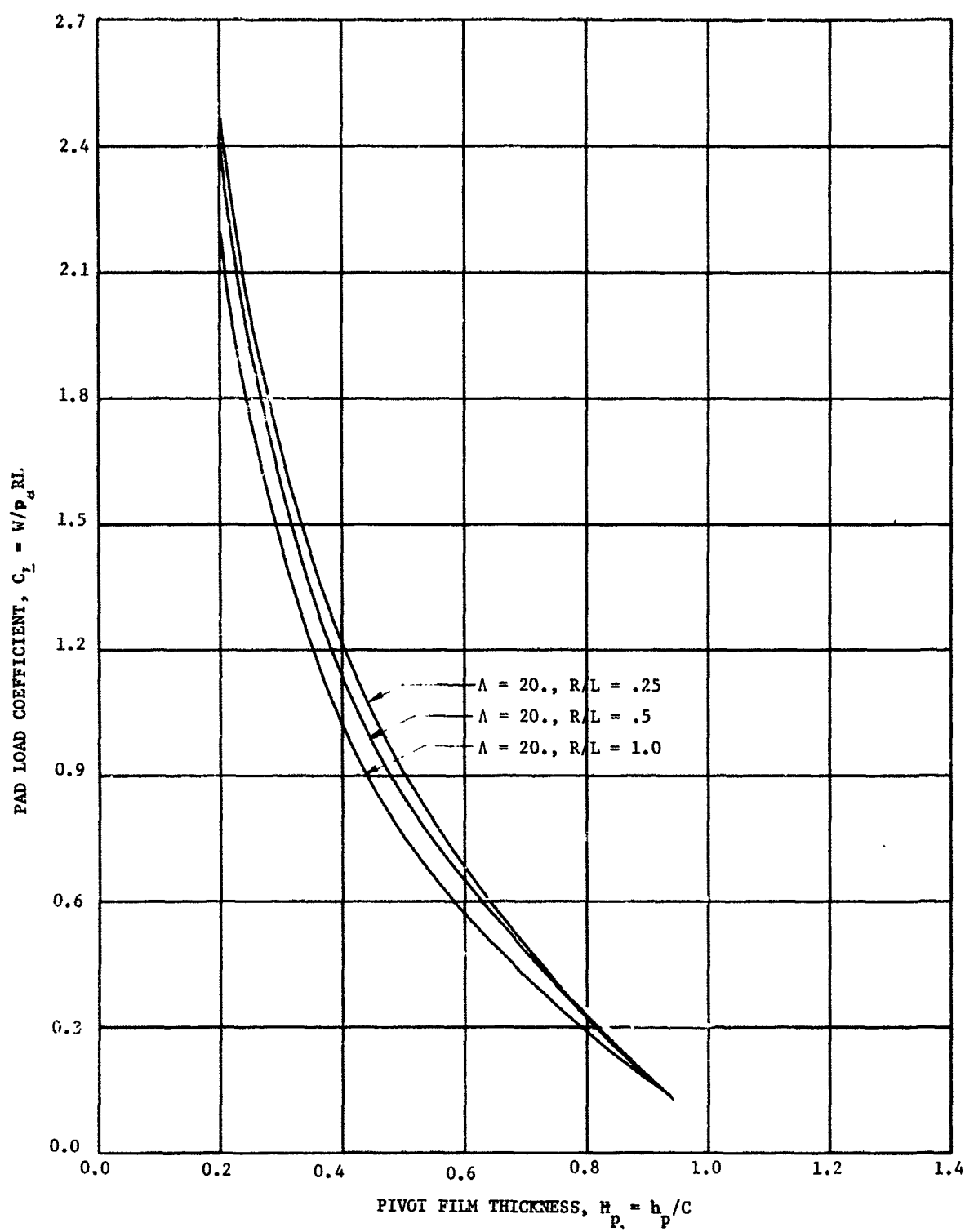
Figure 37. Single Pad Load Coefficient as a Function of Pivot Clearance, $\Lambda = 20$

72
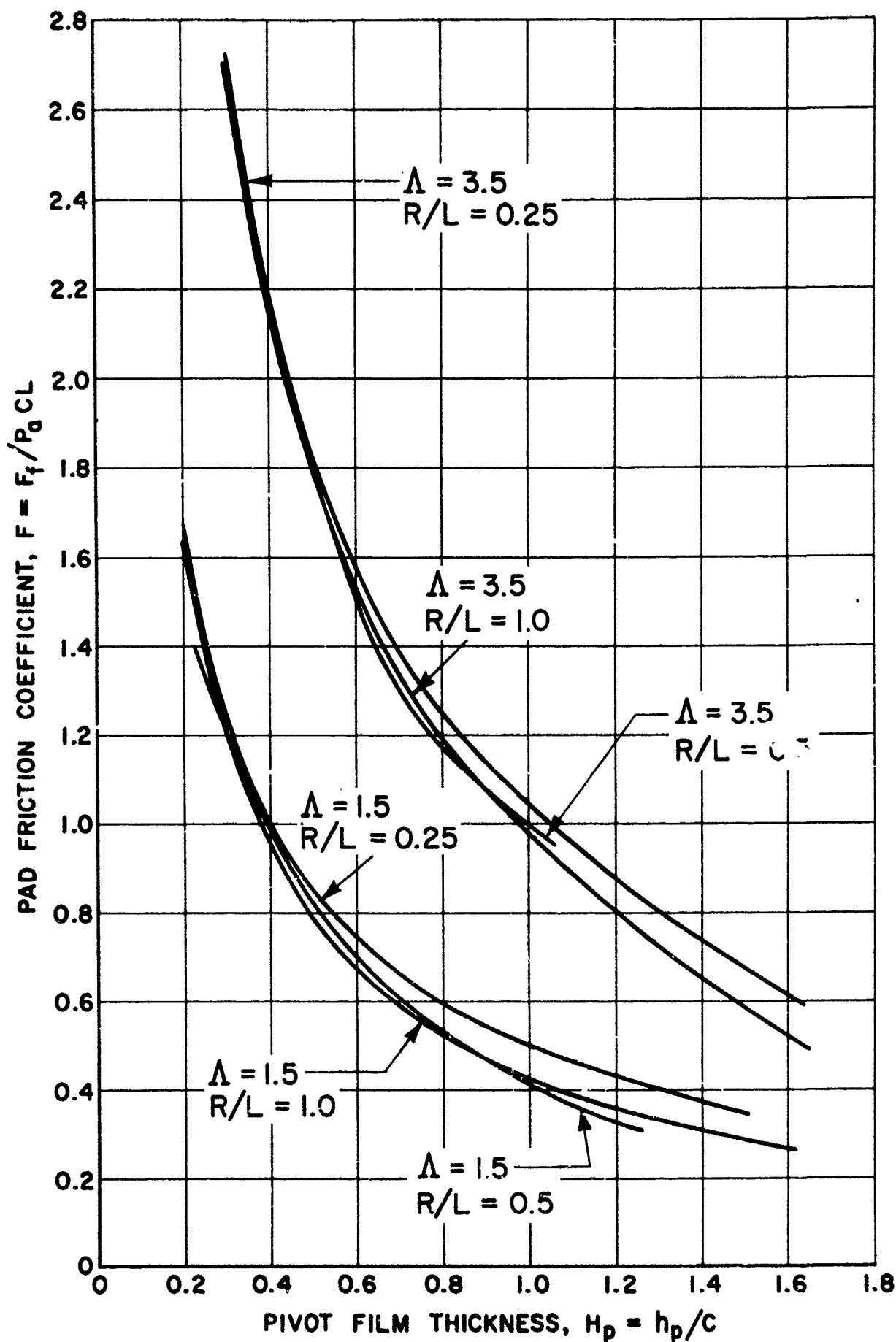
Figure 38. Single Pad Friction Coefficient as a Function of Pivot Clearance, Λ = 1.5, 3.5

73
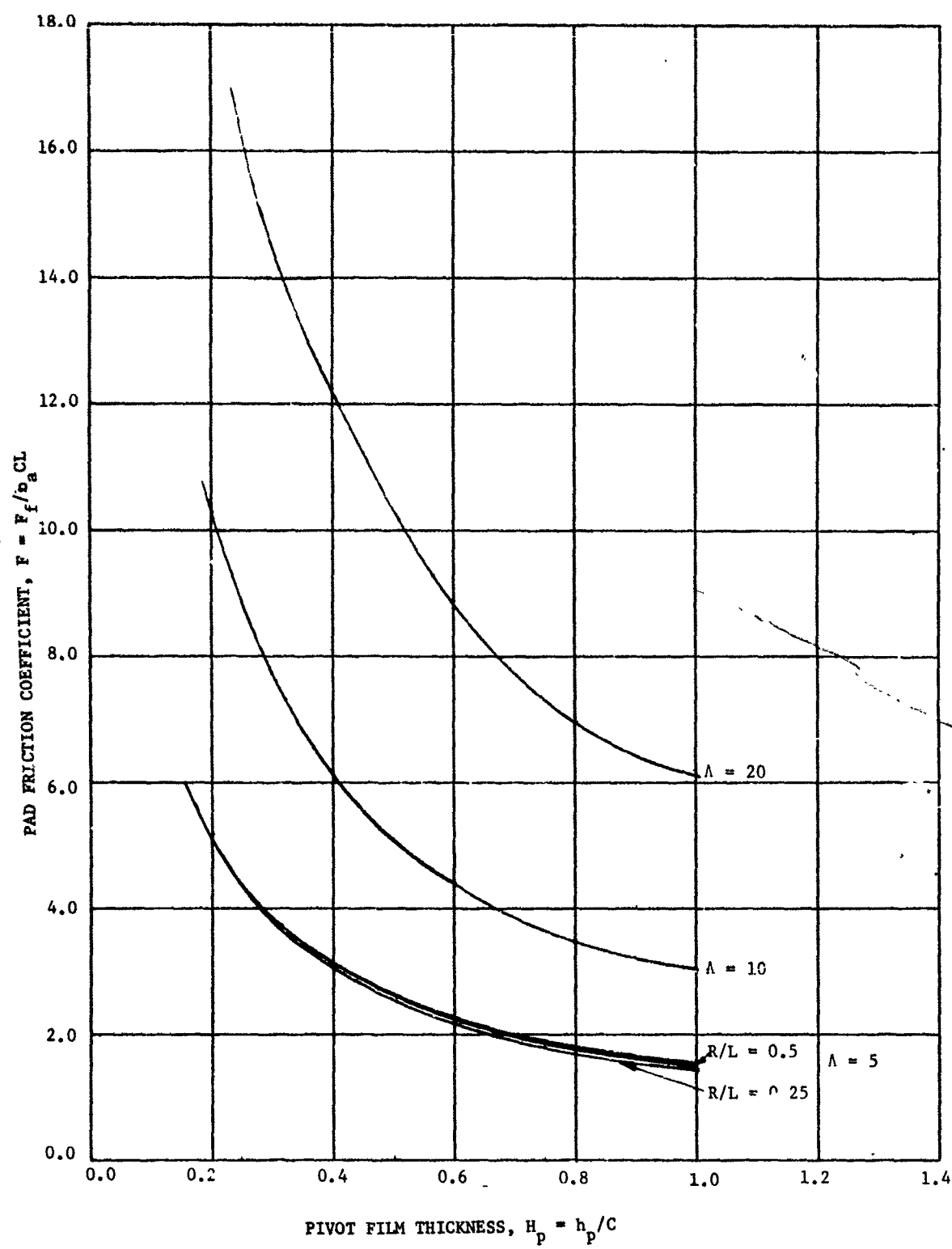
Figure 39. Single Pad Friction Coefficient as a Function of Pivot Clearance, $\Lambda = 5$, 10, 20

74
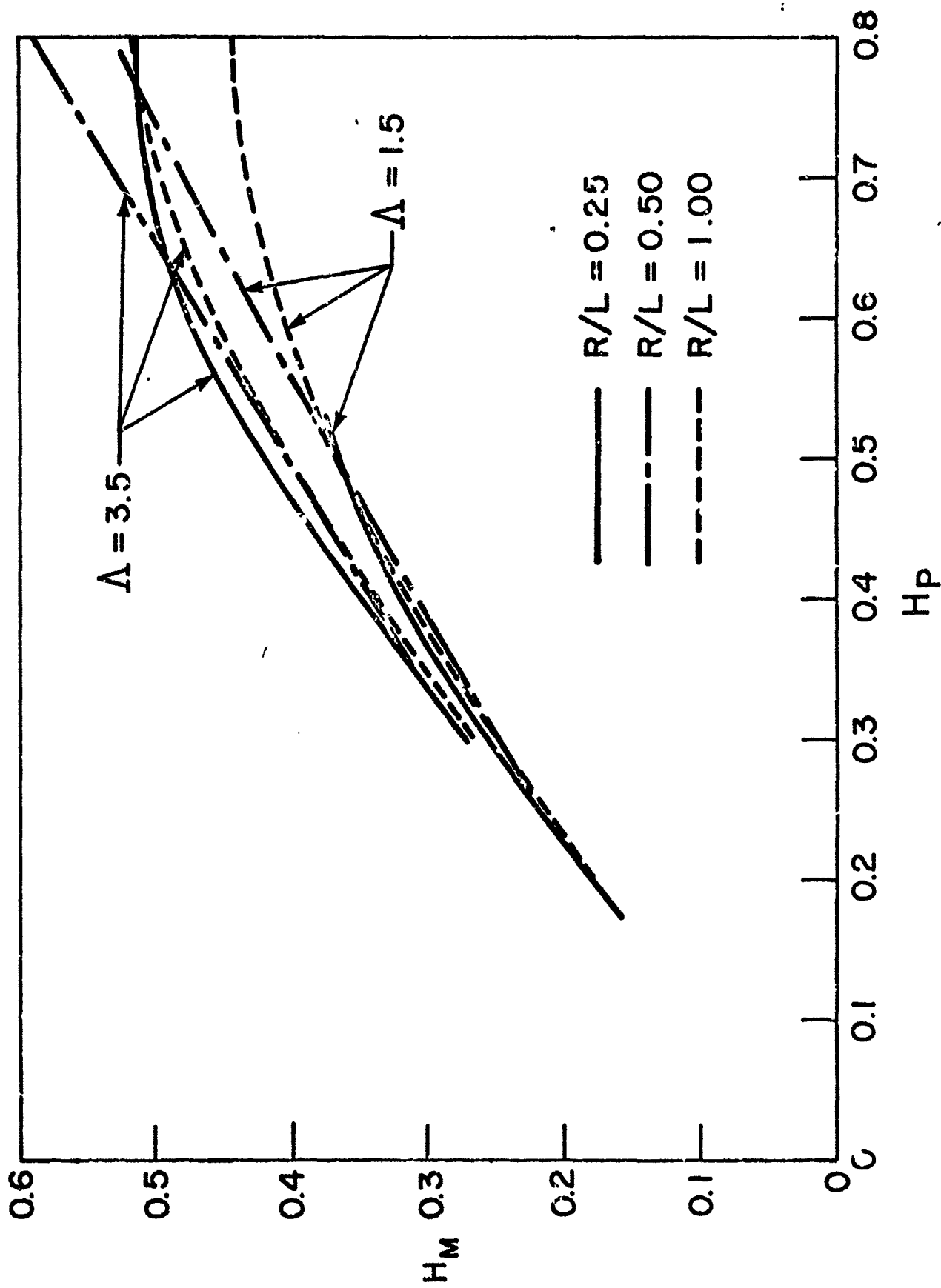
Figure 40. Single Pad Minimum Clearance as a Function of Pivot Clearance, Λ = 1.5, 3.5

75
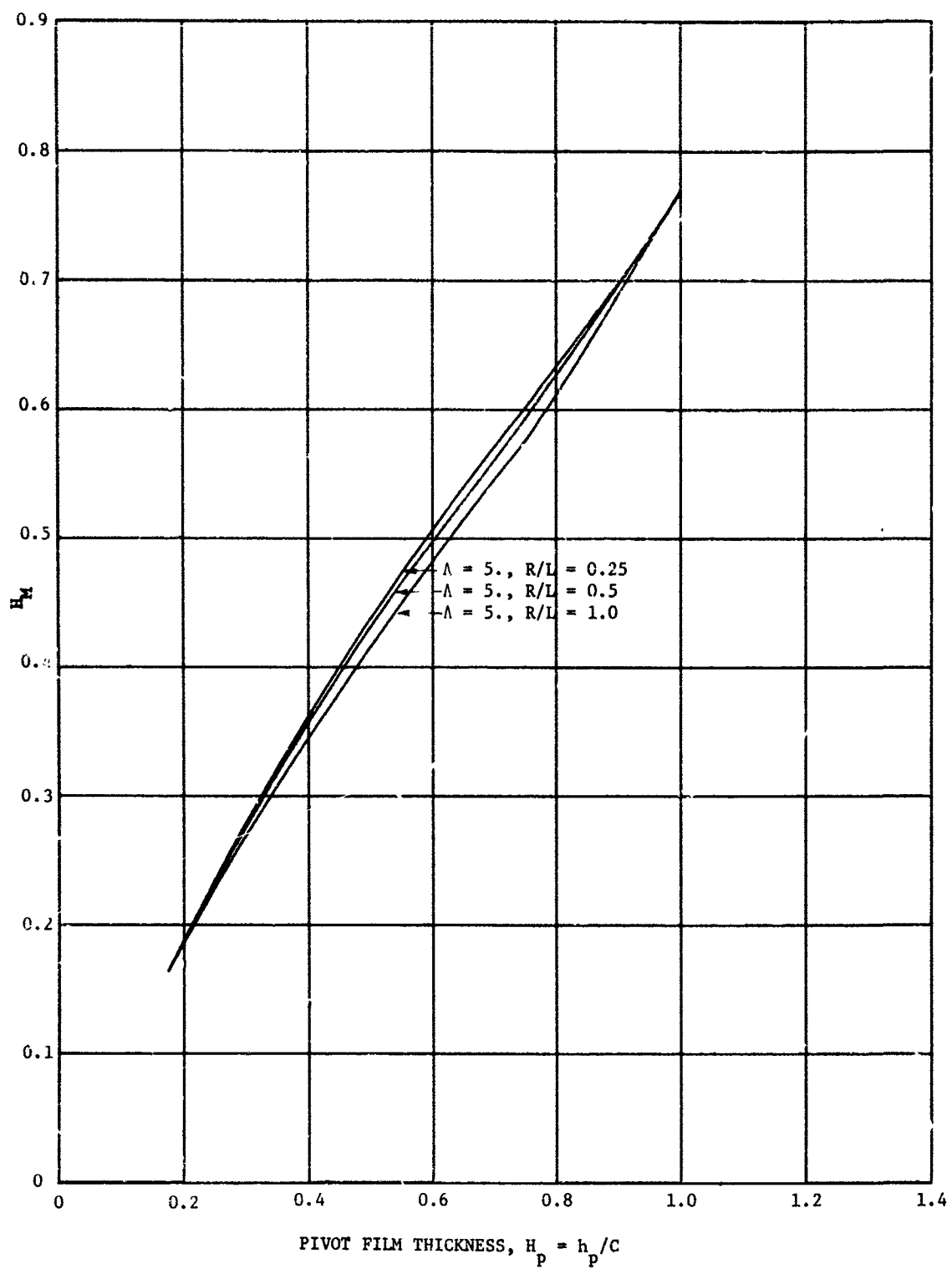
Figure 41. Single Pad Minimum Clearance as a Function of Pivot Clearance, = 5

76
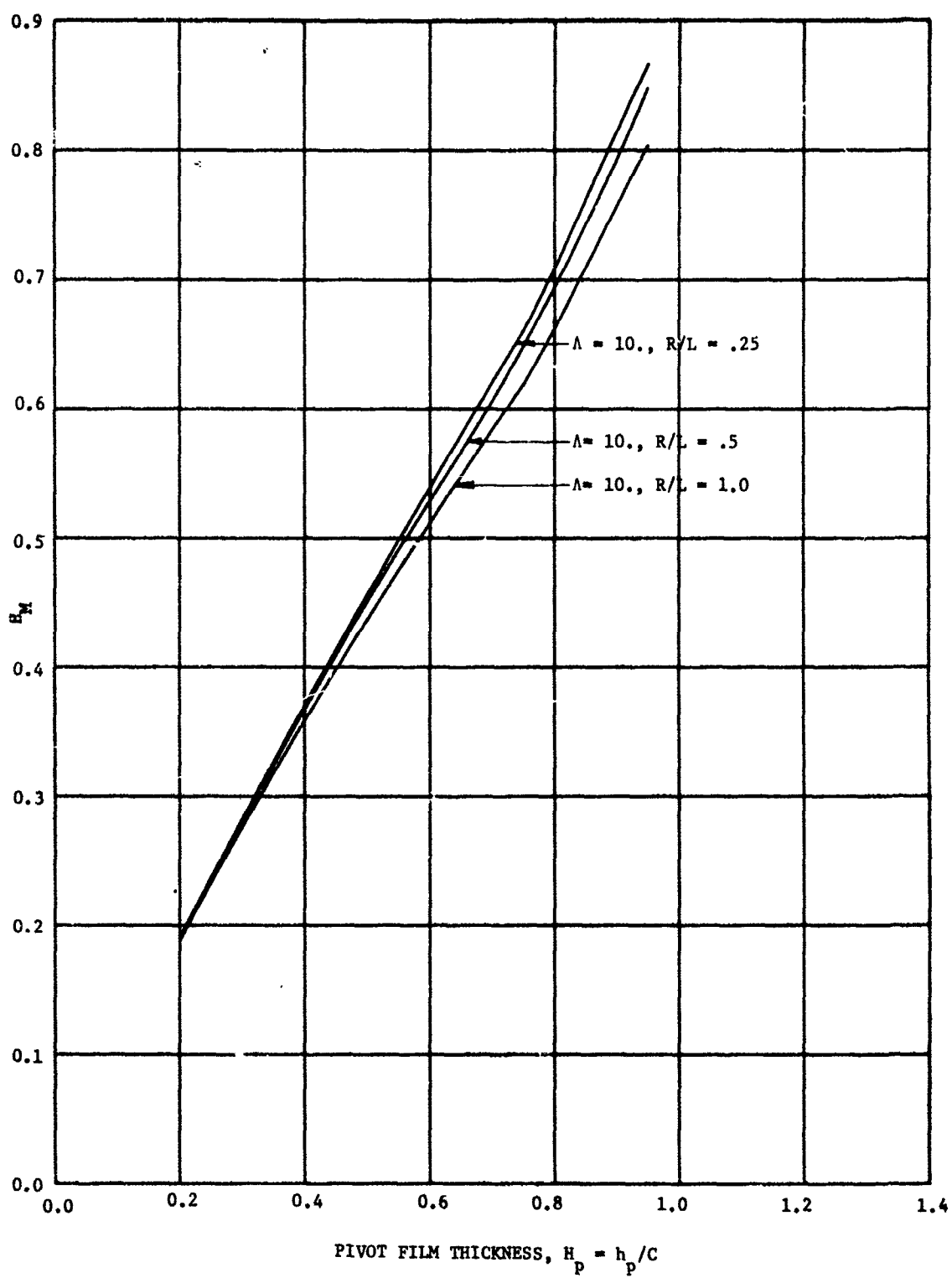
Figure 42. Single Pad Minimum Clearance as a Function of Pivot Clearance, $\Lambda = 10$
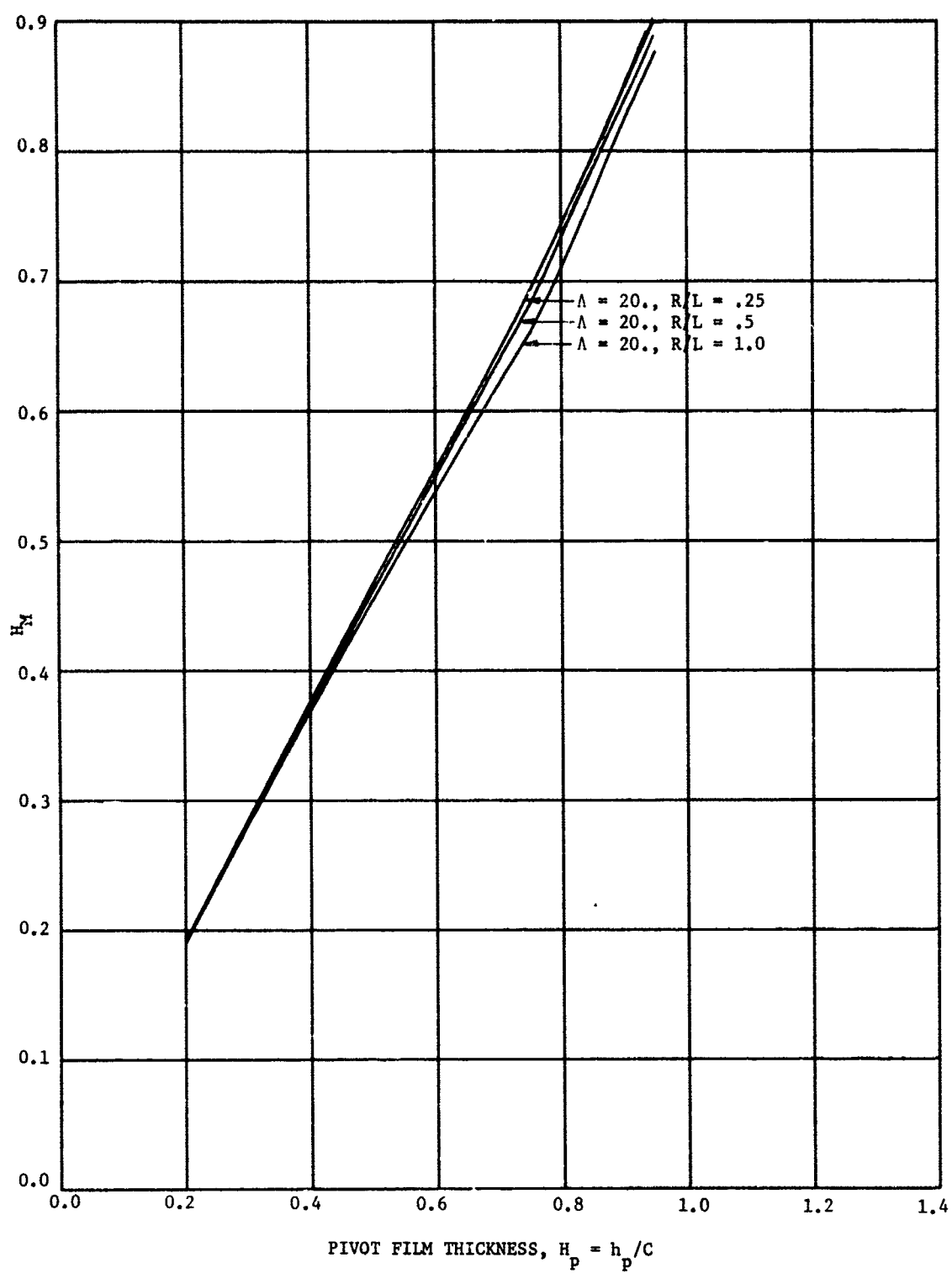
Figure 43. Single Pad Minimum Clearance as a Function of Pivot Clearance, Λ = 20

78

4. BEARING LOAD COEFFICIENT AND PIVOT FILM THICKNESS
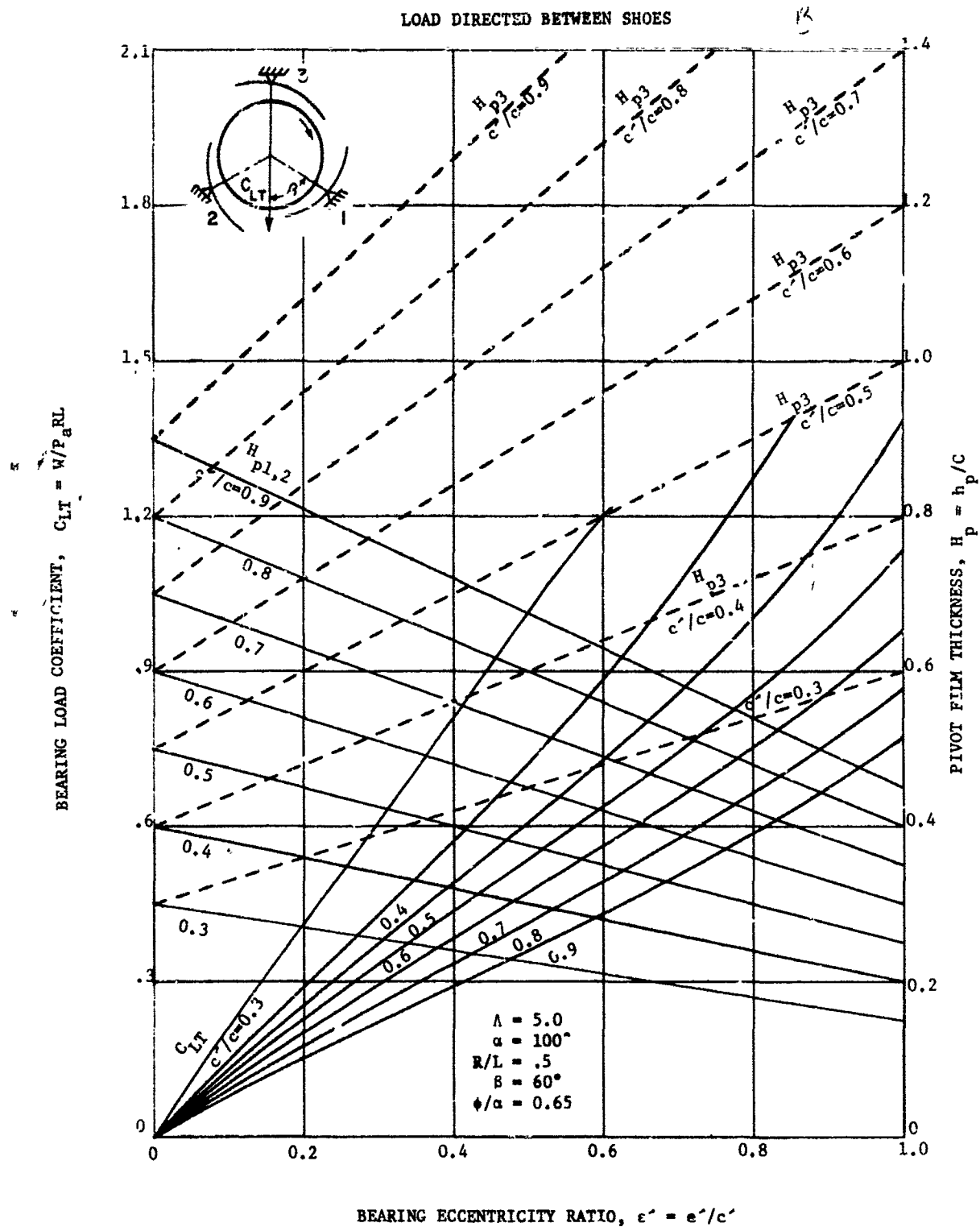
vs. ECCENTRICITY RATIO

(ALL PADS RIGID)
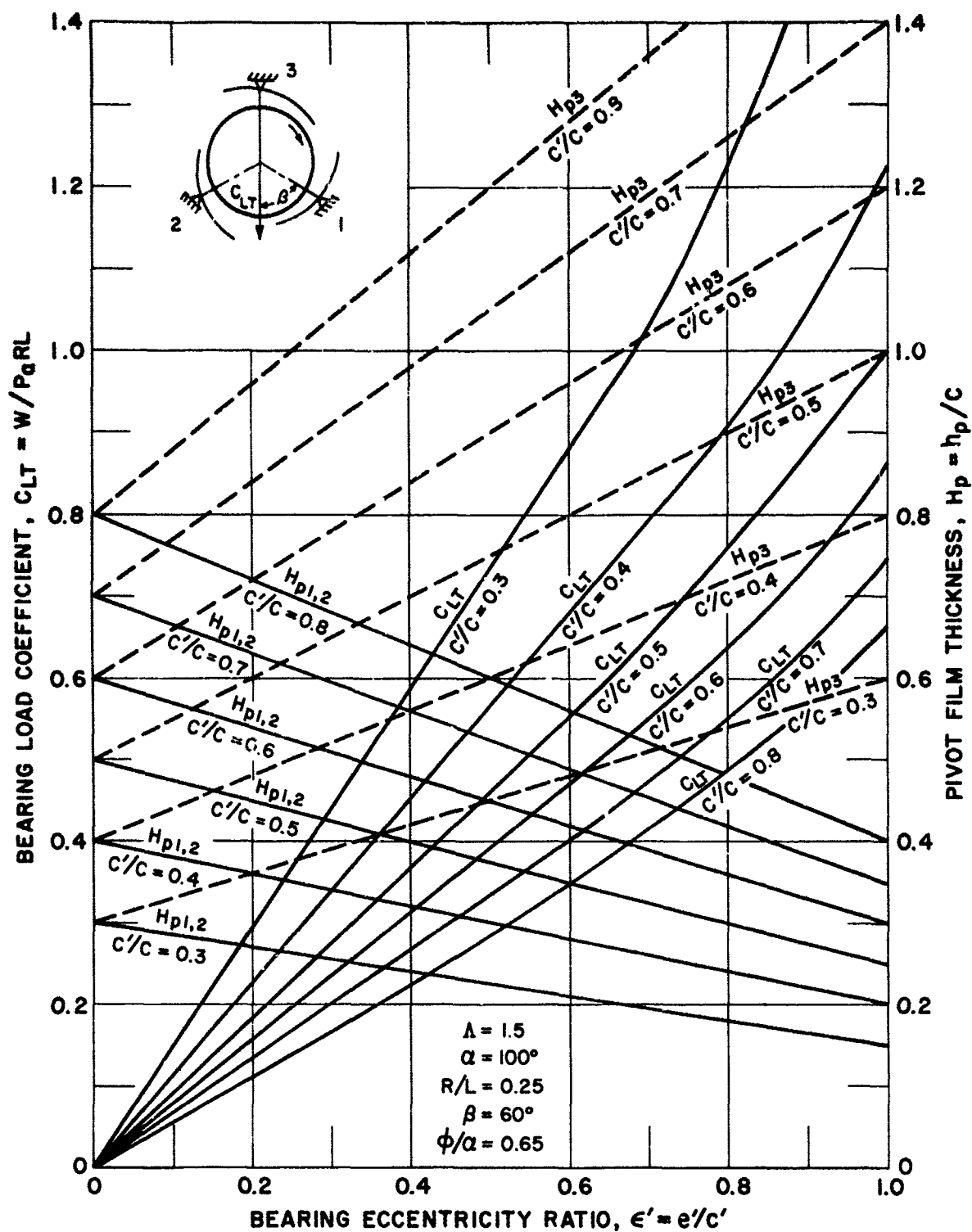
Figure 44. Bearing Load Coefficient and Pivot Clearance vs. Eccentricity Ratio for Load Direction Between Pads with All Pads Rigidly Supported, $\Lambda = 1.5$, $R/L = 0.25$
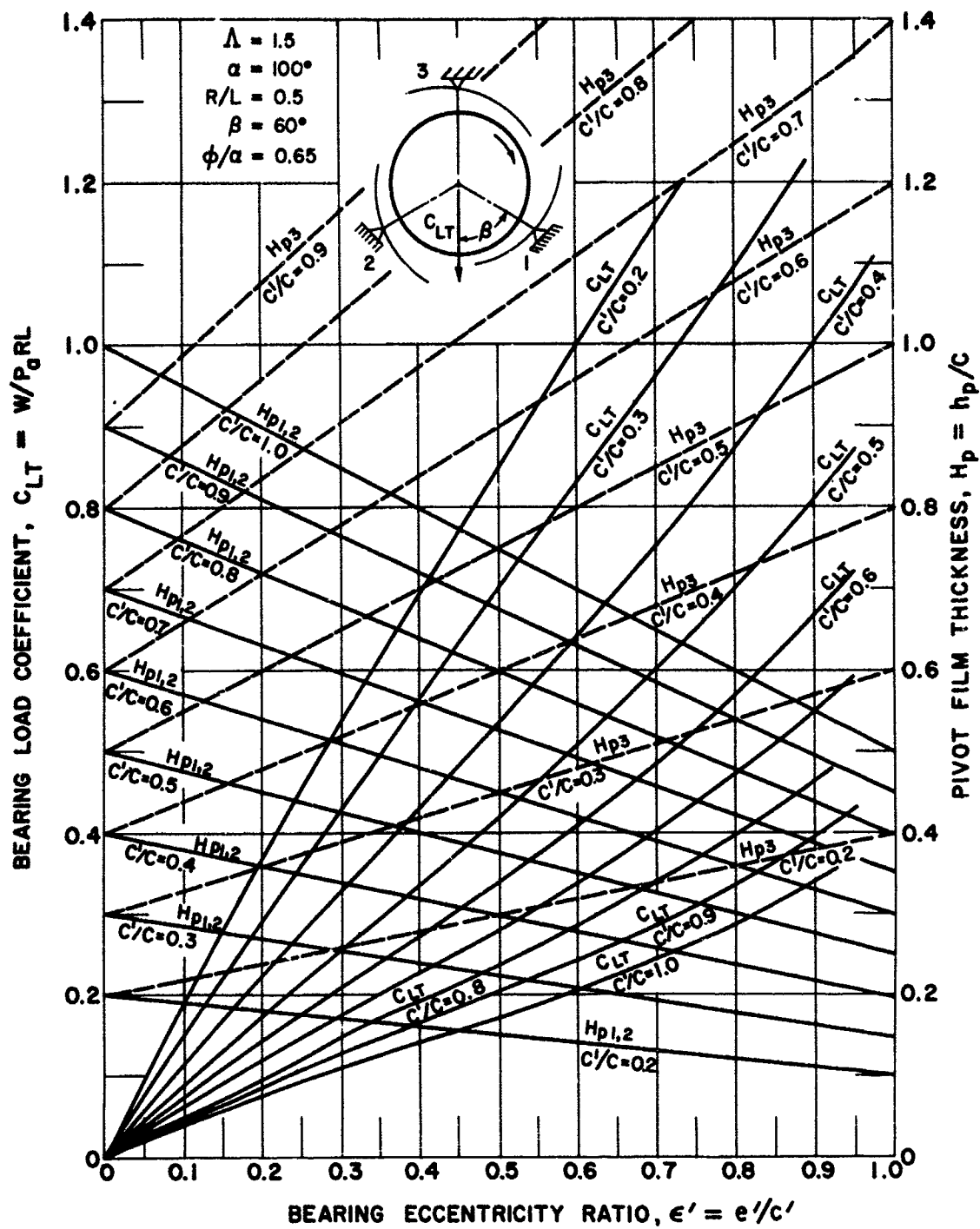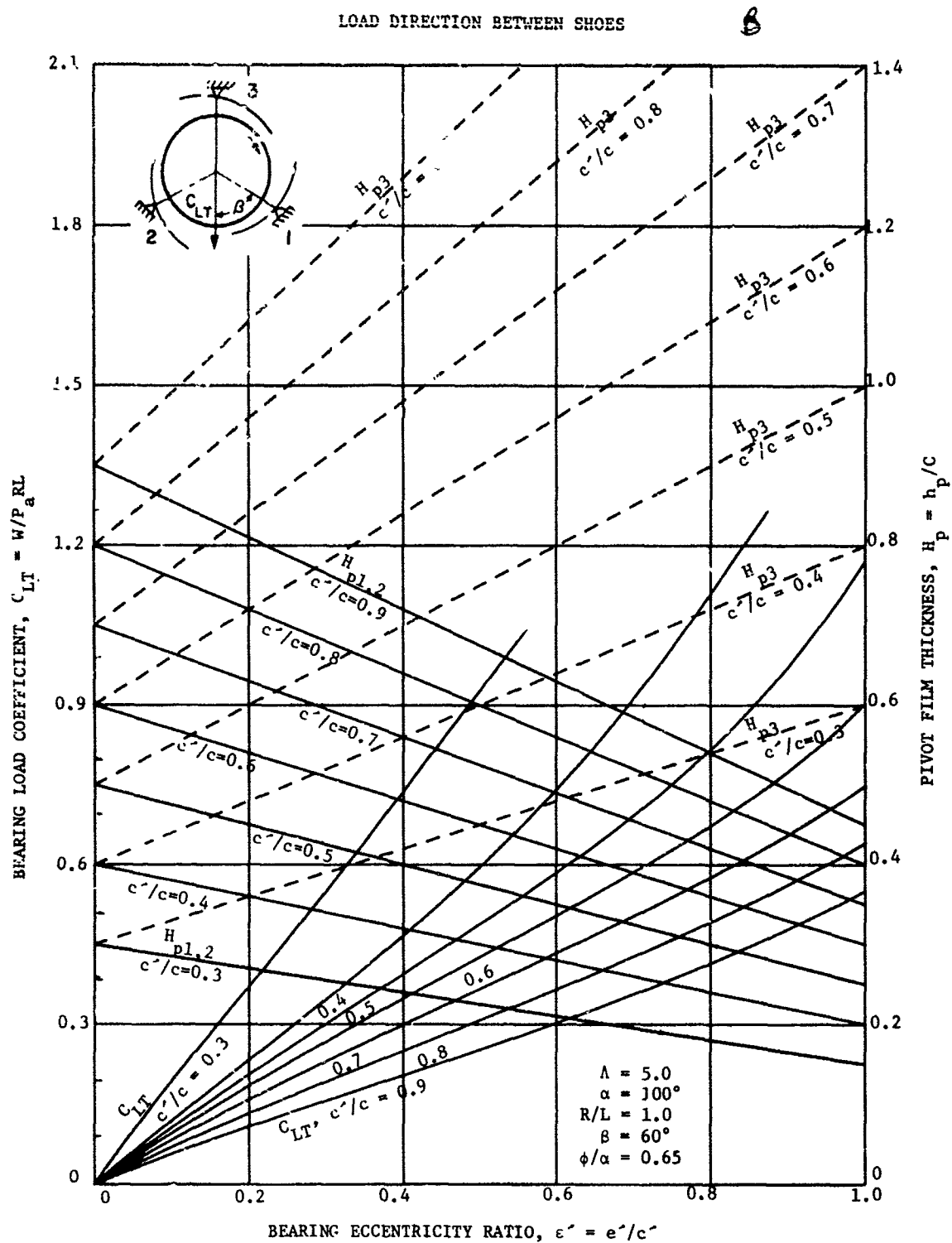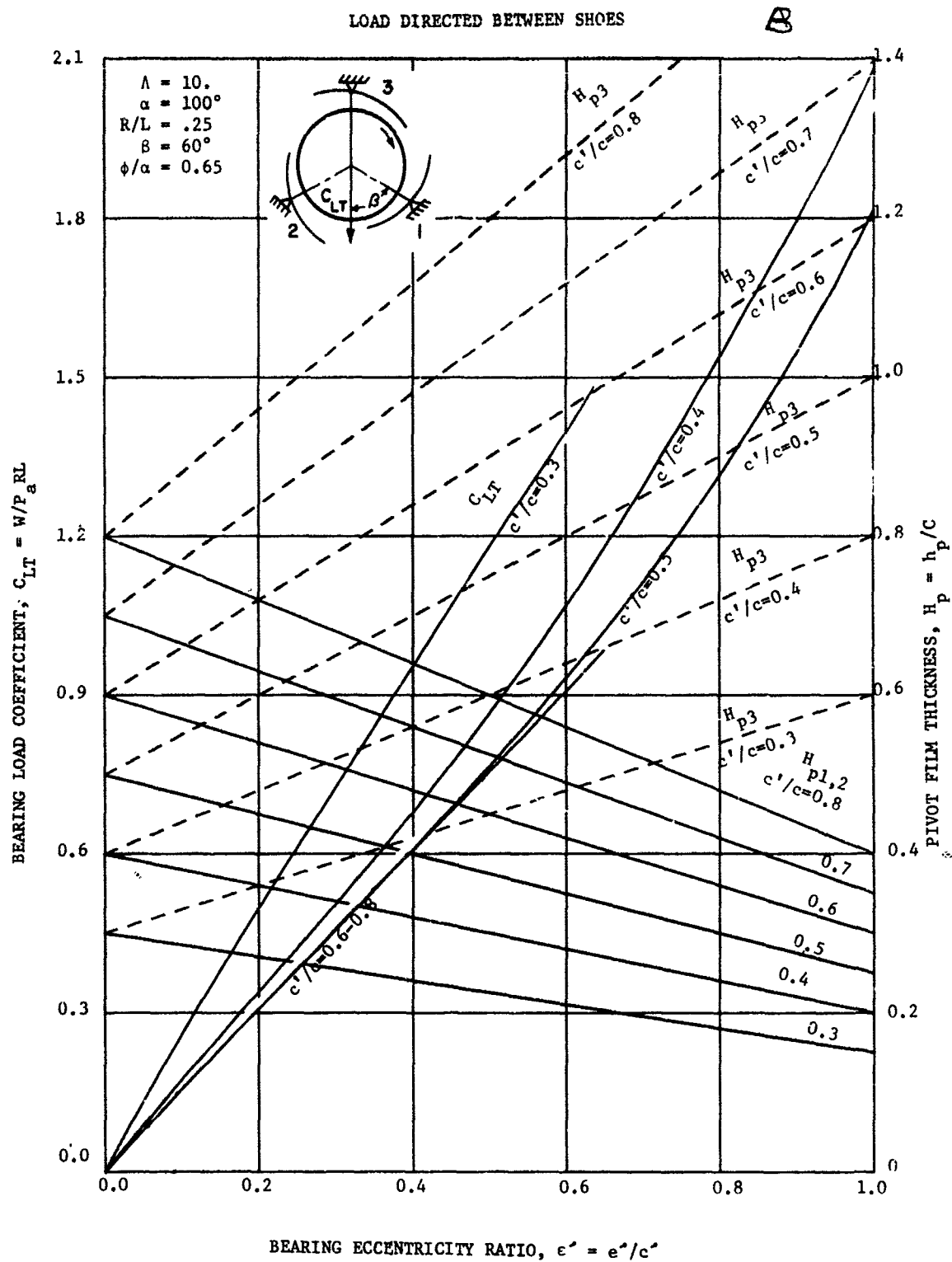
Figure 45. Bearing Load Coefficient and Pivot Clearance vs. Eccentricity Ratio for Load Direction Between Pads with All Pads Rigidly Supported, Λ = 1.5, R/L = 0.5

81
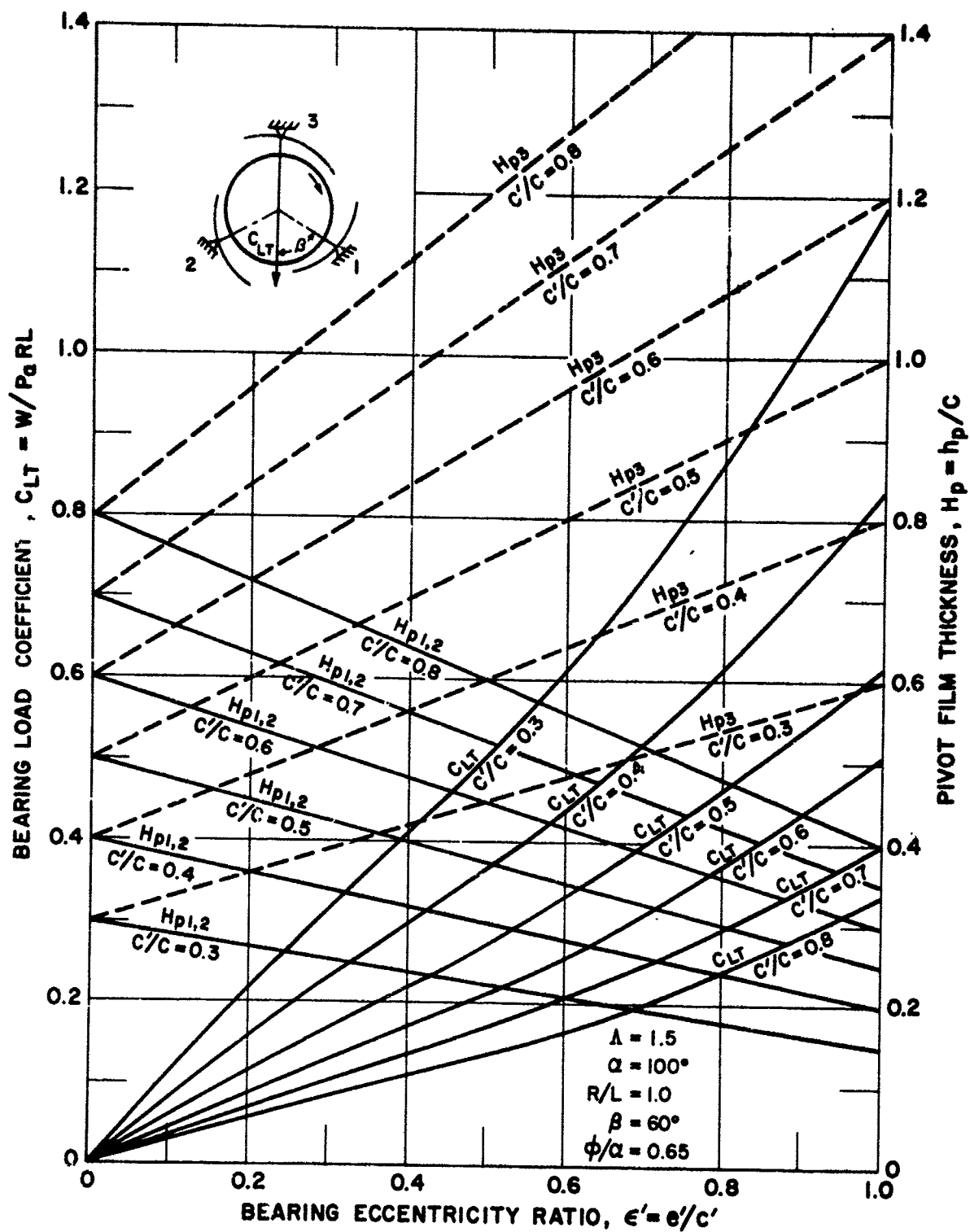
Figure 46. Bearing Load Coefficient and Pivot Clearance vs. Eccentricity Ratio for Load Direction Between Pads with All Pads Rigidly Supported, $\Lambda = 1.5$, $R/L = 1.0$
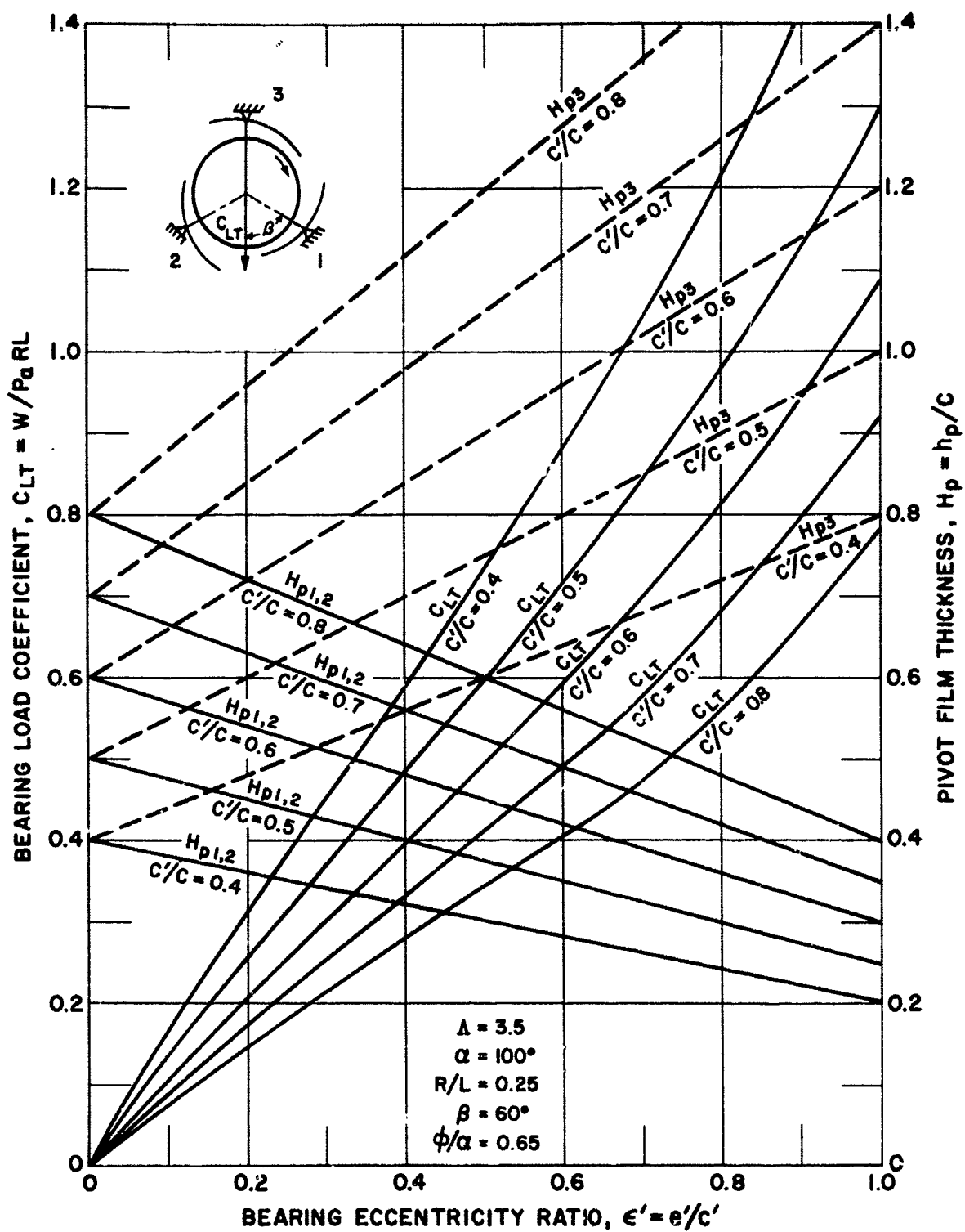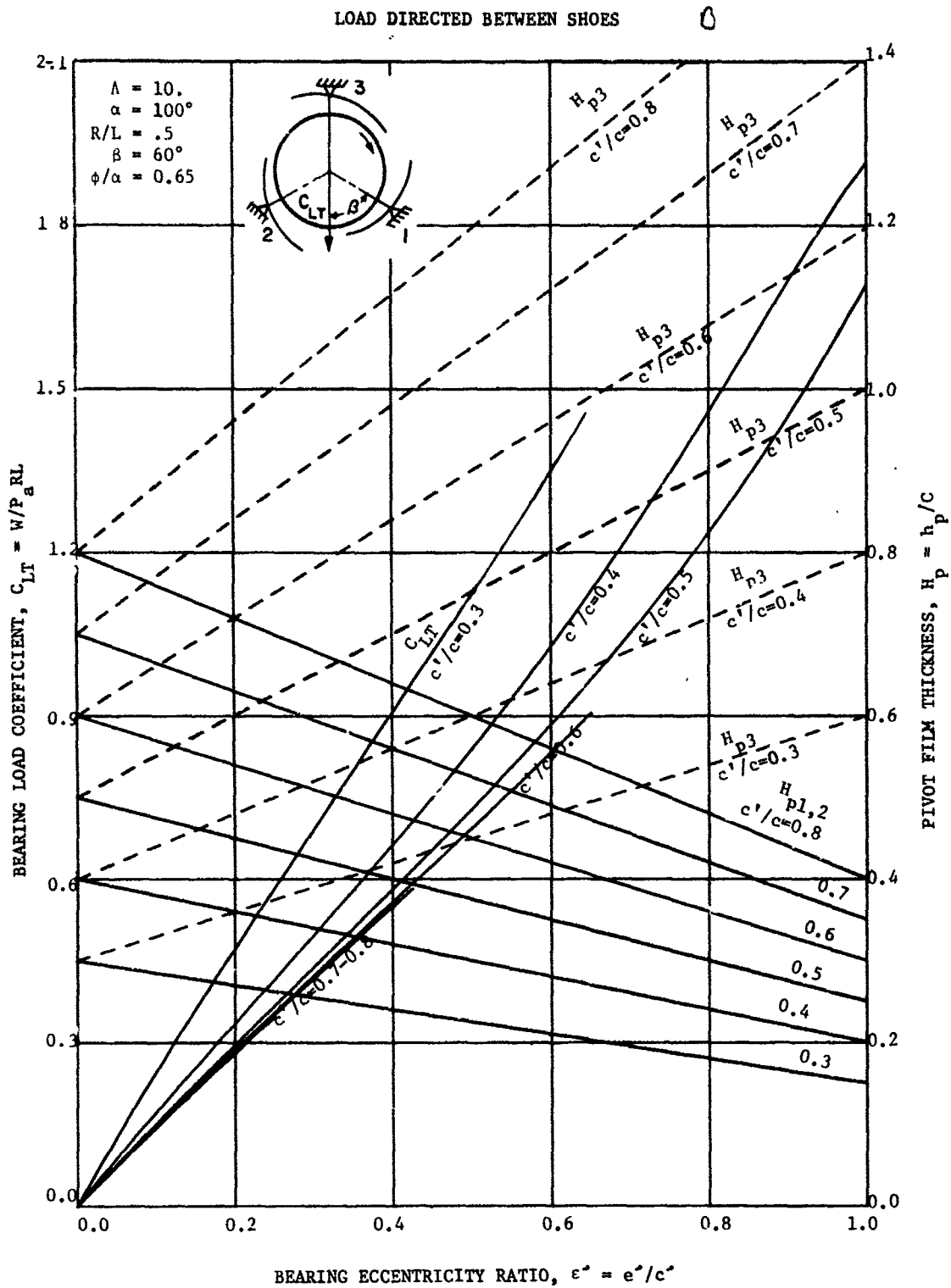
Figure 47. Bearing Load Coefficient and Pivot Clearance vs. Eccentricity Ratio for Load Direction Between Pads with All Pads Rigidly Supported, Λ = 3.5, R/L = 0.25
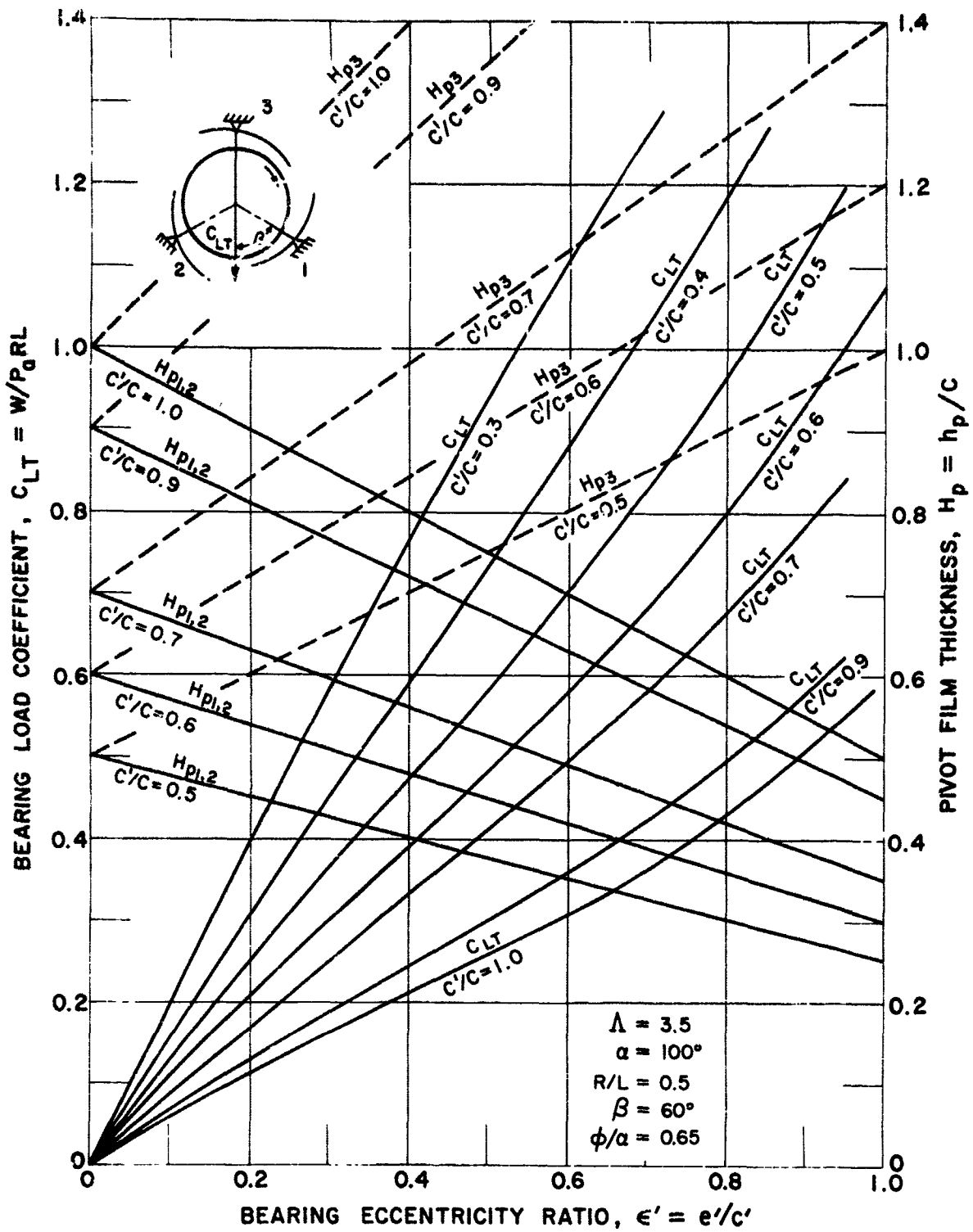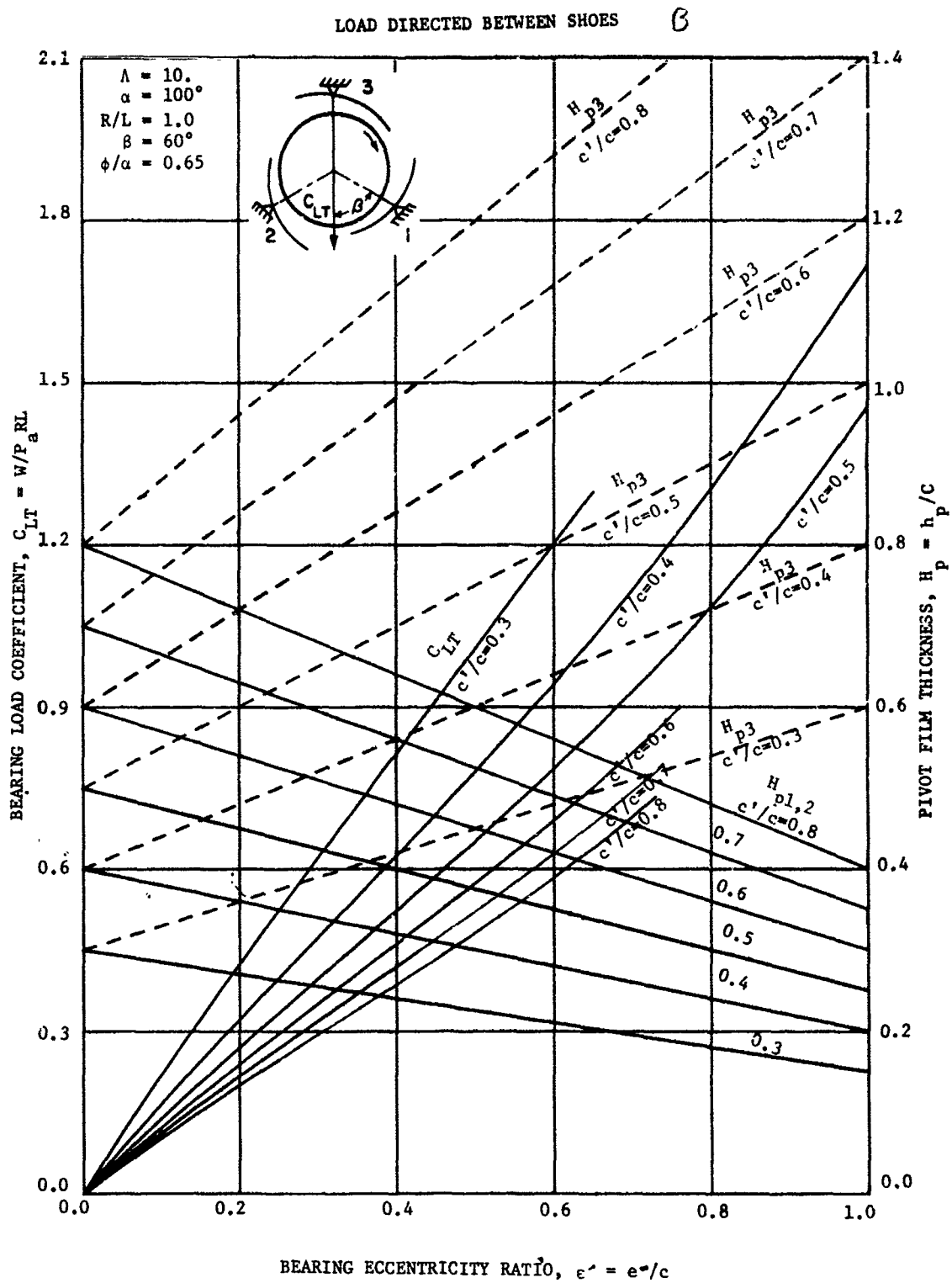
Figure 48. Bearing Load Coefficient and Pivot Clearance vs. Eccentricity Ratio for Load Direction Between Pads with All Pads Rigidly Supported, $\Lambda = 3.5$, $R/L = 0.5$
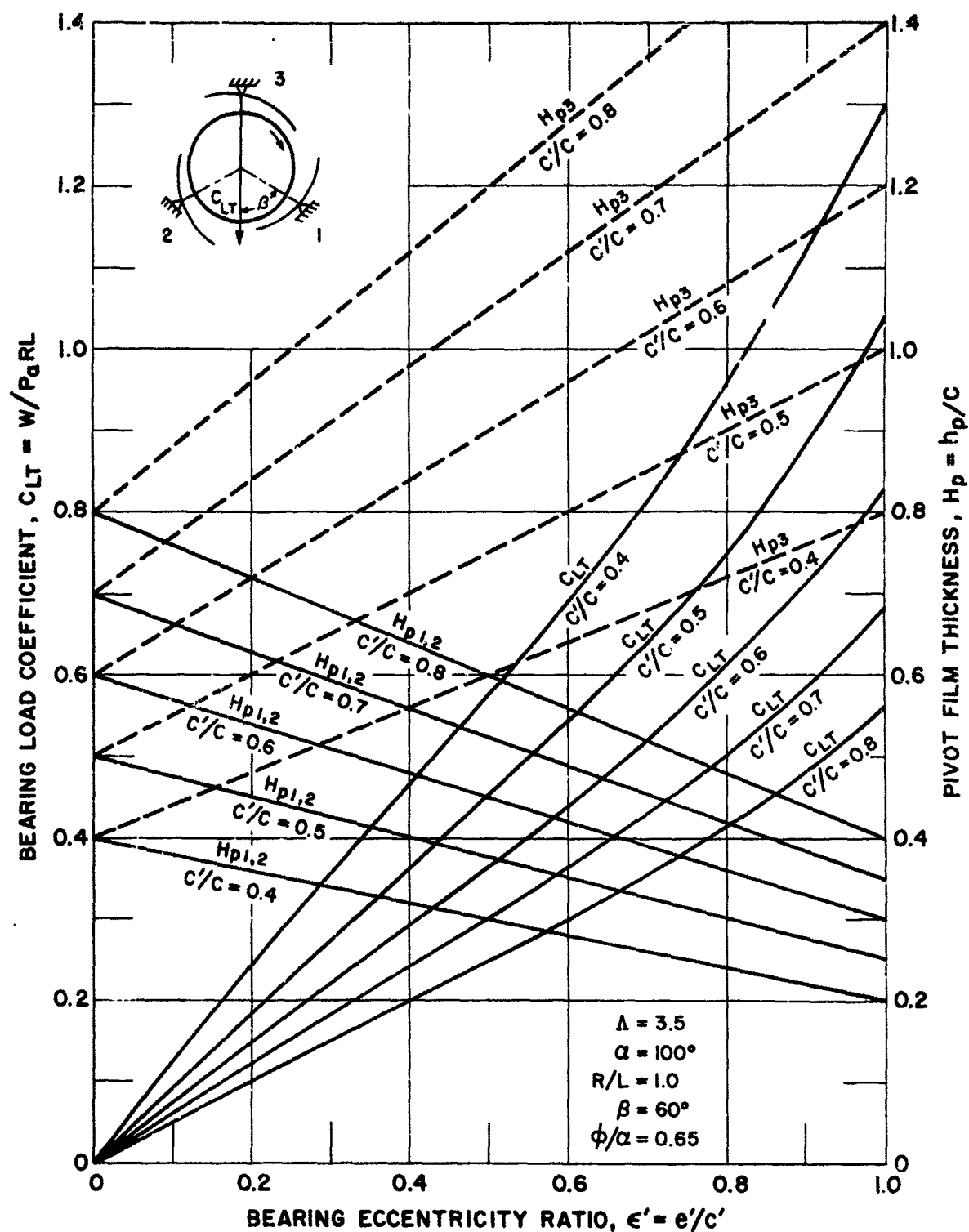
Figure 49. Bearing Load Coefficient and Pivot Clearance vs. Eccentricity Ratio for Load Direction Between Pads with All Pads Rigidly Supported, Λ = 3.5, R/L = 1.0
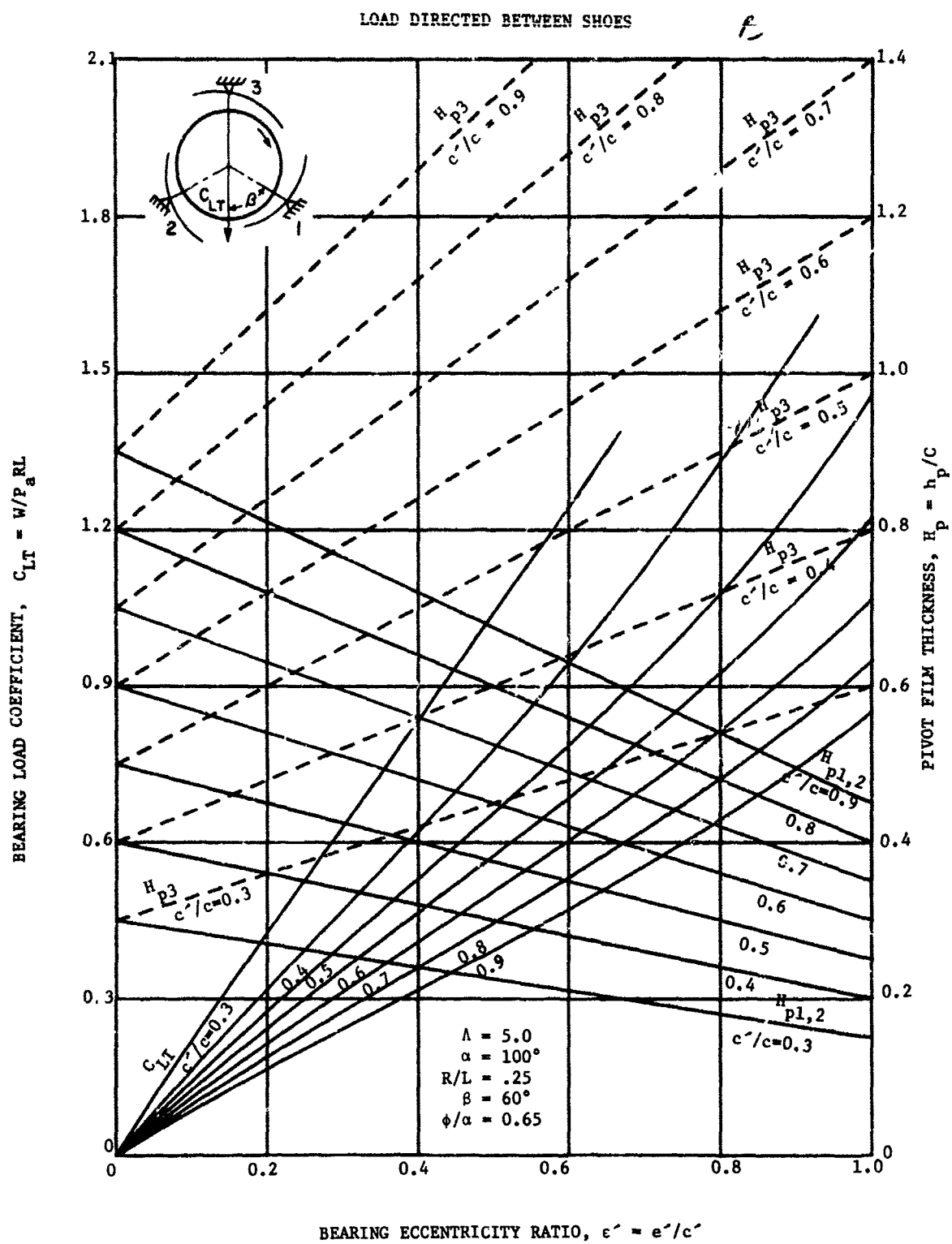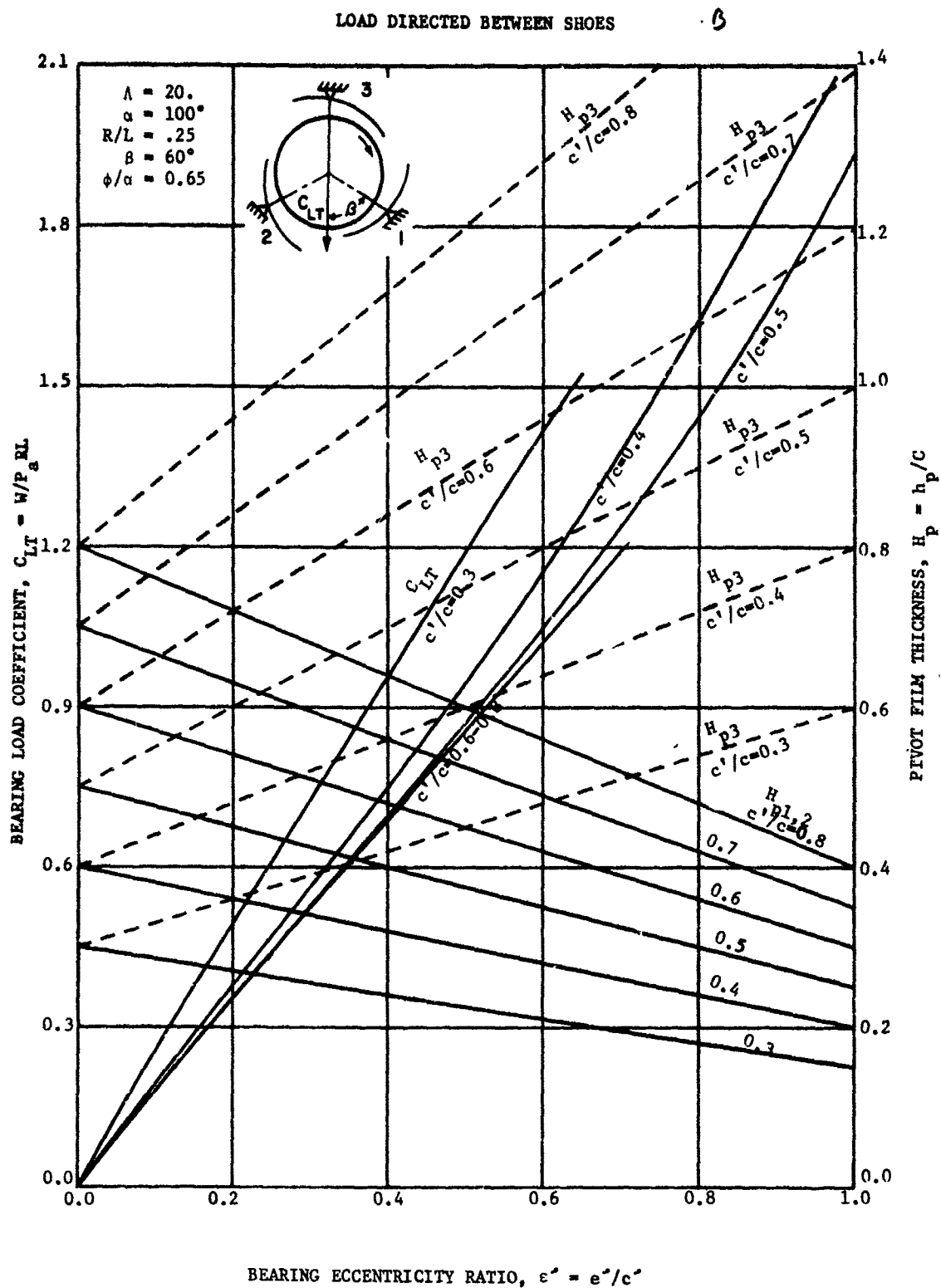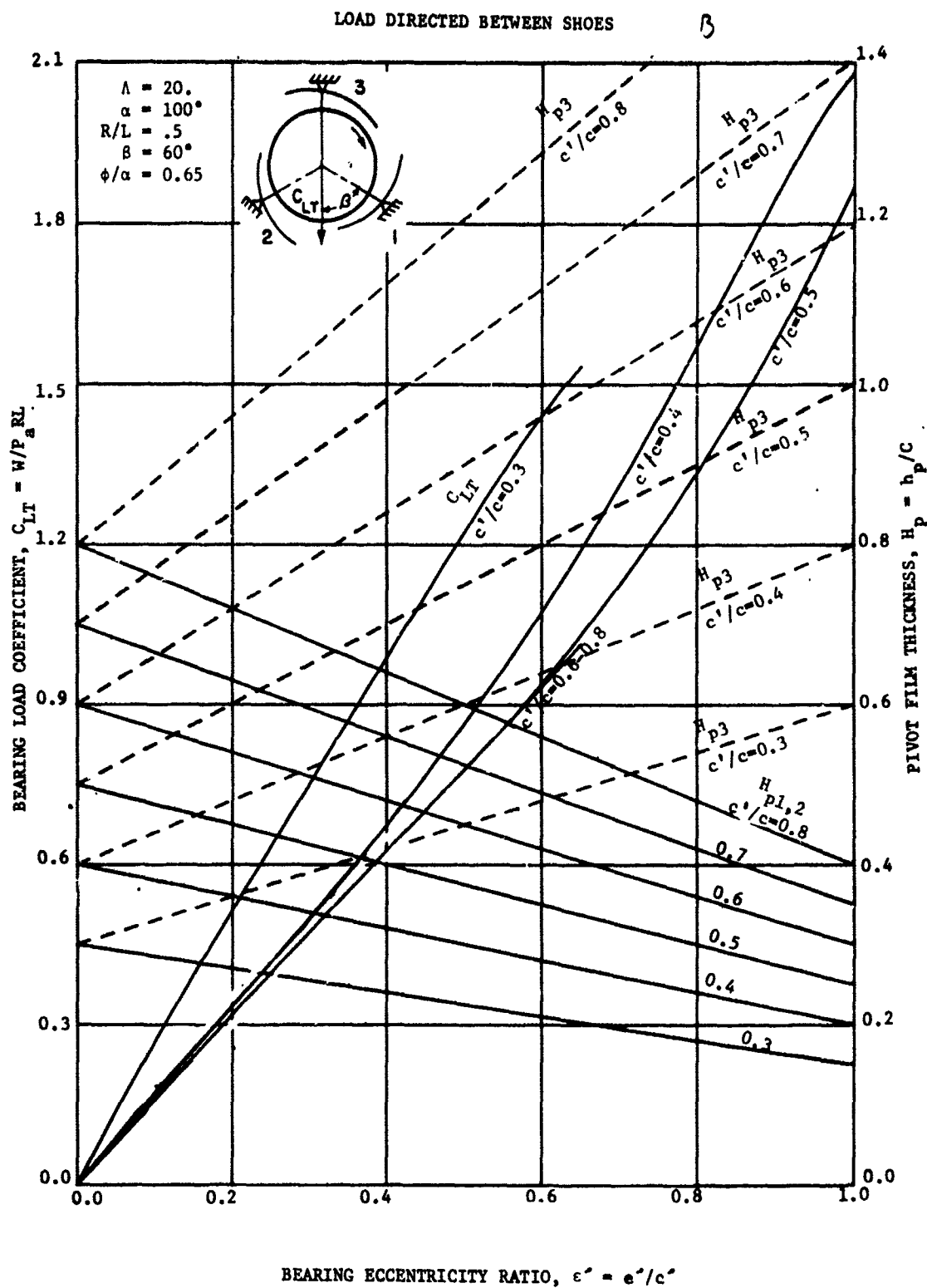
Figure 50. Bearing Load Coefficient and Pivot Clearance vs. Eccentricity Ratio for Load Direction Between Pads with All Pads Rigidly Supported, $\Lambda = 5.0$, $R/L = 0.25$
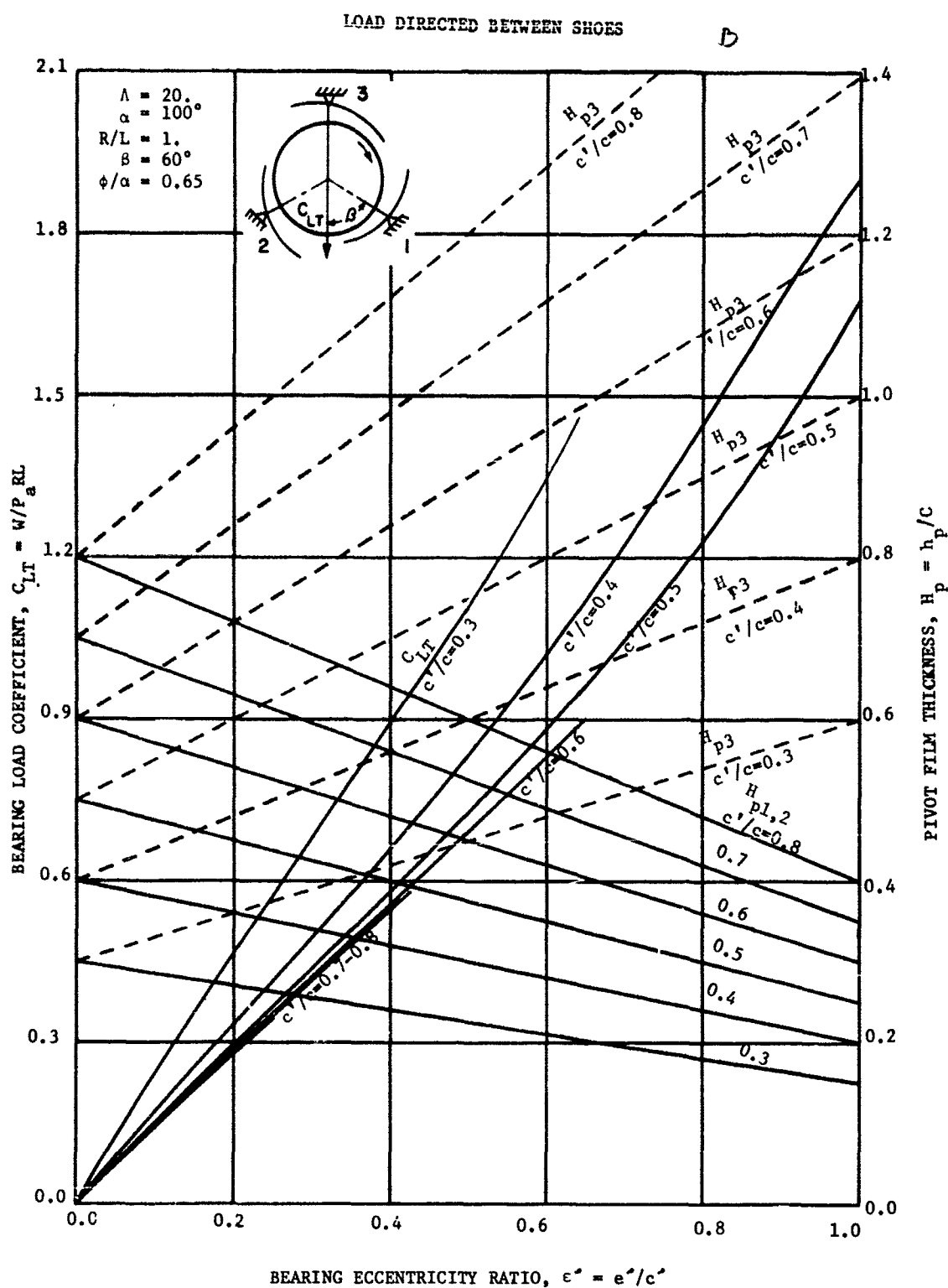
Figure 51. Bearing Load Coefficient and Pivot Clearance vs. Eccentricity
Ratio for Load Direction Between Pads with All Pads Rigidly
Supported, Λ = 5.0, R/L = 0.25

Figure 52. Bearing Load Coefficient and Pivot Clearance vs. Eccentricity Ratio for Load Direction Between Pads with All Pads Rigidly Supported, Λ = 5.0, R/L = 1.0
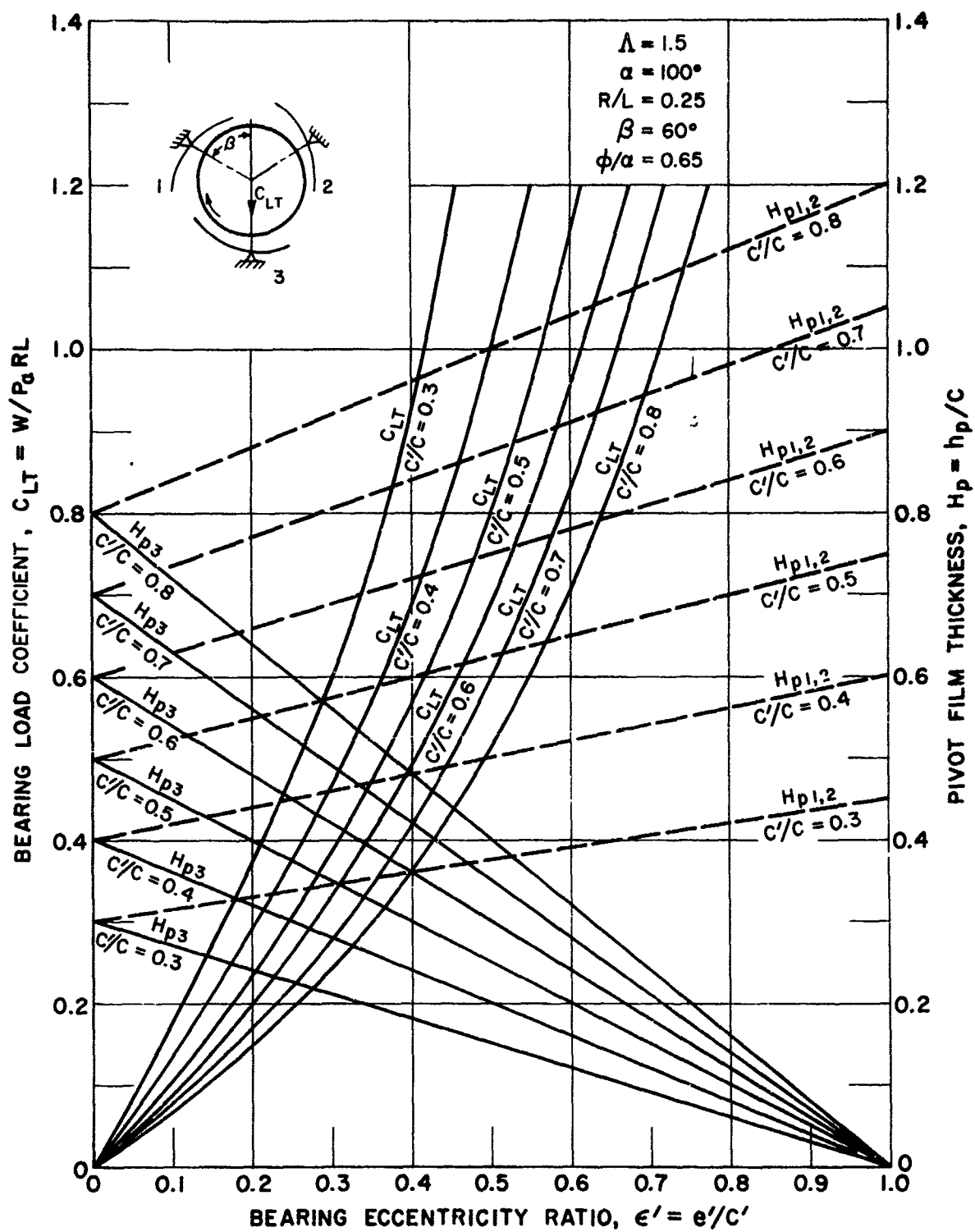
88

Figure 53. Bearing Load Coefficient and Pivot Clearance vs. Eccentricity Ratio for Load Direction Between Pads with All Pads Rigidly Supported, $\Lambda = 10.0$, R/L = 0.25
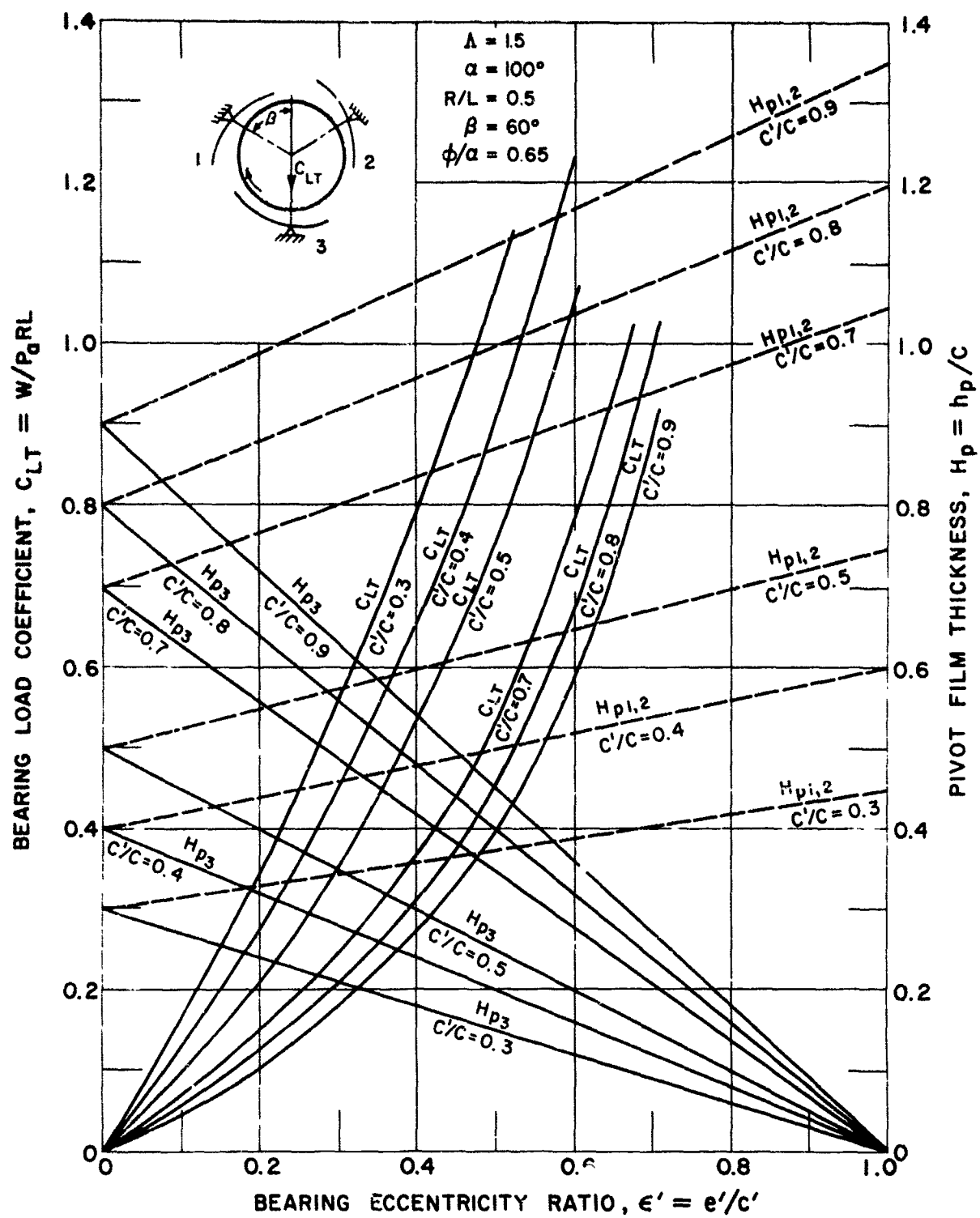
89

Figure 54. Bearing Load Coefficient and Pivot Clearance vs. Eccentricity Ratio for Load Direction Between Pads with All Pads Rigidly Supported, $\Lambda = 10.0$, $R/L = 0.5$

Figure 55. Bearing Load Coefficient and Pivot Clearance vs. Eccentricity Ratio for Load Direction Between Pads with All Pads Rigidly Supported, Λ = 10.0, R/L = 1.0
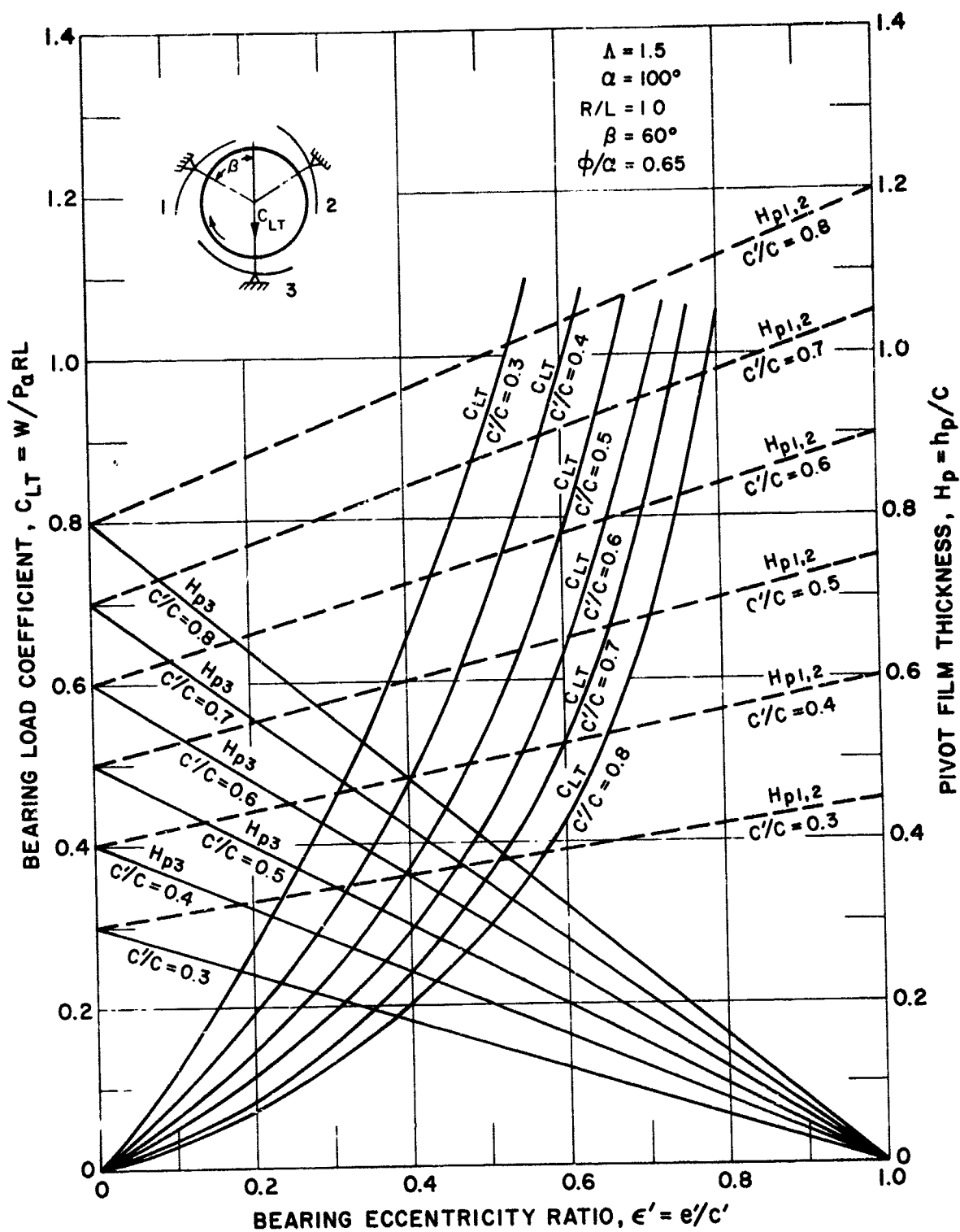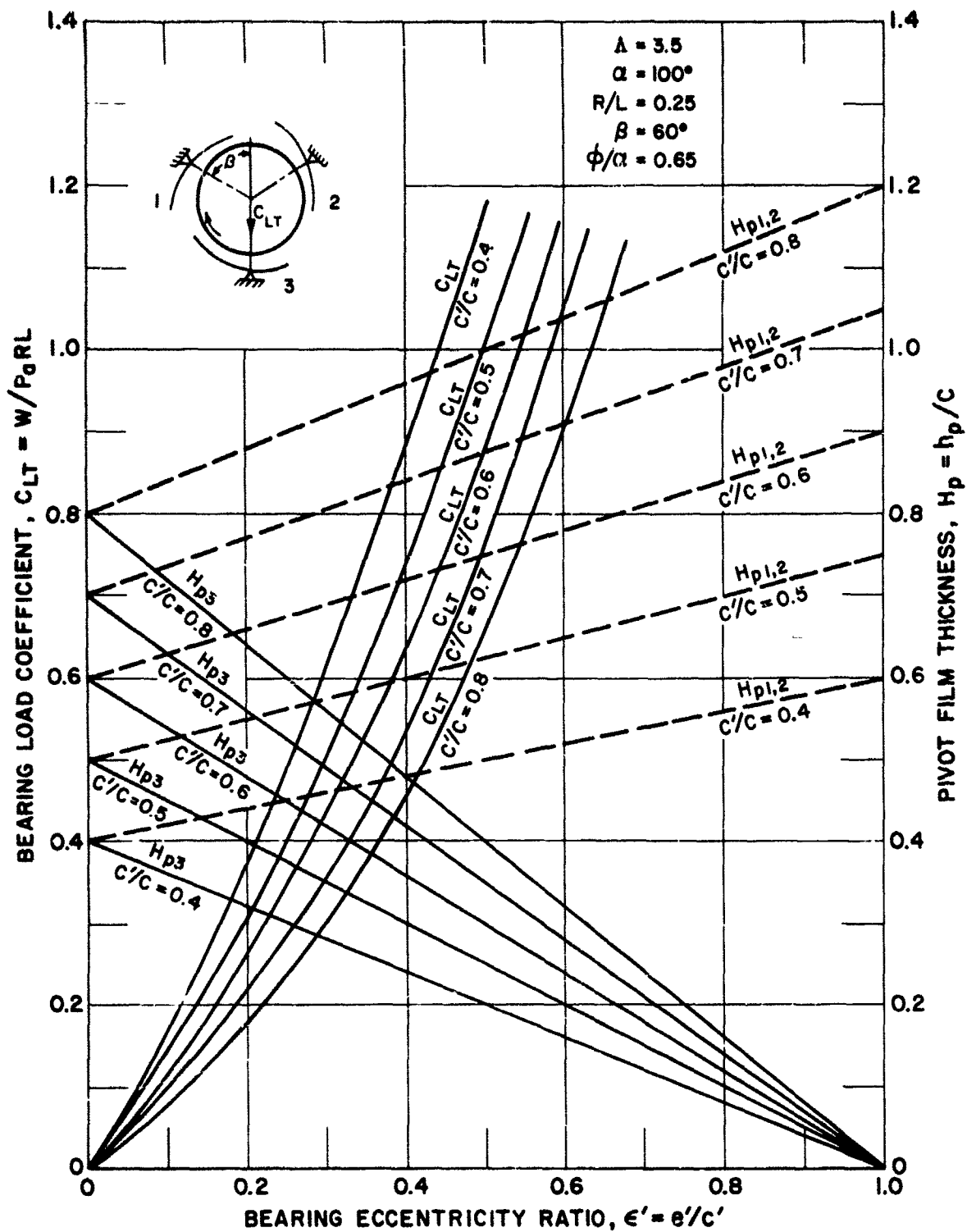
Figure 56. Bearing Load Coefficient and Pivot Clearance vs. Eccentricity Ratio for Load Direction Between Pads with All Pads Rigidly Supported, Λ = 20.0, R/L = 0.25

92

Figure 57. Bearing Load Coefficient and Pivot Clearance vs. Eccentricity
Ratio for Load Direction Between Pads with All Pads Rigidly
Supported, Λ = 20.0, R/L = 0.5

93

Figure 58. Bearing Load Coefficient and Pivot Clearance vs. Eccentricity Ratio for Load Direction Between Pads with All Pads Rigidly Supported, $\Lambda = 20.0$, R/L = 1.0

94

Figure 59. Bearing Load Coefficient and Pivot Clearance vs. Eccentricity Ratio for Load Directed at Pad with All Pads Rigidly Supported $\Lambda = 1.5$, $R/L = 0.25$
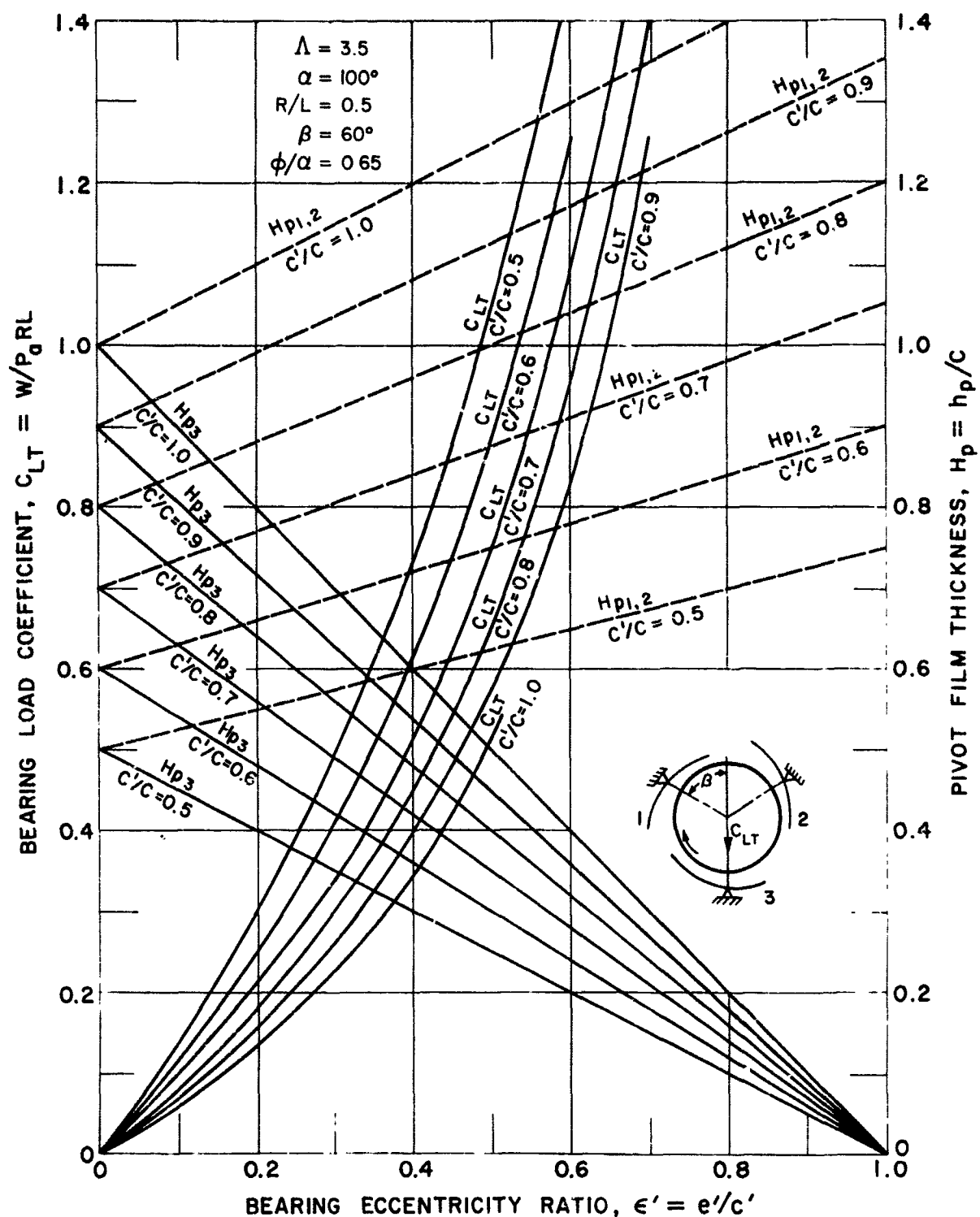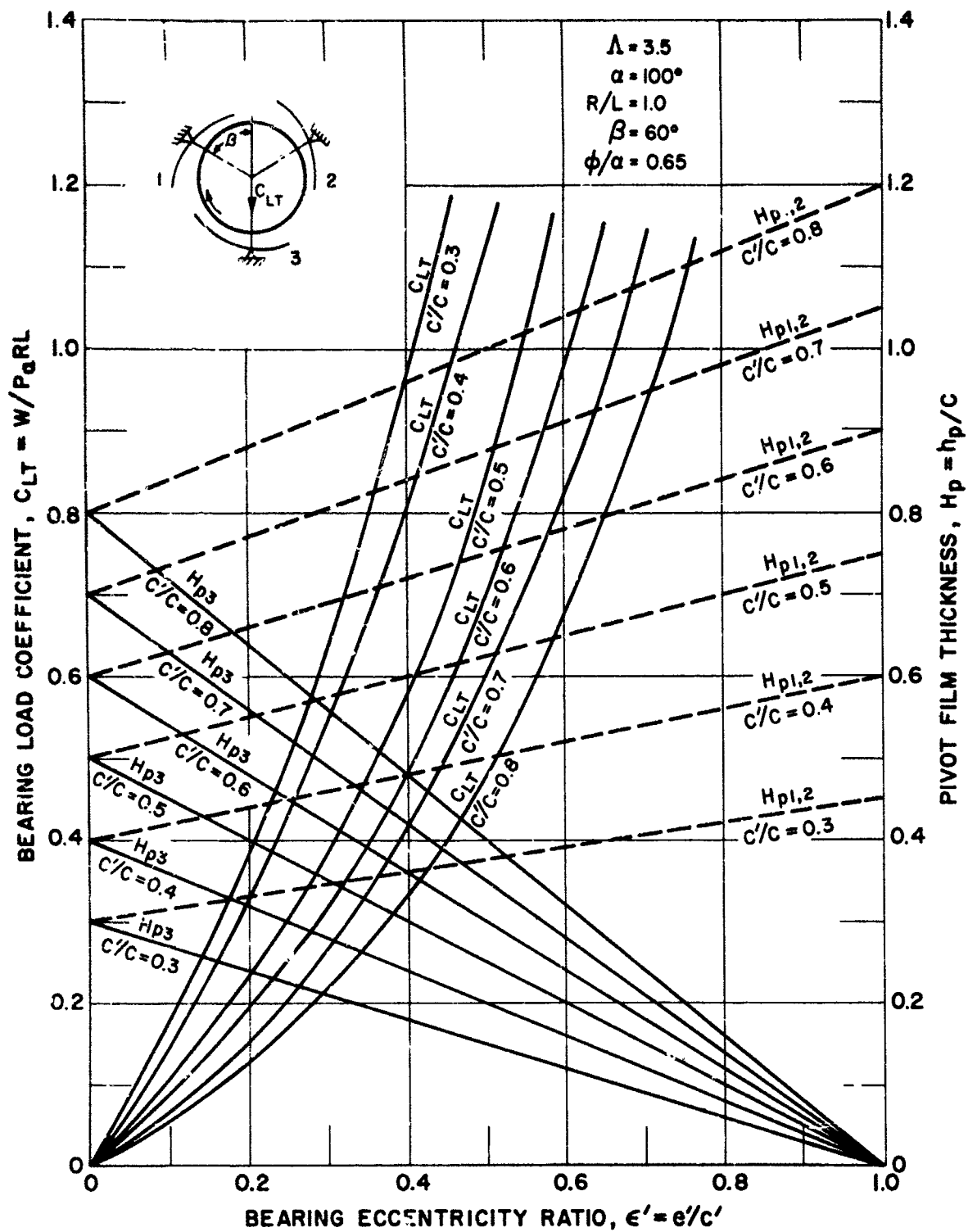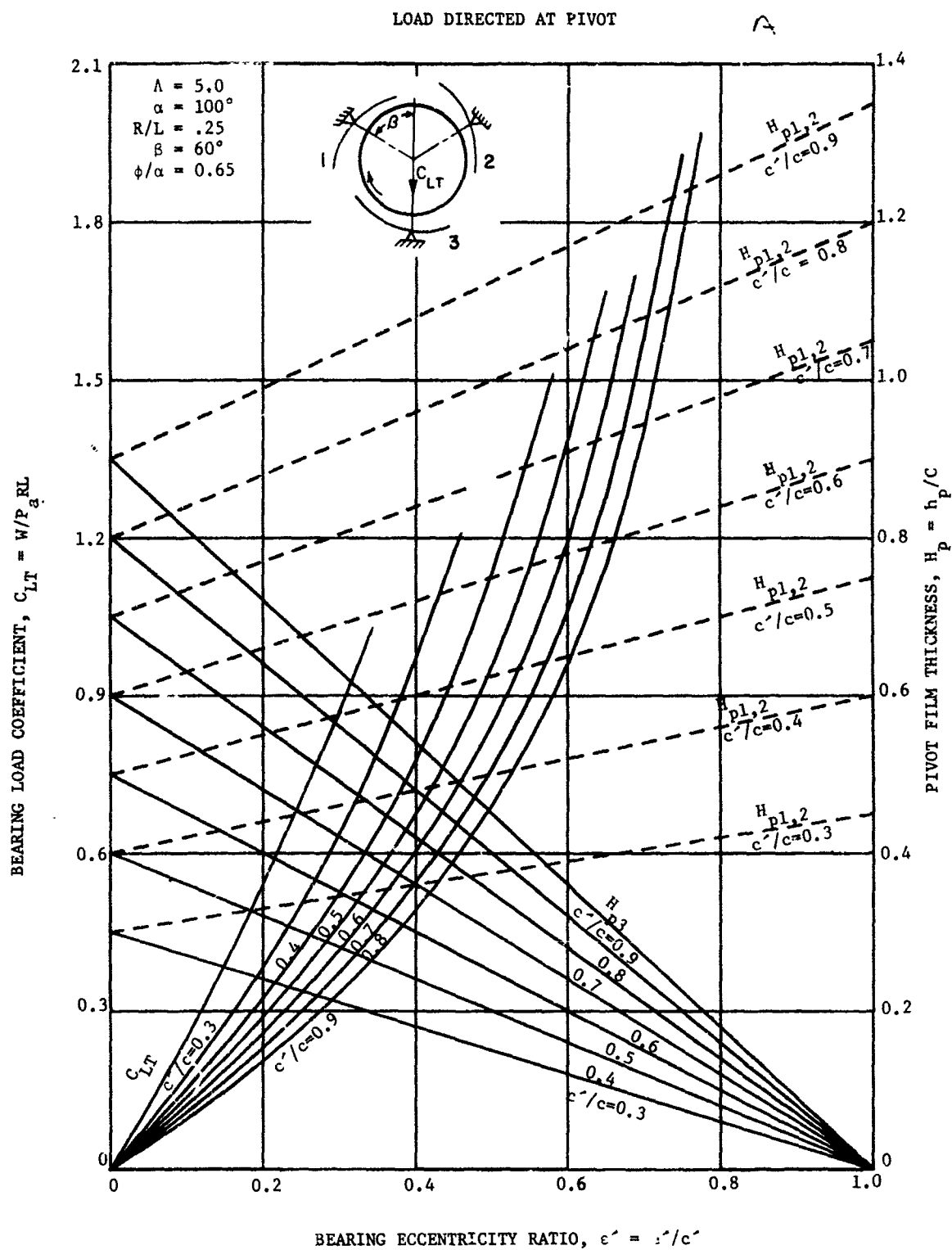
Figure 60. Bearing Load Coefficient and Pivot Clearance vs. Eccentricity Ratio for Load Directed at Pad with All Pads Rigidly Supported, $\Lambda = 1.5$, R/L = 0.5
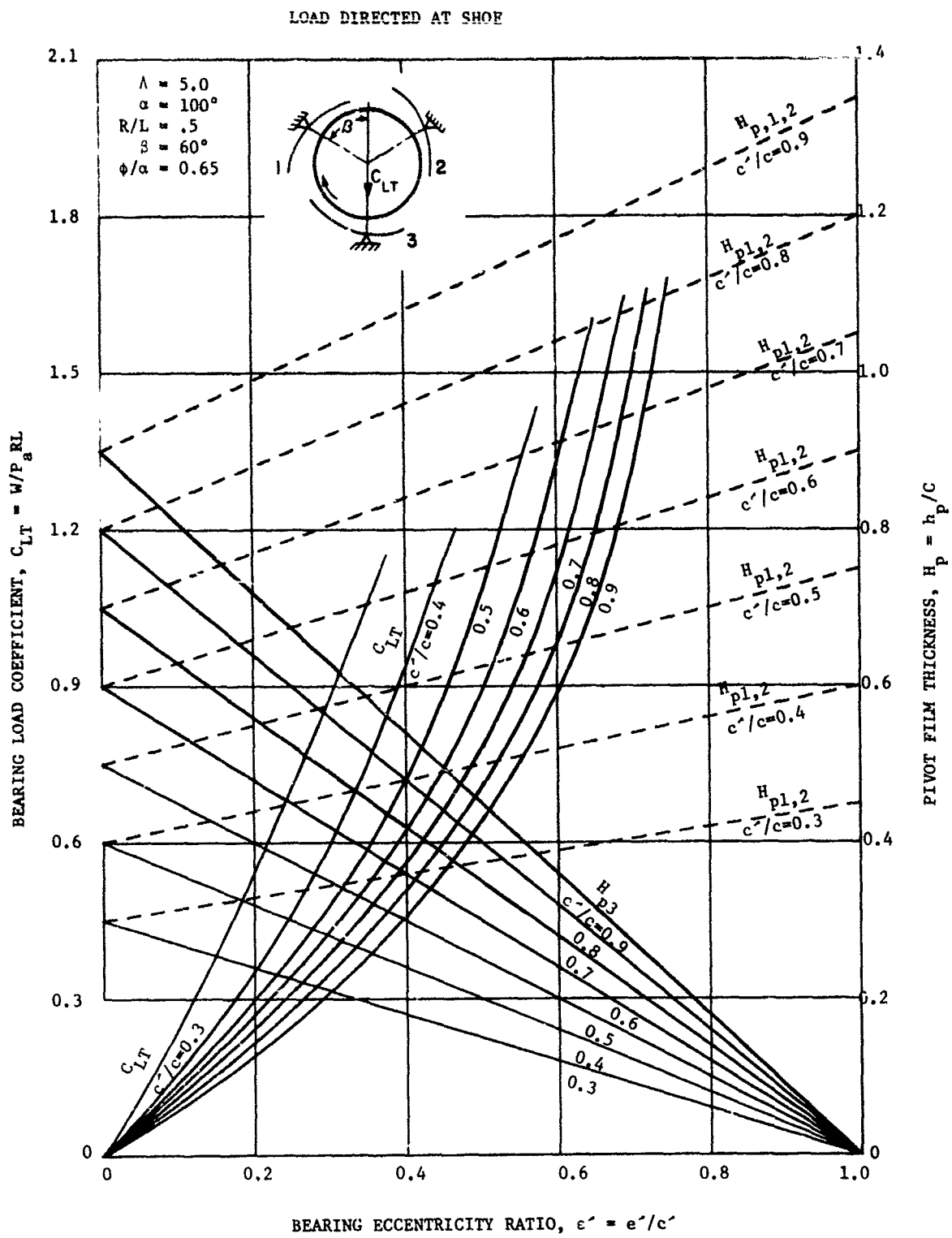
96

Figure 61. Bearing Load Coefficient and Pivot Clearance vs. Eccentricity Ratio for Load Directed at Pad with All Pads Rigidly Supported, $\Lambda = 1.5$, R/L = 1.0
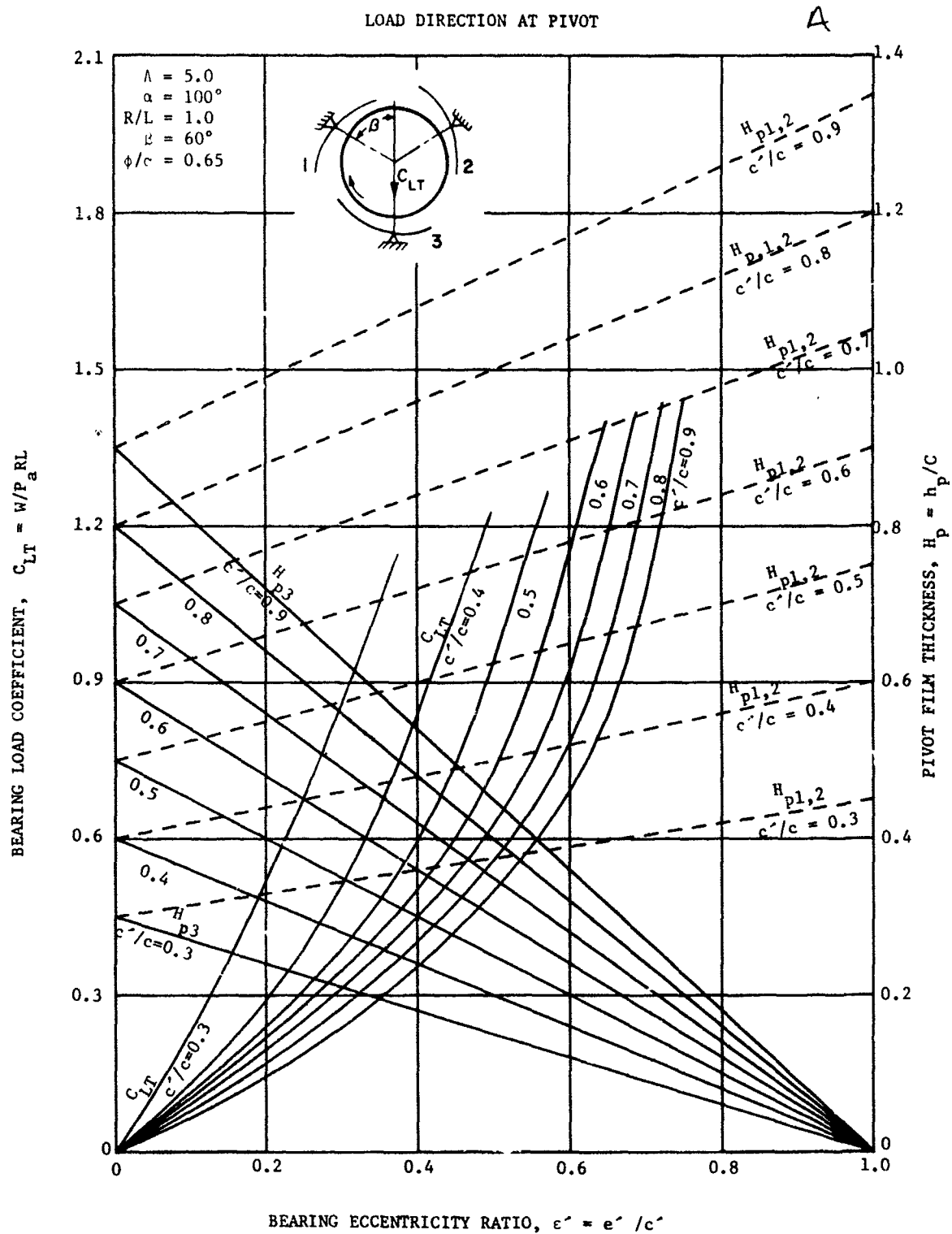
97

Figure 62. Bearing Load Coefficient and Pivot Clearance vs. Eccentricity
Ratio for Load Directed at Pad with All Pads Rigidly Supported,
$\Lambda = 3.5$, R/L = 0.25

Figure 63. Bearing Load Coefficient and Pivot Clearance vs. Eccentricity Ratio for Load Directed at Pad with All Pads Rigidly Supported, $\Lambda = 3.5$, $R/L = 0.5$

Figure 64. Bearing Load Coefficient and Pivot Clearance vs. Eccentricity Ratio for Load Directed at Pad with All Pads Rigidly Supported, $\Lambda = 3.5$, $R/L = 1.0$
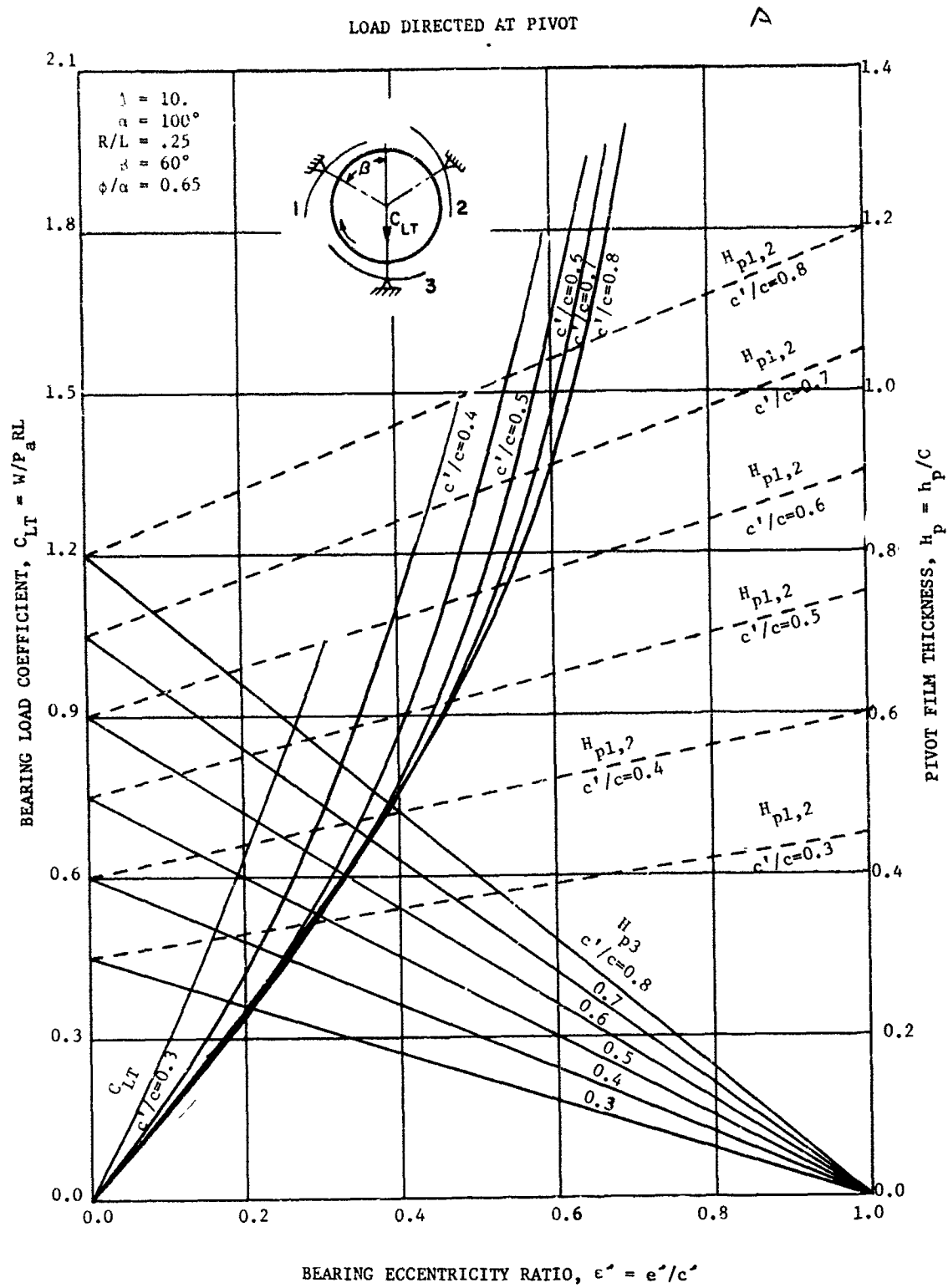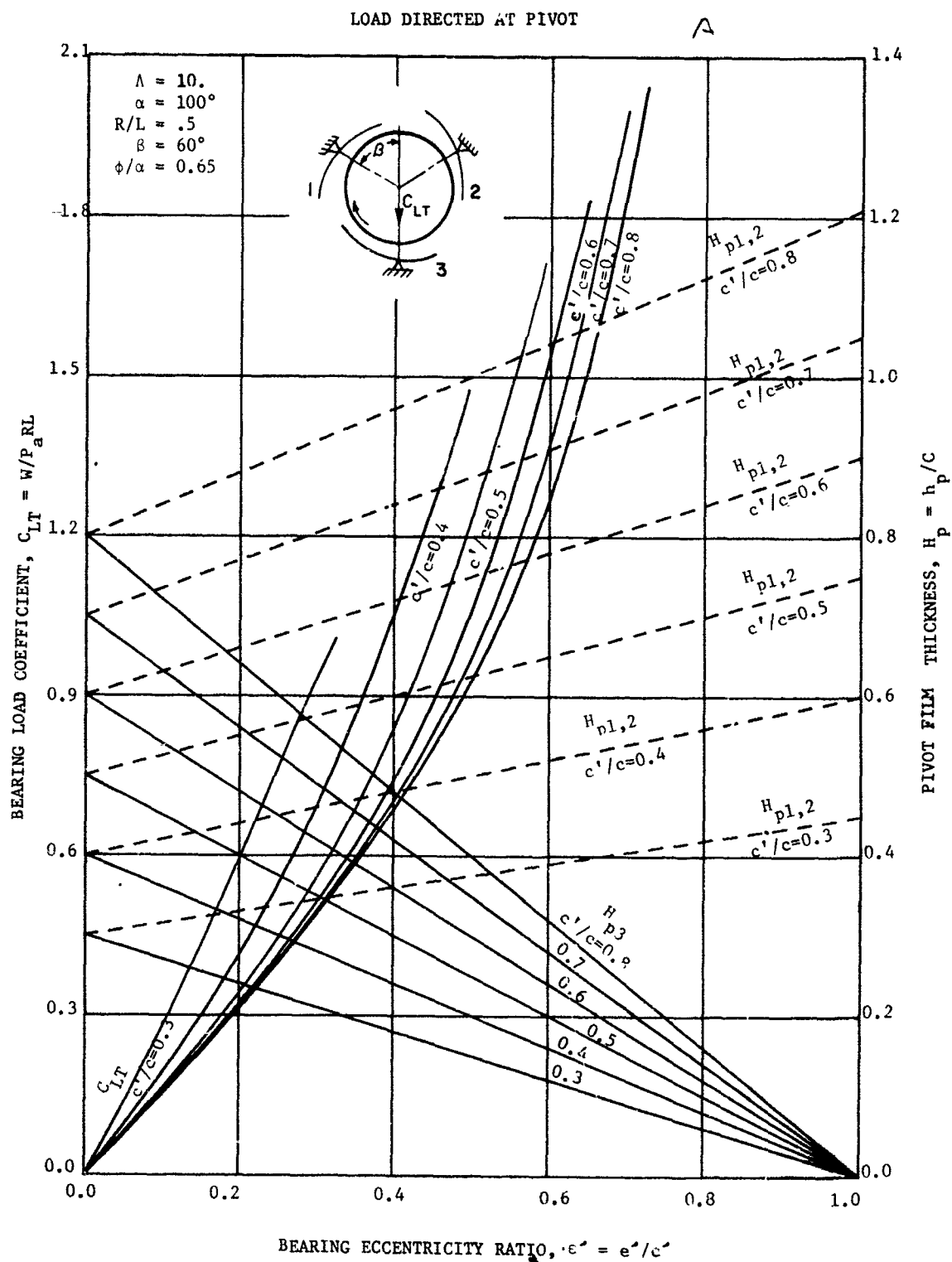
100

LOAD DIRECTED AT PIVOT

Figure 65. Bearing Load Coefficient and Pivot Clearance vs. Eccentricity Ratio for Load Directed at Pad with All Pads Rigidly Supported, Λ = 5.0, R/L = 0.25

101

Figure 66. Bearing Load Coefficient and Pivot Clearance vs. Eccentricity Ratio for Load Directed at Pad with All Pads Rigidly Supported, Λ = 5.0, R/L = 0.5
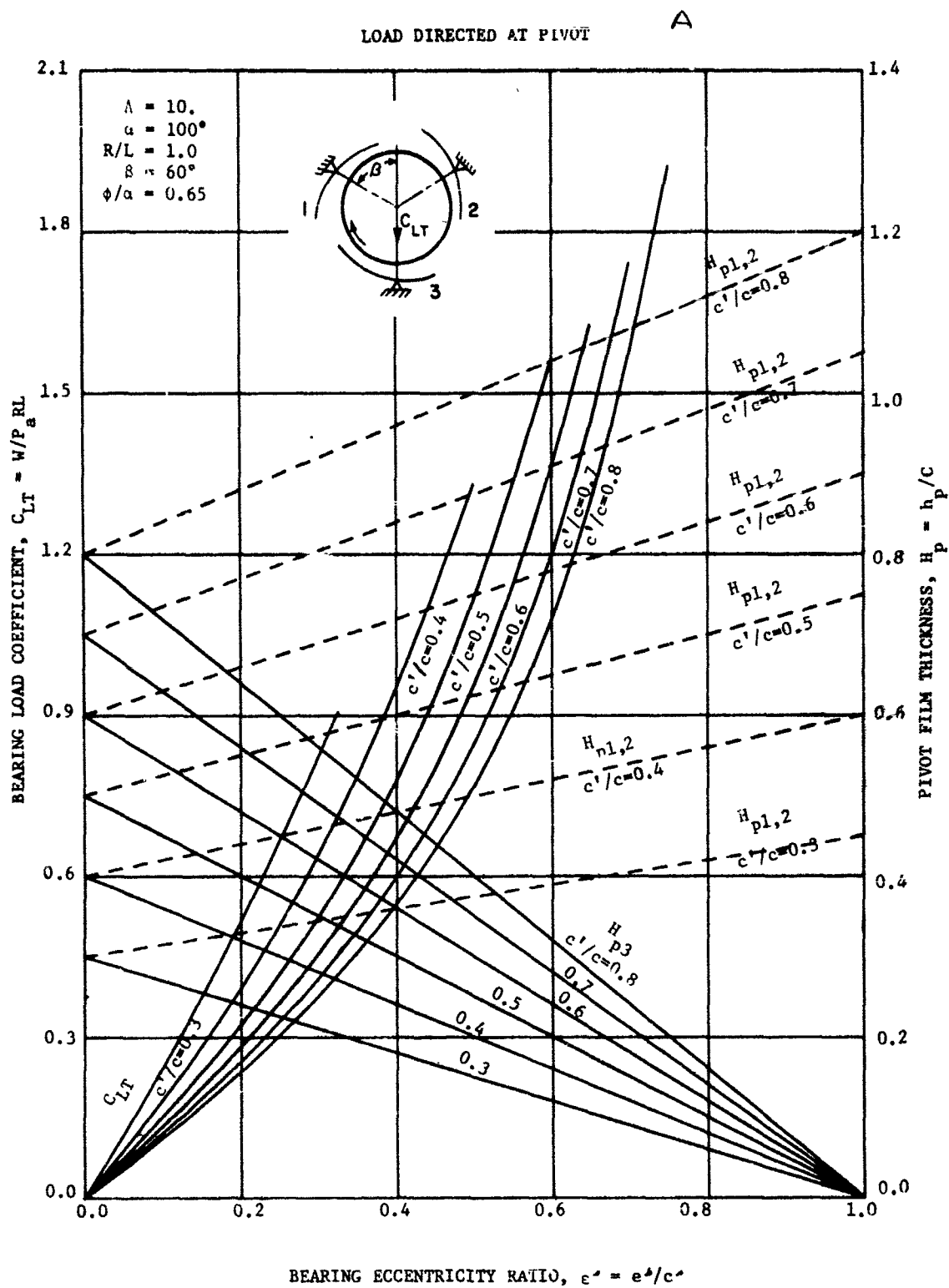
Figure 67. Bearing Load Coefficient and Pivot Clearance vs. Eccentricity Ratio for Load Directed at Pad with All Pads Rigidly Supported, $\Lambda = 5.0$, $R/L = 1.0$
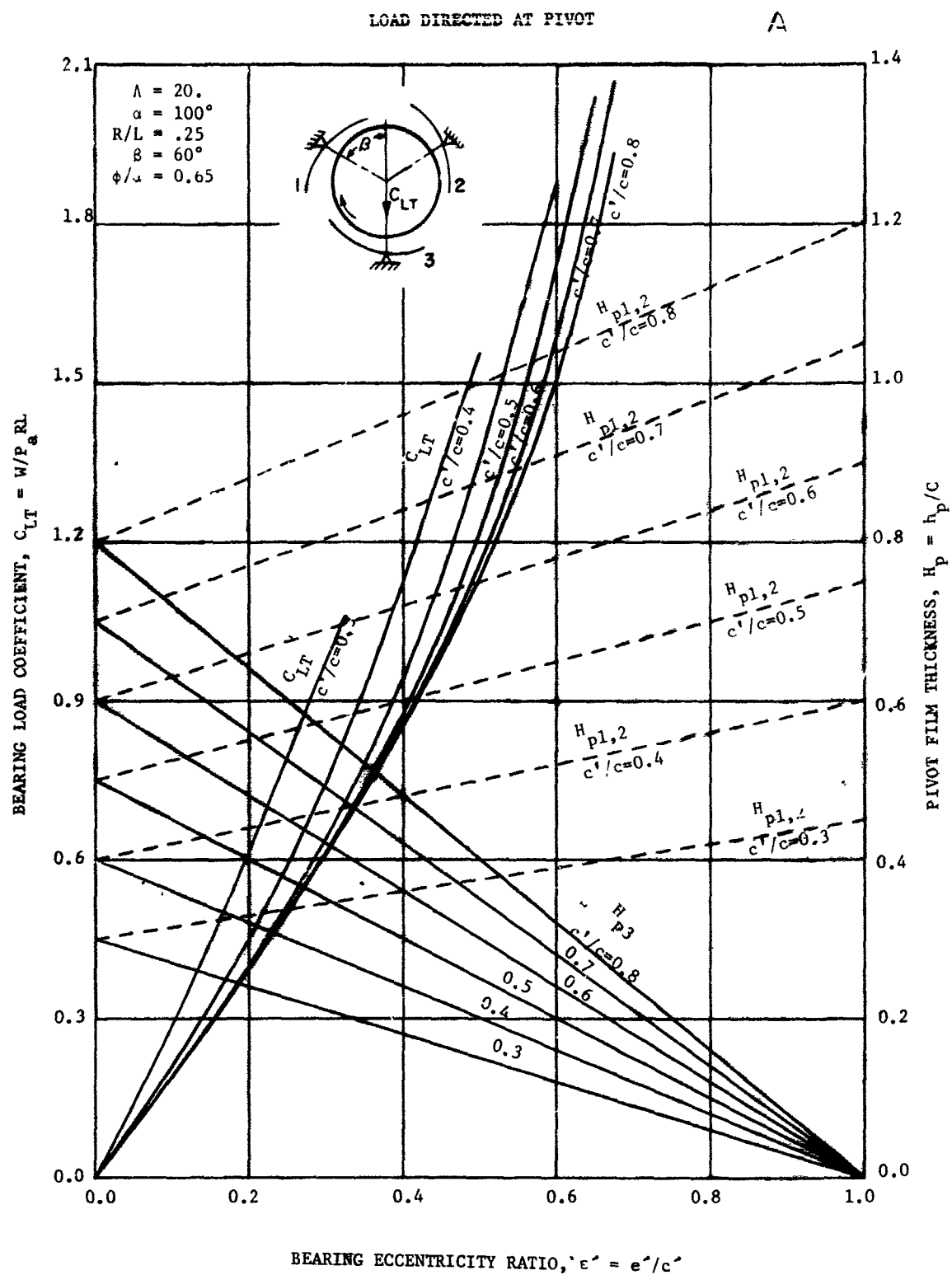
Figure 68. Bearing Load Coefficient and Pivot Clearance vs. Eccentricity Ratio for Load Directed at Pad with All Pads Rigidly Supported, Λ = 10.0, R/L = 0.25

104

Figure 69. Bearing Load Coefficient and Pivot Clearance vs. Eccentricity
Ratio for Load Directed at Pad with All Pads Rigidly Supported,
$\Lambda = 10.0$, R/L = 0.5

Figure 70. Bearing Load Coefficient and Pivot Clearance vs. Eccentricity Ratio for Load Directed at Pad with All Pads Rigidly Supported, $\Lambda = 10.0$, $R/L = 1.0$
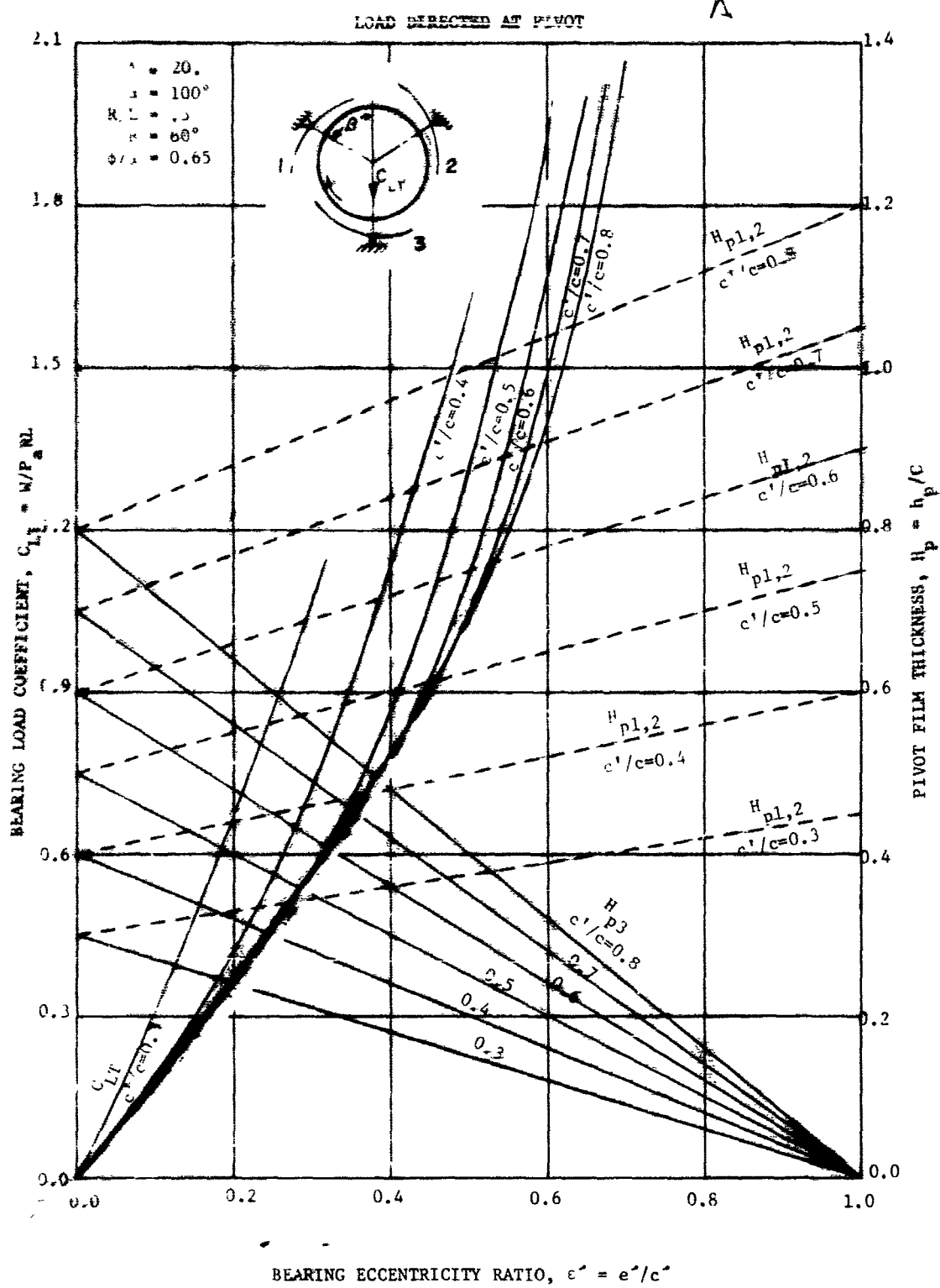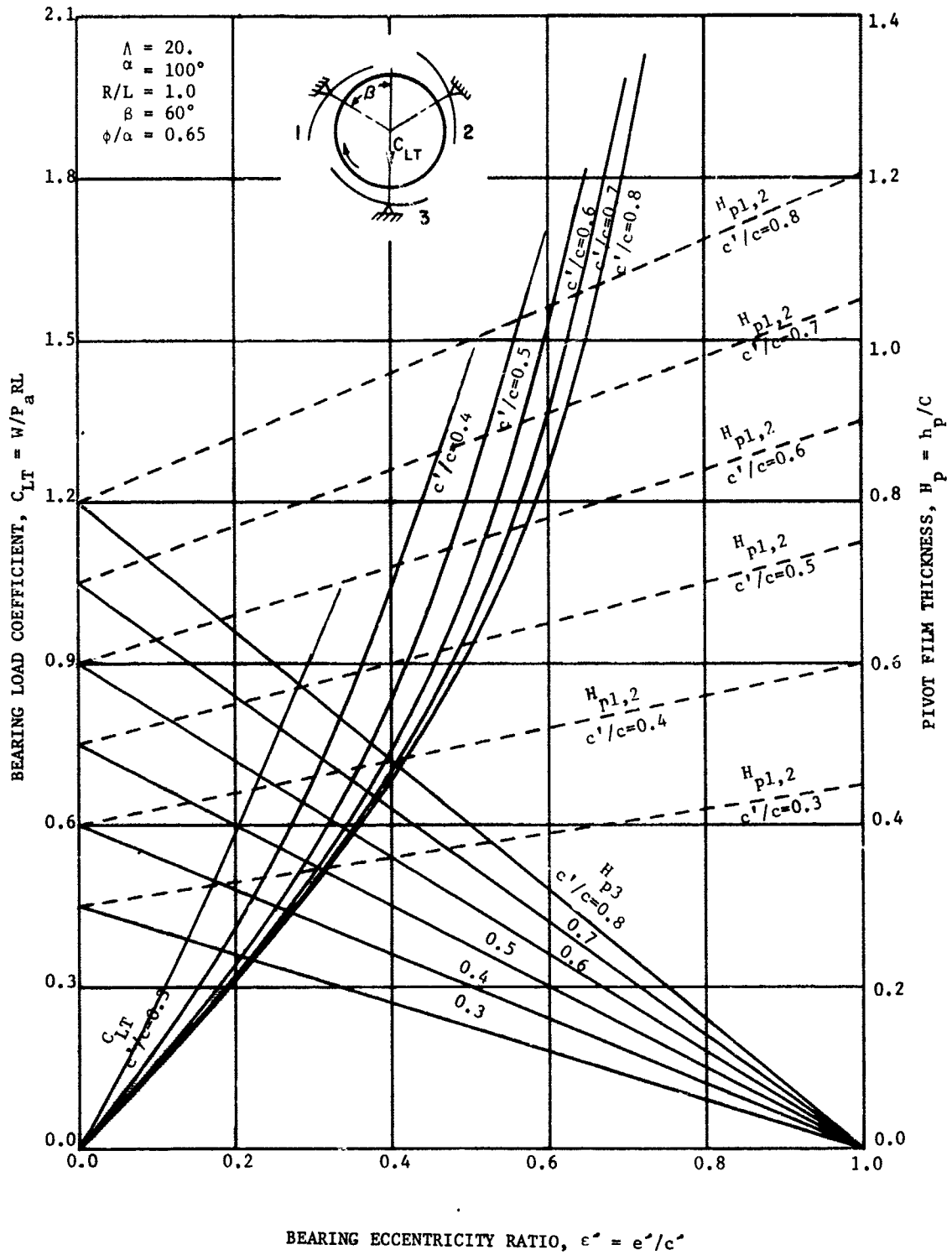
Figure 71. Bearing Load Coefficient and Pivot Clearance vs. Eccentricity Ratio for Load Directed at Pad with All Pads Rigidly Supported, $\Lambda = 20.0$, R/L = 0.25

107

Figure 72. Bearing Load Coefficient and Pivot Clearance vs. Eccentricity Ratio for Load Directed at Pad with All Pads Rigidly Supported, $\Lambda = 20.0$, $R/L = 0.5$

Figure 73. Bearing Load Coefficient and Pivot Clearance vs. Eccentricity Ratio for Load Directed at Pad with All Pads Rigidly Supported, $\Lambda = 20.0$, $R/L = 1.0$

109

5. BEARING LOAD COEFFICIENT AND PIVOT FILM THICKNESS

vs. ECCENTRICITY RATIO
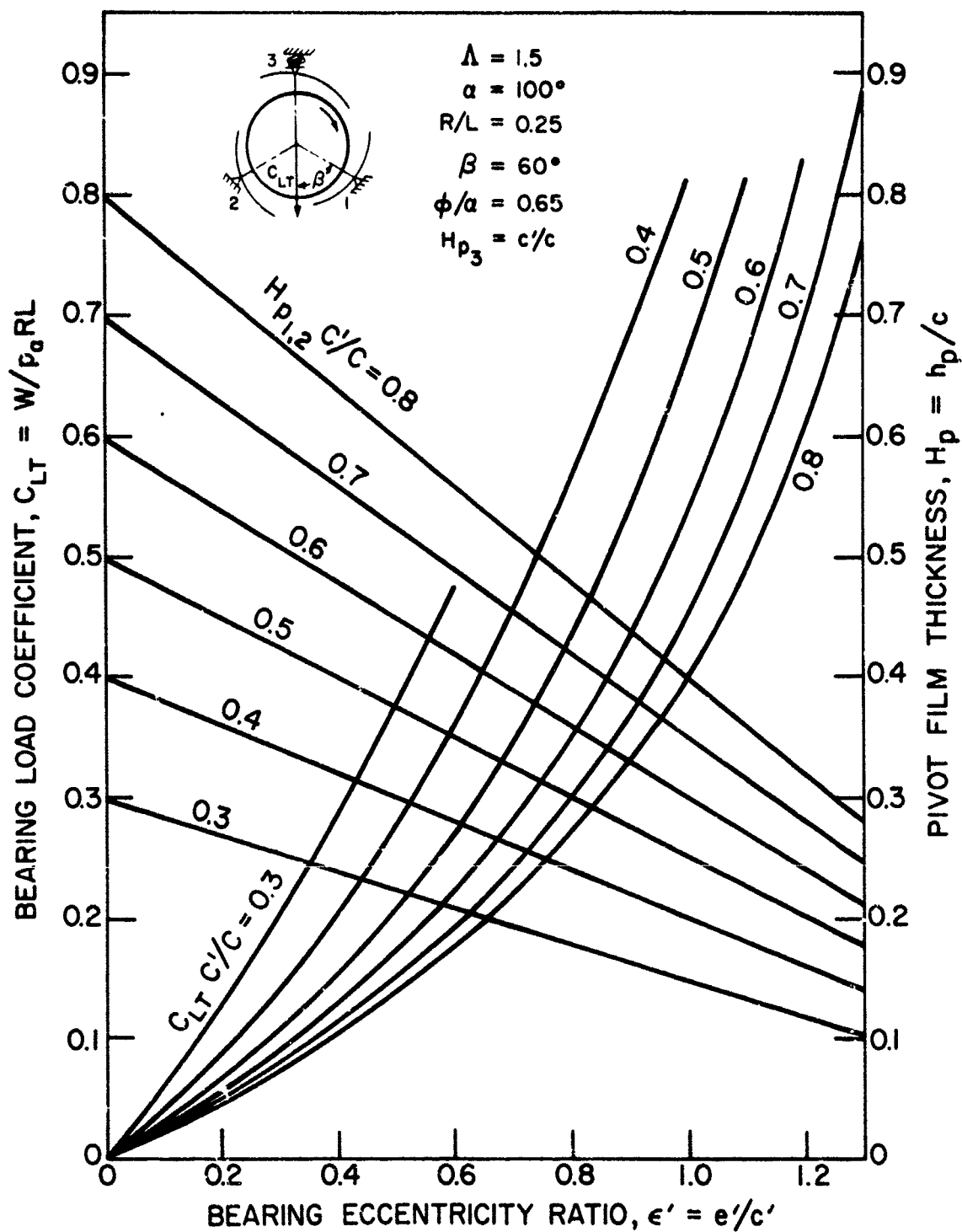
(ONE SPRING LOADED PAD)

Figure 74. Bearing Load Coefficient and Pivot Clearance vs. Eccentricity Ratio for Load Directed Between Pads with Top Pad Spring Loaded, Λ = 1.5, R/L = 0.25
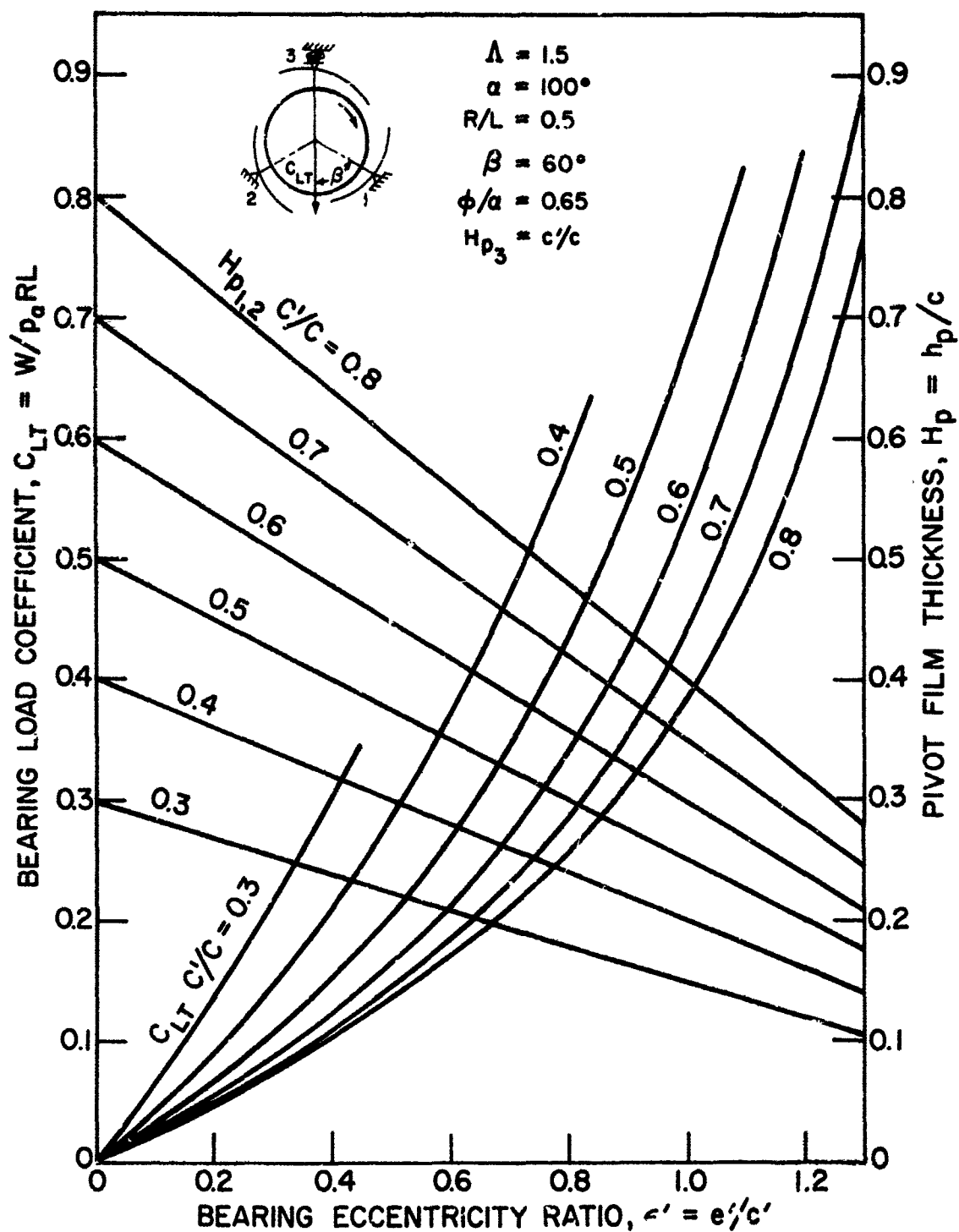
111

Figure 75. Bearing Load Coefficient and Pivot Clearance vs. Eccentricity Ratio for Load Directed Between Pads with Top Pad Spring Loaded, $\Lambda = 1.5$, $R/L = 0.5$
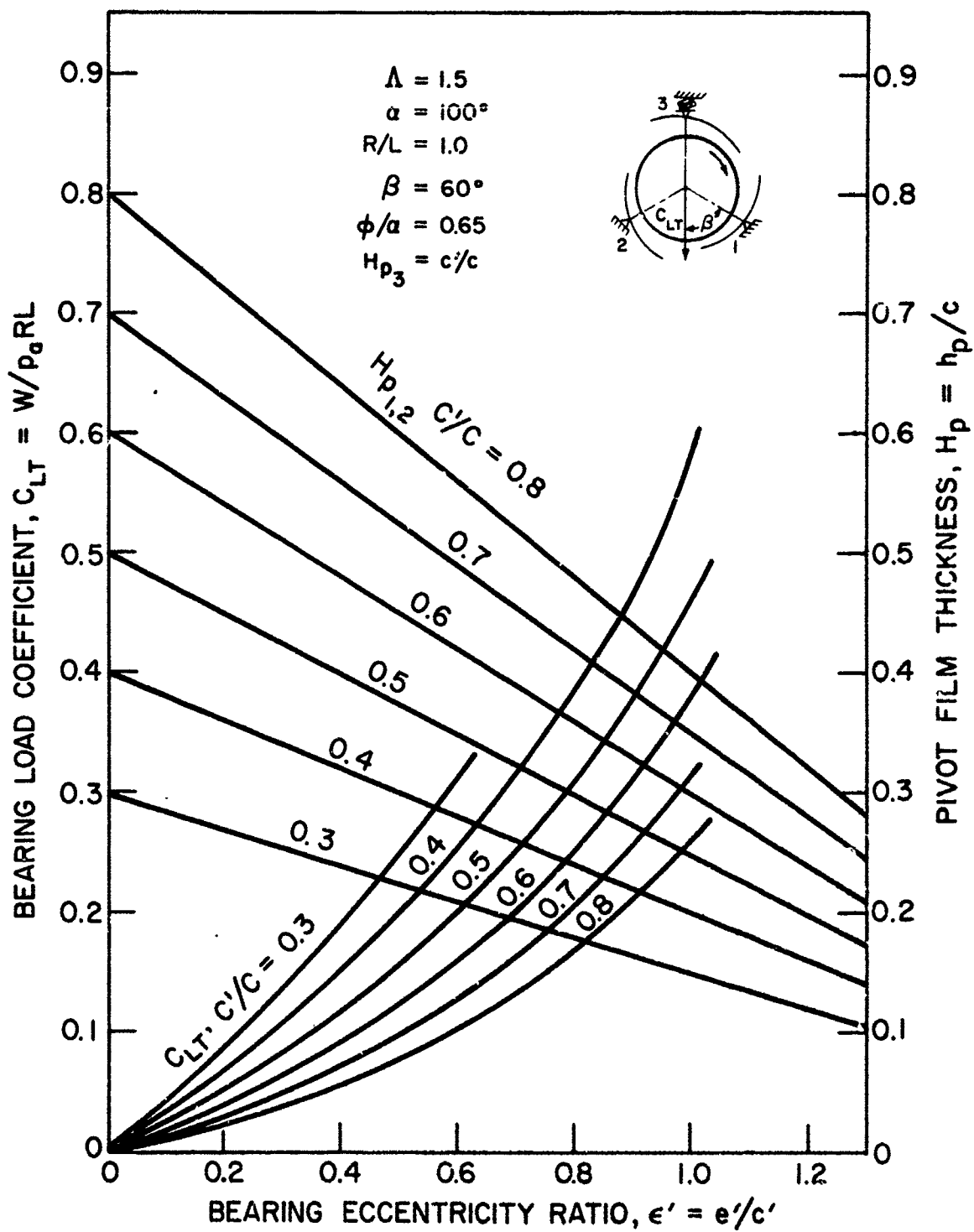
Figure 76. Bearing Load Coefficient and Pivot Clearance vs. Eccentricity Ratio for Load Directed Between Pads with Top Pad Spring Loaded, $\Lambda = 1.5$, $R/L = 1.0$
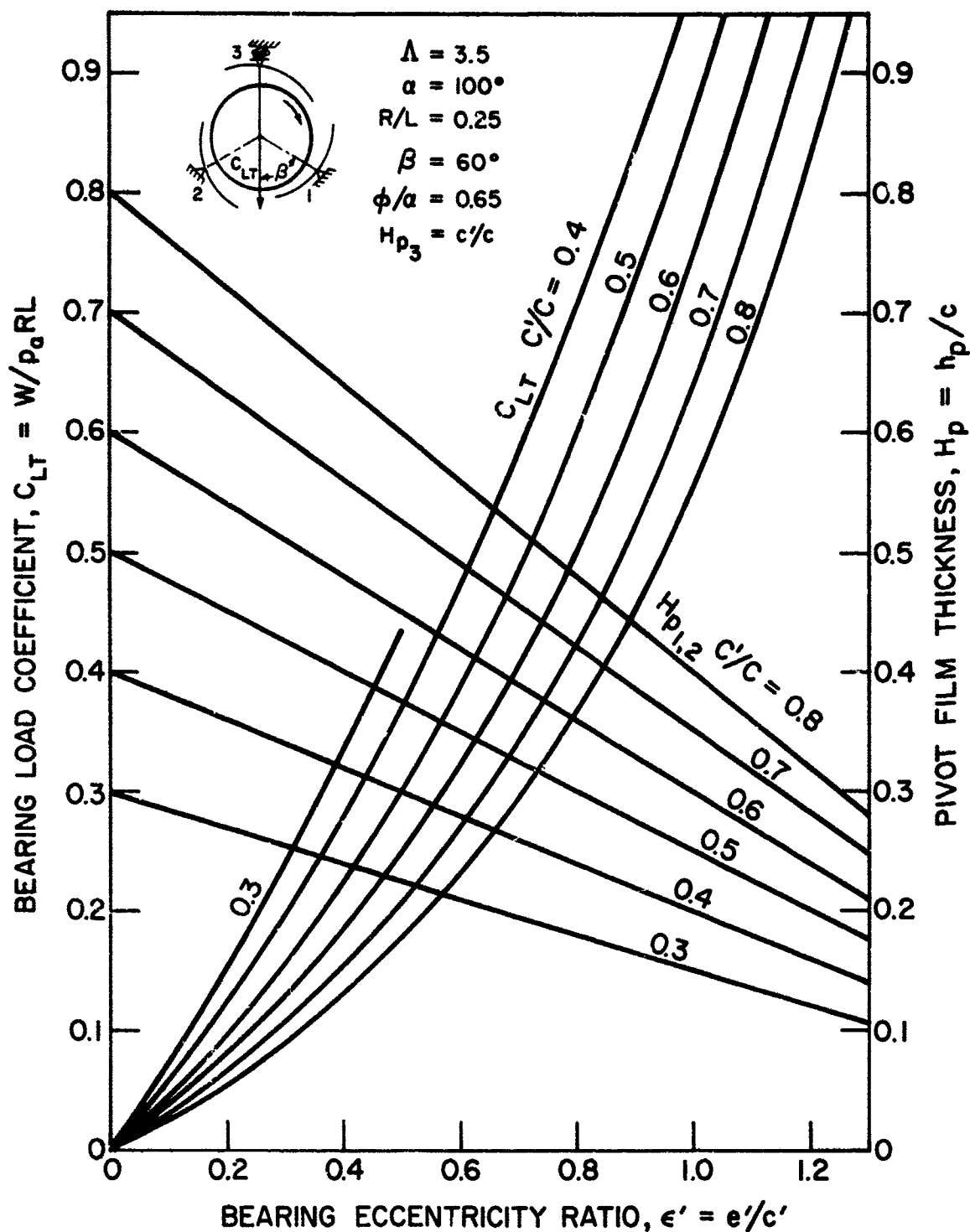
Figure 77. Bearing Load Coefficient and Pivot Clearance vs. Eccentricity Ratio for Load Directed Between Pads with Top Pad Spring Loaded, Λ = 3.5, R/L = 0.25
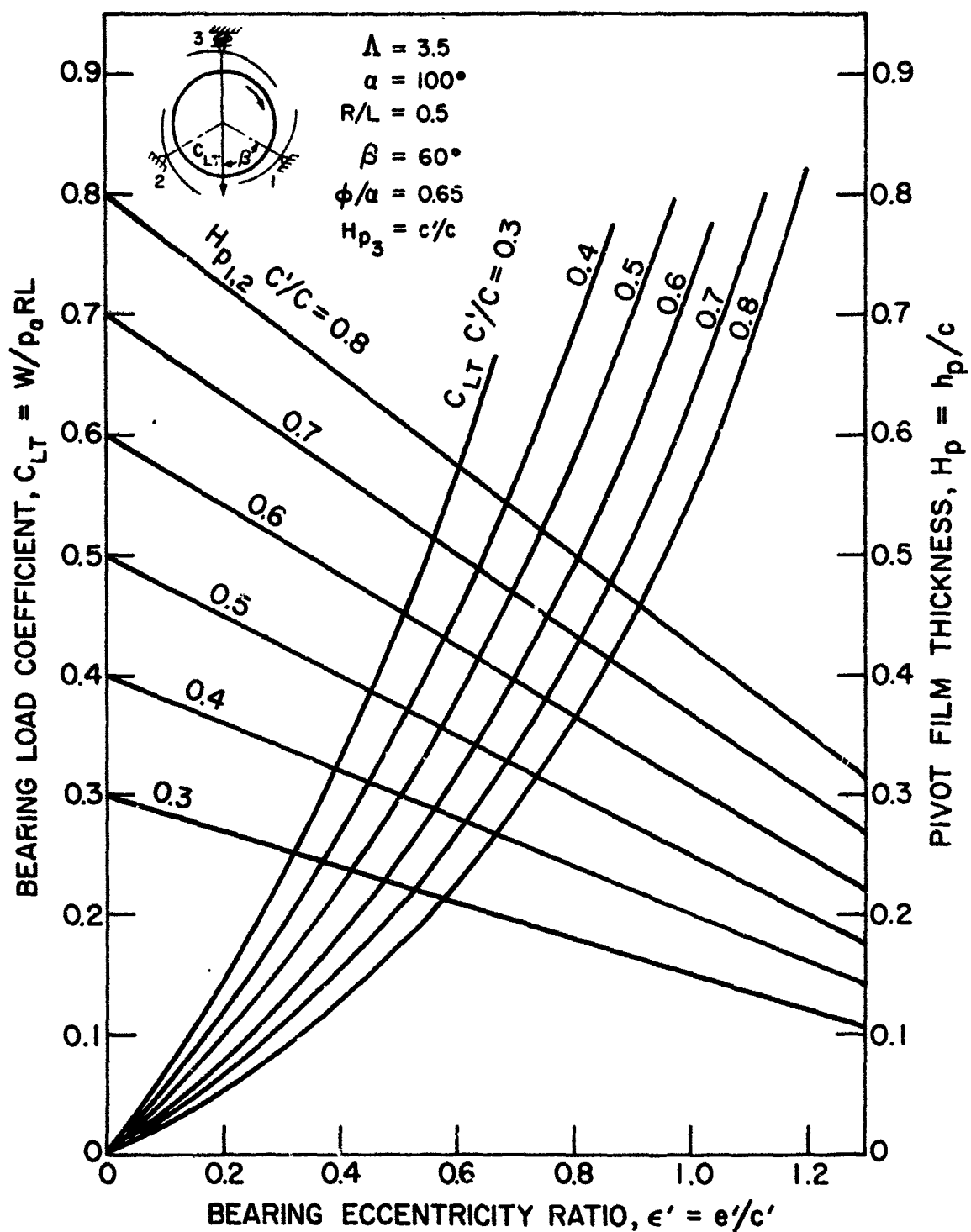
Figure 78. Bearing Load Coefficient and Pivot Clearance vs. Eccentricity Ratio for Load Directed Between Pads with Top Pad Spring Loaded, $\Lambda = 3.5$, $R/L = 0.5$
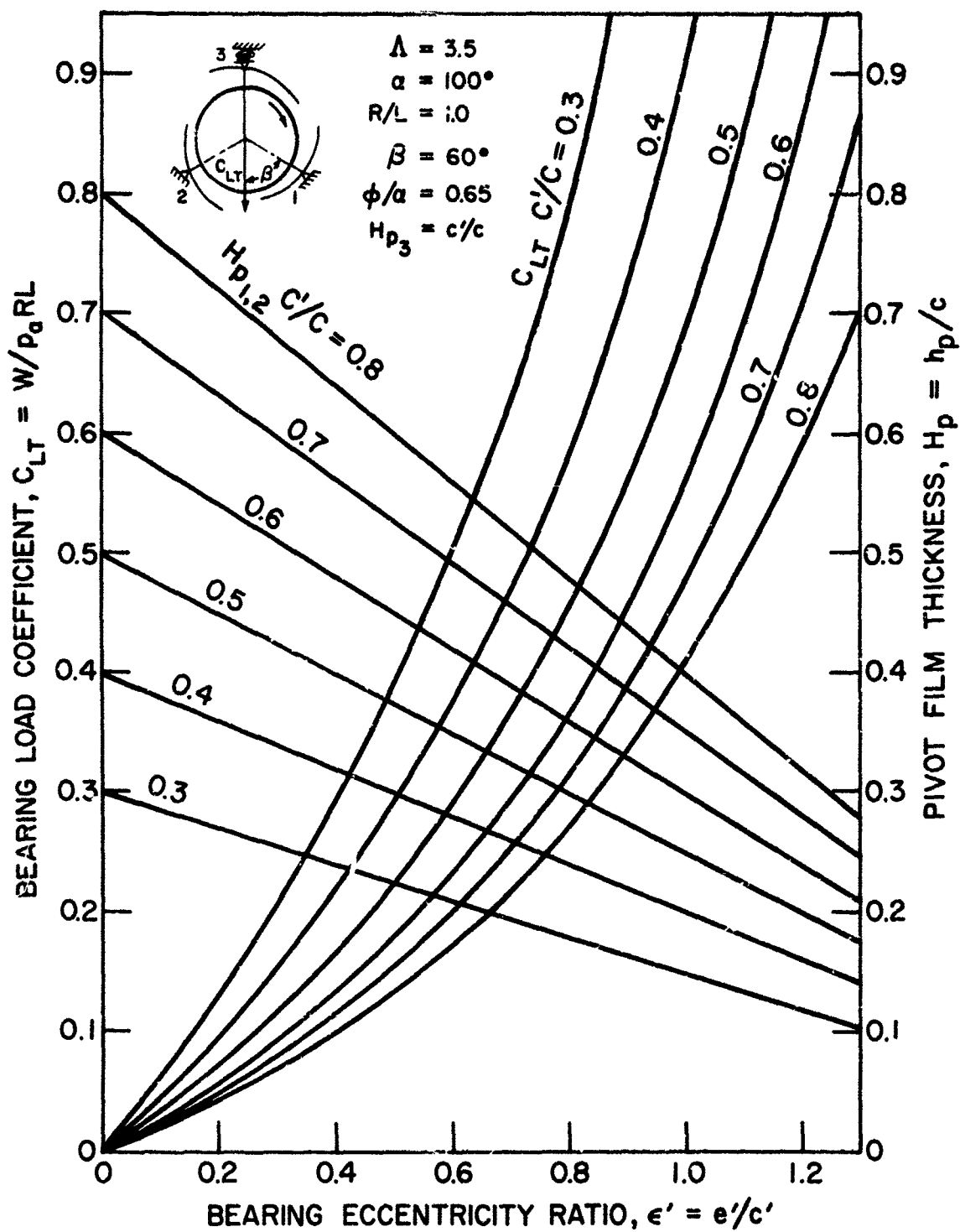
Figure 79. Bearing Load Coefficient and Pivot Clearance vs. Eccentricity Ratio for Load Directed Between Pads with Top Pad Spring Loaded, Λ = 3.5, R/L = 1.0
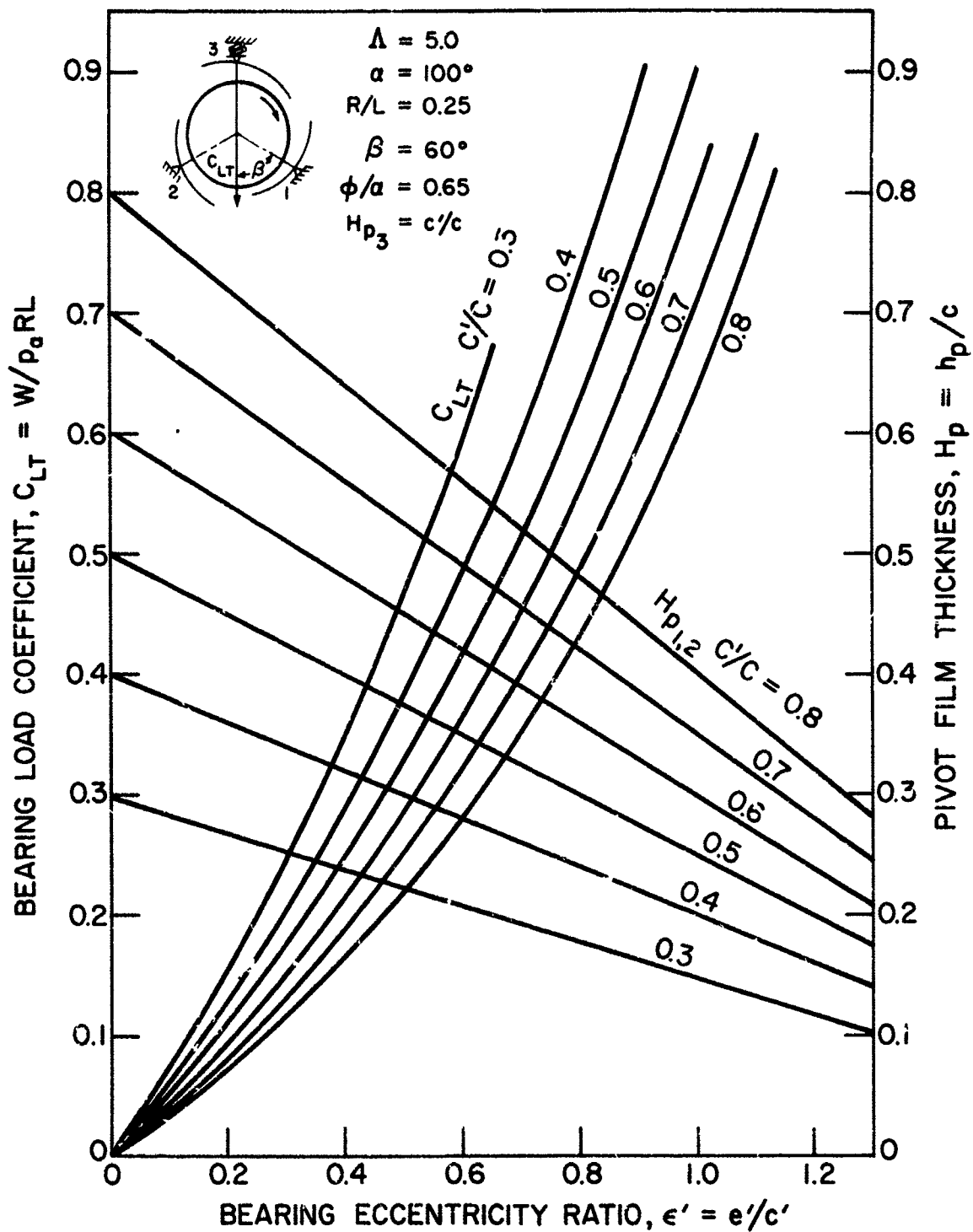
116

Figure 80. Bearing Load Coefficient and Pivot Clearance vs. Eccentricity
Ratio for Load Directed Between Pads with Top Pad Spring
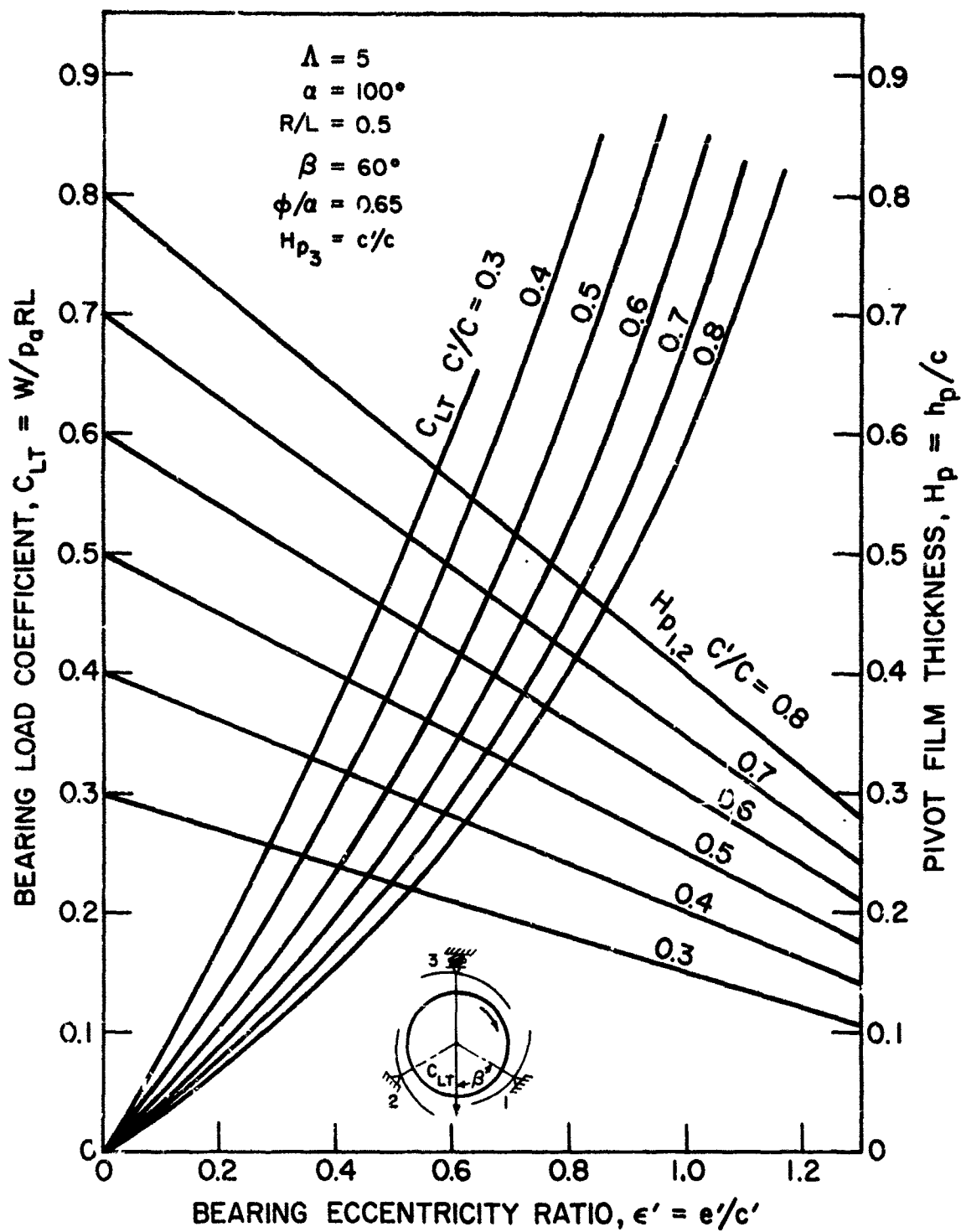Loaded, $\Lambda = 5.0$, $R/L = 0.25$

117

Figure 81. Bearing Load Coefficient and Pivot Clearance vs. Eccentricity Ratio for Load Directed Between Pads with Top Pad Spring Loaded, $\Lambda = 5.0$, $R/L = 0.5$
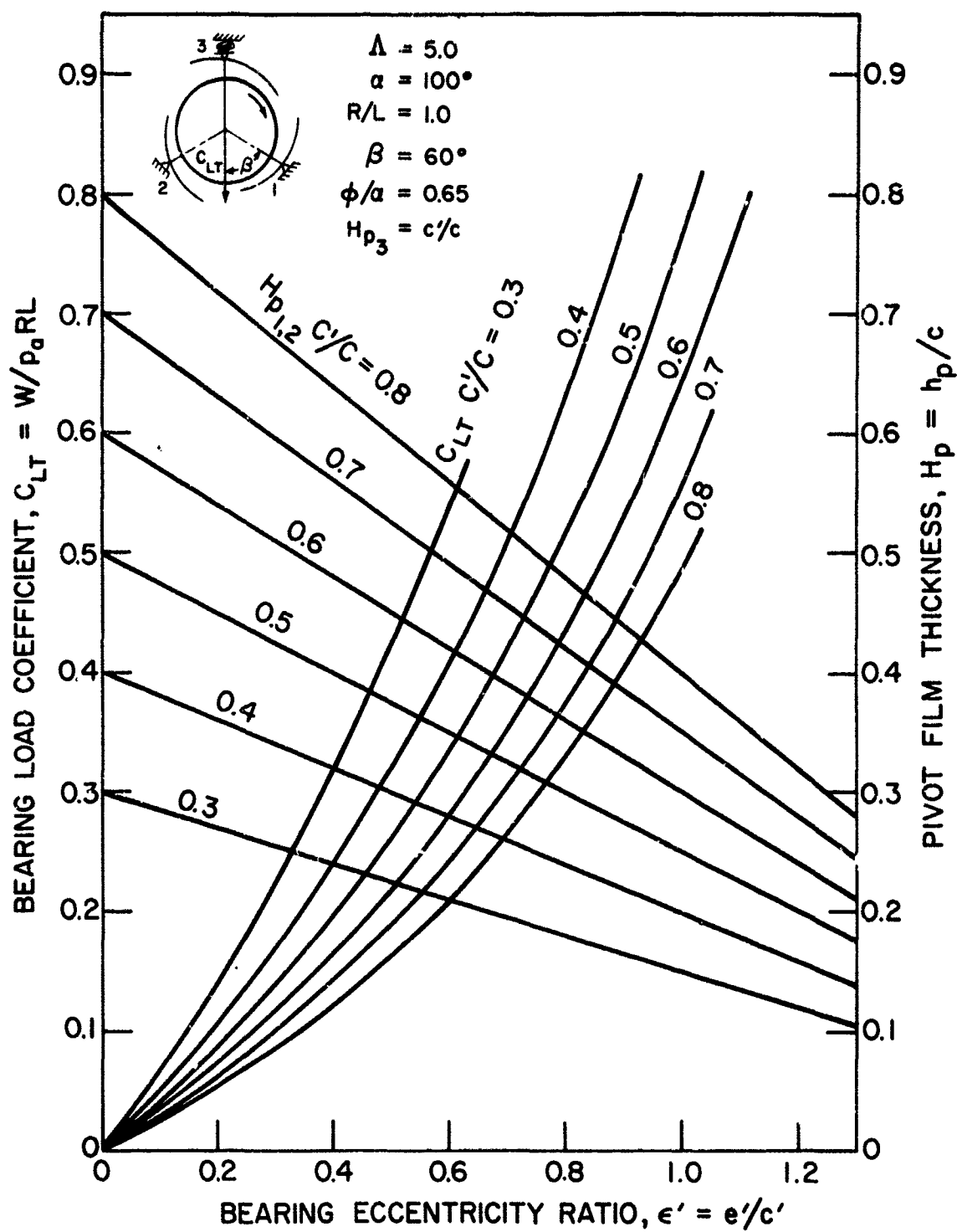
118

Figure 82. Bearing Load Coefficient and Pivot Clearance vs. Eccentricity Ratio for Load Directed Between Pads with Top Spring Loaded, $\Lambda = 5.0$, $R/L = 1.0$

119

Figure 83. Bearing Load Coefficient and Pivot Clearance vs. Eccentricity Ratio for Load Directed Between Pads with Top Pad Spring Loaded, $\Lambda = 10.0$, $R/L = 0.25$

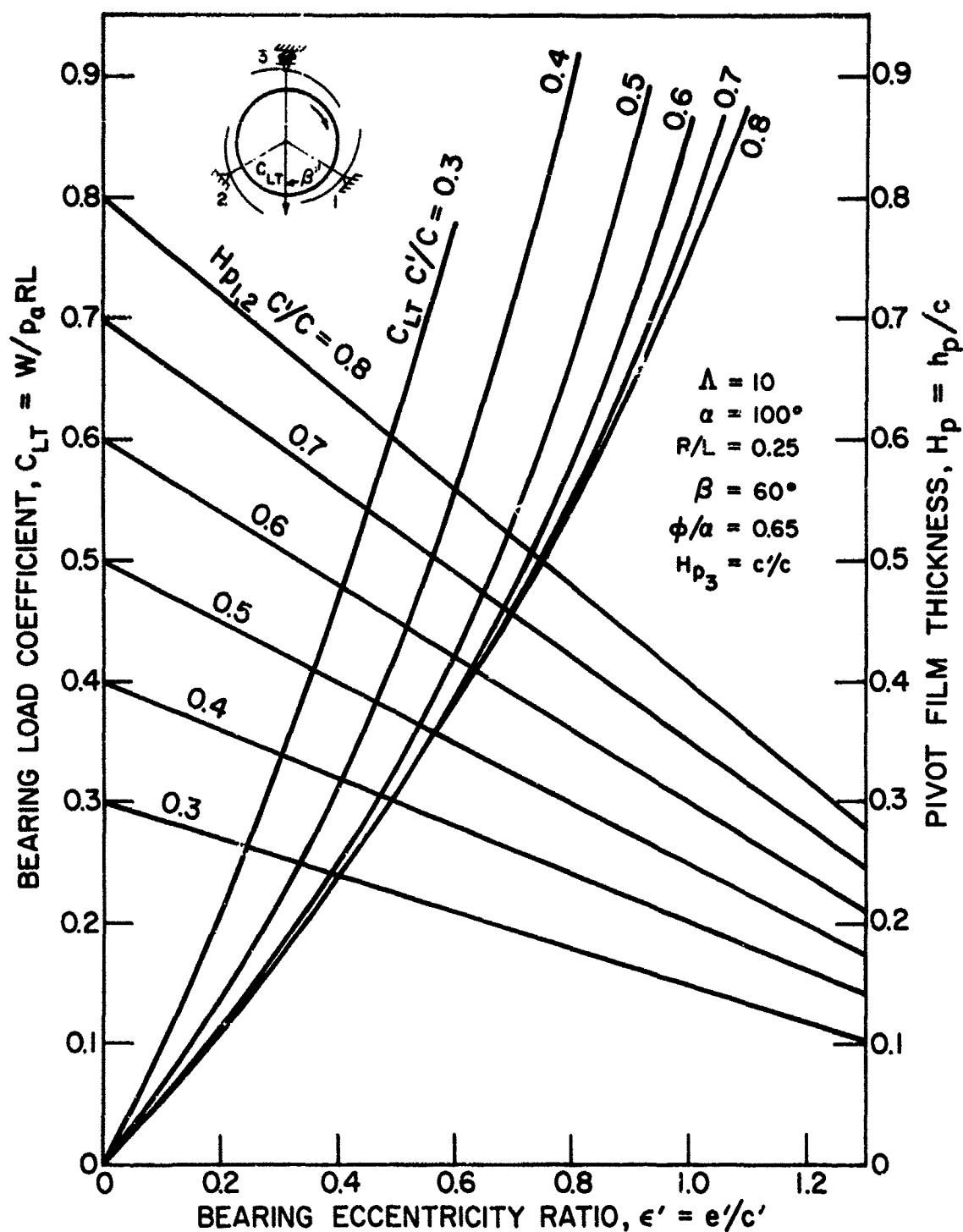Figure 84. Bearing Load Coefficient and Pivot Clearance vs. Eccentricity Ratio for Load Directed Between Pads with Top Pad Spring Loaded, $\Lambda = 10.0$, R/L = 0.5

121
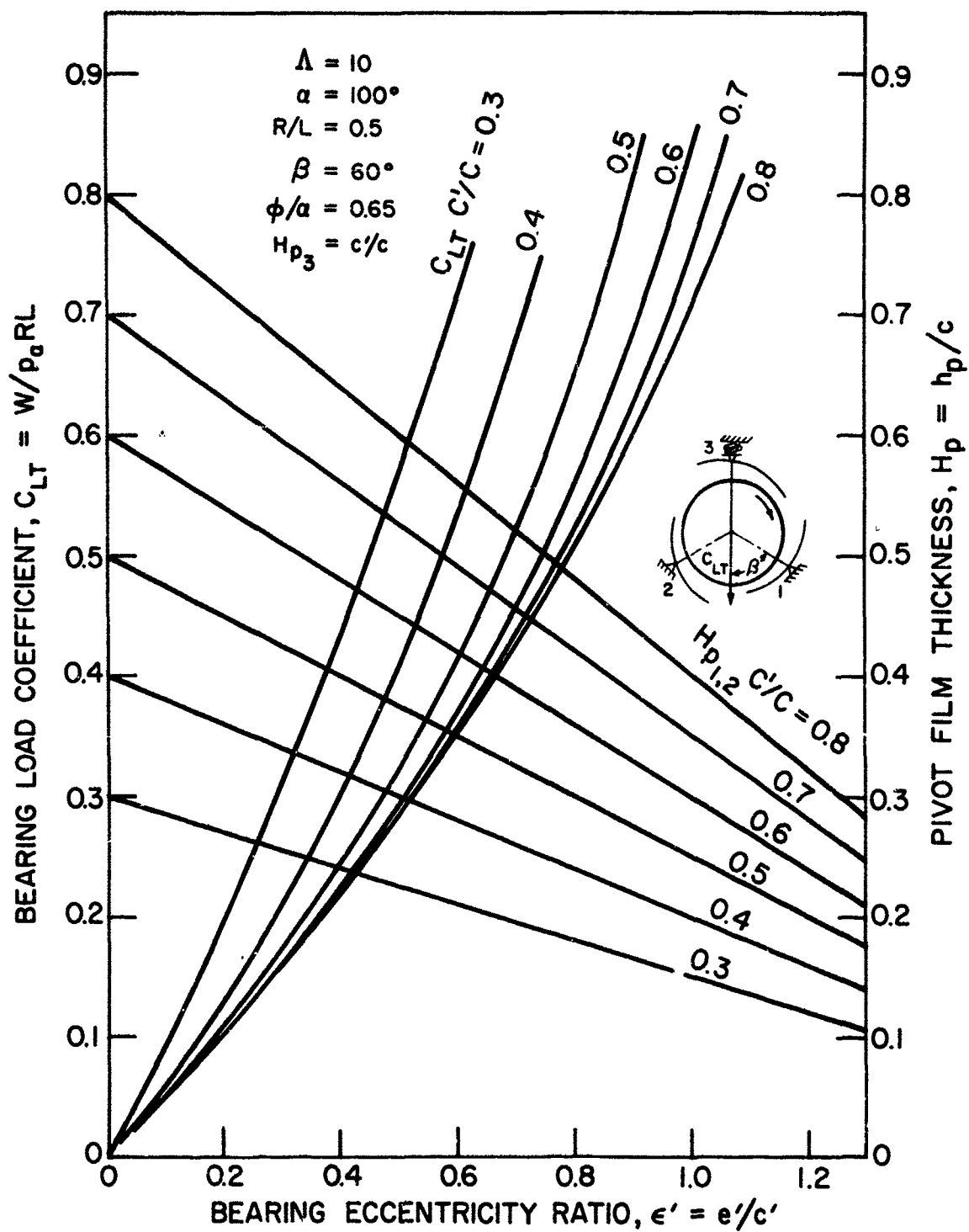
Figure 85.   Bearing Load Coefficient and Pivot Clearance vs. Eccentricity
Ratio for Load Directed Between Pads with Top Pad Spring
Loaded, Λ = 10, R/L = 1.0

122

Figure 86. Bearing Load Coefficient and Pivot Clearance vs. Eccentricity Ratio for Load Directed Between Pads with Top Pad Spring Loaded, $\Lambda = 20.0$, R/L = 0.25
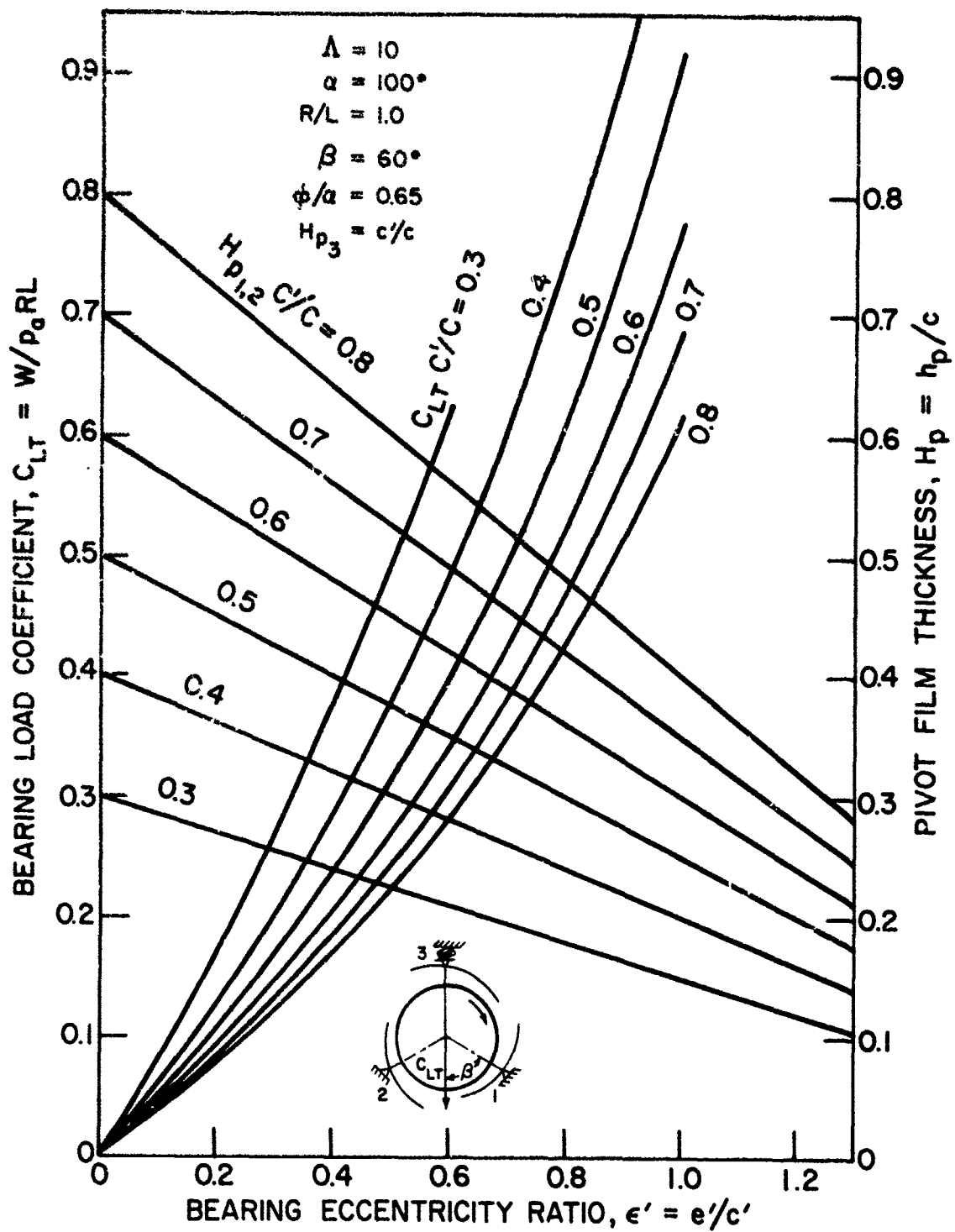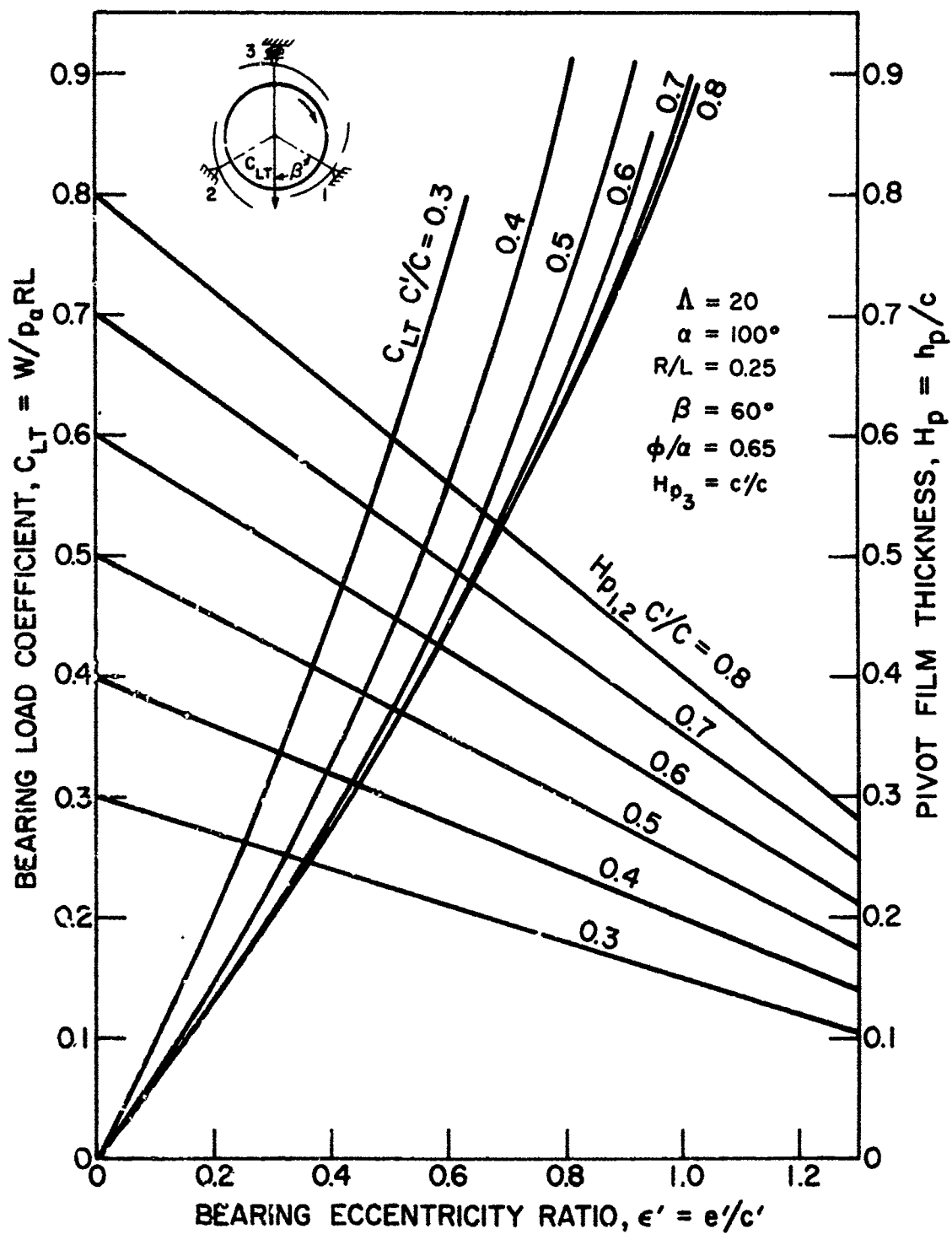
123

Figure 87. Bearing Load Coefficient and Pivot Clearance vs. Eccentricity Ratio for Load Directed Between Pads with Top Pad Spring Loaded, $\Lambda = 20$, $R/L = 0.5$
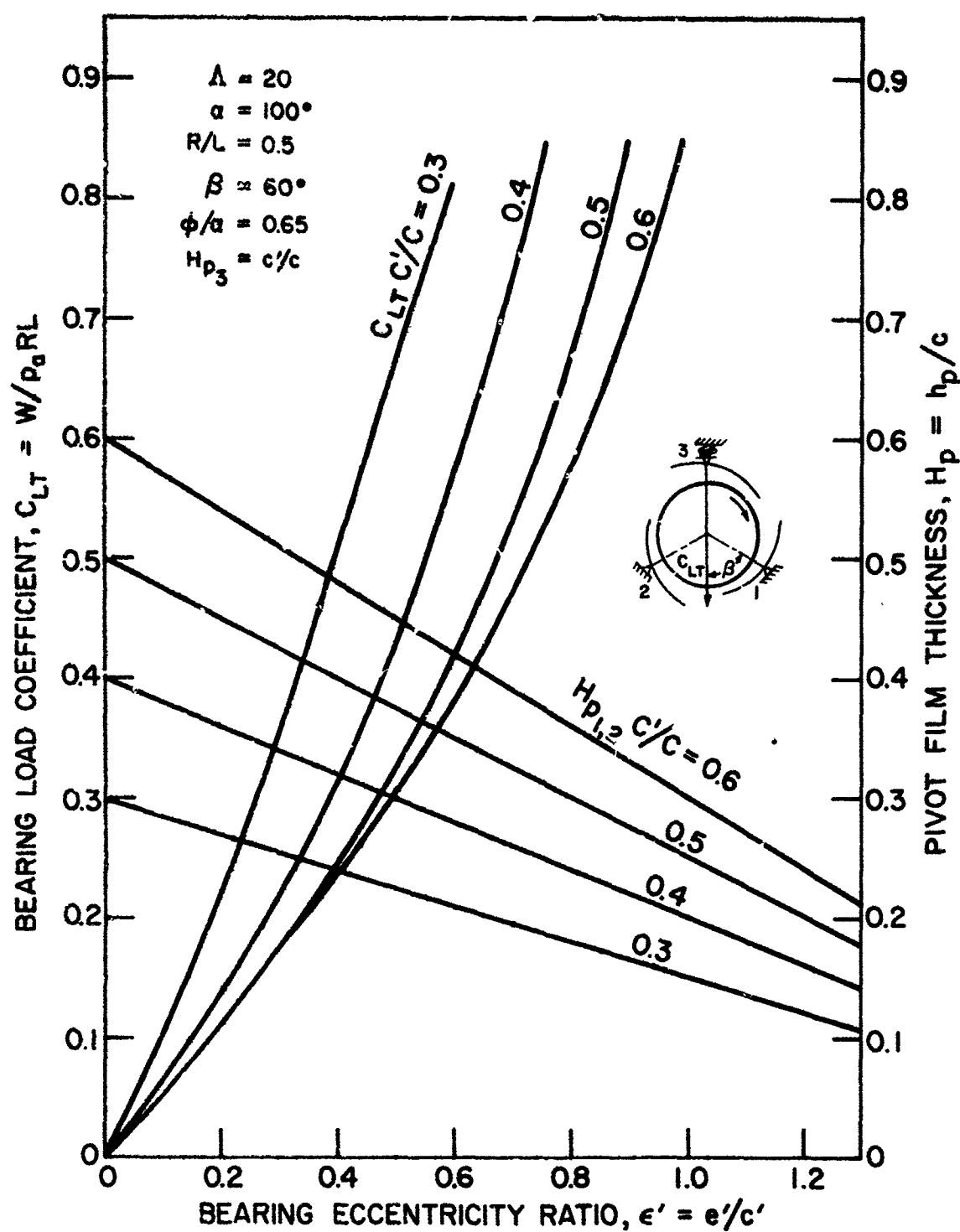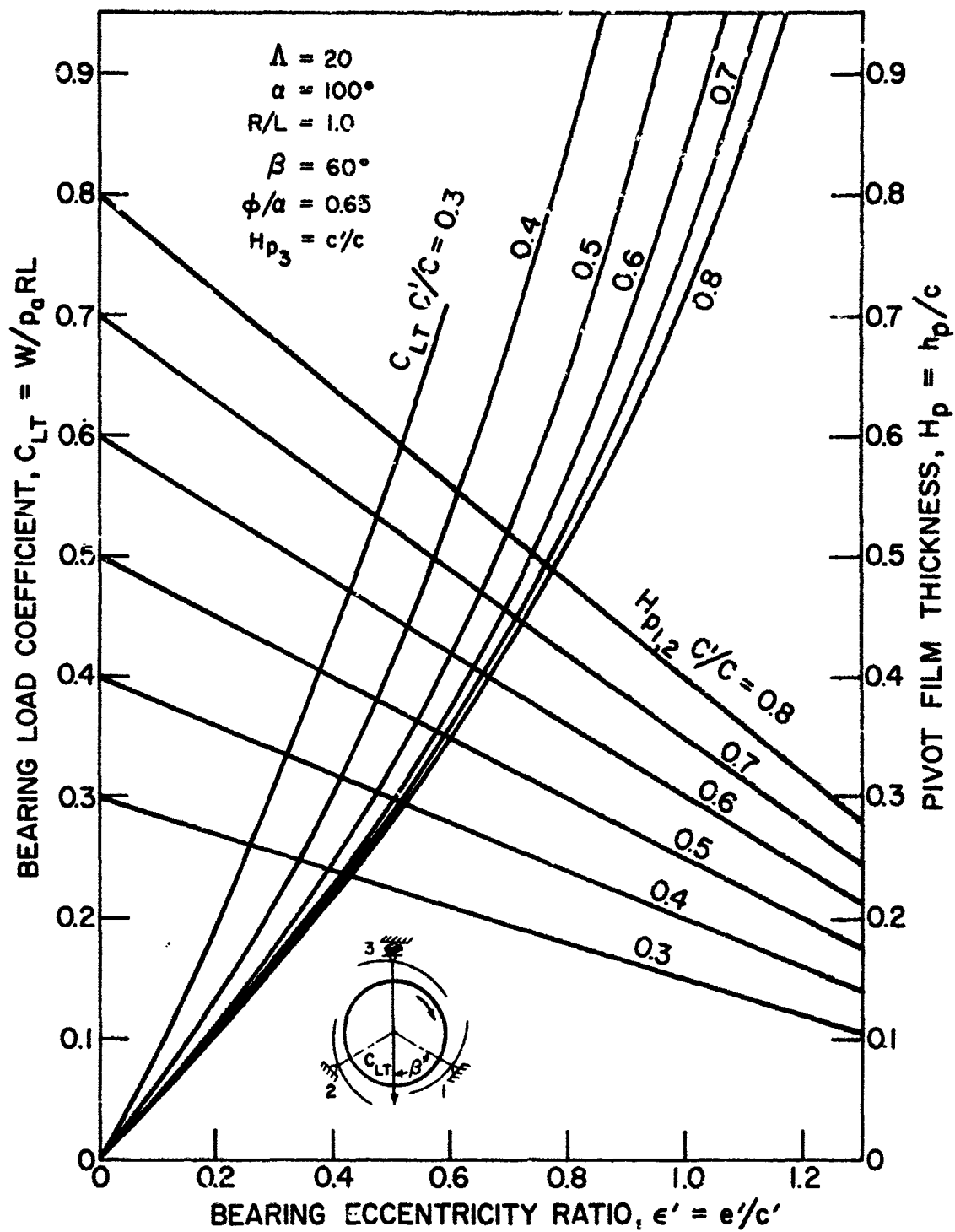
Figure 88. Bearing Load Coefficient and Pivot Clearance vs. Eccentricity Ratio for Load Directed Between Pads with Top Pad Spring Loaded, $\Lambda = 20$, $R/L = 1.0$

Figure 89.   Bearing Load Coefficient and Pivot Clearance vs. Eccentricity
Ratio for Load Directed at Spring Loaded Pad, Λ = 1.5, R/L = 0.5

Figure 90. Bearing Load Coefficient and Pivot Clearance vs. Eccentricity
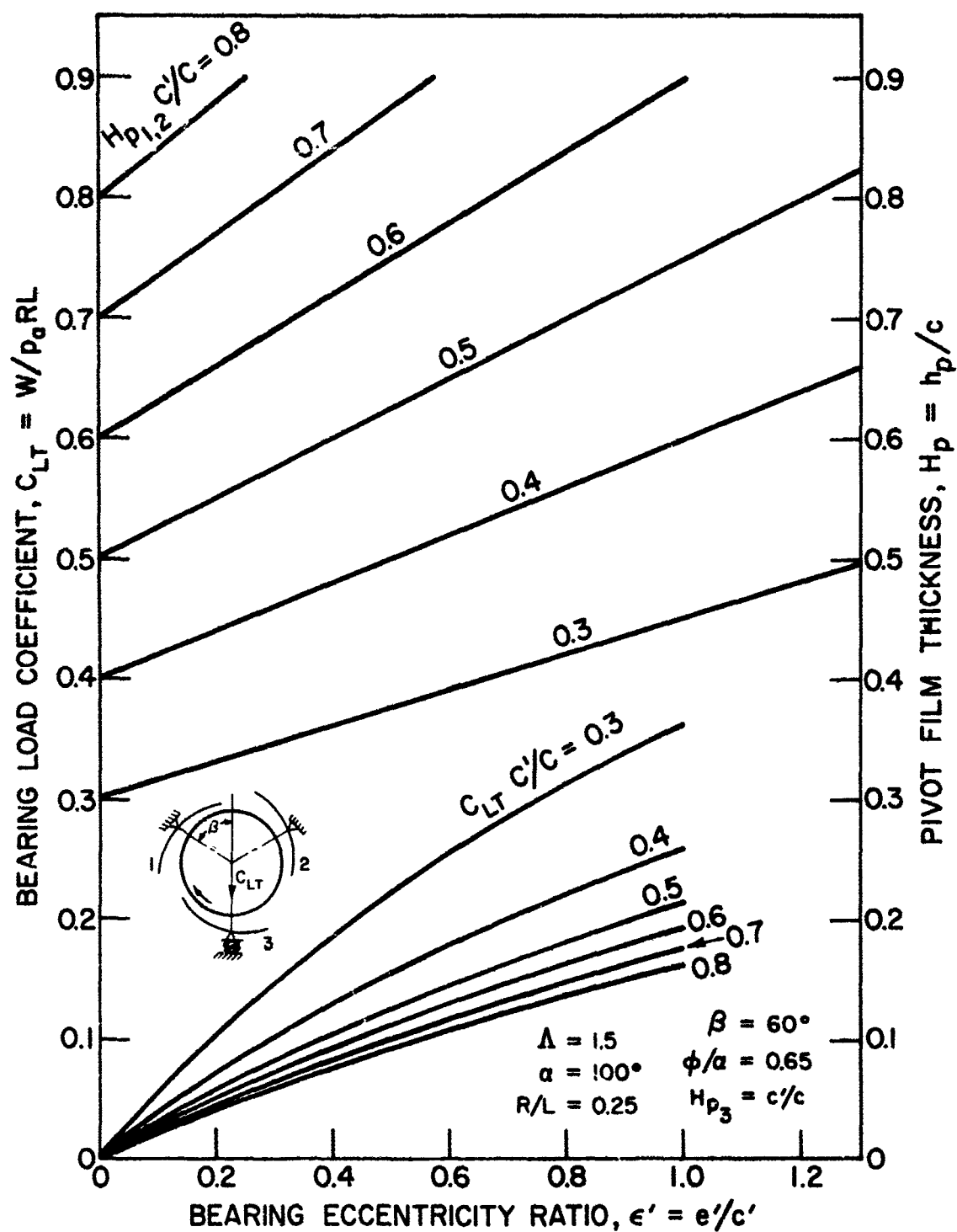Ratio for Load Directed at Spring Loaded Pad, Λ = 1.5, R/L = 0.5

127

Figure 91. Bearing Load Coefficient and Pivot Clearance vs. Eccentricity Ratio for Load Directed at Spring Loaded Pad, $\Lambda = 1.5$, $R/L = 1.0$

128

Figure 92. Bearing Load Coefficient and Pivot Clearance vs. Eccentricity
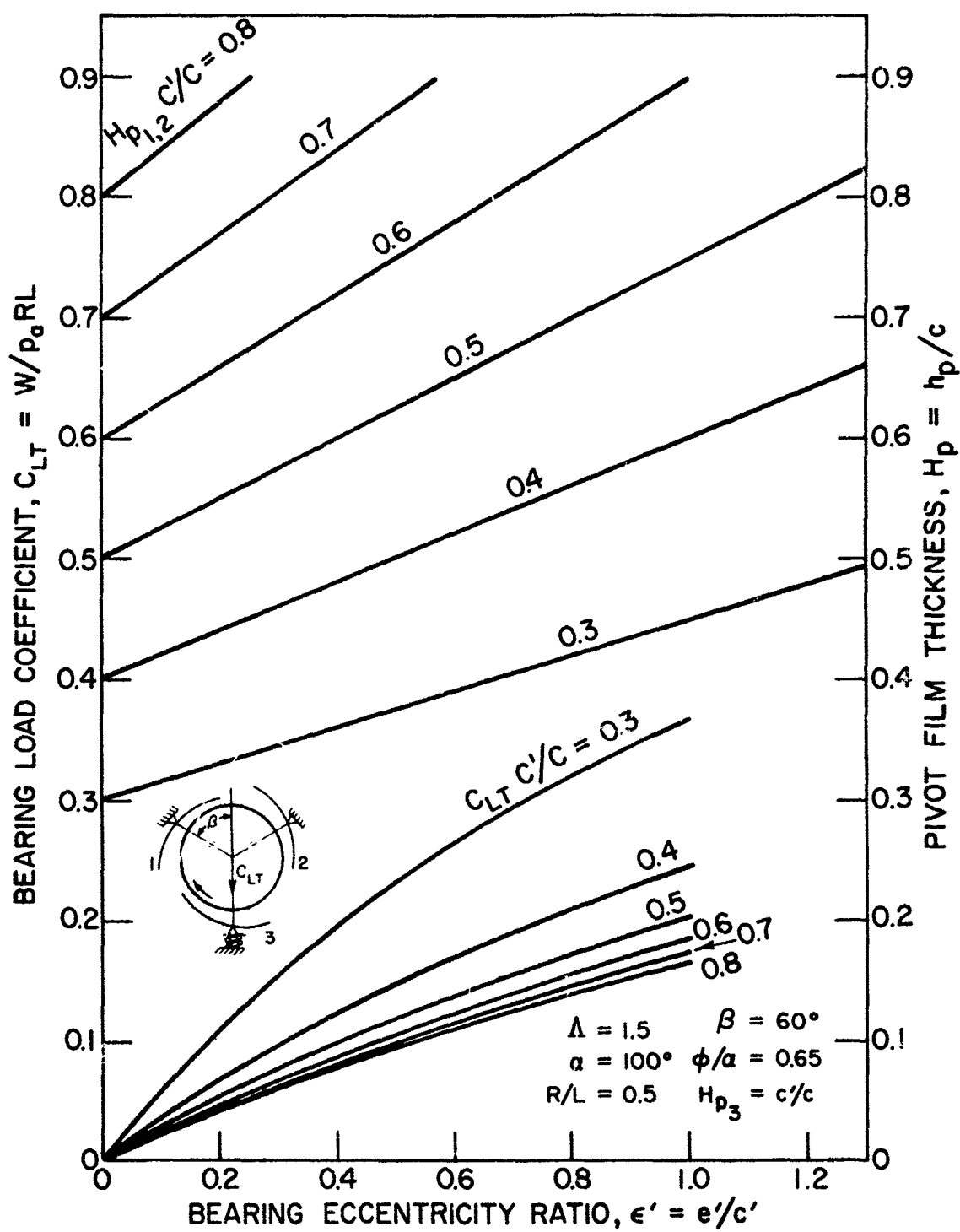Ratio for Load Directed at Spring Loaded Pad, Λ = 3.5, R/L = 0.25

Figure 93. Bearing Load Coefficient and Pivot Clearance vs. Eccentricity Ratio for Load Directed at Spring Loaded Pad, Λ = 3.5, R/L = 0.5

130

Figure 94. Bearing Load Coefficient and Pivot Clearance vs. Eccentricity
Ratio for Load Directed at Spring Loaded Pad, Λ = 3.5, R/L = 1.0

Figure 95. Bearing Load Coefficient and Pivot Clearance vs. Eccentricity Ratio for Load Directed at Spring Loaded Pad, $\Lambda = 5.0$, $R/L = 0.25$
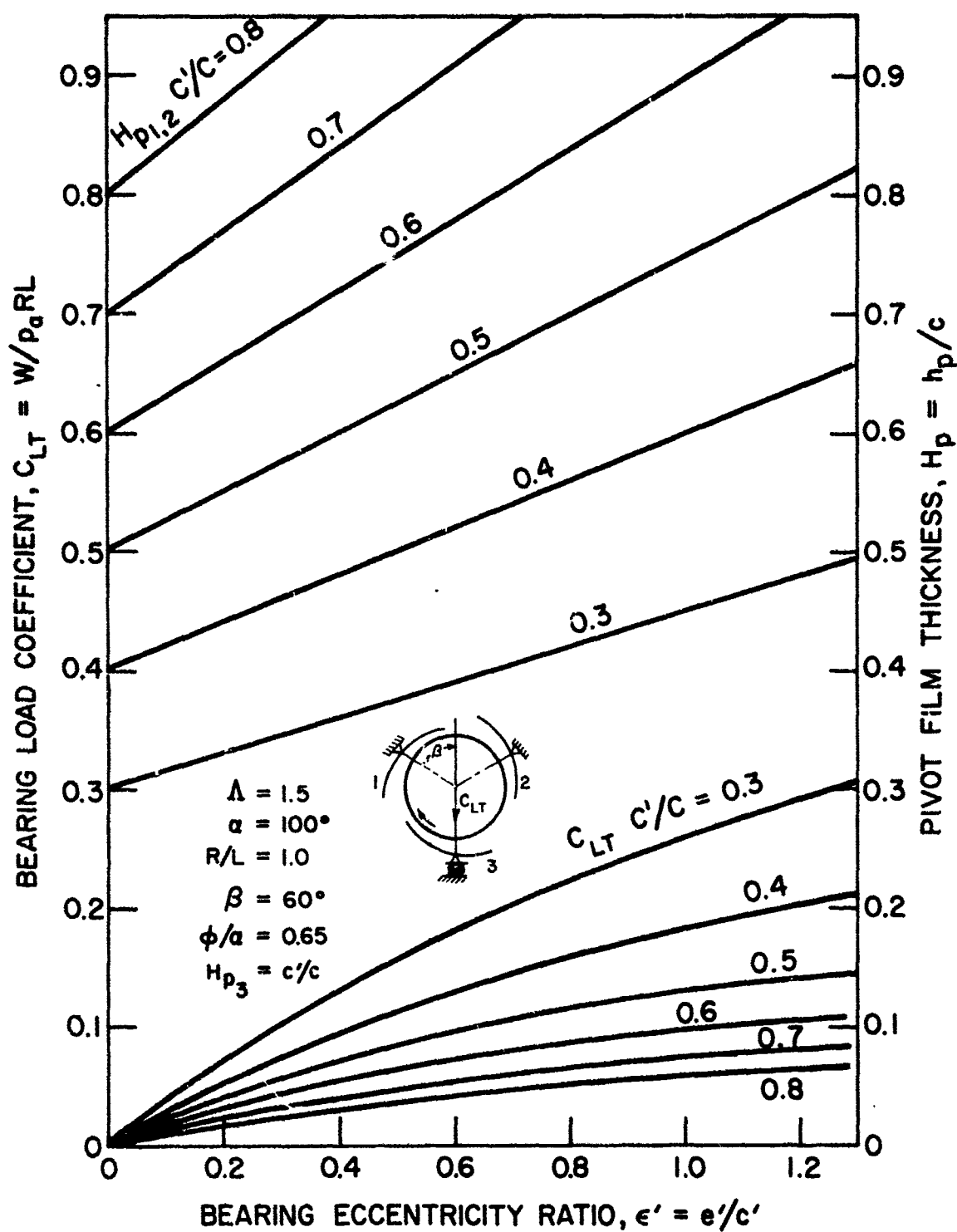
132

Figure 96. Bearing Load Coefficient and Pivot Clearance vs. Eccentricity Ratio for Load Directed at Spring Loaded Pad, $\Lambda = 5.0$, $R/L = 0.5$

Figure 97. Bearing Load Coefficient and Pivot Clearance vs. Eccentricity Ratio for Load Directed at Spring Loaded Pad, $\Lambda = 5.0$, $R/L = 1.0$
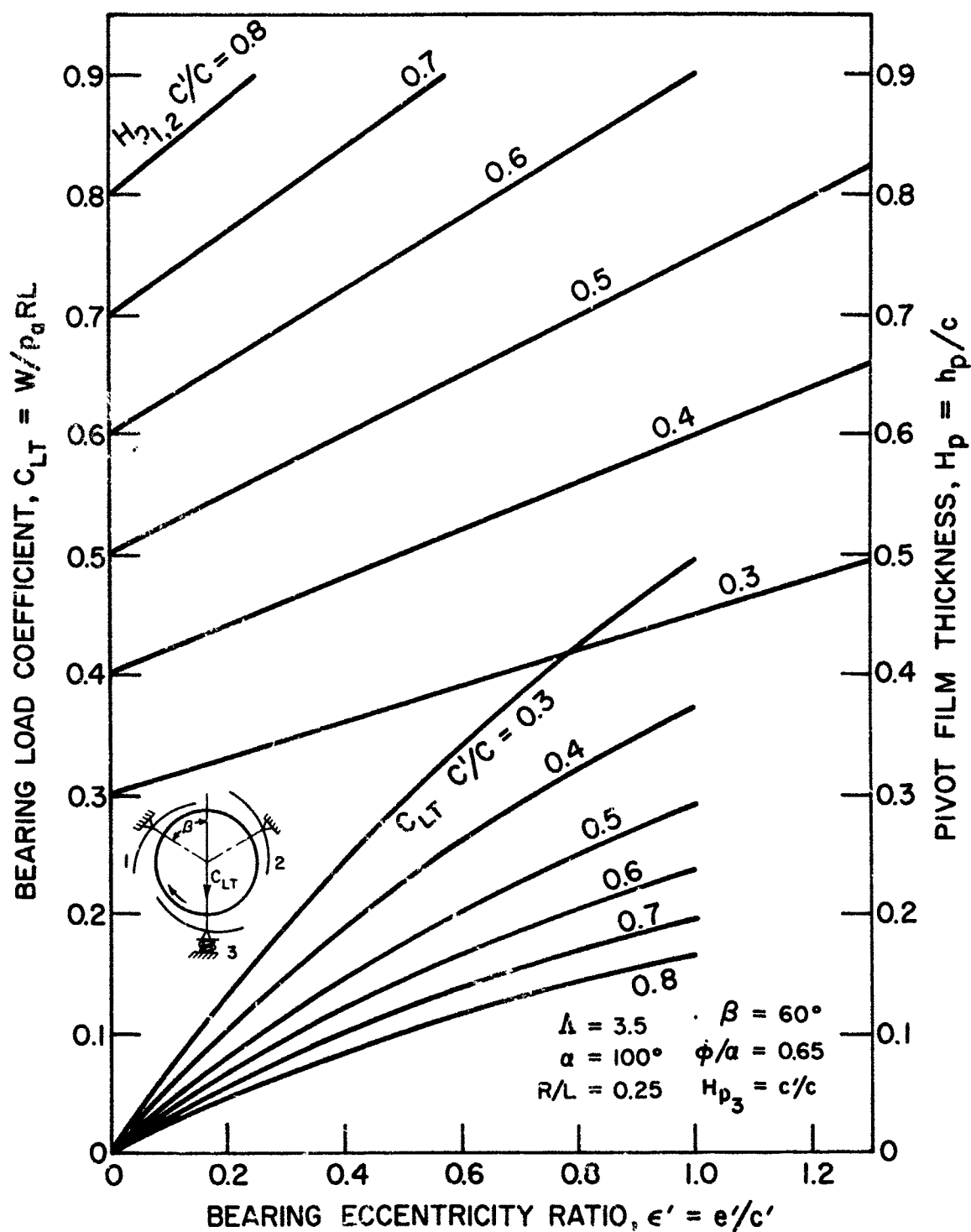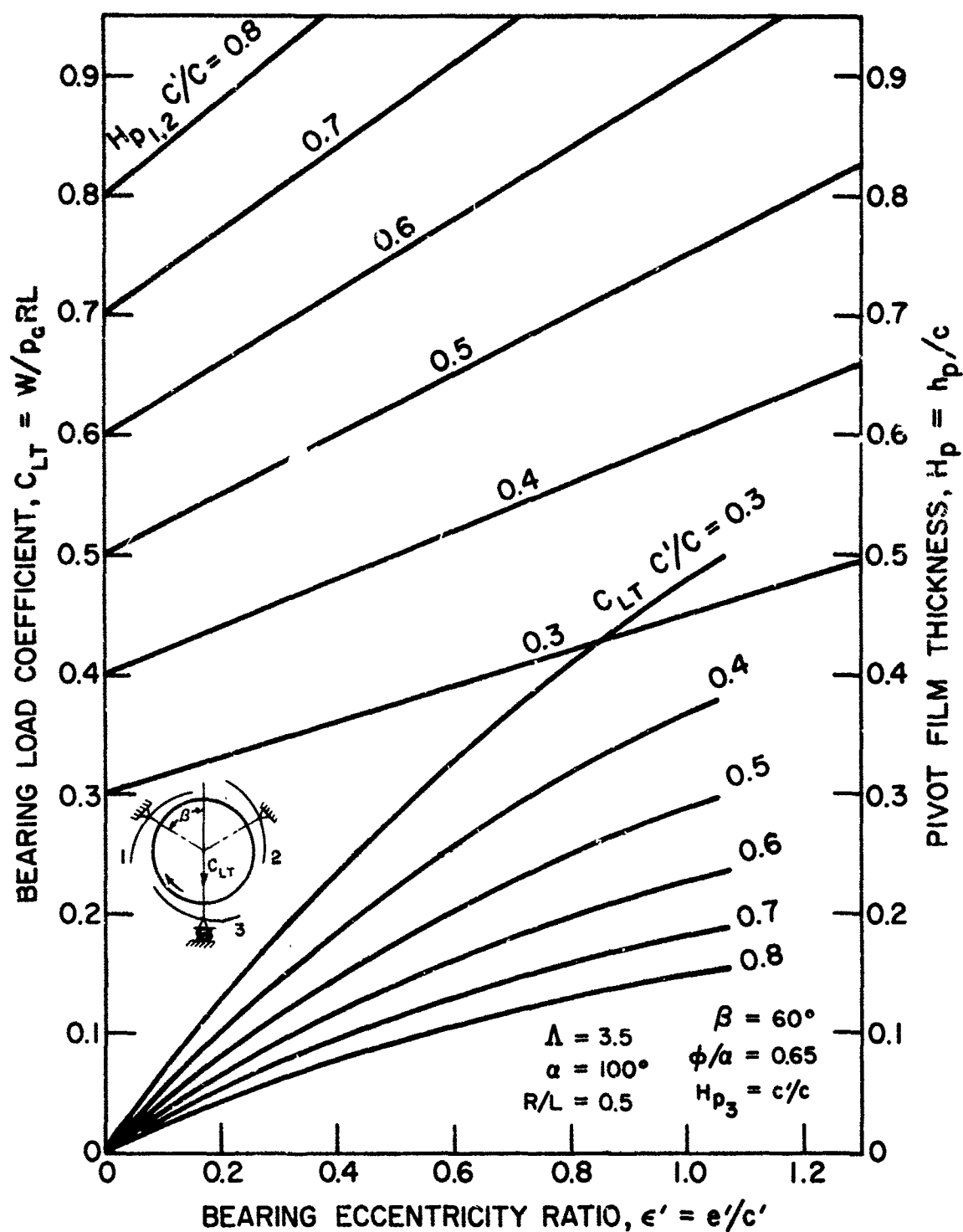
134

Figure 98. Bearing Load Coefficient and Pivot Clearance vs. Eccentricity
Ratio for Load Directed at Spring Loaded Pad, Λ = 10, R/L = 0.25

Figure 99. Bearing Load Coefficient and Pivot Clearance vs. Eccentricity Ratio for Load Directed at Spring Loaded Pad, $\Lambda = 10$, $R/L = 0.5$
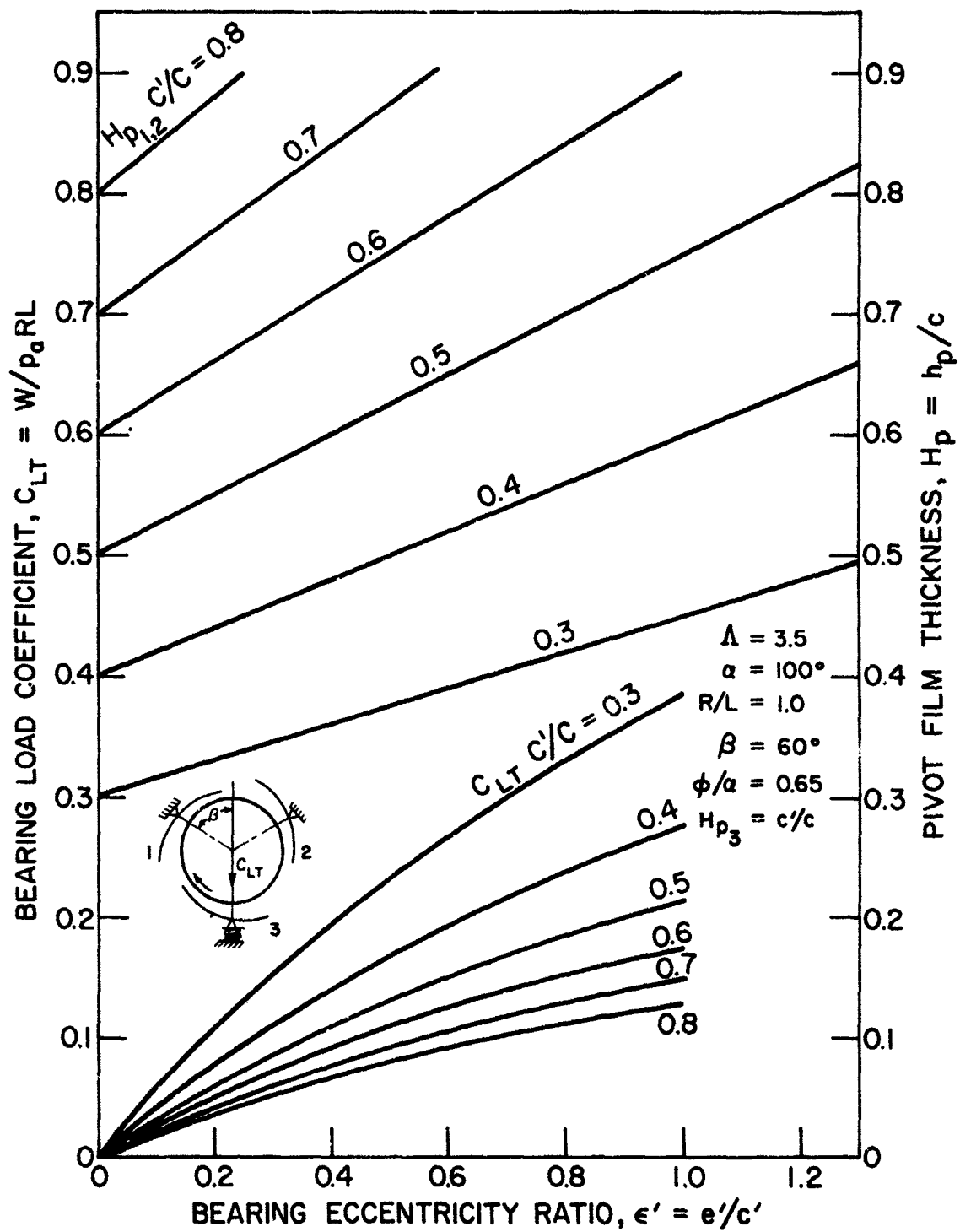
Figure 100. Bearing Load Coefficient and Pivot Clearance vs. Eccentricity Ratio for Load Directed at Spring Loaded Pad, Λ = 10, R/L = 0.25
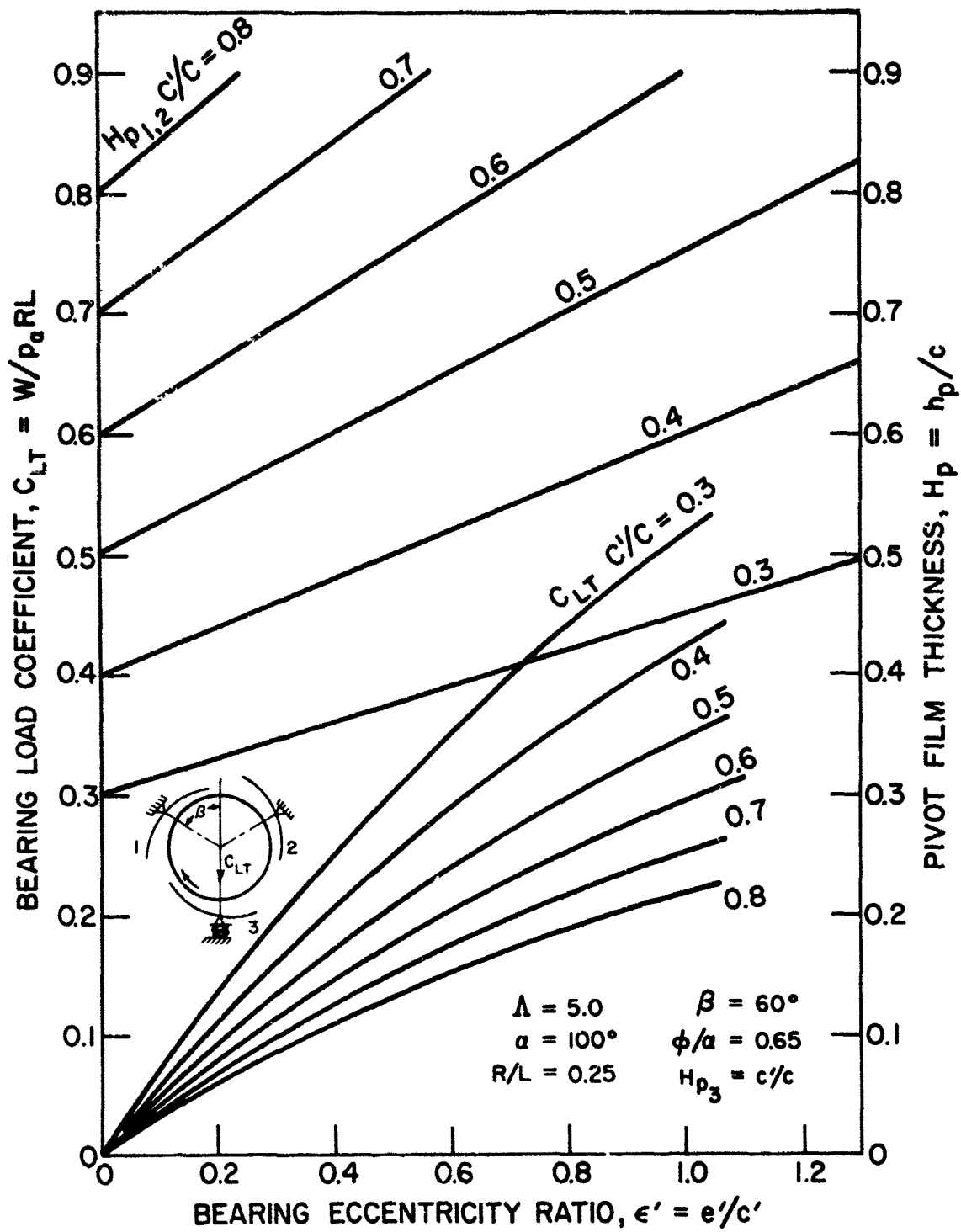
137

Figure 101. Bearing Load Coefficient and Pivot Clearance vs. Eccentricity
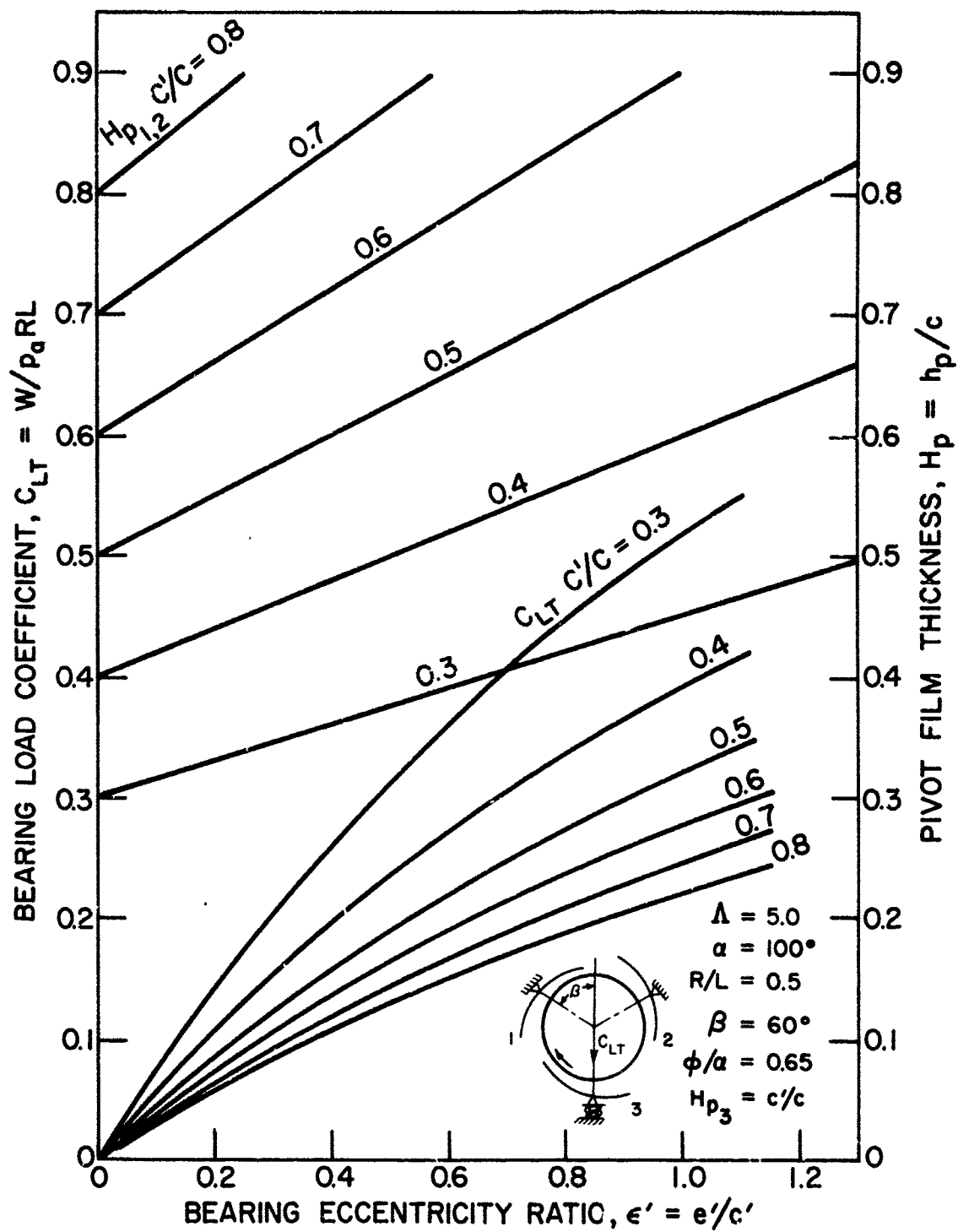Ratio for Load Directed at Spring Loaded Pad, $\Lambda = 20$, $R/L = 0.25$

Figure 102. Bearing Load Coefficient and Pivot Clearance vs. Eccentricity Ratio for Load Directed at Spring Loaded Pad, Λ = 20, R/L = 0.5

139

Figure 103. Bearing Load Coefficient and Pivot Clearance vs. Eccentricity
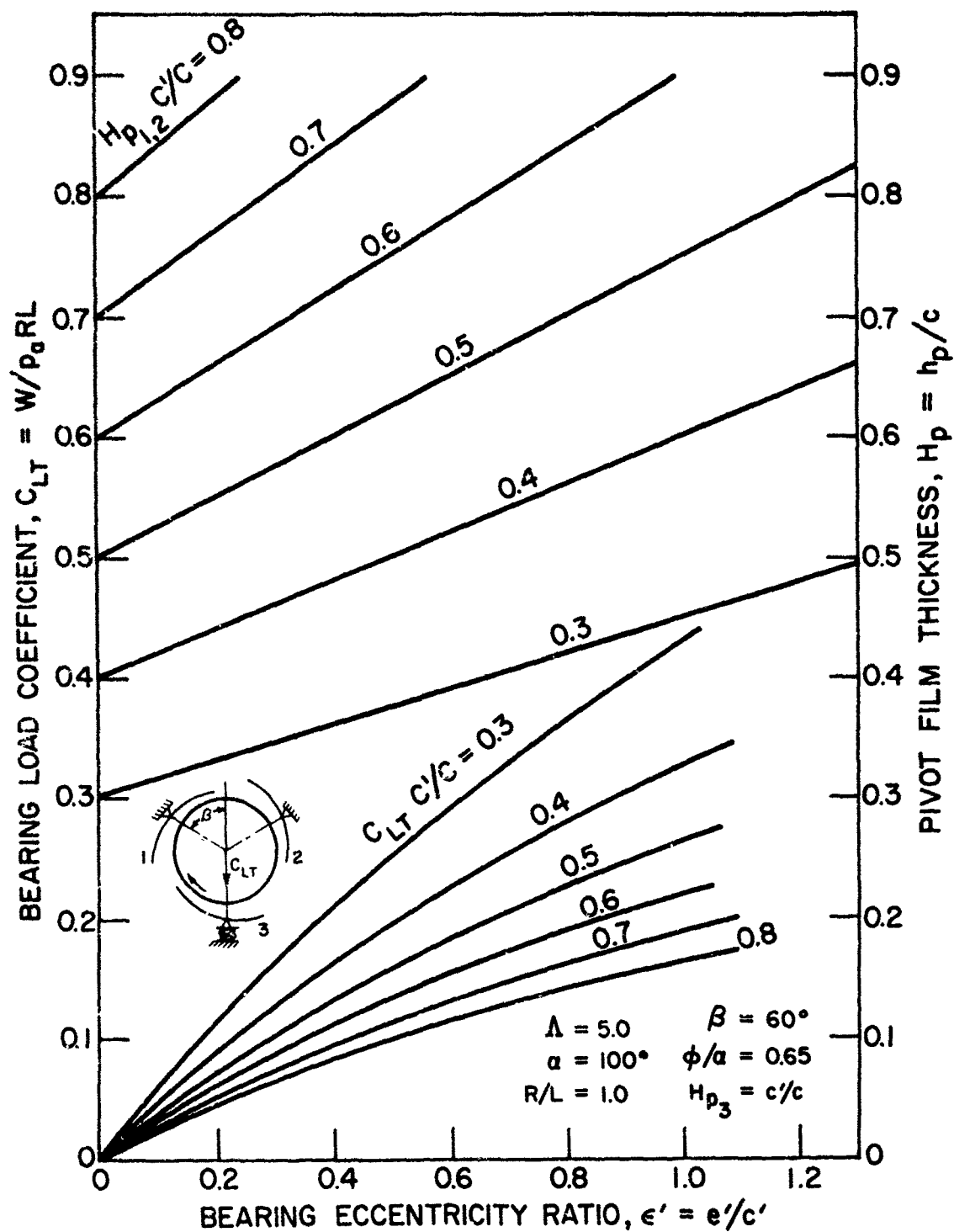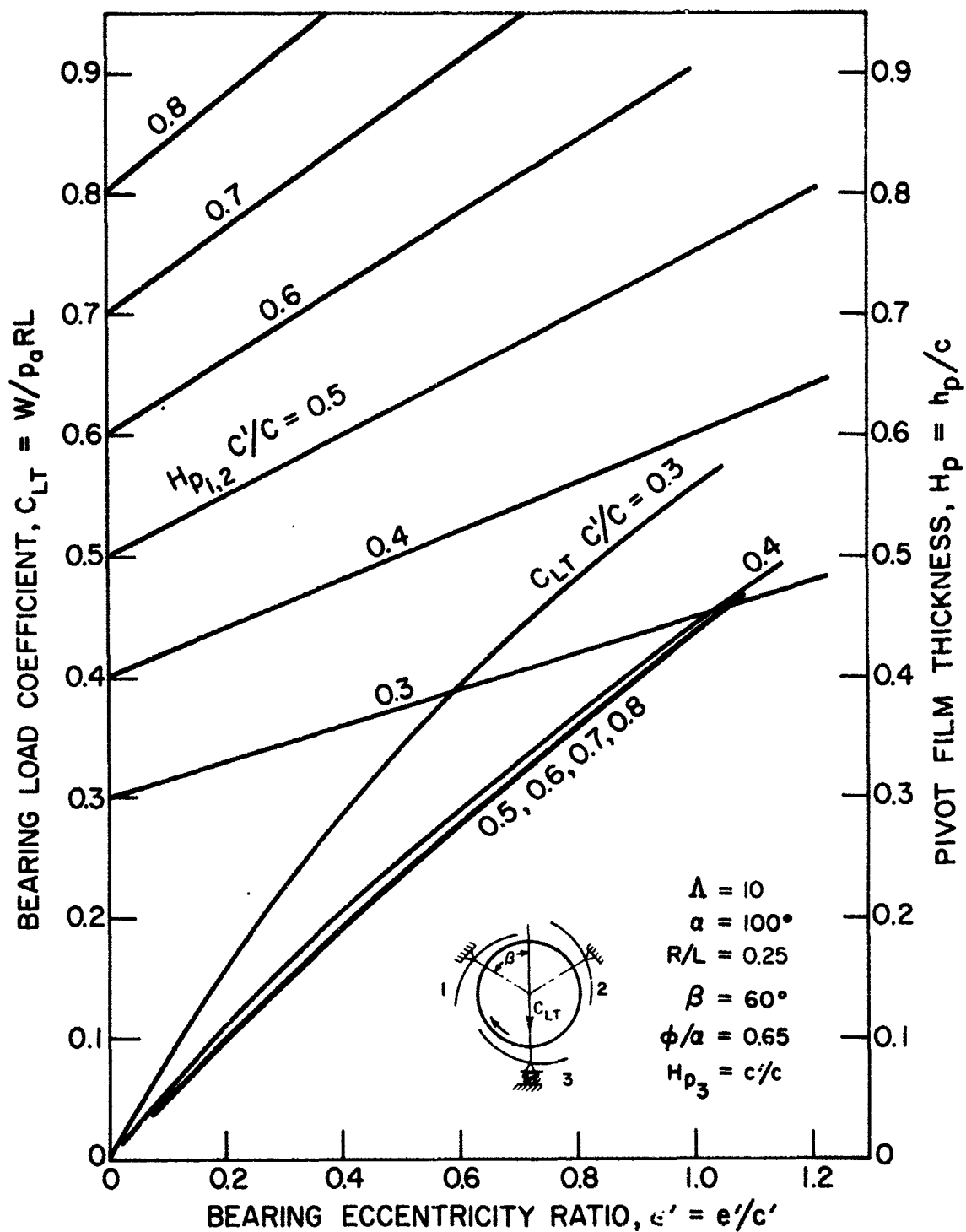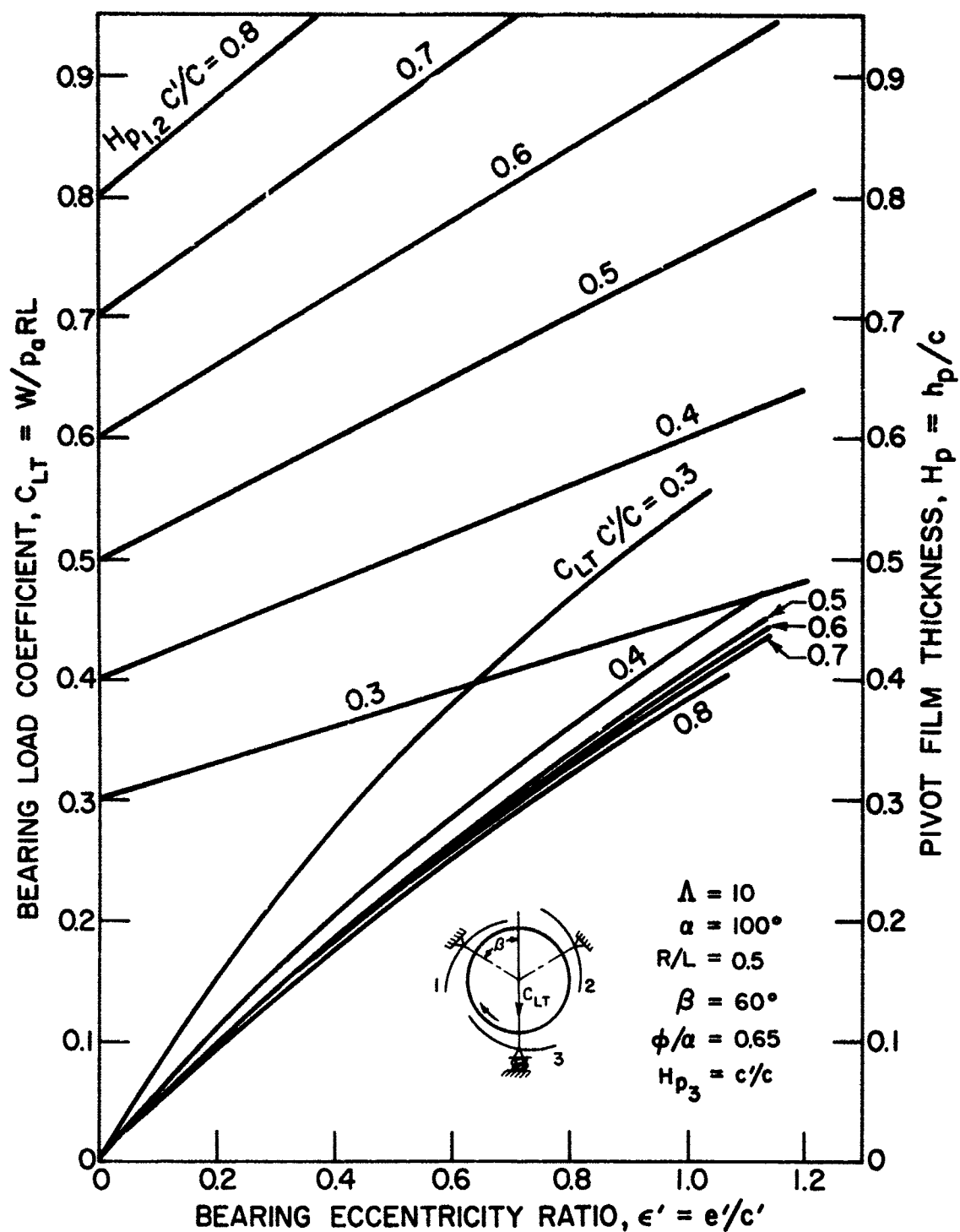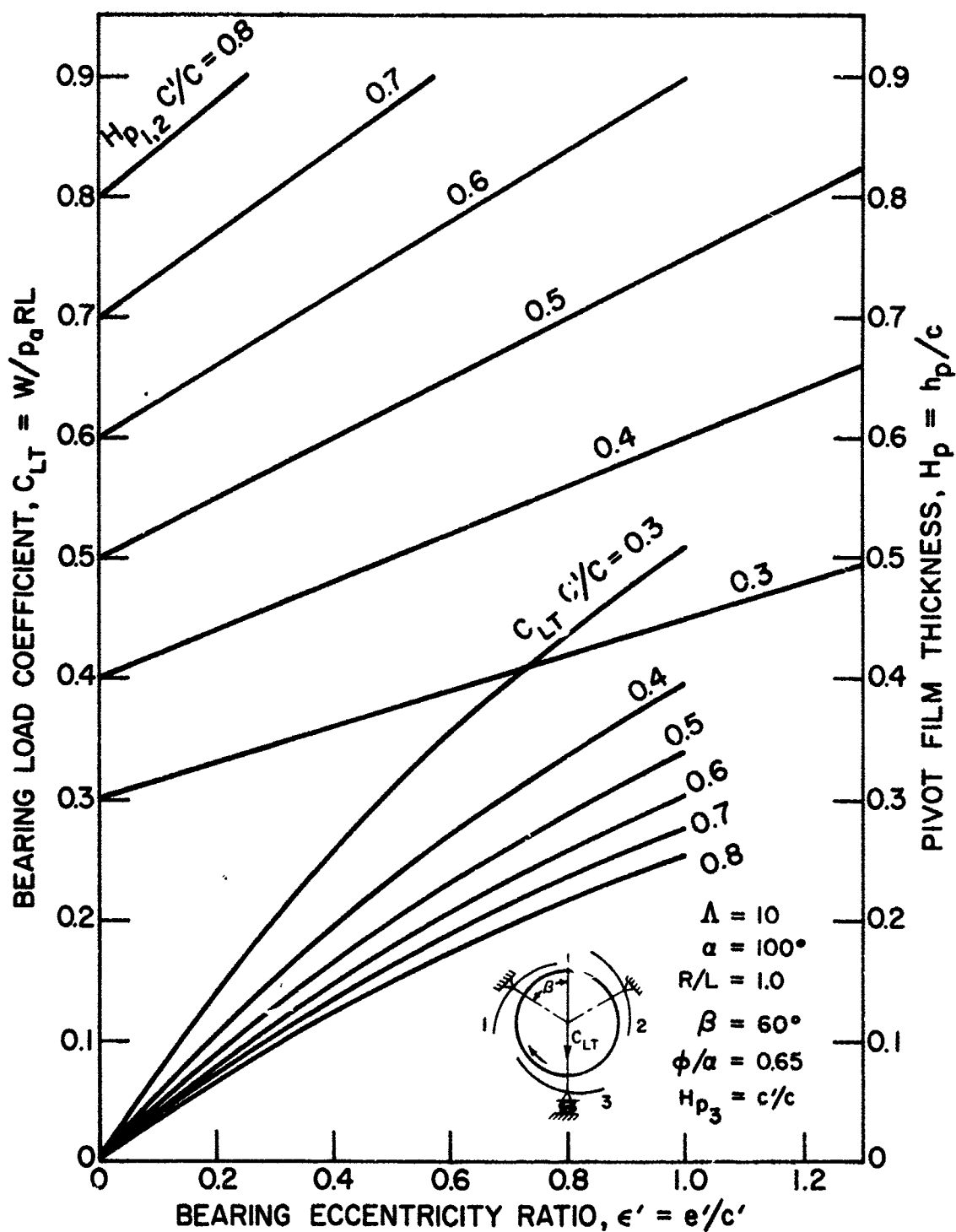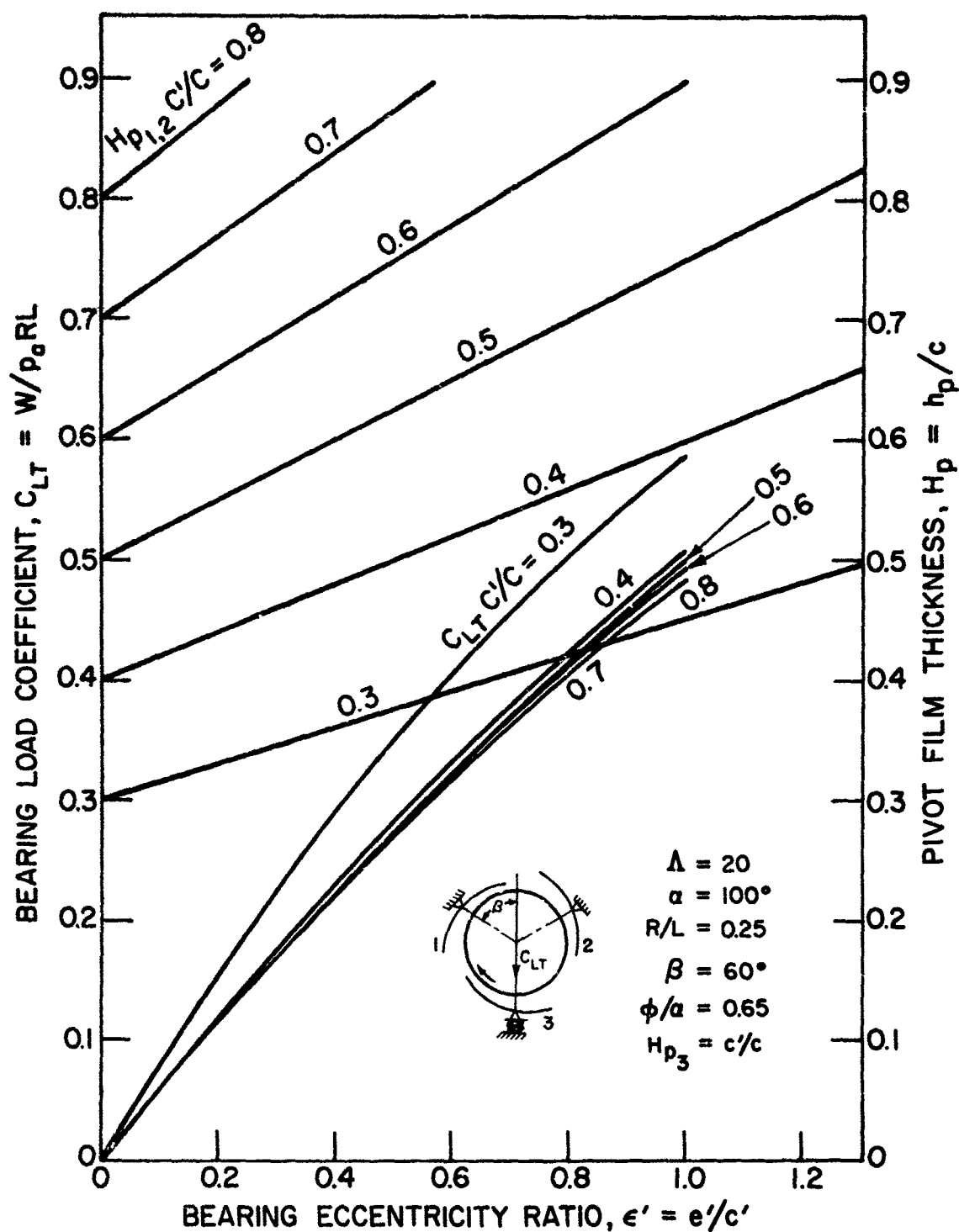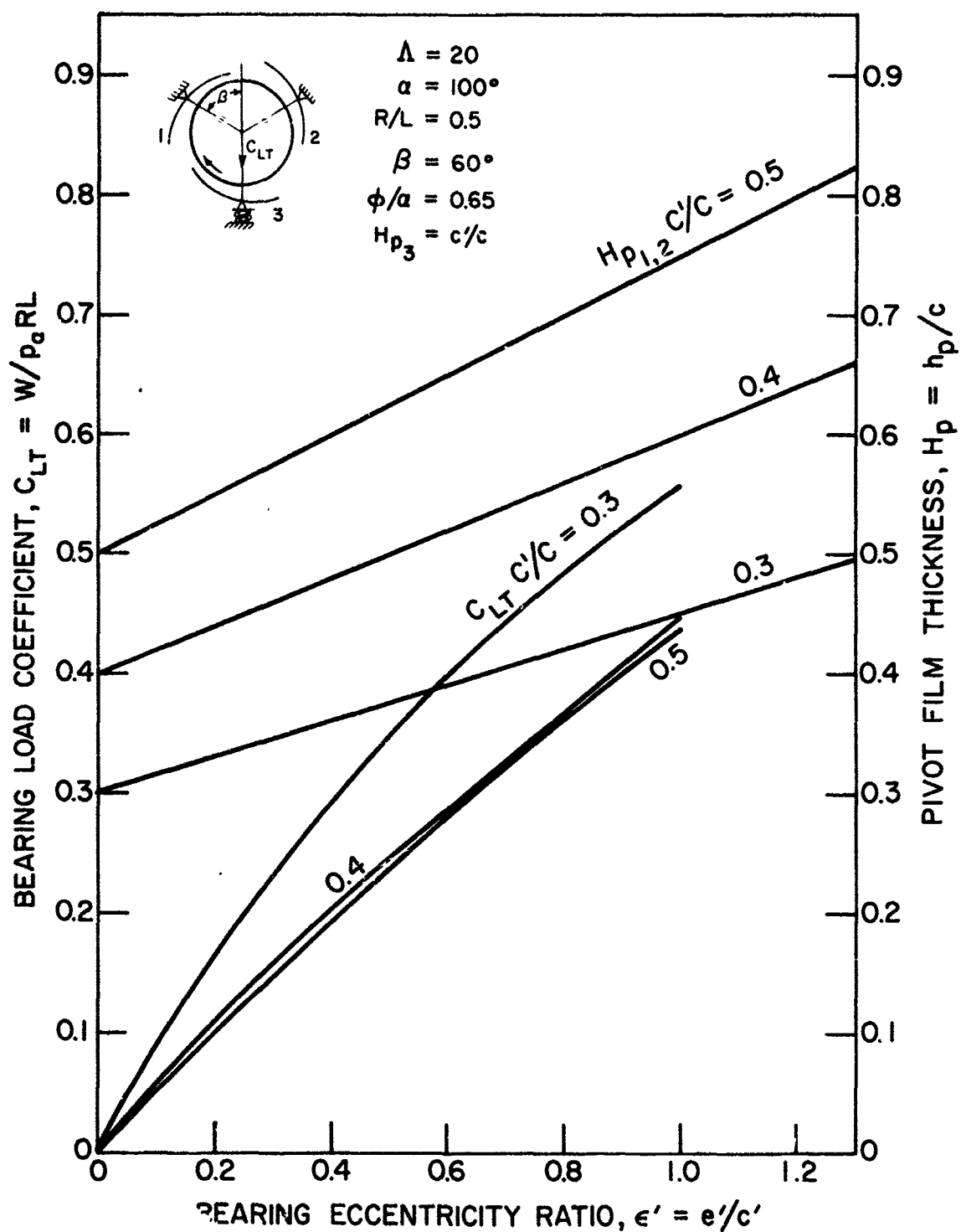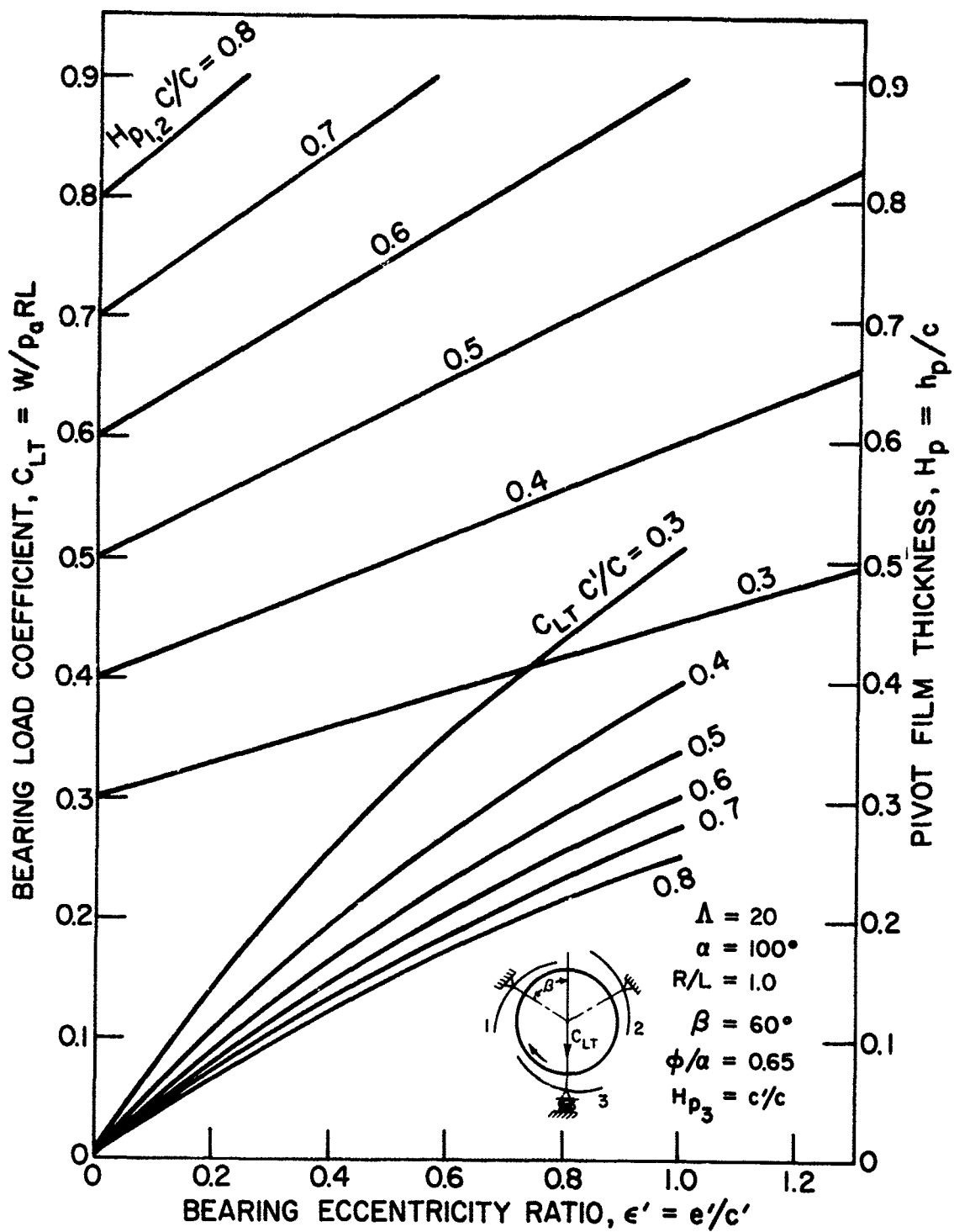Ratio for Load Directed at Spring Loaded Pad, Λ = 20, R/L = 0.5

APPENDIX II
VARIABLE GRID, DU FORT-FRANKEL ANALYSIS OF
GAS-LUBRICATED BEARINGS

1. INTRODUCTION

Solution of high Λ gas-bearing problems have posed numerical problems
because of the very high pressure gradients at the regions of minimum
film thickness. Use of variable grid methods enable a dense grid at
regions of high gradients, and a coarse grid otherwise and circumvents
the problems of numerical instabilities imposed by uniform grids of
spacing that would not absorb excessive computer storage or computational
time.

Another problem inherent in time transient lubrication problems is
repetitive solution of the Reynolds' equation throughout the grid at each
time increment. Implicit formulations are encumbered by large numbers of
matrix inversions while the usual explicit formulation requires very
small time increments for numerical stability. The DuFort-Frankel Method
combines the advantages of explicit solution with reasonable time incre-
ments. Thus, the discussion following incorporates two important
features with regard to gas bearing analysis, namely

a) Variable grid

b) Stable explicit solution for pressure with practical time
increments.

2. ANALYSIS

Making all the standard assumptions for compressible lubrication
theory (contact viscosity, negligible inertia effects, perfect gas, etc.)
the continuity eq can be written

$$\frac{\partial}{\partial t} \int_v \rho\, dv + \int_s \rho\, \overline{V} \cdot \overline{n}\; ds = 0 \qquad [1]$$

where

$$\overline{V} = V_\Theta\, \overline{n}_\Theta + V_z\, \overline{n}_z$$

141

$$V_\Theta = -\frac{1}{R} \frac{\partial p}{\partial \theta} \frac{h^2}{12\mu} + \frac{R\Omega}{2}$$

$$V_Z = -\frac{\partial p}{\partial Z} \frac{h^2}{12\mu}$$

$$dv = hRd\theta dz$$

By non-dimensionalizing [1] with

$$P_a P = p$$

$$\frac{2T}{\Omega_1} = t$$

$$HC = h$$

$$ZL = z$$

$$\Lambda = \frac{6\mu \Omega}{P_a} \left(\frac{R}{C}\right)^2$$

and letting $\frac{P}{p}$ = constant

and $\frac{1}{2} \frac{\partial p^2}{\partial n} = P\frac{\partial p}{\partial n}$

equation [1] becomes

$$\Lambda \frac{\partial}{\partial T} \iint HPd\theta dZ - \int \left[\left(\frac{H^3}{2} \frac{\partial p^2}{\partial \theta} - \Lambda PH\right)dz + \left(\frac{R}{L}\right)^2 \frac{H^3}{2} \frac{\partial P^2}{\partial Z} d\theta\right] = 0 \qquad [2]$$

Integrations are accomplished by accumulation of the net flow emanating from a closed region surrounding each grid point. The equation for each grid point is made algebraic by using finite increments for distances and two point finite differences for derivatives. The region for variable grid, shown dotted on Figure 104, encompasses half the distance between the i, jth point and its neighbors.
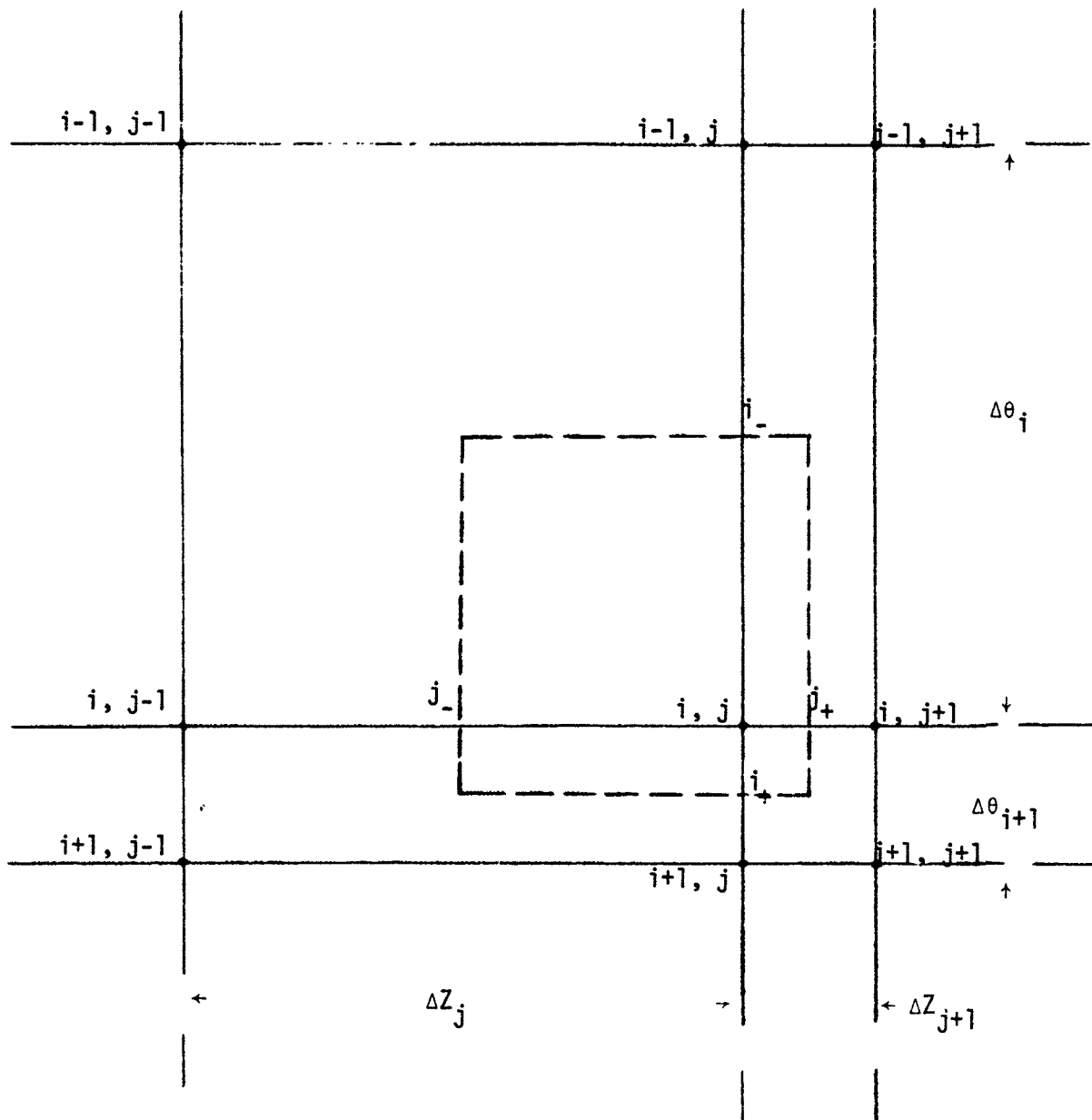
142

Figure 104. Variable Grid Representation

143

The Du-Fort-Frankel technique is introduced by substituting for the pressure at the i, j^{th} point at time t, the average of future and past pressures, i.e.:

$$P_{ij}^{t} = \frac{P_{ij}^{t+1} + P_{ij}^{t-1}}{2}$$ [3]

The formulation of the finite-difference continuity equation is a quadratic of the form:

$$A \, P_{ij}^{2^{t+1}} + B \, P_{ij}^{t+1} + C = 0$$ [4]

where the coefficients are functions of the local film thickness and grid spacing, compressibility parameter and time increment. It can be shown that as $\Delta t \to 0$ the pressure solution to equation [4] converges to the correct solution. Solution of the quadratic equation [4] at each grid point is numerically stable for a reasonably large time increment and computational time is much less than either the usual implicit or explicit schemes described by References 4 and 5.

APPENDIX III

DYNAMIC ANALYSIS AND DESIGN CURVES
FOR TILTING PAD JOURNAL BEARING
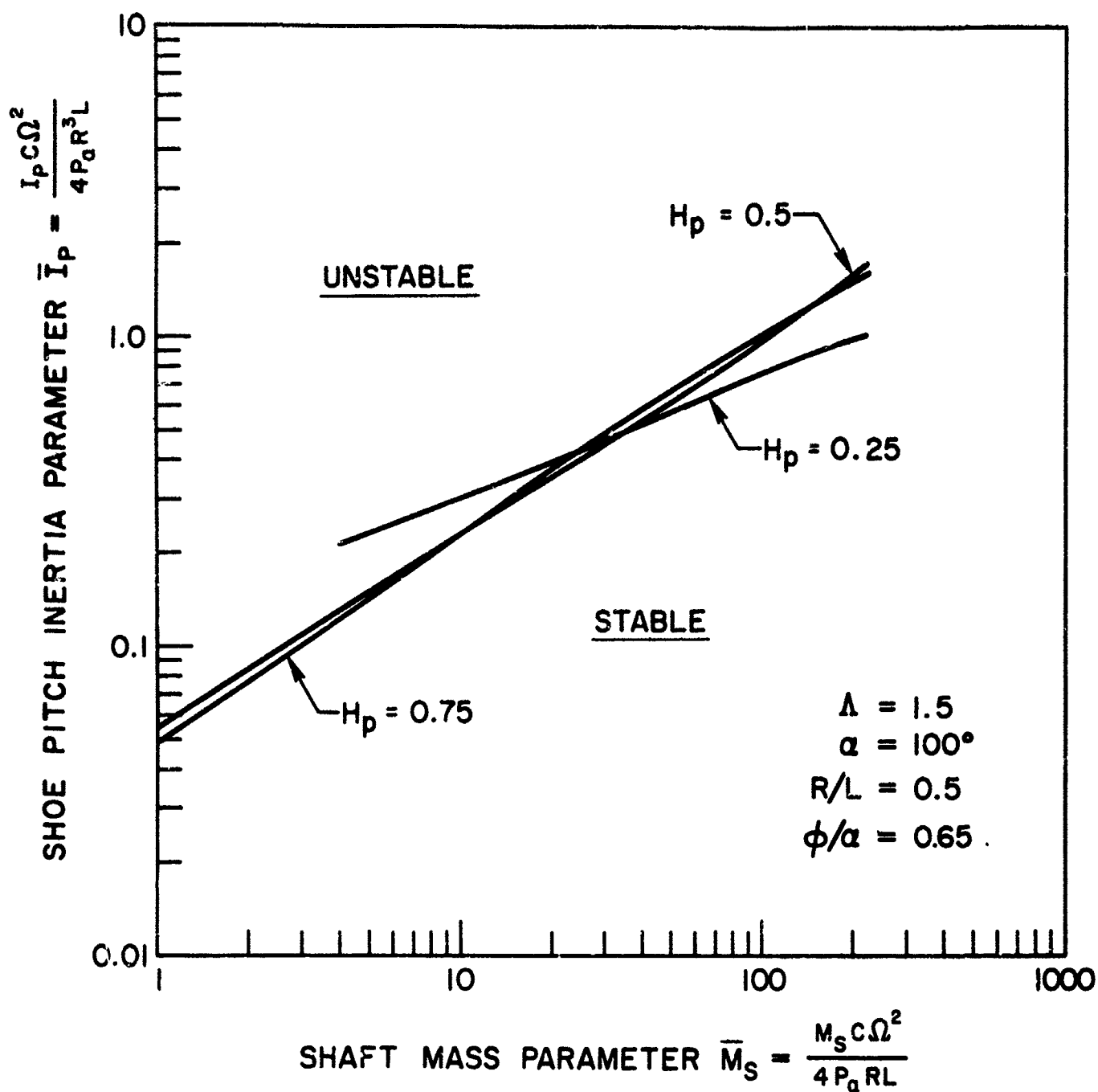
1. STABILITY MAPS

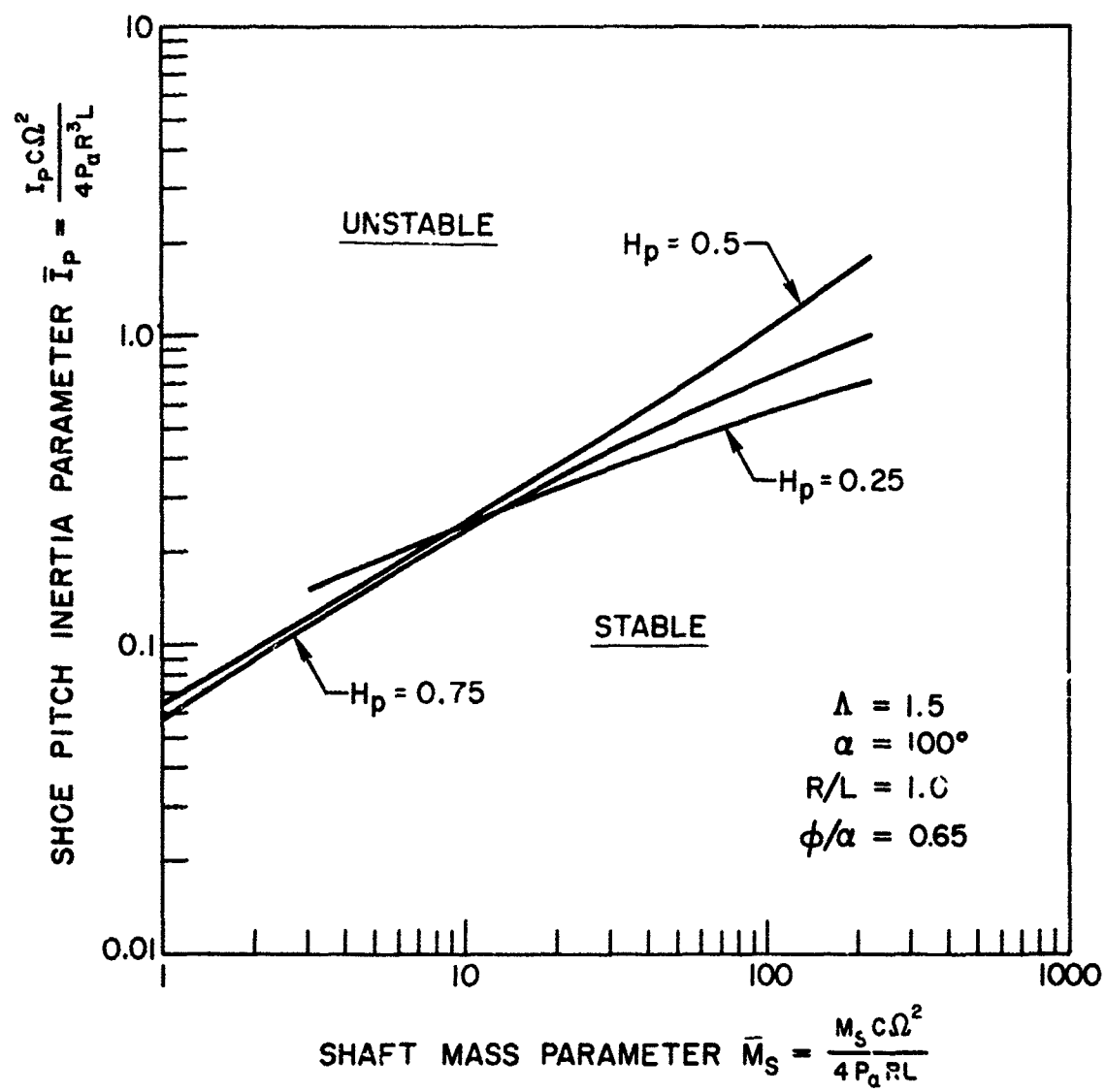Figure 105. Stability Map, R/L = 0.5, Λ = 1.5

146

Figure 106. Stability Map, R/L = 1.0, Λ = 1.5

147

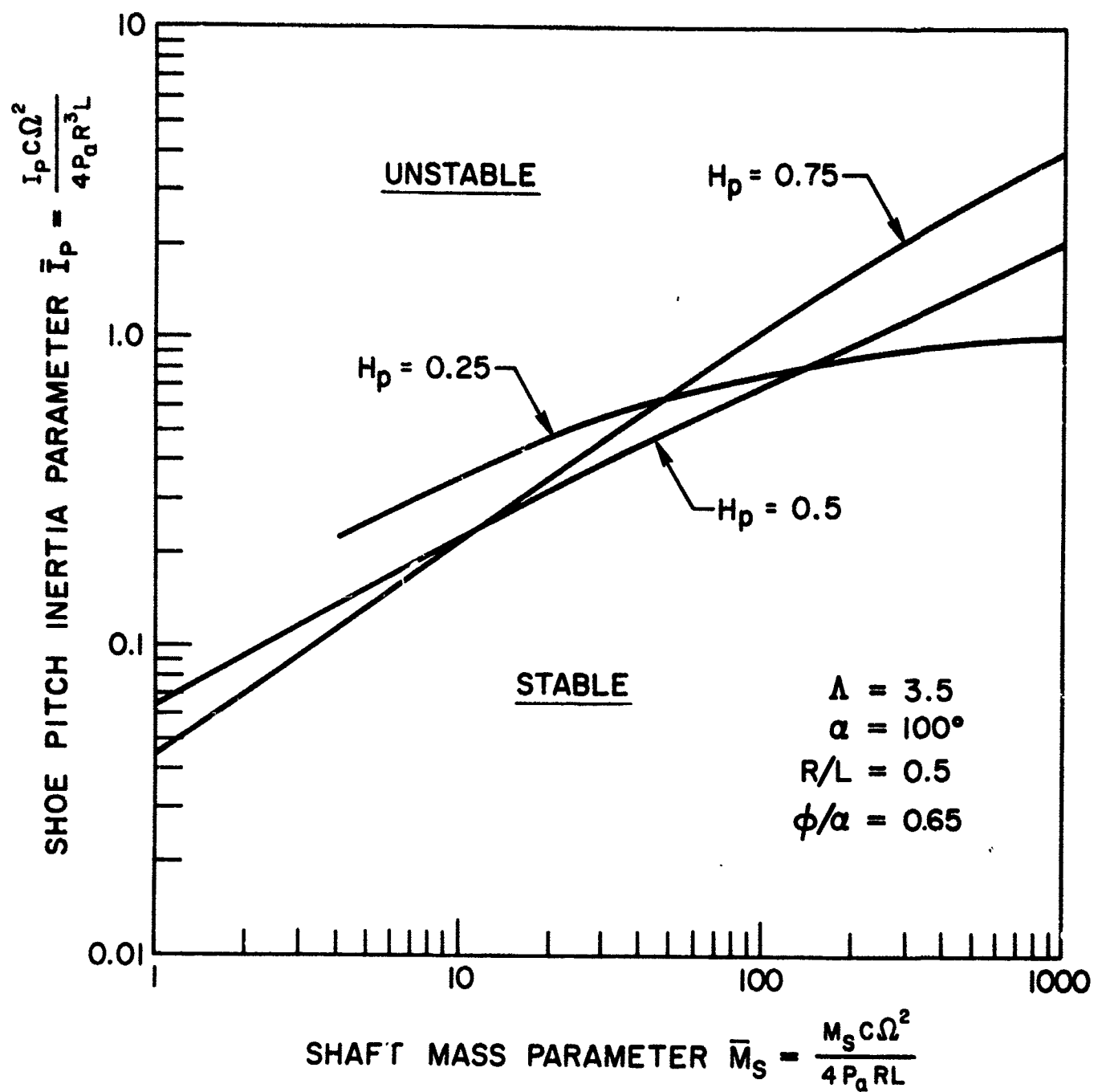Figure 107. Stability Map, R/L = 0.5, Λ = 3.5

148

Figure 108. Stability Map, R/L = 1.0, Λ = 3.5

Figure 109. Stability Map, R/L = 0.5, Λ = 5.0

Figure 110. Stability Map, R/L = 1.0, Λ = 5.0
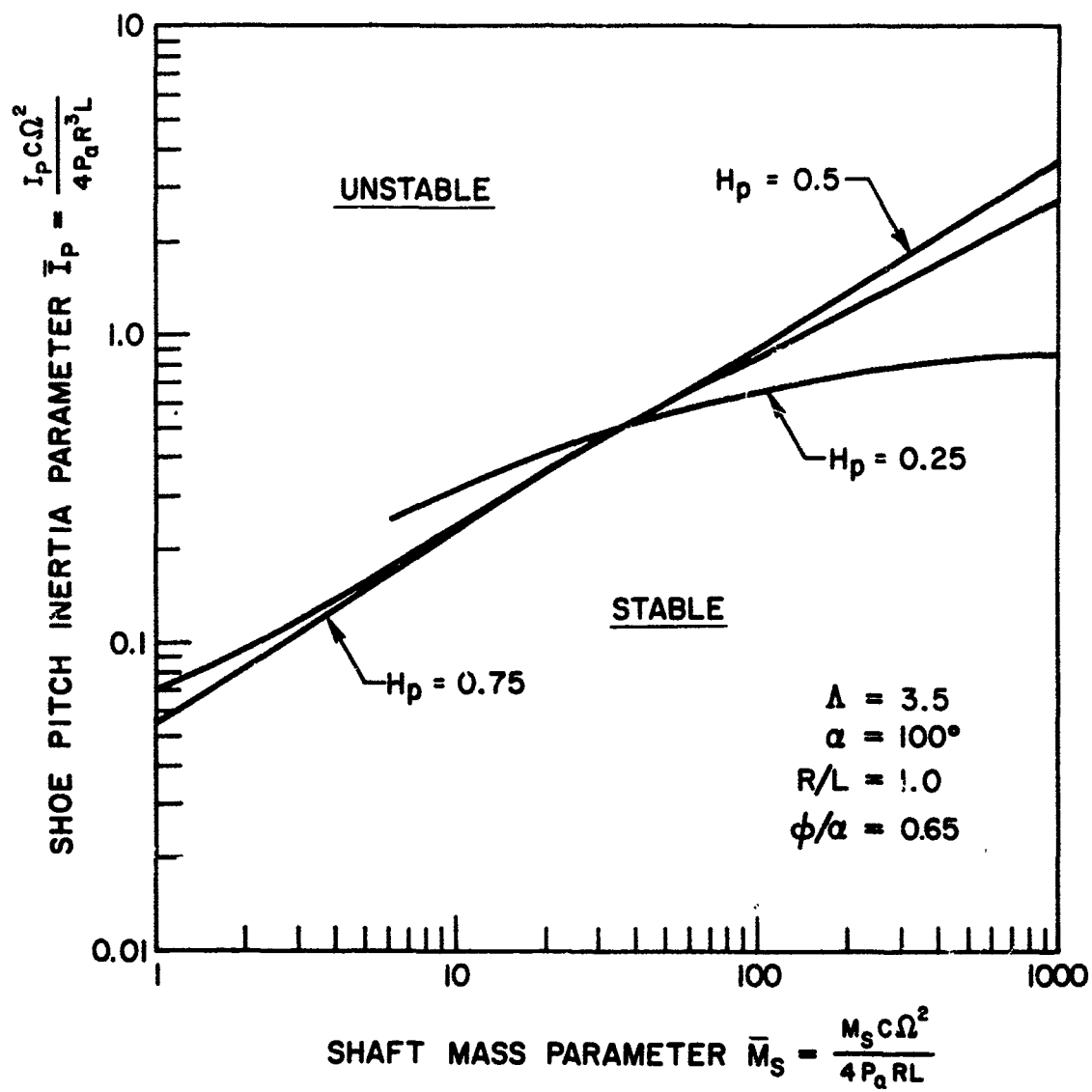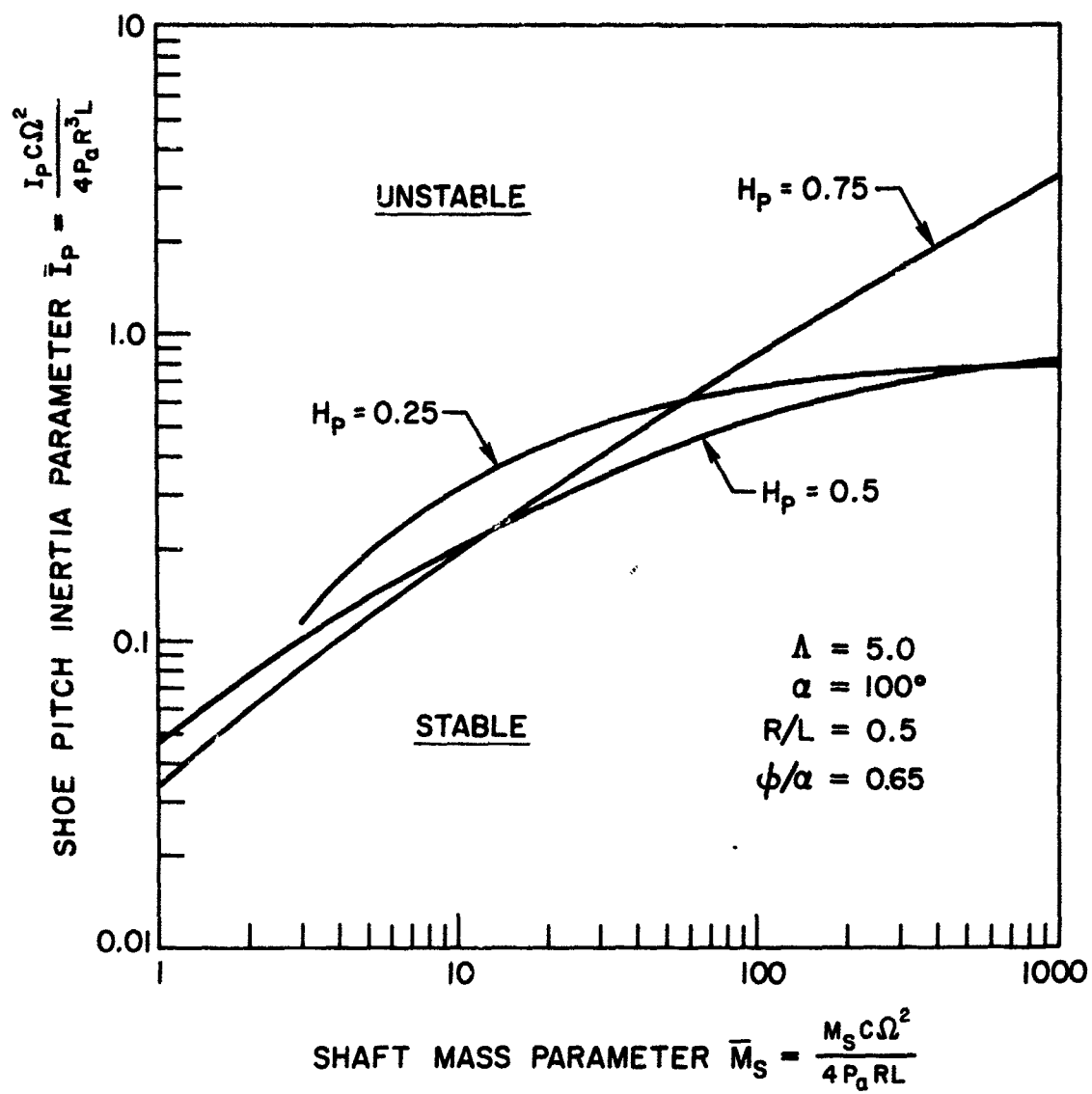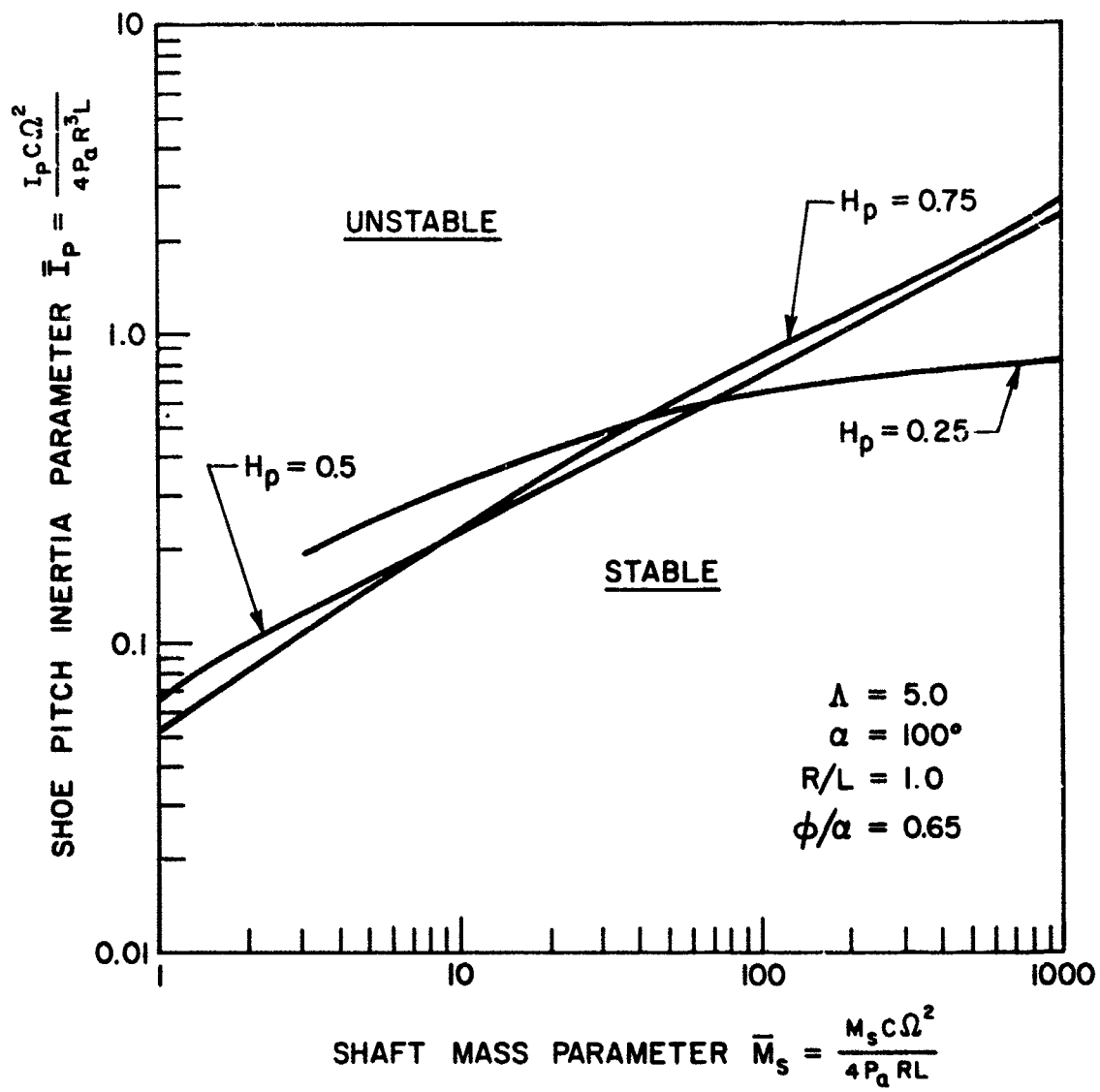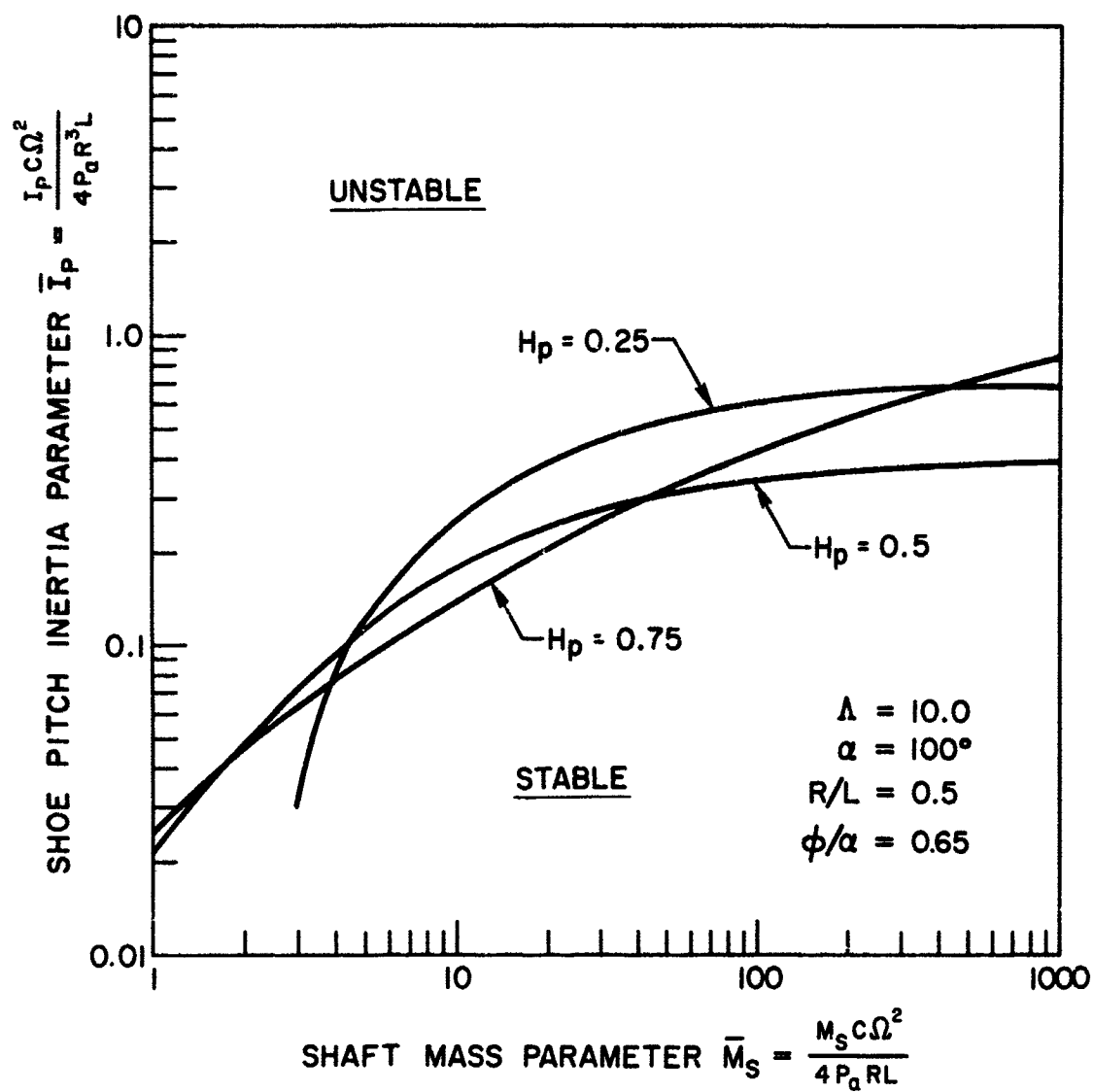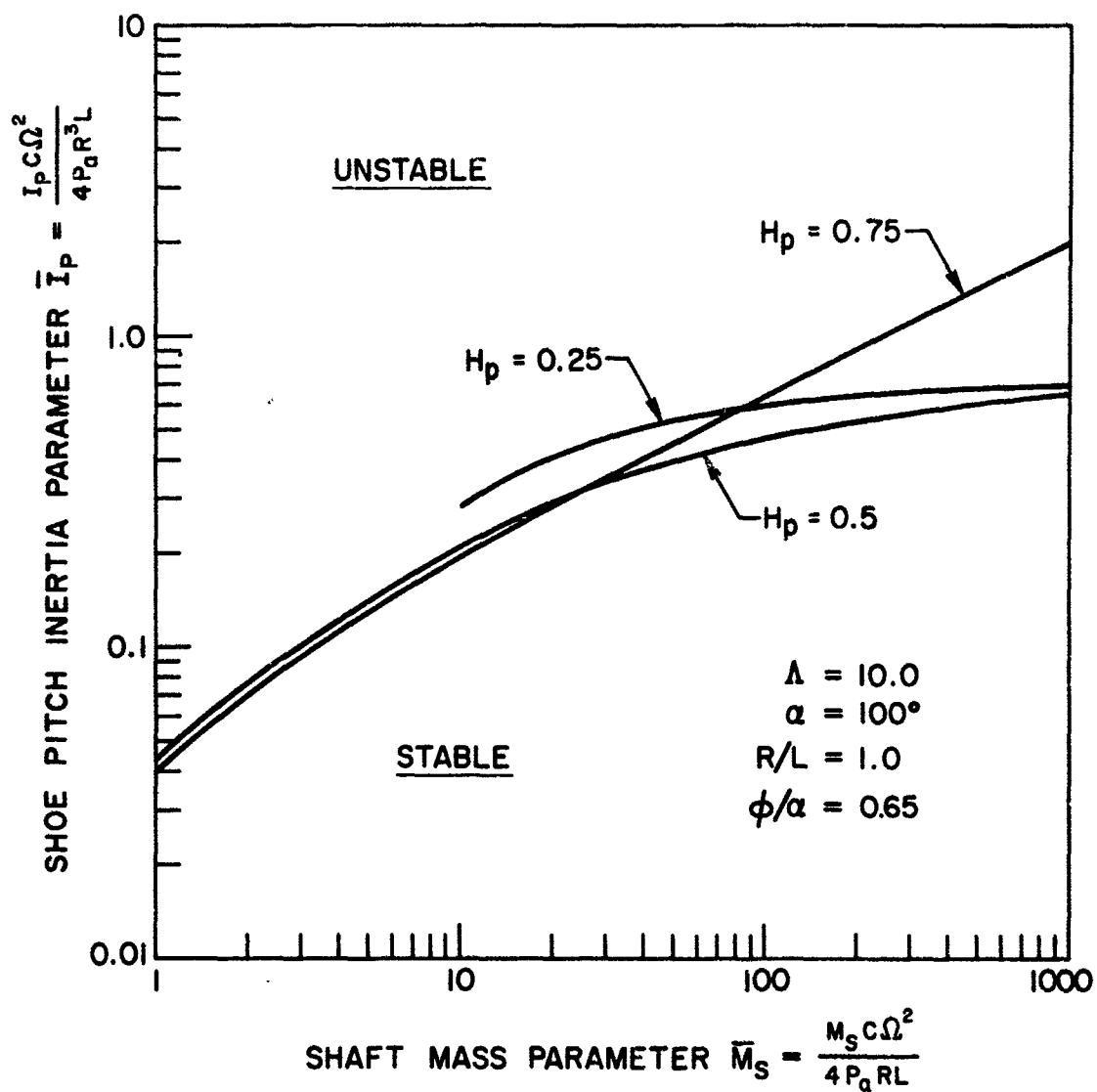
Figure 111. Stability Map, R/L = 0.5, Λ = 10

Figure 112. Stability Map, R/L = 1.0, Λ = 10

153

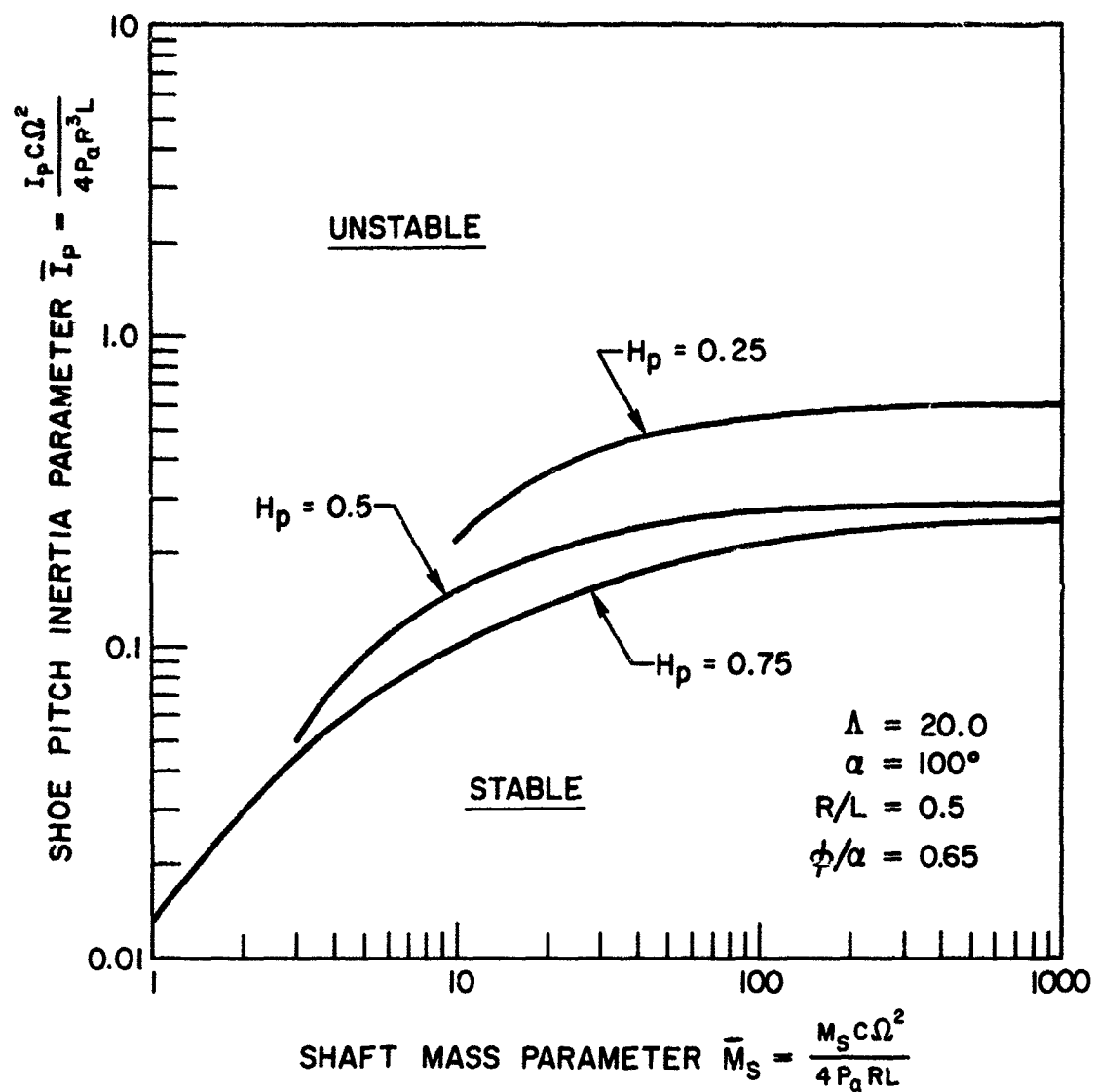Figure 113.   Stability Map, R/L = 0.5, Λ = 20

154

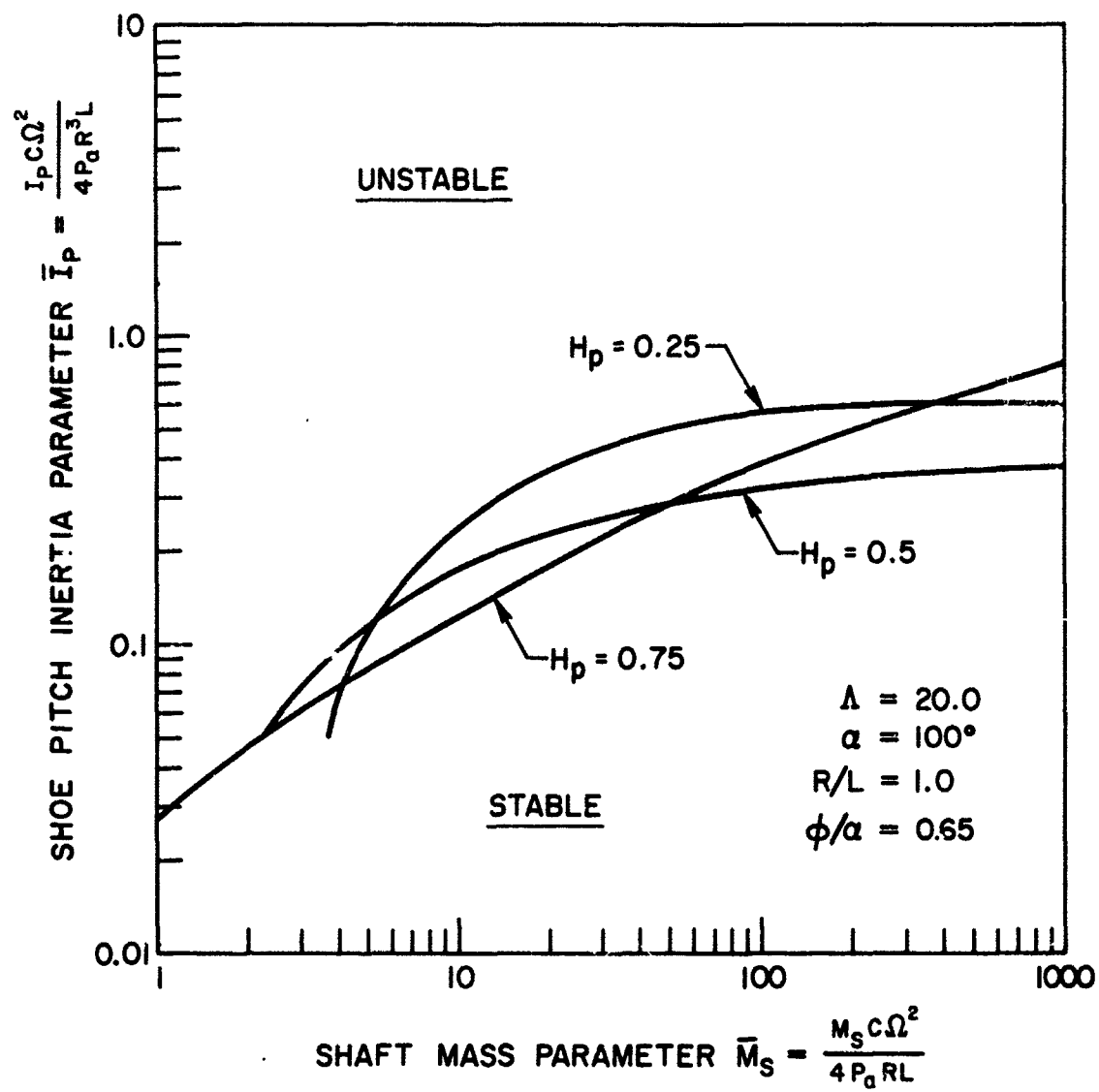Figure 114. Stability Map, R/L = 1.0, Λ = 20

DOCUMENT CONTROL DATA - R & D

(Security classification of title, body of abstract and indexing annotation must be entered when the overall report is classified)

1 ORIGINATING ACTIVITY (Corporate author)	2a. REPORT SECURITY CLASSIFICATION
The Franklin Institute Research Laboratories 20th & Parkway Philadelphia, Pa 19103	Unclassified
	2b GROUP

3 REPORT TITLE

Analysis and Design of Gas-Lubricated Tilting Pad Journal Bearings for Miniature Cryogenic Turbomachinery

4 DESCRIPTIVE NOTES *(Type of report and inclusive dates)*

Final Report   May 1969 through May 1970

5 AUTHOR(S) *(First name, middle initial, last name)*

Wilbur Shapiro   Richard Colsher

6 REPORT DATE	7a. TOTAL NO. OF PAGES	7b. NO. OF REFS
June 1970	169	5

8a CONTRACT OR GRANT NO	9a. ORIGINATOR'S REPORT NUMBER(S)
USAF F33615-69-C-1718	F-C2531
b. PROJECT NO 1470 Task No. 147002	
c	9b. OTHER REPORT NO(S) *(Any other numbers that may be assigned this report)* AFFDL-TR-70-99
d	

10 DISTRIBUTION STATEMENT

This document is subject to special export controls and each transmittal to foreign government or foreign nationals may be made only with prior approval of the Air Force Flight Dynamics Laboratory, FDFM, Wright-Patterson Air Force Base, Ohio.

11 SUPPLEMENTARY NOTES	12 SPONSORING MILITARY ACTIVITY
	Air Force Flight Dynamics Laboratory Air Force Systems Command Wright-Patterson Air Force Base, Ohio

13 ABSTRACT

Extensive steady-state and dynamic design information has been generated for tilting pad journal bearings with emphasis on miniature cryogenic turbomachinery applications. Coverage includes bearing length to diameter ratios of from 0.5 to 2.0 and values of the compressibility parameter from 1.5 to 20. Information was put into a format for use by design engineers and a separate section discusses design procedures plus practical considerations. An experimental program was completed, using room temperature air as the lubricant, which substantiated the analytical information.

Variable grid computerized analysis was required to avoid numerical problems at high values of the compressibility parameter A. These methods proved very successful and represent a significant improvement over constant grid techniques.

DD FORM 1473 (1 NOV 55)

14 KEY WORDS	LINK A		LINK B		LINK C	
	ROLE	WT	ROLE	WT	ROLE	WT
Journal Bearings						
Tilting Pad Journal Bearings						
Gas-Lubricated						
Analysis & Design						
Miniature Cryogenic Turbomachinery						